An Experimental and Numerical Study of the Influence of Room Factors and Hygroscopic Material of Wood Paneling on the Indoor Environment

Yang Li

A Thesis

In the Department

of

Building, Civil and Environmental Engineering

Presented in Partial Fulfillment of the Requirements
For the Degree of Doctor of Philosophy at
Concordia University
Montreal, Quebec, Canada

September 2011

CONCORDIA UNIVERSITY

SCHOOL OF GRADUATE STUDIES

This is to certify that the thesis prepared

By: Yang Li

Entitled: An Experimental and Numerical Study of the Influence of Room Factors and Hygroscopic Material of Wood Paneling on the Indoor Environment

and submitted in partial fulfillment of the requirements for the degree of

DOCTOR OF PHILOSOPHY (Building Engineering)

complies with the regulations of the University and meets the accepted standards with respect to originality and quality.

Signed by the final examining committee:

_____ Chair
Dr. I. Stiharu

_____ External Examiner
Dr. P. Mukhopadhyaya

_____ External to Program
Dr. Y. Zeng

_____ Examiner
Dr. R. Zmeureanu

_____ Examiner
Dr. A. Athienitis

_____ Thesis Co-Supervisor
Dr. P. Fazio

Approved by _____
Dr. M. Elektorowicz, Graduate Program Director

September 23, 2011 _____
Dr. Robin A.L. Drew, Dean
Faculty of Engineering & Computer Science

ABSTRACT

An Experimental and Numerical Study of the Influence of Room Factors and Hygroscopic Material of Wood Paneling on the Indoor Environment

Yang Li, PhD
Concordia University, 2011

Moisture level inside buildings is a key factor influencing the durability of construction, indoor air quality, living comfort, and energy consumption. Previous studies found that this level was related to the room factors including moisture loads and ventilation conditions and to the moisture ab/desorption capacity of hygroscopic material utilized in interior of the building. The phenomenon of the indoor humidity level influenced by the dynamic moisture interaction process between hygroscopic material and indoor air has been recognized as moisture buffering effect. Some materials' buffering properties at the material level have been intensively measured. However, there has not been enough information and testing standard for evaluating material buffering performance at the room level. Meanwhile, the material buffering properties may not be directly representative of the material buffering performance at the room level because the moisture buffering effects are influenced by room factors. This thesis reports on an experimental investigation of the impact of room factors on moisture buffering performance of wood paneling utilized as inner layer of the wall assembly and on the study of the indoor humidity level influenced by room factors and moisture buffering effect of the hygroscopic material. The experimental study presents the moisture responses of wood paneling by moisture ab/desorption kinetic curves, and finds that the buffering effect caused by hygroscopic material is related to not only the buffering

performance of the material but also to the characteristics of the building structure. Under the experimental test conditions, the room characteristics can cause up to 8% variation in RH levels and wood paneling can moderate these variations by up to 30%.

The experimental results showed that to predict indoor humidity levels, the moisture interaction between the wood paneling and indoor air was not negligible, and the room factors dominated the variation of the indoor environment. To further investigate the indoor humidity level influenced by room factors that could not be studied in the experiment and to explain the influences by the mechanisms of HAM transport, a numerical model that coupled the governing equations of momentum, heat, and moisture transport in whole building simulation domain was established. This model which took into account the heat/moisture interaction between indoor air and envelope overcomes the limitations existing in currently available numerical models of coupling moisture transport in the building envelope with indoor CFD simulation and has great application potential in whole building HAM transport studies. The application of this model presented in this thesis includes the investigation of the indoor environment influenced by moisture loads and ventilation designs, the heat/moisture transport through wall system, and the potential damage caused by moisture.

ACKNOWLEDGMENT

This thesis study arose in the time when I began studying at Center for Building Studies (CBS), Concordia University, in Prof. Fazio's building envelope research group. Partially participating in the CRD and SRO projects carried out by this group, I accumulated the knowledge and experience in building science research. This thesis study presented the work I have done under the support of a number of people whose contributions were irreplaceable in helping me to establish this research goals, to finish my thesis experimental tests, and to perform the numerical simulation. It is a pleasure to thank them all for making this research possible.

First I would like to show my gratitude to my supervisor, Dr. Paul Fazio, whose encouragement, guidance and support began from the very early stage of this research. He has made available his support not only by providing the opportunities and grants for this research project, but also by advising the study from the preliminary to the concluding level. I was motivated greatly by his dedication and enthusiasm in research, was encouraged about the research direction selection, and was supervised for the research project proceeding and paper published. I also very much appreciate his expertise, thoughtfulness, and patience.

The success of a large-scale experiment cannot be achieved without the help of a group of people. Among them, I would like to first thank Dr. Rao for his valuable comments in the experimental results analysis. He also helped to solve the experimental problems encountered during the tests and provided program tools to accelerate the analysis of the numerous date obtained by Data Acquisition System (DAS). Thanks are also due to Luc Demers, a fine technician who always helped in the laboratories to make sure all the facilities in the lab ran well, to Tan Minh Phan and Mercy Quarshie, two summer students who traced all the sensors and made schematic drawings of their location and

connection in the DAS, and to our department staffs, Olga Soares, Jacques Payer, Joe Hrib, and many others who helped this research in different ways.

I also have learned a lot from Prof. Marius Paraschivoiu and Prof. Fariborz Haghighat on investigating the physics behind a phenomenon. The inspiration coming from the discussions in their CFD and building science courses has been involved in my research thesis particularly in the numerical simulation part to establish the coupled CFD model in a single simulation environment. This research study also benefited from the discussions with my colleagues, Qian Mao, Xiangjin Yang, Caroline Hachem, and others. They provided me many useful advices on the HAM transport studies.

I also would like to acknowledge the support of my family. I am grateful for my wife Hang Hang who accepts my desire to study and engage in research as part of our family life, and thanks to my daughter Jessie who brings joy in every day of my life.

Finally, I would like to thank those who supported this research: NSERC through the SRO and discovery grants made to my supervisor and the University for providing the financial means and laboratory facilities.

Table of Contents

List of Figures

List of Tables

NOMENCLATURE

Symbol	Explanation	Units
A	Area	m^2
b	Thermal effusivity	$J/(m^2 K \cdot s^{1/2})$
b_m	Moisture effusivity	$kg/(m^2 Pa \cdot s^{1/2})$
Bi	Biot number	-
$Bi_{moisture}$	Moisture Biot number	-
c	Moisture concentration	kg/m^3
C	Coefficient	-
C_g	Water generation amount	g
C_p	Specific heat capacity	$J/(kg \cdot K)$
d_t	Thermal penetration depth	mm
d_m	Moisture penetration depth	mm
D_{AB}	Molecular diffusion coefficient	m^2/s
D_s	Molecular self-diffusion coefficient	m^2/s
D_w	Moisture diffusivity	m^2/s
Ec	Eckert number	-
f_B	Body force	N/m^3
g	Water vapor flux	$kg/(m^2 \cdot s)$
G	Moisture uptake/release amount	g
Gr	Grashof number	-
h_m	Mass transfer coefficient	m/s
h_c	Heat transfer coefficient	$W/(m^2 \cdot K)$
K	Thermal conductivity	$W/(m \cdot K)$

L	Length scale	m
Le	Lewis number	-
$\dot{m}_p$	Indoor vapor production	kg/s
$\dot{m}_{sys}$	Vapor added/removed by HVAC-system	kg/s
M_h	Moisture buffering amount	g
n	Exponent	-
Nu	Nusselt number	-
P	Vapor pressure	Pa
P_{ref}	Reference water vapor pressure	Pa
P_{sat}	Saturation vapor pressure	Pa
Pr	Prandtl Number	-
Q	Volume flow rate	m^3/s
Q_{vt}	Ventilation rate	kg/s
q	Heat flux	W/m^2
Re	Reynolds number	-
R_v	Gas constant for water vapor=461.5	J/(kg·K)
Sc	Schmidt number	-
T	Temperature	K
t_p	Time period	s
U	Flow stream velocity	m/s
V	Room volume	m^3
$\dot{V}_a$	Volume flow rate of outside air	m^3/s
w	Humidity Ratio	$kg_{water\ vapor}/kg_{dry\ air}$
w_{eq}	Equilibrium water content	kg/kg

w_i	Mass fraction of species i	kg/kg
x	Distance	m
$Z_{p,s}$	Surface resistance	$Pa \cdot m^2 \cdot s/kg$

Greek alphabet symbols

Γ	Transfer coefficient corresponding to the driving potential	
Ψ	Driving potential of moisture transport	
Θ	Dimensionless temperature	-
α	Thermal diffusivity	m^2/s
α_c	Convective surface heat transfer coefficient	$w/m^2 \cdot K$
$\overline{\beta}$	Average surface water vapor transfer coefficient	$kg/(Pa \cdot m^2 \cdot s)$
β_{loc}	Local surface water vapor transfer coefficient	$kg/(Pa \cdot m^2 \cdot s)$
β_p	Convective moisture transfer coefficient	$kg/(Pa \cdot m^2 \cdot s)$
δ	Water vapor permeability	kg/(m·s·Pa)
δ^+	Dimensionless wall offset	-
ε	Wall roughness	-
μ	Fluid viscosity	kg/(m·s)
ν	Fluid kinematic viscosity	m^2/s
ρ	Density	kg/m^3
$\underline{\underline{\sigma}}$	Stress tensor	N/m^2
ξ	Moisture capacity	kg/kg
τ	Shear stress	Pa
φ	Relative humidity	-

ϖ	Angular frequency	s^{-1}

Abbreviations

ACH	Air Changes per Hour
AHU	Air Handling Unit
CFD	Computational Fluid Dynamics
CRD	Conceptualized Reference Database
DAS	Data Acquisition System
DEI	Drying by Evaporation Index
EDRH	Effective Dampened Relative Humidity
EPD	Effective Penetration Depth
FSP	Fiber Saturation Point
HAM	Heat, Air and Moisture
HAMSTAD	Heat Air and Moisture Standard Development
HVAC	Heating, Ventilation and Air Conditioning
HIR	Room Hygric Inertia
IEA	International Energy Agency
IRH	Increased Relative Humidity
LFE	Laminar Flow Element
MBC	Moisture Buffering Capacity
MBV	Moisture Buffer Value
MEWS	Management for Exterior Wall Systems
MGR	Moisture Generation Rate
PDE	Partial Differential Equations
PID	Proportional Integral and Differential

RPM	Rotate Per Minutes
RH	Relative Humidity
RH&T	Relative Humidity and Temperature
TMT	Transient Moisture Transfer

CHAPTER 1
INTRODUCTION

1.1 Background

Moisture level inside buildings is a key factor influencing the durability of construction, indoor air quality, living comfort, and energy consumption. Studies have shown that when relative humidity at a surface reaches 70 percent or higher, the problems with mold, corrosion, decay and other moisture related deterioration occur (Lstiburek, 2002). Water and moisture can cause structural damage, reduce the thermal resistance of building materials, change the physical properties of materials, and deform materials (Kalamees, 2006). On the other hand, low humidity levels can cause static electricity, dry skin and hair, and itching and chapping, increasing human discomfort and susceptibility to cold and respiratory illness. Keeping an appropriate room humidity level is important in maintaining a healthy indoor environment for both human comfort and building durability.

The indoor humidity level is the result of the dynamic moisture balance among the moisture gain, moisture loss, and moisture storage inside buildings. There are many large and comprehensive projects at the national and international levels studying the

moisture transport and balance of moisture, both experimentally and numerically. Some of them, related to this thesis research, are briefly introduced.

Moisture Management for Exterior Wall Systems (MEWS) was a four-year project that brought together researchers from IRC's Building Envelope and Structural Program and 11 industry partners. The MEWS methodology offered a way for stakeholders in the building envelope industry to evaluate the ability of building components and systems to manage moisture in any geographic location in North America. The research approach was three-fold: field characterization of wall assemblies, laboratory experimentation on materials and components, and mathematical modeling for prediction of long-term performance under many sets of conditions (Kumaran et al., 2003). The hygrothermal properties of several building materials commonly used in North American were obtained by the project lab tests.

In the 1990s, moisture damages to building envelope occurred in several dramatic envelope failure cases in the North America, such as the leaky Vancouver condos, North Carolina EIFS housing units, and Seattle leaky homes. In order to provide proper design guidelines to avoid these problems, the Collaborative Research and Development (CRD) project on the experimental evaluation of hygrothermal performance of building envelope systems was carried out at Concordia between 2003 and 2008 (Fazio et al., 2007; Alturkistani et al., 2008; Li et al., 2008). This research provided a uniform, measurable and sustaining moisture source in the test, and its mapping methodology

established the DEI (Drying by Evaporation Index) by identifying the correlation between the evaporation rate and the amount of moisture leaving the cavity (Alturkistani et al., 2008). An advanced simulation tool, HAM-BE, was developed to investigate the hygrothermal performance of building envelopes tested in this experiment (Li et al., 2008). This project established a new testing method for evaluating and ranking the performance of different envelope systems (Fazio et al., 2009).

In 2001, the European Commission initiated the project “HAMSTAD” (Heat Air and Moisture Standard Development) to focus on the development of draft standardization procedures on determination methods of moisture transfer properties and a draft methodology for certification of advanced moisture modeling codes (Adan et al., 2004). HAMSTAD included some of the comprehensive projects for developing numerical simulation of heat, air and moisture (HAM) transport in building envelopes. The simulation tools such as DELPHIN, HAM-tools, and TRNSYS ITT were developed. Some of the partners who carried out this project later participated in the Annex 41 tasks of modeling and common exercises.

As moisture studies moved from components to whole building consideration, a better knowledge of the whole building HAM balance and its effects on the indoor environment, energy consumption for heating and cooling, air (de)humidification and construction durability was needed. This search for a better understanding of the HAM balance was the driving force behind the Annex 41 program of the International Energy

Agency (IEA) from 2004 to 2008. Annex 41 had two main objectives: 1) to carry out a detailed exploration of the complex physics involved in whole building HAM response; 2) to perform analysis of the effects of the whole building HAM response on the comfort, enclosure durability and energy consumption (Roels, 2008). In the research program of Annex 41, whole building HAM research methodologies in the modeling principles, experimental investigations, long term performance and technology transfer were proposed and developed.

1.2 Influence of hygroscopic materials on Indoor environment

The indoor environment is influenced by several factors, such as moisture and heat source, ventilation conditions, and the existence of hygrothermal materials. In Annex 41, one important concept about the influence of the materials is the moisture buffering effect. The moisture buffer effect of a room is the capacity of the materials within the room to moderate variations in the relative humidity (Rode et al., 2005). On one hand, moisture buffering provides a passive way to dampen the fluctuations of indoor humidity and temperature, which may be utilized as a way of adjusting indoor condition and saving energy; on the other hand, the buffering phenomenon is a dynamic process of moisture absorbed/desorbed by the envelope materials between indoor and outdoor environment. This transport process involves complex heat, air and moisture responses. The study of moisture buffering helps to understand the complex mechanisms involved in the durability for the building envelope and to provide solutions to envelope failures.

Svennberg et al. (2007) stated that the interest in moisture buffering was not a new issue and they presented a review of such early studies on indoor surface materials from Germany and Sweden. However, it was Annex 41 that first systemically summarized and studied this phenomenon. Rode et al. (2005) described moisture buffering effects at the material level, system level, and room level. The material level was the traditional moisture properties, i.e. the slope of the sorption isotherm. The system level buffering was about the "moisture buffering capacity". The practical Moisture Buffer Value (MBV) was proposed to determine the buffering capacity of the material. This value was mainly, but not only a property of the material because mass transfer coefficient at the boundary had to be considered. The MBV of several materials samples were measured by Round Robin tests conducted by four universities and research institutes that participated in Annex 41. Agreements in MBVs of some materials were obtained. The room level included the buffering effects caused by the building and furnishing materials exposed to the indoor air and the room factors such as moisture load, ventilation rate and indoor climate. Saito (2005a, b), Ojanen and Salonvaara (2004), and Svennberg et al. (2004) studied room level buffering effects in field tests, in large scale climate chamber lab tests, and in fully furnished room tests respectively where different ventilation rates and envelope materials were employed. Fazio et al. (2007) performed full-scale tests to evaluate the impact of five parameters on moisture buffering effect, including moisture load, distribution of indoor environment, condition of moisture generation rate, and hygric properties of surface materials.

A number of whole-building HAM tools were evaluated and benchmarked during Annex 41. BSim, Clim2000, DELPHIN4, Energy Plus, ESP-r, HAMLab, TRANSYS, and WUFI Plus were well known software for the analysis of indoor climate, energy consumption, humidity balance, and/or moisture airborne transport, condensation, and evaporation. Even though some of these existing tools included vapor advection in the air, they did not take into account the vapor mass transfer at the interface between air and building envelope (Woloszyn & Rode 2008b). To obtain detailed information of air flows in buildings and hygrothermal transport through building components, CFD has been combined with the HAM response simulation. Erriguible et al. (2006) modeled 2D convective drying of a porous material with the air flow at the material boundary calculated by a CFD model. Neale (2007) developed a coupled numerical model using CFD simulation in Fluent to determine the heat and moisture transfer coefficients between air and porous material for the HAM simulation in MATLAB. Steeman et al. (2009a) coupled CFD and effective penetration depth (EPD) model to investigate the effect of the assumption of the well-mixed air on the prediction of the indoor temperature and relative humidity and on the hygrothermal behavior of the walls.

1.3 Motivation, objective and approach

The indoor environment study is the fundamental of “whole building” research for the purpose of establishing sustainable buildings and communities. The increasing climate change concern requires building scientists and engineers to find ways to reduce energy consumption and green house gas emissions associated with the use of active HVAC

systems while keeping appropriate indoor conditions. The moisture buffering effects of interior finishing materials of building envelopes have been recognized as a passive way to assist in moderating indoor conditions. In many residential buildings, where only the natural ventilation is available, moisture buffering is an important factor in affecting indoor environment change. In order to predict and utilize the moisture buffering effect, buffering performance of the hygrothermal materials within buildings at the room level must be known. The material's buffering properties at material level have been intensively measured and calculated in experimental studies. However, there is not enough information and testing standard for evaluating material buffering performance at room level. Meanwhile, the material buffering properties may not be directly representative of the material buffering performance at room level because the moisture buffering effects are influenced by room factors such as ventilation conditions, indoor humidity and temperature profiles, and indoor environment initial conditions. To establish reliably the link between the characterization and quantification of the moisture buffering of the interior finishing and furnishing, the moisture buffering performance of these materials at room level needs to be measured experimentally. The relationship between the buffering effects caused by the hygroscopic materials and their hygroscopic performances needs to be found.

In the aspect of simulation, numerical studies have advanced the state of the art in whole building heat, air and moisture response studies. CFD has the advantage to investigate the indoor air movements, the local information of the temperature and

moisture distribution. But currently, the HAM simulation of CFD taking into account the moisture interaction between indoor air and envelope is achieved through the third party programming. This may limit the application of CFD modeling due to the assumptions by the programming party and its limited extendibility to fit new simulation conditions. To simulate the indoor environment change under given moisture loads and to explain how the air movement caused by buoyancy forces and ventilations influences indoor temperatures and humidity levels, the CFD modeling to couple the momentum, heat, and moisture in whole building domain including indoor air and wall systems are highly desirable.

The aim of this thesis research is to develop a methodology and carry out a full scale experiment to measure the buffering response of wood material in various room conditions, and to develop a coupled CFD model taking into account the heat and moisture transfer through the wall system to simulate the indoor environment changes under different moisture loads and ventilation conditions. The objectives include:

- To obtain an understanding of the nature of moisture buffering at the room level. With the better understanding comes the opportunity of a better prediction on how moisture buffering affects the indoor condition, and how to maximally use these effects in certain design consideration.
- To develop an experimental method to calculate the interior wall surface moisture buffering effect by measuring the RH&T distribution difference between non-hygroscopic and hygroscopic tests.

- To investigate moisture responses of wood paneling at room level and study the performance influenced by the room factors including ventilation conditions, moisture loads, and indoor environments.
- To analyze the relationship of the moisture buffering effect to the test room caused by wood paneling and its hygroscopic performances at room level.
- To develop a numerical model coupling the momentum, heat, and mass transfer inside room and through envelope in a single simulation environment.
- To study the indoor environment influenced by different ventilation strategies and to investigate the potential damage caused by high humidity levels by using the coupling model.
- To find out the main factors dominating the heat and moisture fluxes in the wall system under mixed convection condition of the indoor environment through the numerical investigation.

A combination of experimental measurements, calculations and numerical simulations are utilized as an approach to accomplish the above goals set for this thesis research.

The experimental investigation on the buffering effects of wood paneling at room level was carried out inside the Environmental Chamber at Concordia University by taking advantage of the existing test hut, data acquisition system, installed sensors, and sensor calibrations for the test room and inside walls. These test facilities had been previously used in the sub-project of Annex 41 conducted by PhD students Sergio Vera and Xiangjin

Yang under the supervision of Prof. Fazio and were supported by a number of technicians, outside construction workers, co-op students, and Dr. Jiwu Rao. In that sub-project, the moisture transport in the two-story test hut and the indoor conditions influenced by different hygrothermal materials and furniture were investigated. To study the moisture buffering performance of wood paneling at room level , the wood paneling installed at the interior of the first floor room of this two-story test hut as well as the sensors embedded inside the wall system were adopted in this thesis experimental tests. The wood paneling was subjected to controlled moisture loads applied in different amounts and schedules, with varied forced convection, ventilated and non-ventilated indoor condition, and with cold outside environment. The temperature and relative humidity changed in the test room, at the inlet and outlet of the ventilation system, and inside the wall cavity were monitored for all test scenarios. A formulation was developed to calculate the amount of moisture change in the wood paneling.

To study the influence of moisture loads and different ventilation strategies on indoor environment with the heat and moisture interaction between indoor air and wood paneling taken into account, the mathematical coupling between the indoor conditions obtained by CFD calculations and heat/mass diffusion inside porous walls described by diffusion equations need to be implemented. In this thesis, the conservation equations of momentum, heat, and mass were described in a single simulation environment--COMSOL. The coupling process among these equations and between the sub-domain of

the indoor air and the walls were developed by establishing the relationship of the variables in each governing equation and inside each sub-domain. The solver parameters related to solve these coupled equations were chosen according to the numerical algorithm. The results of the simulation were validated by comparing the experimental results. Then, the validated model was utilized to investigate the room factors which were not tested in the experiment, such as the locations of the ventilation vents, and to study the phenomena that could not be studied in the experiment, such as the heat and moisture fluxes, and the potential damage on wall surface caused by mold. In this thesis, only steady state analysis in the numerical investigation was performed.

1.4 Outline

The thesis consists of 8 chapters. The introductions of the background, motivation and objectives have been presented in this chapter. In Chapter 2, the critical points of current studies on moisture buffering and "whole building" HAM responses including substantive findings, theoretical and methodological contributions, experimental and numerical results are reviewed. Chapter 3 describes the fundamental theories utilized in this thesis study. These theories include the terminologies related to the description and calculation of hygroscopic material properties, the mathematical description of convective heat and moisture transfers, and the deduction of the formulation applied in this thesis experimental study. Chapter 4 introduces the experimental protocol. The experimental setup including construction of the test room, sensors location, and data acquisition system; the quantity of the room factors tested in the experiment, such as

the moisture loads, ventilation conditions; and the experimental procedure are presented in this chapter. The experimental results are analyzed in Chapter 5. The moisture buffering performance of wood paneling under different test conditions, the influence of wood paneling on the indoor environment affected by room factors, and the relationship of the moisture response of the wood paneling, its buffering effect to the test room and the room factors are elaborated. Chapter 6 presents the numerical modeling. The coupling process including the coupling between the momentum, heat and mass equations in whole simulation domain, the coupling of heat and mass between indoor air and wall system is described. The numerical model is validated by comparing its results with the experimental results. In Chapter 7, the numerical investigations of the influence of room factors on indoor humidity levels at steady state, of the impact of the ventilation vents position changes on indoor environment, of the dominating factors to the heat and mass transport through the wall systems, and of the potential local damage caused by extreme temperature and humidity conditions are performed. Chapter 8 summarizes the major findings, contributions, and future work.

CHAPTER 2
LITERATURE REVIEW

This chapter presents a literature review of current studies on the moisture buffering phenomenon and HAM transport in buildings. The existing efforts in defining and describing the buffering effects are reviewed in the first section. The overall review about impacts of moisture buffering on the indoor environment, energy consumption as well as its calculation by numerical simulation in whole building is followed. Finally, a summary of the literature review is presented in the last section.

2.1 Defining and Measuring Moisture Buffering

2.1.1 Moisture Buffering Value (MBV)

The hygroscopic materials used in building structures have the ability to reduce the extreme values of humidity levels in indoor environments when the rooms are subjected to moisture load changes. This phenomenon is investigated in some earlier studies (Rode et al., 2001, 2003; Salonvaara, 1998; Padfield, 1999; Simonson et al., 2001a, 2001b; Karagiozis et al., 1999; Mitamura et al., 2001) and has been recognized as moisture buffering effects.

The traditional material properties such as moisture capacity, vapor permeability, density, and moisture sorption isotherm (to be presented in Chapter 3), which are found in the steady state situation, can be used to describe this phenomenon. In the NORDTEST project (Rode et al. 2005), the concept called moisture buffering value (MBV) and its theory were developed. Based on the heat-moisture transfer analogy, the moisture flux, *g(t)* , on the surface of a hygroscopic material under the rectangular signal loads (e.g. 8 hour of high moisture load followed by 16 hour of low load without load in a one-day cycle) can be calculated by the Fourier transformation method. The accumulated moisture uptake and moisture release, *G(t)*, is expressed as:

$$G(t) = \int_0^t g(t)dt = b_m \cdot \Delta p \cdot h(\alpha)\sqrt{\frac{t_p}{\pi}} \qquad (2.1)$$

where

b_m is the moisture effusivity, $J/m^2 \cdot K \cdot s^{1/2}$

Δp is the vapor pressure difference, Pa

t_p is the time period, s

$$h(\alpha) = \frac{2}{\pi}\sum_{n=1}^{\infty}\frac{\sin^2(n\pi\alpha)}{n^{3/2}} \approx 2.252[\alpha(1-\alpha)]^{0.535} \qquad (2.2)$$

For the 8/16 hr scheme, α=1/3, h(α)=1.007, and the accumulated moisture uptake is reduced to

$$G(t) \approx 0.568 \cdot b_m \cdot \Delta p\sqrt{t_p} \qquad (2.3)$$

The theoretical Moisture Buffer Value (MBV), also called ideal MBV in the project, is defined as the moisture exchange *G*(t) normalized with the change in the surface relative humidity, ΔRH, i.e.

$$MBV_{ideal} \approx \frac{G(t)}{\Delta RH} = 0.00568 \cdot p_s \cdot b_m \cdot \sqrt{t_p} \qquad (2.4)$$

To measure the MBV of hygroscopic materials, the concept of the practical MBV as well as the experimental measurement condition and set up is proposed in the project and later is standardized as (Rode and Grau, 2008):

> "The standardized Moisture Buffer Value (MBV) indicates the amount of water that is transported in or out of a material per open surface area, during a prescribed period of time, when it is subjected to specific variations in relative humidity of the surrounding air with a specified velocity. When the moisture exchange during the period is reported per open surface area and per % RH variation, the result is the MBV. Standardized exposure is 8 h of 75% RH, and 16 h of 33% RH. The unit for MBV is $kg/(m^2 \cdot \%RH)$."

The ideal MBV is derived from material hygroscopic properties and belongs to the material level definition as stated in Section 1.2, while the practical MBV measured from experiments includes the effect of the vapor resistance of the surface air film and is a

system level definition. The surface resistance is assumed as zero in the ideal MBV calculation formula. With this assumption, the calculated ideal MBVs of some materials are about three times higher than the measured values presented in the NORDTEST project report. (Abadie and Mendonca, 2009).

2.1.2 Sorption Kinetic Curves

Using sorption kinetic curves of hygroscopic materials to predict moisture buffering capacities has been suggested and studied. The first-order, pseudo-second-order and general forms of kinetics models for the adsorption process were proposed by Lagergren (1898), Ho and McKay (1999) and Delgado et al. (2005), respectively, as:

$$\frac{dw}{dt} = k_1(w_{eq} - w) \tag{2.5}$$

$$\frac{dw}{dt} = k_2(w_{eq} - w)^2 \tag{2.6}$$

$$\frac{dw}{dt} = k_n(w_{eq} - w)^n \text{ for } n > 1 \tag{2.7}$$

where w_{eq} is the equilibrium sorption capacity, k terms are the kinetic parameters.

The solutions to (2.5)—(2.7) are:

$$\log(w_{eq} - w) = \log(w_{eq}) - \frac{k_1 t}{2.303} \tag{2.8}$$

$$\frac{1}{w_{eq} - w} = \frac{1}{w_{eq}} + k_2 t \tag{2.9}$$

$$\frac{1}{(n-1)(w_{eq}-w)^{n-1}} = \frac{1}{(n-1)w_{eq}^{n-1}} + k_n t \text{ for } n > 1 \quad (2.10)$$

An experimental method to determine the equilibrium water content (i.e. w_{eq}) based on the sorption kinetic curves was developed by Jantti et al. (1970) with the adsorption equation and calculation as:

$$w(t) = w_{eq} \frac{t/\tau}{1 + t/\tau} \quad (2.11)$$

$$w_{eq}(t_2) = \frac{w(t_1)w(t_2) + w(t_2)w(t_3) - 2w(t_1)w(t_3)}{2w(t_2) - w(t_1) - w(t_3)} \quad (2.12)$$

where $w(t_1)$, $w(t_2)$ and $w(t_3)$ are the moisture content measurements at three different times and $\Delta t = t_2 - t_1 = t_3 - t_2$. This provided a quick way to determine the equilibrium moisture content.

Six hygroscopic material samples were tested by Delgado et al. (2005) under several cycles of square waves of RH loads at a constant temperature similar to the test conditions performed in the NORDTEST project. The moisture buffering value based on these test conditions were obtained, and the equilibrium moisture content, kinetic parameters of the sorption curves, as well as other pertinent parameters such as initial sorption rate and the time to reach 50% equilibrium water content were measured and calculated.

The major findings and conclusions of Delgado et al. (2005) included:

1. The sorption of water vapor by these building materials proceeded in accordance with the pseudo-second-order model, except for cement plaster. The experimental values do not deviate from the lines by more than 12% and the correlation coefficients are about 0.99. The values of w_{eq} and k_2 obtained in the initial and stable cycles are very similar.

2. The advantage of using the kinetics models for adsorption/desorption processes is the possibility that the end of a sorption process, w_{eq}, may be predicted, using only a few hours experiment, with a good agreement of the results.

3. The MBV retrieved from these experiments can be an easy way of comparing different building materials or building elements in terms of their moisture buffer capacity. The MBV corresponding to an amount of moisture adsorbed in a predefined cycle can be predicted from the knowledge of w_{eq} and kinetics coefficients. The sorption kinetics analyzed can provide a better insight on moisture buffer performance.

2.1.3 Moisture transfer coefficient

A key factor in evaluating the moisture buffering capacity of a hygroscopic material is the amount of water it can absorb and release in the different load conditions. This amount of water is significantly affected by the surface transfer coefficient. The theory of mass transfer coefficient is analogized to heat transfer as:

$$h_m = \frac{h_c}{\rho c_p Le^{2/3}} \tag{2.13}$$

where h_m is the convective mass transfer coefficient (m/s), h_c is the convective heat transfer coefficient ($w/m^2 \cdot K$), c_p is the specific heat ($J/kg \cdot K$), Le is the Lewis number. This equation, relating convective heat and mass transfer, is the well-known *Chilton-Colburn analogy*. The analogy itself has been the subject of many research projects that proved or disproved the accuracy of the results for a variety of conditions (Neale 2007).

Rode et al. (2005) summarized the convective moisture transfer coefficient, $\beta_p (kg/p_a \cdot m^2 \cdot s)$, and the surface resistance, $Z_{p,s} (p_a \cdot m^2 \cdot s/kg)$, by using the Lewis relation and choosing exponent ¾ recommended for interior surfaces in buildings as:

$$Z_{p,s} = \frac{1}{\beta_p} = \frac{\rho \cdot c_p \cdot R_v \cdot T}{\alpha_c} \cdot Le^{3/4} \tag{2.14}$$

where:

ρ air density (1.205 kg/m^3 at 20 °C)

c_p heat capacity of air at constant pressure (1005 $J/kg \cdot K$)

R_v gas constant for water vapor (461.5 $J/kg \cdot K$)

T temperature (K)

α_c convective surface heat transfer coefficient ($w/m^2 \cdot K$)

Le Lewis number

$$Le = \frac{a}{D} = \frac{2.1 \times 10^{-5} m^2/s}{2.5 \times 10^{-5} m^2/s} = 0.84 \text{ (At 20 °C)}$$

The general moisture transfer resistance in a building can be assumed to be 5×10^7 $m^2\cdot s\cdot p_a/kg$.

The determination of moisture transfer coefficients in the current research on moisture buffering was mostly based on the above analogy. Osanyintola et al. (2005) used the Transient Moisture Transfer (TMT) facility (Fig. 2.1) to measure the moisture buffering performance of spruce plywood under three different Reynolds numbers, Re =1000, 2000, and 4000, which corresponds to convective heat transfer coefficients (h_c) of 2.5, 3.5, and 8.1 $w/m^2\cdot K$ respectively and convective mass transfer coefficients (h_m) of 0.0021, 0.0029, 0.0067 m/s respectively. The Moisture Buffering Capacity (MBC) defined as the average amount of the sum water absorbed and released in a steady state cycle in this research were 22.5, 24.9, and 26.2 g/m^2 corresponding to these three Re conditions.

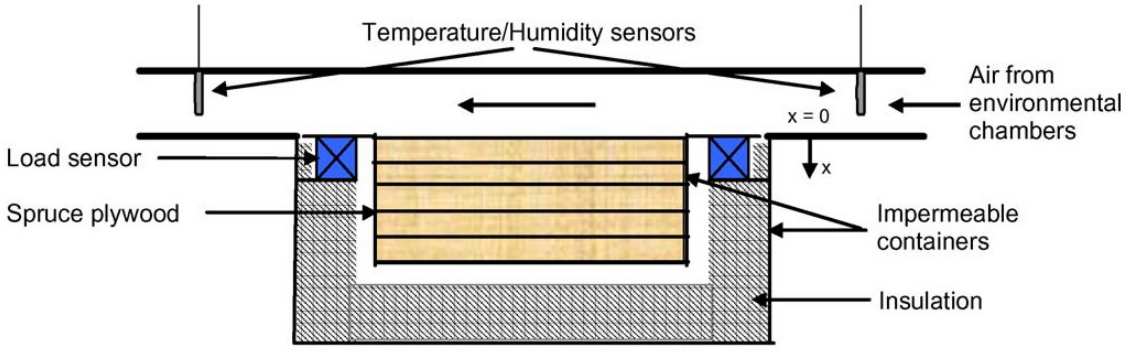

Fig. 2.1 Schematic of the TMT facility (From Osanyintola et al., 2005)

Roles and Simonson (2006) performed a numerical simulation to study the influence of the surface film resistance on MBVs of four hygrothermal materials. The simulation

results were presented as Table 2.1. Different materials had different MBV changes for a changed surface resistance, and a sudden drop of MBV was observed for wood fibre board when increasing the surface film resistance from 1×10^{8} to $3.3\times10^{8} m^{2}\cdot s\cdot p_{a}/kg$.

Table2.1 ***Influence of the surface film resistance on the obtained MBV (in g/m^2.%RH) for the four materials investigated.***

Surface resistance $\times$ 10^7 (m^2sPa/kg)	WFB	PW	ACC	GP
33	0.55	0.47	0.56	0.61
10	1.55	0.64	0.75	0.86
5	1.86	0.69	0.82	0.94
3.3	1.99	0.71	0.83	0.97
1	2.20	0.74	0.86	1.01
Negligible (0.0033)	2.31	0.76	0.89	1.03

Note: This table is adopted from Roles and Simonson (2006). WFB stands for the wood fiber board, PW for plywood, ACC for aerated cellular concrete, and GP for gypsum plaster

A study of local surface water vapor transfer coefficient in a ventilated test room based on a coupled CFD-EPD model was performed by Steeman et al. (2009). Since the commercially available CFD packages do not allow for the simulation of the coupled heat and moisture transport in hygroscopic materials, the effective penetration depth (EPD) model to simulate the hygrothermal behavior of the walls was combined into the CFD package. To couple the CFD and EPD models, the water vapor mass fraction at the surface of the wall for a given time step was obtained from the previous step results of the EPD model, then the water vapor flux from the air to the wall at this time step was calculated by the CFD model and input into EPD to generate next step's mass fraction value on the wall surface. The coupled CFD-EPD model was first validated by a non-hygroscopic wall configuration test with 8 hours of moisture jet coming from the inlet

and then applied to this test again without changing any conditions except including the wall hygroscopic interaction.

The local surface water vapor transfer coefficient β_{loc} and the average surface water vapor transfer coefficient $\overline{\beta}$ in Steeman et al. (2009) were defined as:

$$\beta_{loc} = \frac{g}{p_{sur} - p_{ref}} \tag{2.15}$$

$$\overline{\beta} = \frac{\overline{g}}{\overline{p_{sur}} - \overline{p_i}} = \frac{(1/A)\int g dA}{(1/A)\int p_{sur} dA - \overline{p_i}} \tag{2.16}$$

where g is the water vapor flux. The term p_{ref} is the reference water vapor pressure (also called free stream water vapor pressure); it is the volume average indoor water vapor pressure $\overline{p_i}$ as:

$$p_{ref} = \overline{p_i} = \frac{\int p_i dV}{V} \tag{2.17}$$

The simulation results of Steeman et al. (2009) showed that the local surface water vapor transfer coefficient was not constant over the surface area and varied between 0.8×10^{-8} s/m and 3×10^{-8} s/m in the first hour of the moisture generation and decreased to 1.8×10^{-8} s/m after 8 hours. But the average surface water vapor transfer coefficient remains constant during the whole period of testing.

2.1.4 Other moisture buffering measurements

Another notable standard for characterizing building materials with respect to moisture buffering is the "test method of ad/desorption performance of building materials to regulate indoor humidity", the Japanese industrial standard JIS A 1470-1 (JIS 2002). With the similar objectives and measurement principles as the NORDTEST protocol, this test standard used a square wave signal with 24 hours high RH followed 24 hours low RH. Three humidity levels, 33% to 53%, 53% to 75%, and 75% to 93% were chosen as the load signals. The specimen thickness was equal to the product thickness. The surface film resistance was set to $4.8\times10^{7}\pm10\%\ \ m^{2}\cdot s\cdot p_{a}/kg$. The test results were reported as moisture masses absorbed and released by the test materials as well as the moisture content profiles with respect to time.

Yang W.; Fazio, P.; Kumaran, M.K. (2008) measured the moisture buffering capacities of five building materials commonly used in North America: gypsum, plywood, OSB, fiberboard, and stucco. The test conditions were same as the NORDTEST condition, 8 hours 75% RH followed 16 hours 33% RH with a constant temperature of 23 °C. The MBV values were calculated, the absorption and desorption curves were plotted and fitted into Eqs. (2.18) & (2.19) for gypsum, and Eqs. (2.20) & (2.19) for the other materials.

$$\Delta m_{ab} = a + be^{-t} \tag{2.18}$$

$$\Delta m_{de} = a + b\exp(-t/c) \tag{2.19}$$

$$\Delta m_{ab} = a + bx^{c} \quad (2.20)$$

where a, b, and c were fitting coefficients.

Highly absorbing materials, such as sodium polyacrylate and cellulose-based material, are super absorbent polymers and combination of cellulose and super adsorbent polymers respectively, and are used in several industrial sectors ranging from personal hygiene to medical field. The moisture buffering capacities of these materials were investigated by Cerolini et al. (2008). In their test, the materials were wound in a nonwoven fabric and then placed in a non absorbing plastic container to facilitate the weighing procedure. The container was covered with a perforated sheet metal to simulate the presence of a surface closure and sealed with aluminum adhesive tape as shown in Fig. 2.2. The same moisture load scheme as NORDTEST project was applied.

Comparing the moisture buffering results of gypsum to perlite material, this study found that the super absorbent polymer reacted more quickly than the other materials to RH changes in both the adsorption and desorption phases. However polyacrylate showed a hysteretic behavior that may cause the loss of its sorption properties. Therefore the cellulose-based material seemed to be the most suitable for moisture buffer applications.

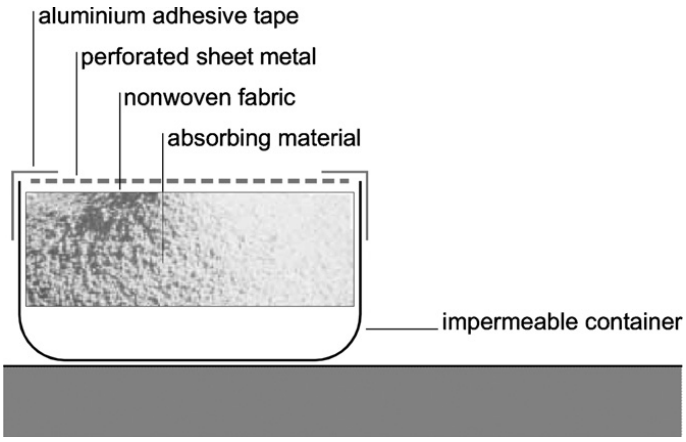

Fig. 2.2 Test setup of closing and sealing systems used for the loose materials (from Cerolini et al., 2008)

Svennberg (2006) studied the moisture buffering of furniture in the indoor environment. In one project, two bed systems, one of a homogenous mattress and the other of a multilayer type, were tested in a Sweden house subjected a diurnal temperature and RH variations. The systems were mathematically analyzed and the noticeable differences of microclimatic conditions in the two systems had been observed. The moisture uptake in a chair seat as a response to daily RH variations was studied in another project. The comparison between chair measurements and analytical solution showed that the latter provided a good representation of the moisture uptake. An addition of internal resistance in the analytical solution and using truer boundary conditions would further improve the agreement.

There were also some large scale experimental studies on the moisture buffering. However, these studies were mostly focusing on the moisture buffering impact on indoor room conditions instead of on the moisture buffering measurement. This subject

as well as the influence of moisture buffering on energy consumption are reviewed in the next section.

2.2 Moisture buffering studies in whole buildings

The moisture buffering phenomenon, as stated in Chapter 1 and reviewed in the previous section, is a dynamic process that the hygroscopic materials inside building dampen the variation of the indoor air humidity levels. One goal of studying the moisture buffering is to predict the buffering effects of the hygroscopic materials and utilize it to control indoor environment and to achieve energy saving. In this section, the existing studies on the impact of moisture buffering on indoor environments and energy consumption are reviewed, and the currently numerical simulations for the whole building moisture response studies are also presented.

2.2.1 Moisture buffering effect on indoor environment and its prediction

Indoor humidity is an important factor in keeping human body in a healthy condition. Toftum et al. (1998) studied the influences of the indoor humidity level on the human skin humidity and respiratory comfort. Fang et al. (1999) and Kurnitski et al. (2007) investigated the indoor air quality related to the humidity condition. Bornehag et al. (2001, 2004) found that the appropriate indoor humidity could prevent mold growth and reduce health risks due to sick building syndromes such as asthma, allergic symptoms, and airway infections.

Several large-scale, lab and field experiments on moisture buffering effects have been performed by Simonson et al. (2000), Rode et al. (2001), Svennberg et al. (2004), Mitamura et al. (2004), Ojanen and Salonvaara (2004), Satio (2005a), Holm et al. (2007) and Yang (2010). Different hygrothermal materials including plywood, coated and uncoated gypsum board, cellular concrete, unpainted wood, as well as the furnished room with desk, table, book, chair carpet were used as moisture buffering objects to dampen the indoor environment variations of temperatures and relative humidity, especially for the relative humidity change. Different moisture load schemes ranging from simple square wave at constant generation rate to complex signal of mimicking daily occupancy schedule with different moisture generation rates at different time periods had been used in these experiments. The studies found that the buffering effects of the hygroscopic materials depended on many factors, including the type and area of the buffering objects exposed to the moisture, the ventilation rate, the moisture generation rate, and the outdoor climate conditions.

A method of comparative testing, with the ceiling, floor, and walls of a testing house located in Helsinki, Finland covered by plastic sheets (Fig.2.3) in one case and the regular enclosure of the same house in another, was adopted in Simonson et al. (2004). The measured indoor humidity ratios as a function of time for the different ventilation rates with and without a plastic vapor retarder were measured. The reduction of moisture buffering effects as the ventilation rates increased was observed, as shown in Fig.2.4.

The fact that moisture buffering effects have significant impacts on the indoor environment, especially on the humidity change has been recognized and verified. To be as a passive way to save energy consumption is one of the applications of the moisture buffering. Atthajariyakul et al. (2004) proposed a systematic approach to determine the optimal indoor-air condition by simultaneously setting the time-dependent variables to appropriate reference values for real-time control implementation of the HVAC system. This HVAC control methodology used RH as one of the control parameters and the results showed that the buildings with this control strategy consumed less energy than the traditional approach while providing desired thermal comfort and air quality. Barbosa and Mendes (2008) combined heat, vapor and liquid transfer in porous elements and the HVAC systems and built an integrated model for both the HVAC system and multi-zone building hygrothermal simulation. The simulation results showed that the monthly peak load could be 13% lower when moisture was taken into account as compared with the situation disregarding the presence of moisture. Therefore, they concluded that when moisture within the construction was neglected, HVAC system might be oversized.

Fig. 2.3 Sealing the test room with polyethylene plastic (from Simonson et al., 2004)

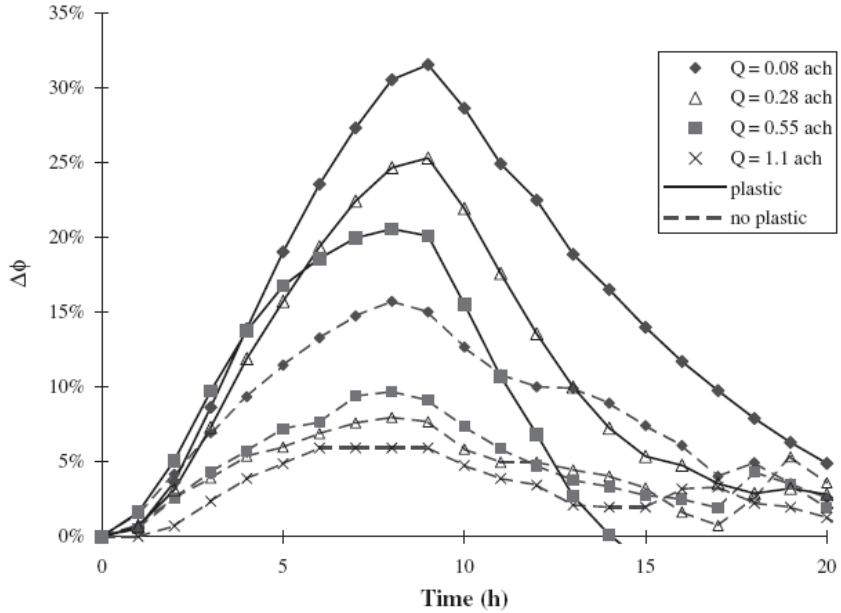

Fig. 2.4 Change in relative humidity in the test room after the humidity generator was turned on for different ventilation rates with and without plastic (from Simonson et al., 2004)

Olalekan et al. (2005) studied the effect of hygroscopic materials on energy consumptions in buildings by dividing the potential energy savings into “direct”, which means the energy required for the heating and cooling of a building, and “indirect”, which means the possible savings due to a lower ventilation rate, a higher indoor temperature in the winter and a lower one in the summer. The investigation found that the “direct saving” could be 5-30% of the cooling energy and 2-3% of the heating energy, and the “indirect saving” was in the range of 5% to 20%.

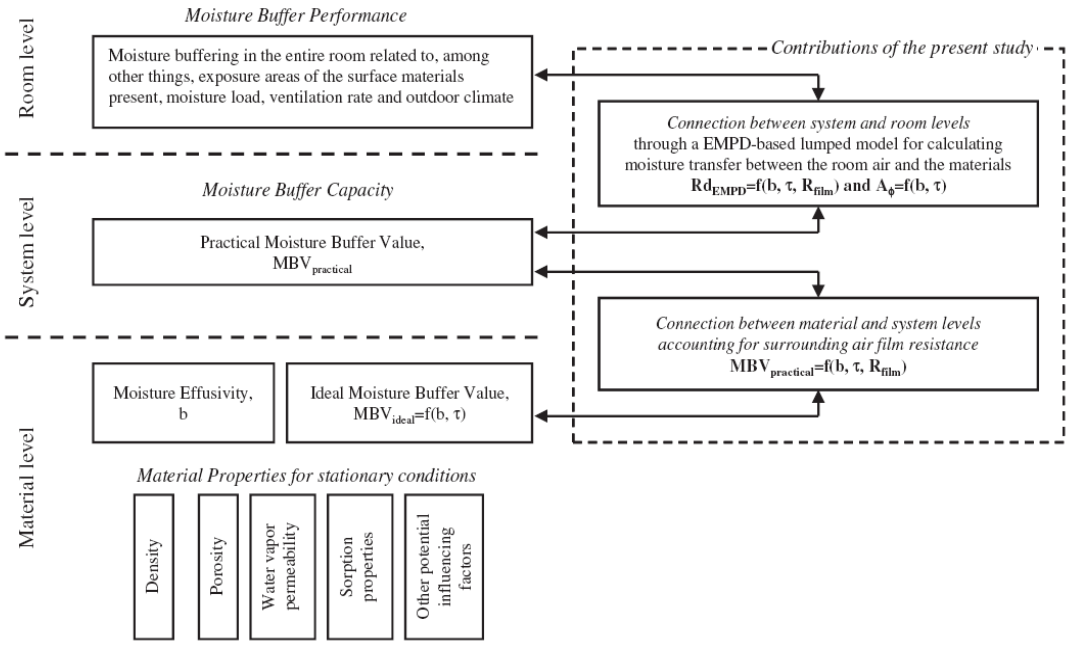

Fig. 2.5 (Left side) Descriptive levels from the NORDTEST Project of the moisture buffer effect in the built environment. (Right side) Contributions of the present work (from Abadie and Mendonça 2009)

To utilize the moisture buffering effects efficiently requires a reasonably accurate prediction of the buffering performance of the hygroscopic material in the building. The measurements of the material properties and the room factors have to be combined

together to achieve this prediction. Abadie and Mendonca (2009) summarized this combination and the contribution of their work as shown in Fig. 2.5. These studies, most of them were implemented by numerical simulation, will be reviewed in the next section. There was an effort to derive and use a single-element to characterize the moisture buffering performance of interior elements and to corroborate their superposition to the moisture buffering potential of a room-enclosure. Janssen and Roels (2008) proposed a weighting factor α for considering the room factor of moisture production interval as:

0 h < production interval $\leq$ 2h: α =0.0
2 h < production interval $\leq$ 6h: α =0.5
6 h < production interval $\leq$ 10h: α =1.0

Then the enhancement of MBP characterization of the material and buffering objects, MBV*, was defined as:

$$MBV^* = \alpha \cdot MBV_{8h} + (1-\alpha) \cdot MBV_{1h} \quad (2.21)$$

In this equation, the MBV_{8h} is the calculation according to the NORDTEST protocol and MBV_{1h} is the measurement of the accumulated moisture after just one hour at the high RH level within the 8/16 h test.

Janssen and Roels (2008) proposed a new term, the room hygric inertia, as:

$$HIR^* = \frac{(\sum A_k \cdot MBV_k^* + \sum MBV_l^*)}{V} = \alpha \cdot HIR_{8h} + (1-\alpha) \cdot HIR_{1h} \quad (2.22)$$

where k is the index for wall finishing and l is the index for buffering objects in the room, V is the volume of room, and HIR_{8h} / HIR_{1h} are the room hygric inertia with the superposition of interior finishes and objects which was proposed by Ramos and de Freitas (2006) as Eq. 2.23.

This methodology for qualitative and quantitative assessments of interior moisture buffering by introducing a moisture production factor α into the calculation provided a missing link between currently available approaches for characterization and quantification of moisture buffering in rooms.

$$I_h = \frac{\sum_i \omega_i S_i + \sum_j \Omega_j}{V} \qquad (2.23)$$

Where I_h is moisture buffering capacity (MBC) by cubic meter of room volume (kg/m^3), w_i is MBC of element i (kg/m^2), S_i is the surface of element i (m^2), Ω_j is the total MBC of element j (kg), and V is the room volume (m^3).

2.2.2 Moisture transport in whole building

A common way to evaluate the moisture amount absorbed and released by the hygroscopic enclosure is by calculating the moisture distributing in each part of building according to the transport mechanism. Example of this method can be seen from Yang, Fazio, Ge & Rao (2011) in which the moisture buffering amount was calculated by the total moisture generation in the test room subtracting the moisture taken away by ventilation, air leakage and diffusion through the wall system. With a computer

simulation approach, a complicated interacting mechanism among these building components was modeled by Zhang (2005) as Fig. 2.6.

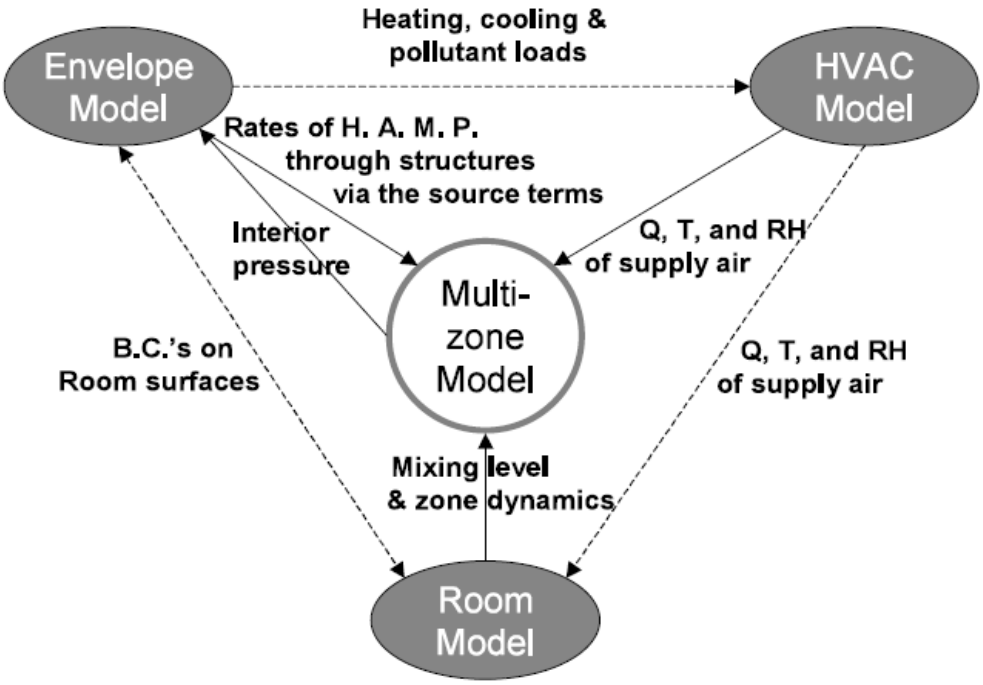

Fig. 2.6 Interaction among the component models (from Zhang, 2005)

There are many models with different degrees of complexity for predicting HAM transfers in the building envelope systems. Chen et al. (2004) established a phenomenological equation with the determination of the coefficients of heat and moisture to describe the migration process of heat and mass in unsaturated porous building materials. Qin et al. (2005) provided an analytical approach to calculate the coupled heat and moisture transfer in the porous building materials. The coupled system was solved by using the Laplace transformation and transfer function method. Janssen et al. (2006) investigated the hygrothermal responses of the building

components under atmospheric excitation. Abadie and Mendes (2005) compared the analysis of response-factor methods and finite-volume based methods for predicting heat and moisture transfer through porous building materials. The envelope model has been well developed and the transfer equations for moisture and heat in building components are currently undergoing standardization (Janssen et al., 2006). Straube and Burnett (2001) summarized 5 factors in performing the building envelope simulation including 1) Geometry of the enclosure with all macro building details; 2) Interior and exterior boundary conditions; 3) Material properties and their variation with temperature, moisture content, and age, as well as their chemical interaction with other materials; 4) Physics, chemistry, thermodynamics, and mathematics of combined heat, air, and moisture transport; and 5) Performance thresholds, i.e. the conditions under which a material or assembly will cease to perform as intended.

HVAC systems are modeled in many building simulations. The HVAC model should include the dynamic response characteristics of the HVAC components as well as other performance aspects such as pressure and flow delivery of fans, efficiency of air cleaner, and flow resistance of air damper, and energy consumption (Zhang, 2005). The HVAC models have been developed extensively (e.g. Knabe and Le 2001; Hensen, 1991; Lam et al., 1997; and Novak et al., 2004) and many available software packages (e.g. EnergyPlus, ESP-r) include HVAC systems in their building models.

The room models which focus on the resolution of the spatial distribution of temperature, humidity and air flow profiles inside a room had been built mostly by using

the computational fluid dynamics (CFD) techniques. Liu et al. (2002) studied the air flow and moisture distribution inside a ventilated test room (1.22×1.21×1.5 m3) and ventilation rate of 3.8 h^{-1} by using a standard κ-ε turbulent model, and a good agreement was obtained between the modeling simulation and experimental results. Teodosiu et al. (2003) investigated the uncertainties influenced by boundary conditions by performing a numerical simulation on a full-scale test room with mixed ventilation (Fig.2.7). The results showed that the perturbation of the air supply as the boundary conditions may have a major effect on the prediction of the cold jet separation from the ceiling.

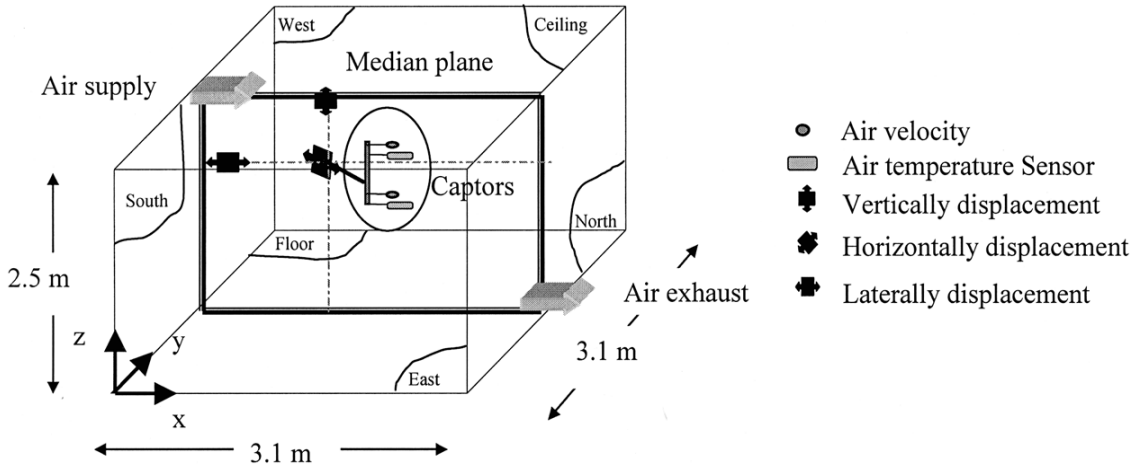

Fig. 2.7 Experimental set up (from Teodosiu et al., 2003).

The integration of all the sub-models into a whole building simulation poses a great challenge, and it was a main subtask of Annex 41. The Annex 41 report (2008) summarized current integration efforts in coupling these models into a whole building simulation tool. In order to develop numerical codes to couple the transfer of water vapor between the air and the material surface, the moisture transfer within material,

and the moisture storage within the material, simplified coupling methods were often adopted. In these models, the moisture balance for the indoor air in a room was described so-called multi-zone models with the assumption of well mixed air properties. The governing equation can be as (Woloszyn and Rode 2008a):

$$\dot{m}_p + \dot{m}_{sys} + \frac{\dot{V}_a}{R_v T_i}(p_e - p_i) = \frac{V}{R_v T_i}\frac{dp_i}{dt} + \sum_j A_j \beta_j (p_i - p_{s,j}) \quad (2.24)$$

where,

$\dot{m}_p$ indoor vapor production (kg/s)

$\dot{m}_{sys}$ vapor added/removed by HVAC-system (kg/s)

R_v gas constant for vapor (461.5 $J/kg\cdot K$)

T_i indoor air temperature (K)

p_i and p_e partial water vapor pressures of the indoor and outdoor air (Pa)

$\dot{V}_a$ volumetric flow rate of outside air (m^3/s)

V room volume (m^3)

A_j area of the interior surface of wall j (m^2)

β_j convective surface film coefficient for vapor transfer (s/m)

$p_{s,j}$ vapor pressure at the interior surface of wall j (p_a)

Woloszyn and Rode (2008b) also provided (in Annex 41) a summary of these models in simulating the whole building heat-air-moisture transfer, as seen in Table 2.2. Note that, in many cases, the moisture transfer coefficient between the air in the room and the wall was assumed or defined by the users.

Table 2.2 General features of whole building Heat, Air and Moisture models (from Woloszyn and Rode, 2008)

Name	Granularity	Envelope	Air	Furniture (impact on moisture)	HVAC systems
BSim	Multi-zone, capable of zonal model	1D Heat+Moisture, airflow through envelope under development	Interzonal flows (including cross flow through large openings), natural and mechanical ventilation	Approximated as interior building envelopes	Most of the typical systems
BUILDOPT-VIE	Multi-zone	1D Heat+Moisture	Well mixed zone, interzonal flow	No	Some of the typical systems with ideal behaviour
Clim2000	Multi-zone, capable of zonal HA model	1D Heat, vapour diffusion through envelope under development	Interzonal flows (including cross flow through large openings), natural and mechanical ventilation	Lumped model for moisture buffering (rendering+furniture)	Most of the typical systems, with detailed representation of some systems
DELPHIN	1 zone	1D/2D Heat+Air+Moisture	1 well mixed volume	No	No
EnergyPlus	Multi-zone	1D Heat	Interzonal flows (including cross flow through large openings), natural and mechanical ventilation	Approximated as interior building envelopes	Some of the typical systems, with capabilities of detailed representation of most systems & controllers
ESP-r	Multi-zone, capable of CFD	Standard 1D Heat, capable of 1D/2D/3D Heat, or 1D Heat+ Moisture	Interzonal flows (including cross flow through large openings), natural and mechanical ventilation	No	Most of the typical systems, with detailed representation of systems
NPI	1 zone	1D Heat+Moisture	1 well mixed volume	Yes	No
IDA-ICE	Multi-zone	1D Heat+Air+Moisture	Interzonal flows (including cross flow through large openings), natural and mechanical ventilation	For moisture buffering: approximated as interior building envelopes	Most of the typical systems, with detailed representation. Possibility to create own systems
HAMFitPlus	Multi-zone	1D/2D Heat+Air+Moisture	Single zone: well mixed zone. Multi-zone: coupled with COMIS	Approximated as interior building envelopes	Some of the typical systems
HAMLab	Multi-zone, capable of CFD	Standard 1D Heat+Moisture capable of 1D/2D/3D Heat+Air+Moisture	Interzonal flows (including cross flow through large openings), natural and mechanical ventilation, CFD capabilities	One parameter for all moisture storage in each zone	Some of the typical systems, with capabilities of detailed representation of some systems & controllers
HAM-Tools	Multi-zone	1D Heat+Air+Moisture	Well mixed volumes, interzonal flows, natural and mechanical ventilation	Approximated as interior building envelopes	Most of the typical systems, 2D and 3D floor heating systems
PowerDomus	Multi-zone	1D Heat+Moisture, airflow through envelope under development	Well mixed volumes, natural and mechanical ventilation. Possible link with COMIS is under analysis	Approximated as interior building envelopes	Most of the typical systems, with detailed representation of systems
SimSPARK	Zonal model	1D Heat+Moisture	Zonal, represents airflows in one room and intra-rooms, including ventilation	Approximated as interior building envelopes	Some of the typical systems, including solar DEC
TRNSYS	Multi-zone	1D Heat	Interzonal flows, ventilation, extensions possible using COMIS	Lumped model for moisture buffering (rendering+furniture)	Most of the typical systems, including many solar components, with detailed representation of systems
TRNSYS ITT	Multi-zone	1D Heat+Moisture	Well mixed zone, zonal model or interactive coupling with CFD available	Lumped models for heat and moisture buffering	All of the TRNSYS modules
WUFI-Plus	1 zone	1D Heat+Moisture	1 well mixed zone	Approximated as interior building envelopes	Most of the typical systems, including heat recovering
Xam	1 zone	1D Heat+Moisture	1 well mixed zone	No	Hourly schedule of H&M gain/sink

One of the popular model based the simplified lumped approach is the effective moisture penetration depth (EMPD) model. It has been used to simulate moisture absorption and desorption in the building material. With different material property assumptions, different codes are developed based on this model. For example, in EnergyPlus, non-isothermal conditions are assumed, which the temperature used in the EMPD model comes from the solution of energy conservation equations, and the property of moisture capacity of the material is not constant but a function of the relative humidity of the layer, while in TRNSYS, the isothermal conditions are assumed, and the moisture capacity is constant.

The advances in 3D airflow modeling by using CFD to determine the local moisture transfer coefficient has not been widely applied in the coupled simulations. Paepe (2008) in Annex 41 report imputed this to two limitations. One is the computational time that, as an example, the annual simulations of whole building by CFD are beyond the capacity of the current computational resources. The other is the problem of validation. Only a few simulation studies took this approach. Steeman et al. (2008), as reviewed in Section 2.1.3, coupled an EMPD model with a CFD model in FLUENT so that the CFD code could be used to solve the moisture transfer in the material. Neale (2007) solved the heat and mass transfer for boundary layers close to a wall by implementing vapor transfer equations in MATLAB and coupled it with Fluent. This approach was validated and compared with the experimental data, but the post-processing was complicated due to non-single simulation environment.

2.3 Summary

In the first section of this chapter, the characterization of moisture buffering is reviewed in terms of MBV, kinetic curves, and film coefficient. The MBV term combines material hygroscopic properties to describe this dynamic effect. Kinetic curves present this dynamic process in time domain, and the equilibrium state may be predicted by a few measurement steps. The film coefficient which is mainly affected by the local conditions influences the moisture amount absorbed and released by the buffering material in this process. Other measurement method and different material types as well as the other objects such as furniture buffering evaluation are also reviewed.

The moisture buffering effects can be utilized to moderate indoor environment and reduce energy consumption. To have this utilization, the whole building moisture responses to the different moisture load profiles and ventilation conditions have to be understood and predicted. Currently, the numerical simulation methods are mainly employed for this calculation. These topics are reviewed in the second section of this chapter.

The review indicates that the link between the characterization of the material buffering capacity and its utilization has not been well established. To have a reasonably precise prediction of the moisture buffering effects, the material's buffering properties characterization is not sufficient, and the material buffering performance at room level has to be investigated. Currently the evaluation of the material performance based on simplified simulation model has provided an assessment of indoor condition. However,

extensive experimental data are still needed to enhance this assessment. Meanwhile, since the detailed information of the microclimate inside rooms cannot be obtained from these models, the CFD model involving the moisture interaction process between the indoor air and the hygroscopic material is required. All of these reasons become the motivation of this research. As introduced in the previous chapter, this research includes a comprehensive experimental investigation to evaluate impact of the buffering material on indoor environment under different room factors, and a numerical model in a single simulation environment to study the moisture interaction with the hygroscopic materials and to predict the spatial responses of indoor moisture and temperature under different room factors.

CHAPTER 3

BASIC THEORIES FOR HAM TRANSPORT

This chapter consists of three sections. The building material's hygroscopic properties and relative concepts encountered in the literature review chapter, such as moisture sorption isotherm, moisture effusivity, and penetration depth, are explained in the first section. The principles of moisture transport as well as the fundamental governing equations and dimensionless numbers used in fluid flow, heat and mass transfer analysis are given in the second section. The third section presents the moisture balance in the room and enclosure. The experimental tests formulation in this research is derived in this part.

3.1 Definition of hygroscopic material properties

In this section, material properties are introduced mathematically. For the experimental and numerical study about the properties measurement and determination one can refer to Carmeliet and Roels (2001), Jirickova and Cerny (2006), and Derluyn et al. (2006).

3.1.1 Moisture sorption isotherm

Moisture Sorption Isotherm, which is usually displayed graphically by a regression curve, describes the relationship between water content and the equilibrium humidity of a material at constant temperature. Sorption isotherms are often used as empirical models which do not make statements about the underlying mechanisms and measured variables (Roles et al., 2004). An example of the spruce wood material sorption isotherm is given as Fig. 3.1:

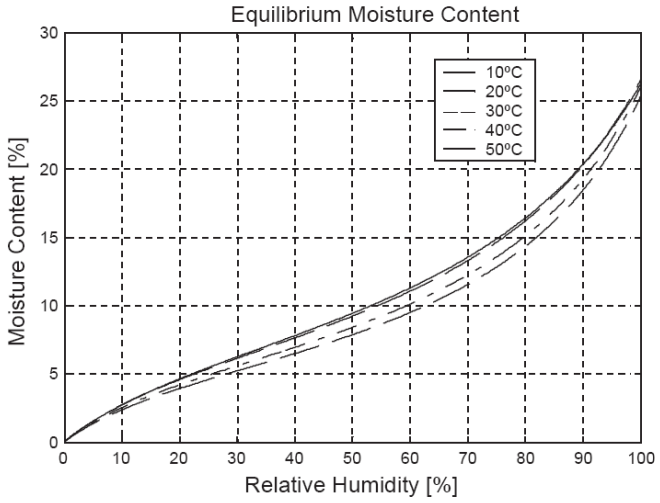

Fig.3.1 Equilibrium moisture content of wood at various temperatures versus the relative humidity (from Hameury, 2005)

3.1.2 Moisture capacity, ξ

The moisture capacity, ξ, which is also called storage capacity, is the derivative of the moisture sorption isotherm (Fig.3.2). It is used in solving the isothermal moisture transport equation, and is generally expressed by parametric functions covering both

the hygroscopic and over-hygroscopic regime (Carmeliet and Roels, 2001). Its unit is kg/kg.

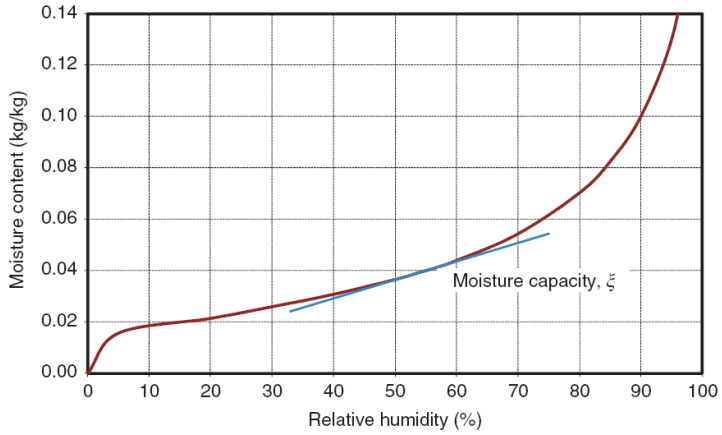

Fig. 3.2 Sorption curve for aerated concrete. The slope of the curve indicates the moisture capacity, $\xi = du/d\varphi$ (kg/kg), where u is the moisture content (kg/kg – mass of absorbed moisture per dry mass of the material), and φ is relative humidity (-) (from Rode and Grau, 2008).

3.1.3 Water vapor permeability, δ

In building science, water vapor permeability, δ ($kg/m \cdot s \cdot p_a$), describes the ability of a material to transmit the water vapor. It is defined in:

$$w = -\delta \frac{dp}{dx} \qquad (3.1)$$

where

w = mass of vapor transmitted over unit time (kg/s)

p = vapor pressure (p_a)

x = distance along the flow path (m)

δ = permeability ($kg/m \cdot s \cdot p_a$)

For the standard methods to measure water vapor permeability one can refer to McCullough et al. (2003).

3.1.4 Moisture diffusivity D_w

The moisture diffusivity, $D_w(m^2/s)$, combines the transport and retention properties into one property. It describes how fast the moisture potential propagates through the material (Rode and Grau, 2008) as:

$$D_w = \frac{\delta \cdot p_s}{\rho \cdot \xi} \tag{3.2}$$

where p_s is the saturation vapor pressure (Pa). A method using TDR (time domain refrectometry) to measure moisture diffusivity was presented by Pavlik et al. (2006).

The moisture diffusivity has the same unit with thermal diffusivity α and kinematic viscosity ν.

3.1.5 Moisture effusivity b_m

In thermodynamics, the thermal effusivity, $b(J/m^2 \cdot K \cdot s^{1/2})$, of a material is defined as the square root of the product of the material's thermal conductivity and its volumetric heat capacity.

$$b = \sqrt{\kappa \rho c_p} = \kappa / \sqrt{\alpha} \tag{3.3}$$

where $\kappa(W/m\cdot K)$ is the thermal conductivity, $\rho(kg/m^3)$ is the density, $c_p(J/kg\cdot K)$ is the specific heat capacity, and $\alpha(m^2/s)$ is the thermal diffusivity. The product of ρ and c_p is known as the volumetric heat capacity. A material's thermal effusivity is a measure of its ability to exchange thermal energy with its surroundings.

Analogue to this definition, Rode et al (2005) described moisture buffering capacity by the moisture effusivity, $b_m(kg/m^2\cdot Pa\cdot s^{1/2})$ which derived from vapor permeability (δ_p , $kg/m\cdot s\cdot Pa$), dry density of the material ($\rho_0, kg/m^3$), moisture content (w , kg/kg), relative humidity (φ), and the saturation vapor pressure (P_s, Pa) as:

$$b_m = \sqrt{\frac{\delta_p \cdot \rho_0 \cdot \partial w/\partial\varphi}{P_s}} \tag{3.4}$$

3.1.6 Moisture Penetration depth d_m

The thermal penetration depth d_t is obtained from the exact solution for a semi-infinite slab with temperature T_i subjected to a sudden temperature change T_0 on its surface. In this situation, assuming constant thermal diffusivity, the one dimension unsteady conduction Eq. (3. 5) needs to be solved with the initial condition (3.6) and boundary condition (3.7) and (3.8).

$$\frac{\partial T}{\partial t} = \alpha\frac{\partial^2 T}{\partial x^2} \tag{3.5}$$

$$T(x,0) = T_i \tag{3.6}$$

$$T(0,t) = T_0 \tag{3.7}$$

$$T(\infty,t) = T_i \tag{3.8}$$

The semi-infinite slab problems are typically solved by Fourier integrals and Laplace transforms. White (1988) presented the exact solution in using similarity theory by defining a single variable η as Eq. 3.9 and correspondingly the dimensionless temperature Θ as Eq. 3.10. Then the governing Eq. (3.5) changes to a simple ordinary differential Eq. (3.11) with the exact solution (3.12).

$$\eta = \frac{x}{2\sqrt{\alpha \cdot t}} \tag{3.9}$$

$$\Theta = \frac{T - T_i}{T_0 - T_i} \tag{3.10}$$

$$\frac{d^2\Theta}{d\eta^2} + 2\eta\frac{d\Theta}{d\eta} = 0 \tag{3.11}$$

$$\Theta = \frac{T - T_i}{T_0 - T_i} = 1 - \frac{2}{\sqrt{\pi}}\int_0^{\eta} e^{-z^2}\,dz = erfc(\eta) \tag{3.12}$$

The function $erfc$ is called the complementary error function. This solution is used to calculate the thermal penetration depth d_t which is defined as the interior position at which the temperature change is 1% of $(T_0 - T_i)$, i.e. $\Theta = 0.01$. From the tabulate solution, to have $\Theta = 0.01$, the single variable $\eta = d_t / 2\sqrt{\alpha \cdot t} = 1.82$ (Eq. 3.9 with $x = d_t$), so the penetration depth d_t can be calculated as:

$$d_t = 3.64\sqrt{\alpha \cdot t} \tag{3.13}$$

Cunningham (1992) obtained the analytical solution for the effective moisture penetration depth for the semi-infinite material in one-sided case which is subjected to cyclic moisture concentration load, and the moisture EPD is equal to $\sqrt{D_w / 2\varpi}$ (Eq. 3.14) for a constant vapor diffusion coefficient and under isothermal conditions.

$$d_m = \sqrt{D_w / 2\varpi} \tag{3.14}$$

where ϖ is the angular frequency of the cyclic load (s^{-1}).

Eq. 3.15 is obtained by substituting (3.2) into (3.14). This equation is used in many numerical codes as effective penetration depth model reviewed in the previous chapter to describe moisture buffering. Rode et al. (2004) defined the moisture penetration depth as the depth at which the amplitude is dampened to 1% of the amplitude at the surface and gave Eq. 3.16. The reality is that unlike the thermal penetration depth, the moisture vapor penetration depth cannot be measured currently, and the value for most common materials is still unknown.

$$d_m = \sqrt{\frac{\delta \cdot p_s \cdot t_p}{\rho \cdot \xi \cdot \pi}} \tag{3.15}$$

where t_p is the time period of the cyclic variation (s).

$$d_p = 4.61\sqrt{D_w \cdot t_p / \pi} \tag{3.16}$$

where d_p is the moisture vapor penetration depth (m).

3.2 Principles of moisture transfer

The material properties related to moisture transport were described in the previous section, the theories of HAM transport including characterizing fluid flow, heat and mass diffusion, and analogy of heat and mass transfer in building science are reviewed in this section. These theories are the fundamentals of the numerical study presented in later chapters.

3.2.1 Convection flow characterized by dimensionless numbers

The governing equations of a convection fluid flow are derived from the principles of conservation of mass, momentum, and energy. The constitutive relation for stress in a Newtonian fluid with constant viscosity is shown in Eq. 3.17, and the governing equations can be expressed in the tensor form as (3.18)-(3.20):

$$\underline{\underline{\sigma}} = -p\underline{\underline{I}} + [\lambda \underline{\underline{I}} \nabla \cdot \vec{V} + \mu(\nabla \vec{V} + \vec{V}\nabla)] \tag{3.17}$$

Continuity

$$\frac{\partial \rho}{\partial t} + \nabla \cdot (\rho \vec{V}) = 0 \tag{3.18}$$

Momentum

$$\rho \frac{\partial \vec{V}}{\partial t} + \rho(\vec{V} \cdot \nabla)\vec{V} = -\nabla p + \lambda \nabla(\nabla \cdot \vec{V}) + \mu[\nabla^2 \vec{V} + \nabla(\nabla \cdot \vec{V})] + \rho \vec{f}_B \tag{3.19}$$

Energy

$$\rho\frac{\partial e}{\partial t}+\rho\vec{V}\cdot\nabla e=-p\nabla\cdot\vec{V}+[\lambda\underline{\underline{I}}\nabla\cdot\vec{V}+\mu(\nabla\vec{V}+\vec{V}\nabla)]\cdot\nabla\vec{V}+\nabla\cdot(\kappa\nabla T) \qquad (3.20)$$

where in the above equations,

$\underline{\underline{\sigma}}$ is the stress tensor

I is the unit tensor

$\vec{V}=u\hat{i}+v\hat{j}+w\hat{k}$

$\nabla=\frac{\partial}{\partial x}\hat{i}+\frac{\partial}{\partial y}\hat{j}+\frac{\partial}{\partial z}\hat{k}$ in the Cartesian coordinate system

$\vec{f}_B$ is body force, and for the force due to gravity, $\vec{f}_B=g\hat{k}$

e can be obtained from the caloric equation of state, frequently, $e=c_pT$.

These governing equations, which describe the convection of fluid flow in the internal and external as well as for the compressible and incompressible, are highly nonlinear, and the analytical solutions for complex boundary conditions cannot be obtained. Hence, these equations must be solved numerically.

Different numerical models are available to describe the fluid flow based on the flow characteristics, and the dimensional analysis plays an important role in characterizing the flows. In this section, some dimensionless numbers are introduced, which are relevant in identifying the flow characteristics in the test room in this thesis. The more detailed description of the numerical model and the coupling process are described in Chapter 6.

- Nusselt number Nu

The Nusselt number is the ratio of convective to conductive heat transfer across (normal to) the boundary. A large Nusselt number means an efficient convective heat transfer. The Nusselt number is defined as Eq. 3.17:

$$Nu_L = \frac{hL}{\kappa} = \frac{Convective \quad Heat \quad transfer}{Conductive \quad Heat \quad transfer} \tag{3.17}$$

Where *h* is convective heat transfer coefficient, *k* is thermal conductivity of the fluid, *L* is the characteristic length.

- Reynolds number Re

The Reynolds number Re is the ratio of inertial forces ($U\rho$) to viscous forces (μ / L). In the viscous force dominated laminar flow, the Re number is small while in the inertial force dominated turbulent flow, the Re number is large. For example, for a fully developed flow inside a pipe, the laminar flow occurs when $\mathrm{Re} < 2300$, and it becomes turbulent when $\mathrm{Re} > 4000$. For an external flow along a flat plate, the transition from the laminar to the turbulent occurs at approximately $\mathrm{Re} = 5 \times 10^5$. The Reynolds number is defined as (3.18):

$$\mathrm{Re} = UL / \nu \tag{3.18}$$

where U is the average velocity for the internal flow and the stream velocity for the external flow, L is the length scale that is the diameter D for internal flow and the distance x for external flow; and ν is the fluid kinematic viscosity with the unit of m^2 / s

- Prandtl Number Pr

The Prandtl number Pr is a dimensionless number approximating the ratio of momentum diffusivity (kinematic viscosity ν) and thermal diffusivity α as Eq. 3.19:

$$\mathrm{Pr} = \frac{\nu}{\alpha} = \mu c_p / \kappa \tag{3.19}$$

For the incompressible fluid flow past a flat plate at the steady state with the constant free stream velocity, no heat generation and neglecting the dissipation effects, the thicknesses of the velocity and thermal boundary layers can be correlated by the Pr number. When $\mathrm{Pr} = 1$, the shape of the velocity and temperature profiles is identical.

- Grashof number Gr

For the natural convection developed along a vertical plate, neglecting friction, the Grashof number Gr is defined by the "local Reynolds number" $u_{avg} x / \nu$, i.e.:

$$Gr_x = (u_{avg} x / \nu)^2 = g(1 - \frac{\rho_w}{\rho_\infty})(\frac{x^3}{\nu^2}) = \frac{g \Delta \rho x^3}{\nu^2 \rho_\infty} \tag{3.20}$$

In free convection, the Grashof number takes the place of Reynolds-number-squared in the forced convection. This number may assess the relative importance of a streaming motion superimposed on a buoyant heat transfer situation by:

Free convection: $Gr_x / \mathrm{Re}_x^2 >> 1$ (3.21)

Mixed convection: $Gr_x / \mathrm{Re}_x^2 \cong 1$ (3.22)

Forced convection: $Gr_x / \mathrm{Re}_x^2 << 1$ (3.23)

The definition of Gr_x in Eq. 3.20 is not convenient for engineering analysis, where temperature rather than density differences are more useful. An appropriate definition can be obtained by introducing the coefficient of the thermal expansion β:

$$\beta = -\frac{1}{\rho}(\frac{\partial \rho}{\partial T})_p \quad (3.24)$$

For ideal gas,

$$\beta \equiv 1/T \quad (3.25)$$

The Grashof number can be expressed as:

$$Gr = g\beta(T_w - T_\infty)L^3 / \nu^2 \quad (3.26)$$

- Eckert number Ec

$$Ec = \frac{U^2}{c_p \Delta T} = \frac{Kinetic \quad Energy}{Enthalpy} \quad (3.27)$$

Eckert number Ec expresses the relationship between a flow's kinetic energy and enthalpy, and is used to characterize dissipation, if the Eckert number $Ec << 1$, then the

dissipation is negligible. For the free convection, substituting the U in Ec number by the velocity $(g\beta\Delta TL)^{1/2}$, the Eckert number is with the form of (3.28)

$$Ec = \frac{U^2}{c_p \Delta T} = \frac{g\beta\Delta TL}{c_p \Delta T} = \frac{g\beta L}{c_p} = \frac{L}{c_p / g\beta} \tag{3.28}$$

The scale $c_p / g\beta$ is equal to 30 and 2030 km for the air and water respectively. So the vertical length scale L in most cases is much smaller than $c_p / g\beta$, and $Ec << 1$. This is the reason that most CFD software neglects the dissipation when perform natural convection analysis.

3.2.2 Governing equations and mechanisms of moisture transfer and its analogy to heat transfer

The mechanisms of moisture transfer in air include convection which is described in the previous section and diffusion which is based on the theory of mass diffusion. The diffusion process of a mixture of n species with individual masses of m_1, m_2, m_3, … m_n contained in a volume v can be described as follows:

The mass fraction of any species i is:

$$w_i = m_i / m = \rho_i / \rho \quad \text{with} \sum_{i=1}^{n} w_i = 1 \tag{3.29}$$

where ρ_i is the density of species i, and ρ is the density of this mixture

In a flowing mixture, each species moves with a different velocity $\vec{V}_i$ and mass flow rate $\rho_i \vec{V}_i$, and then the bulk mass flow per unit area is:

$$\vec{G} = \dot{m}'' = \rho \vec{V} = \sum_{i=1}^{n} \rho_i \vec{V}_i \tag{3.30}$$

where $\vec{V}$ is the bulk velocity.

And the diffusion mass flux of species i is defined as:

$$\vec{g}_i = \rho_i (\vec{V}_i - \vec{V}) \tag{3.31}$$

Fick's law of mass diffusion states that the diffusion mass flow is proportional to the gradient of the concentration of the species. In a mixture of two species A and B, the Fick's law is expressed as:

$$\vec{g}_A = -D_{AB} \nabla \rho_A = -\rho D_{AB} \nabla w_A = \rho_A (\vec{V}_A - \vec{V}) \tag{3.32}$$

where D_{AB} is called the molecular diffusion coefficient with the unit of m^2/s.

The mechanisms of moisture transport in porous materials include diffusion, saturated viscous flow, and liquid transport. Depending on the pore size of the materials, the molecules of moisture have different patterns diffusing through the materials. When the mean free path is relatively short compared to the pore size, the mechanism of the moisture diffusion can be described by Fick's Law. As introduced in the previous paragraph, the flux of the moisture transport is related to the driving force of the

concentration. When the pores dimensions range in diameter between 2 and 50nm, the free path of the moisture particles is relatively long compared to the pore size, and particles collide frequently with the pore wall. This diffusion mechanism is called Knudsen diffusion and is described by the Einstein relation as (Malek and Coppens, 2003):

$$D_s(c) = \lim_{t\to\infty} \frac{1}{6Nt} \left\langle \sum_{i=1}^{N} \left| r_i(t) - r_i(0) \right|^2 \right\rangle \tag{3.33}$$

where D_s is the self-diffusion coefficient, which depends on the concentration c, t is time, N is the total number of particles in the system, and r_i is the position vector of particle i.

Surface diffusion occurs on the surface of the pore where the moisture molecules jump between the adjacent adsorption sites (Jaguste and Bhatia, 1995). The viscous flow occurs when the transverse section of the channel is large compare to the mean free path of the moisture flow, and the Reynolds number of the flow is small. The viscous flow can be described by Brinkman equation as (Whitaker, 1986):

$$\beta \nabla^2 q + q = -\delta \nabla P \tag{3.34}$$

where q is the flow flux (kg/m^2·s), P is the pressure gradient (Pa), δ is the permeability of the porous medium (kg/m·s·Pa), β is an effective viscosity term.

The liquid transport mechanisms are described as hydrodynamic flow and capillary flow. The hydrodynamic flow is induced by pressure differentials along a pore channel (Weber

and Kimmich, 2002), while the capillary flow can be described by Washburn's equation as (Noble and Arnold, 1991):

$$L^2 = \frac{\gamma D t}{4\eta} \tag{3.35}$$

where *L* is the penetration distance in to the capillary (m), γ is the surface tension (N/m), *D* is the pore diameter (m), *t* is the time (s), η is the dynamic viscosity (Pa·s).

Generally, in building science, the moisture transport is described as a product of a transfer coefficient and a gradient of the driving potential (Gudum, 2003)

$$\vec{g}_x = -\Gamma \cdot \frac{d\Psi}{dx} \tag{3.36}$$

where

$\vec{g}_x$ is the moisture transfer in the x-direction

Ψ is the potential, e.g. vapor concentration, vapor mass fraction, vapor pressure, relative humidity, suction pressure, capillary pressure, and gravity.

x is the coordinate

Γ is the transfer coefficient corresponding to the driving potential

This generic equation has the same form as Fourier's law in heat conduction Eq. 3.37 and the Newtonian's law of relationship of shear stress and velocity as Eq. 3.38, respectively.

$$\vec{q}'' = -k\nabla T = -k \cdot \frac{dT}{dx} \text{ in x direction} \tag{3.37}$$

where *k* is the thermal conductivity with the unit of W/(m·K)

$$\tau = \mu \frac{du}{dy} \tag{3.38}$$

where μ is the viscosity with the unit of kg/(m·s)

Despite of the same form of the three equations (Eqs. 3.36-3.38), the first item in each of the three equations has different order of the geometric entity. The heat and moisture flow flux are vectors, while viscous stress τ is a tensor. The analogy between momentum and heat can be achieved by the Prandtl number, and the analogy between heat and mass transfer is achieved with the analogous variables listed in Table 3.1.

Table 3.1 Heat transfer and analogous mass transfer variables (from White 1988)

Heat Transfer Variables	Analogous Mass Transfer Variables
Temperature, T	Moisture density, ρ_A
Thermal diffusivity, $\alpha = k/\rho c_p$	Mass diffusivity, D_{AB}
Bulk velocities, u, v	Bulk velocities, u, v
Heat generation rate, $\dot{q}/\rho c_p$	Moisture generation rate, $\dot{m}_A$
Prandtl number, Pr	Schmidt number, Sc

The last item in the table for moisture transfer variables is Schmidt number, Sc (Eq. 3.39). Recall that the diffusion coefficient D_{AB}, kinematic viscosity $\nu = \mu/\rho$, and thermal diffusivity α have the same unit of m^2/s, and the Pr number is given in Eq. 3.19 as extended fluid property, the other two dimensionless numbers of fluid properties are defined as (3.39) and (3.40):

- Schmidt number $Sc = \nu / D_{AB}$ (3.39)
- Lewis number $Le = \alpha / D_{AB} = Sc / \mathrm{Pr}$ (3.40)

Generally, gases have Schmidt and Lewis number near unity indicting that momentum, heat, and mass transfer effects are of comparable magnitude. Liquids have large Sc and Le indicting small diffusion rates compared to momentum and heat transfer.

For moisture transfer in a stationary medium, with no bulk flow or moisture generation, the mass diffusion equation is described as:

$$\frac{\partial \rho_A}{\partial t} = D_{AB} \nabla^2 \rho_A \quad (3.41)$$

This is mathematically identical to the unsteady heat conduction equation

$$\frac{\partial T}{\partial t} = \alpha \nabla^2 T \quad (3.42)$$

In the unsteady heat conduction analysis, the Biot number Bi defined as (3.43) plays an important role. The Biot number (Bi) is the ratio of the heat transfer resistances inside of and at the surface of a body. It determines whether or not the temperature inside a body varies significantly in space when the body surface is subjected to a thermal gradient. For a small Bi number, the body may be regarded as uniform temperature field inside body while for a large one, the non-uniformity of temperature fields exist.

- $Bi = \frac{hL}{k}$ (3.43)

where h is the convective heat transfer coefficient ($W/m^2 \cdot K$), L is the characteristic length (m), and k is the thermal conductivity of the body ($W/m \cdot K$)

A similar number called moisture Biot number was proposed by (Rode at al. 2004) as Eq.3.44 in studying the moisture transferring into a sample material, and Fig. 3.3 shows that a decreasing moisture Biot number corresponds to a lower moisture transfer rate.

- $$Bi_{moisture} = \frac{L}{\delta_v \cdot Z_{s,v}} \qquad (3.44)$$

where L is the thickness of the sample (m), δ_v is the water vapor permeability (m^2/s), $Z_{s,v}$ is the moisture surface resistance (s/m).

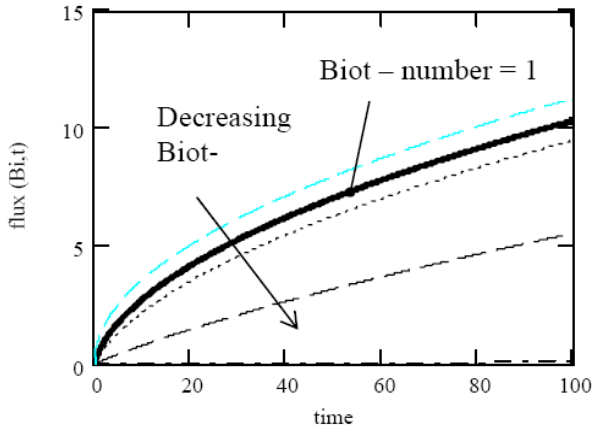

Fig. 3.3 Moisture uptake as a function of time (t) and moisture Biot number (From Rode et al. 2004)

The theories covering the moisture transport including bulk movement and diffusion in different medium have been summarized. The principles of mass transfer and governing equations of fluid dynamics and mass transfer are the essential in numerical simulations

of whole building moisture transfer by using CFD analysis. The numerical model and the relevant theories of CFD techniques to solve the fluid flow will be given in Chapter 6 where the model is described.

3.3 Governing equation of the moisture balance in the experimental study

In this section, the formulation of this thesis experimental test is derived. The experiment which is described in detail in next chapter consists of two steps: first, the non-hygroscopic tests in which the hygroscopic material on the wall surface is covered by plastic sheets so that there is no moisture interaction between indoor air and wall systems, and second, the hygroscopic tests in which the plastic sheets are removed (Fig. 4.1 and 4.2). The moisture balance for the test room can be described as:

$$\frac{\partial}{\partial t}(\rho V w_i) = \dot{m}_p + \dot{m}_{sys} + \dot{Q}_a w_{dif} - \dot{m}_{wall} \tag{3.45}$$

where

ρ room air density (kg/m^3)

V room volume (m^3)

w_i indoor humidity ratio (kg/kg)

t time (s)

$\dot{m}_p$ indoor vapor production (kg/s)

$\dot{m}_{sys}$ vapor exchange rate by HVAC system (kg/s)

$\dot{Q}_a$ mass flow rate of air leakage (kg/s)

$\dot{w}_{dif}$ humidity ratio difference between outdoor and indoor (kg/kg)

$\dot{m}_{wall}$ moisture exchange rate between indoor and wall system (kg/s)

Eq. 3.45 is the differential equation stating that the indoor humidity level is the result of the moisture balance of moisture generation inside room, moisture gains/loss from the ventilation, air leakage and through the walls, and moisture storage inside the test room. The last item on the right side of the equation is the moisture interchange between the wood wall and the test room. The time integral of this item represents the moisture amount absorbed or released by the wall system, which is defined as the moisture buffering amount M_h in this research. Defining the time when moisture starts generating from the moisture source at the center of the test room as time t_0, at any time t_1, the $M_h(t_1)$ can be obtained by the integral of the equation from time t_0 to time t_1. The time integral of Eq. 3.45 is:

$$\underbrace{\int_{t_0}^{t_1} \frac{\partial}{\partial t}(\rho V w_i)dt}_{(1)} = \underbrace{\int_{t_0}^{t_1} \dot{m}_p dt}_{(2)} + \underbrace{\int_{t_0}^{t_1} \dot{m}_{sys} dt}_{(3)} + \underbrace{\int_{t_0}^{t_1} \dot{Q}_a w_{dif} dt}_{(4)} - M_h(t_1) \qquad (3.46)$$

The item on the left side of Eq. 3.46 is the changing amount of the moisture amount inside the test room and can be rewritten as:

$$\underbrace{\int_{t_0}^{t_1} \frac{\partial}{\partial t}(\rho V w_i)dt}_{(1)} = V \cdot \rho_a \cdot \left[w_i(t_1) - w_i(t_0)\right] \qquad (3.46a)$$

The first item on right side of Equation 3.46 is the amount of moisture generation in the experiment. The generation rate is controlled by the moisture generation system (Fig. 4.12) and designed to have same constant value Cg in both two test steps with little error. Then this item can be rewritten as:

$$\underbrace{\int_{t_0}^{t_1} \dot{m}_p dt}_{(2)} = C_g \cdot (t_1 - t_0) \qquad (3.46b)$$

The second item on the right side of Eq.3.46 is the moisture increased amount due to ventilation system. As the test protocol in next chapter stated, the ventilation system used in this experiment is designed as closed system. The mixture air inside room will be driven out to be conditioned and sent back to the test room again. Then we have:

$$\underbrace{\int_{t_0}^{t_1} \dot{m}_{sys} dt}_{(3)} = \int_{t_0}^{t_1} \dot{Q}_{vt} [w_{inlet}(t) - w_{oulet}(t)] dt \qquad (3.46c)$$

where $\dot{Q}_{vt}$ is the ventilation rate (kg/s), and $w_{inlet}(t)$ and $w_{outlet}(t)$ are the function of humidity ratio at inlet and outlet, which can be measured by the experimental sensors.

The third item is the moisture infiltration due to the air leakage which is deduced as follows:

$$\underbrace{\int_{t_0}^{t_1} \dot{Q}_a w_{dif} dt}_{(4)} = \dot{Q}_a \int_{t_0}^{t_1} [w_e(t) - w_i(t)] dt \qquad (3.46d)$$

Same as Eq. 3.46c, the indoor and outdoor humidity ratio can be obtained from the sensors measurements, but the air leakage rate needs to be tested.

Then for hygroscopic test, the Eq. 3.46 is written as:

$$M_h(t_1) = C_g \cdot (t_1 - t_0) + \int_{t_0}^{t_1} \dot{Q}_{vt} \cdot [w_{inlet}(t) - w_{oulet}(t)]dt + \int_{t_0}^{t_1} \dot{Q}_a \cdot [w_e(t) - w_i(t)]dt - V \cdot \rho_a \cdot [w_i(t_1) - w_i(t_0)] \quad (3.47)$$

For the non-hygroscopic tests, the walls were covered by plastic sheets. It means there is no moisture interaction between the indoor humidity air and the wall system. The superscript *n* is used to denote the non-hygroscopic step, and Eq. 3.47 can be rewritten again to describe the non-hygroscopic test with M_h equal to zero.

$$0 = C_g^n \cdot (t_1 - t_0) + \int_{t_0}^{t_1} \dot{Q}_{vt} \cdot [w_{inlet}^n(t) - w_{outlet}^n(t)]dt + \int_{t_0}^{t_1} \dot{Q}_a \cdot [w_e^n(t) - w_i^n(t)]dt - V \cdot \rho_a \cdot [w_i^n(t_1) - w_i^n(t_0)] \quad (3.48)$$

The outdoor condition is the same for every case, i.e. $w_e(t)=w_e^n(t)$. Then the hygroscopic buffering can be obtained by subtracting Eq. 3.48 from Eq. 3.47, as:

$$M_h(t) = (C_g - C_g^n) \cdot (t - t_0) + \int_{t_0}^{t} \dot{Q}_{vt} \cdot [(w_{outlet}^n(t) - w_{oulet}(t)) + (w_{inlet}(t) - w_{inlet}^n(t))]dt + \int_{t_0}^{t} \dot{Q}_a \cdot [w_i^n(t) - w_i(t)]dt + V \cdot \rho_a \cdot \{[w_i^n(t) - w_i^n(t_0)] - [w_i(t) - w_i(t_0)]\} \quad (3.49)$$

The term C_g-C_g^n and $w_{inlet}(t)=w_{inlet}^n(t)$ are expected to be very small, because they are controlled by the moisture generation system and the AHU respectively.

The time integral equation of the moisture balance inside the test room has been deduced and presented in this section as the theory of the experimental work. The experimental data will be analyzed based on Eq. 3.49 to calculate the moisture buffering amount caused by the wood paneling. Due to the non-homogenous condition of the temperature and moisture distribution profiles inside the test room, this equation need to be further developed, and the air leakage of the test room also needs to be investigated before this equation is applied to the calculation. This work is presented in the next chapter.

3.4 Summary

In Chapter 3, the theories and concepts related to the moisture transport process and to hygroscopic materials absorbing/releasing moisture are reviewed. In the first section of this chapter, several terminologies regarding the moisture transport and storage inside porous materials are elaborated. The first item introduced, moisture sorption isotherm, is useful to understand the moisture buffering performance of wood paneling investigated in the thesis experimental work. The other items including moisture capacity, water vapor permeability, and moisture diffusivity are utilized when the non-linear governing equations of the moisture transport inside the wall system are derived in this thesis' numerical model in Chapter 6. The moisture penetration depth is an

important concept in current moisture buffering studies, especially in the numerical models. Detailed explanation of moisture penetration depth is provided to recognize the advantages and limitations of using the penetration depth method to simulate whole building moisture transport and to understand how the thesis numerical model overcomes the limitations existing in current whole building HAM models. In the second section of this chapter, the governing equations and mechanisms of moisture transport in air and inside porous materials are presented. Those theories are the fundamental of establishing the numerical models in investigating the indoor environment influenced by room factors. The more detailed description of the equations applied in the thesis numerical model and their coupling process are presented in later chapters where the equations were utilized, especially in Chapter 6, “Numerical simulation”. In the last section of this chapter, the equations governing the moisture balance in the test room are derived.

CHAPTER 4

EXPERIMENTAL SETUP, PROTOCOL, AND PRELIMINARY EXPERIMENTAL RESULTS

The moisture buffering performance of interior finishing of a room wall, as stated in the literature review, has not been extensively investigated at the room level in full-scale setups. In order to study the wood wall panel's moisture buffering responses in a room, in this thesis research, a comprehensive experimental investigation of the influence of the room factors including moisture loads, the ventilation conditions, and the RH initial conditions inside the test room on the moisture ab/desorption by wood paneling and on the indoor environment were carried out in an environmental chamber. The moisture ab/desorption kinetic curves of the wood paneling were presented. The relationship of the moisture buffering performance of wood paneling and its buffering effect to the indoor environment under different test conditions were analyzed. This chapter on the experimental protocol includes the description of the experimental objective, methodology, setup, equipments, test scenarios, and preliminary test results.

4.1 Objective and scope of the experimental study

The current moisture buffering studies reviewed in Chapter 2 can be divided into two main categories: the characterization of material hygroscopic property, that is at the

material level, and the investigation of the buffering effects in whole building environment at the room level. At the material level, the material buffering property is measured in experiments or calculated in simulations and determined as the mass of the moisture absorbed/desorbed when the specimen is subjected to a cyclic change of the surrounding environment. One way to describe this property is by the sorption curves where the mass change with respect to time is presented by the absorption/adsorption equations. The form of the equations and the correlation coefficients in the equations need to be determined for the different materials. The other well-accepted way to characterize this buffering property is the moisture buffering value (MBV). Theoretically, this value can be calculated by the Fourier transform when the material is tested under a square wave of RH signal. Practically, this value is defined by the moisture amount exchanged during a cycle and normalized by the open surface area of the hygroscopic material and the % RH variation.

The moisture buffering at room level has been studied in some large-scale experiments and field tests. The moisture buffering effects of different hygroscopic materials under different ventilation rates and moisture generation regimes have been investigated. Recently, the room level moisture buffering value, defined as the superposition of the moisture buffering potential of the interior finishes and objects in the room and referred to as the room's hygric inertia (HIR), has been proposed and developed. Among these studies, the concept of moisture buffering value based on material level tests has been widely adopted. However, the material buffering properties may not be directly representative of the material buffering performance at room level because the

moisture buffering effects are influenced by room factors such as ventilation conditions, indoor humidity and temperature profiles, and indoor environment initial conditions. To establish reliably the link between the characterization and quantification of the moisture buffering of the interior finishing and furnishing, the moisture buffering performance of these materials at room level needs to be measured experimentally. To obtain the material's buffering performance, having it tested when it is made to be a part of the wall system and put it in the real room condition is a better solution.

This experimental research focused on the study of measuring the buffering performance of a wood frame wall system at room level, and its buffering effect on indoor environment. Since wood material is commonly used in the light frame building envelope systems, it was chosen to be the interior layer of the wall in this experiment project.

The main objective of this experiment was to measure and calculate the capability of wood paneling of exchanging moisture under various room conditions, to analyze the relationship between the buffering effect caused by the hygroscopic materials and their hygroscopic performance, and to investigate the influence of moisture buffering effect under different room conditions on indoor environment. Comparing the changes of moisture amount inside the test room with the non-hygroscopic tests which the wood paneling was covered by non-hygroscopic material, the buffering amount could be calculated. The parameters considered in the experiment are explained in detail in the following paragraphs, and the methodology will be explained in next section.

Firstly, the ventilation factor was considered. Since the light-weight wall systems are mostly used in the residential building such as house, apartments, condominiums, as well as townhouses. In these structures, the ventilation is mainly caused by the natural convection or mix convection where the forced convection is not a dominant factor in the indoor room condition, so a room condition without and with lower controlled air exchange rate was applied in the experiment. The common ventilation rates are expressed as the number of times that the whole interior volume of air is replaced per hour, and are referred to as air changes per hour (ACH). For residential buildings, a minimum ventilation rate of 0.35ACH is required by the International Mechanical Code (IMC-2009) (Mudarri, 2010). In the experiment, three levels of ventilation rates were chosen. The non-ventilated condition was chosen as a reference to which other ventilated conditions are compared with and was denoted as 00 ACH. In ventilated condition, the controlled air change rates were 0.5, and 0.75 ACH respectively. To explore how forced convection can affect the buffering performance, 2 test cases using an auxiliary fan with different blow level to mock the forced convection were performed.

The second factor was about the moisture loads. This is another main factor in current moisture buffering studies. In this experiment, at 00 ACH condition, the 25g/h (gram per hour), 33 g/h, 42g/h MGRs were applied for 8 hours in one day cycle to compare with other cases in order to investigate the influence of moisture loads, ventilation rates, indoor RH initial conditions, and the effects of forced convection on wood paneling moisture absorption. These values of the MGR under the non-ventilated condition were

chosen so that the indoor RH level could be kept in the range of 45% to 75%. This range of RH level is close to the indoor environmental condition in real life, and ensures that no condensation occurs. To maintain these RH levels in ventilated conditions, the MGRs need to be increased. For the ventilated conditions, 42g/h, 58.5g/h, and 91g/h MGRs were applied. The minimum MGR in ventilated tests was equal to the maximum rate in the non-ventilated tests. These two test scenarios could make the ventilation condition and non-ventilation condition comparable. The moisture generation time was set to 8 hours in a daily test cycle. This time period is consistent with most moisture buffering studies, such as Rode et al. (2005), Osanyintola and Simonson (2006). In addition to the tests with 8 hours moisture generation, one scenario with 24 hours MGR at 42g/h was included. The main reason to have this scenario was to generate experimental data to compare with the steady-state simulation results introduced in Chapter 7.

The initial condition of the indoor environment was also considered in three test scenarios (cases 3, 5 and 6). The tests which were under non-ventilated condition were repeated with the same load (42 g/h moisture generation rate) except for different initial RH levels inside the test room. These three tests were set to study the influence of initial indoor environment on wood paneling moisture buffering performance. The detailed test parameters are presented in Table4.1.

Table 4.1 Presentation of test cases and loading conditions

Test stage	Test Case Number	Ventilation Rate (ACH)	Moisture Generation Rate (g/h)	Moisture Generation Time (h)	Initial Condition of test room (%RH)	Forced convection using auxiliary fan at south wall
Series 1: Non-ventilated Tests	1	00	25	8	25%	No
	2	00	33	8	20%	No
	3	00	42	8	30%	No
	4	00	42	8	28%	fan[ζ] at low flow
	5	00	42	8	23%	No
	6	00	42	8	33%	No
Series 2: Ventilated Tests	7	0.5	42	8	25%	No
	8	0.5	58.5	8	30%	No
	9	0.5	58.5	8	25%	fan[ζ] at medium flow
	10	0.5	91	8	25%	No
	11	0.75	42	8	30%	No
	12	0.75	58.5	8	30%	No
	13	0.5	42	24	28%	No

Notes: 1. Each test includes two steps: step 1, non-hygroscopic; step 2, hygroscopic.

2. All tests were carried out with winter conditions of -5°C and 60% RH in the climate chamber outside, with 20 °C and 34 %RH in the supply air at the inlet.

3. [ζ] Auxiliary fan at south wall to create air flow on the surface of the wall

4.2 Methodology of experimental tests

The moisture buffering performance of the wood paneling at room level was obtained by calculating the moisture exchange in the wood paneling when it was installed on the interior wall of the test room and the designed moisture loads applied in the room. In order to get the change value, two test steps were performed for each defined room

condition: the non-hygroscopic material test (Fig. 4.1) and the hygroscopic material test (Fig. 4.2). In the non-hygroscopic test, the plastic panel covered the wood paneling, so there was no interaction between the test room and the building enclosure. Later, the test was repeated with nothing changed except for the plastic panels being removed. It was assumed that the same air leakage existed as in a normal residential building, but it would not pass though the wall panel; so, the wall was made airtight (Fig. 4.3). Then, the moisture changes inside the room between the two steps were deemed to have been caused by the wood panel buffering.

Fig. 4.1 Non-hygroscopic test: wood panels were covered by plastic sheets (Plaskolite 4 mm x 1220 mm x 2435 mm)

Fig. 4.2 Hygroscopic test: wood panels were subjected to moisture loads generated inside the room.

Fig. 4.3 Joints between wood panels were sealed with elastomeric latex sealant.

The formula to describe the moisture balance about the two-step tests has been derived in Chapter 3, and is repeated here for convenience.

$$M_h(t) = (C_g - C_g^n)\cdot(t-t_0) + \int_{t_0}^{t} \dot{Q}_{vt}\cdot[(w_{outlet}^n(t) - w_{oulet}(t)) + (w_{inlet}(t) - w_{inlet}^n(t))]dt$$
$$+ \int_{t_0}^{t} \dot{Q}_a \cdot [w_i^n(t) - w_i(t)]dt + V\cdot\rho_a\cdot\{[w_i^n(t) - w_i^n(t_0)] - [w_i(t) - w_i(t_0)]\} \qquad (3.49)$$

There are some advantages in using this methodology to obtain the moisture buffering of the wood paneling. Firstly, the wood paneling was tested in the real room condition. The test hut was designed and assembled with components used in the industry. The experiment results represent the real situation. Secondly, the air leakage is difficult to control and yet has influence on the experimental results. In this experiment, for the two step test, since the temperature and RH value of the outside environment were kept the same, i.e. $w_e = w_e^n$, where *n* denotes non-hygroscopic tests. Then the factor of air leakage in the moisture buffering calculation is expressed by $\dot{Q}_a[w_i^n(t) - w_i(t)]$ as shown in Eq. 3.49. This expression means that the experimental methodology allows the measurement of the air leakage rate weighted by the difference of the indoor humidity ratio between the two steps of tests. This method significantly reduces the error caused by the uncertainty of the air leakage because the value of $w_i^n(t) - w_i(t)$ is much smaller than the difference of the moisture content between the indoor and outdoor. Thirdly, errors exist in the data recorded in the experimental studies. The effects on the results of some sensors are especially large, such as at those placed at the inlet and the outlets in this experiment. For this project, there are 33 RH&T sensors being used inside the test room. The indoor humidity ratio presented as the last item in Eq. 3.49 can be calculated by the averages of the humidity ratios measured from these sensors. For the inlet and

outlet conditions, if it is assumed that for the same sensor, its measurement error is the same in the different test steps, then this experimental methodology can largely reduce the errors caused by the sensors measurement. As shown in Eq. 3.49, the calculation related to ventilation includes mathematical expression of $(w^n_{outlet}(t) - w_{oulet}(t)) + (w_{inlet}(t) - w^n_{inlet}(t))$. This expression indicates that in the calculation of the moisture buffering amount, the measurement errors by the sensors located at the inlet and outlet in the non-hygroscopic steps, i.e. the errors in item w^n_{inlet} and w^n_{outlet}, will be mostly reduced by w_{inlet} and w_{outlet} measured in the hygroscopic steps.

In this section, the methodology of the experiment and its advantages are presented. The equipment, monitoring system and the preliminary test results will be described in the next section.

4.3 Test facilities and setup

4.3.1 Environmental chamber

The environment chamber used in this investigation consists of two large boxes and specimen frames as shown in Fig. 4.4. The cold box is 7.5m high, 4.4 m wide and 3.6 m long. The mechanical equipment (including a 5 ton screw compressor, 12,000 CFM recirculation fan and 25 kW re-heating heater) can provide temperature control from -40 °C to 50 °C. The hot box is of the same height and width as the cold box and it is 6.1m in length. The temperature ranging from 5 °C to 50 °C and relative humidity between 10 to 90% can be controlled. The hot and cold box can be joined together to form a large

(7.5m high by 4.4m wide by 10.5m deep) climatic chamber (Fig. 4.5). The walls of the chamber are made of 150 mm foamed polyurethane boards, laminated between 0.8 mm aluminum sheets outside and 0.8 mm stainless steel sheets inside (Fazio et al 1997). Fig. 4.6 shows a photo taken from the outside of the chamber.

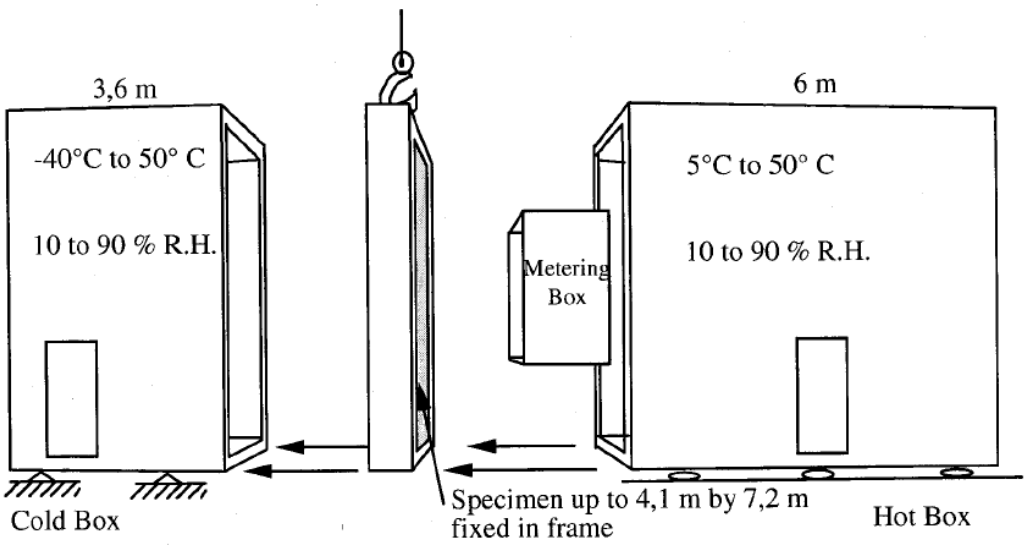

Fig. 4.4 Schematic representation of Environmental Chamber (from Fazio et al., 1997)

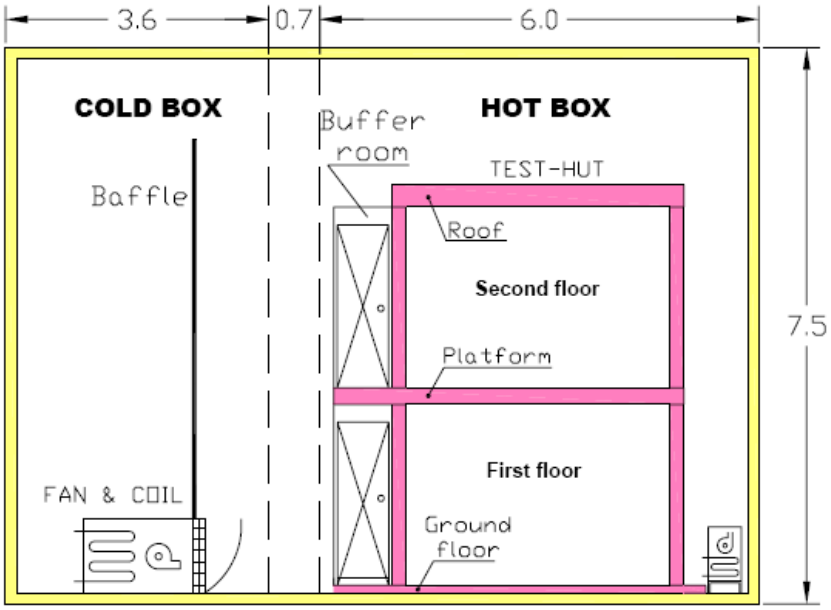

Fig. 4.5 Two-story test hut inside Environment Chamber (From Fazio et al., 2007)

Fig. 4.6 Outside view of environment chamber

4.3.2 Test hut

The first floor of the two-story test hut which was built during the Annex 41 sub-project to study the buffering impact on indoor environment (Yang, 2010) and moisture transport inside rooms (Vera, 2007) was used in this experiment. The objectives and methodology in this thesis experiment were different from the previous buffering impact study. Some parameters investigated and results obtained from the previous studies, such as some heavier moisture loads in ventilation condition, which were not carried out in this thesis experiment, can be utilized to supplement this study. A more detailed description about the test hut, the specification about the test sensors and the

relative nominal can be found in the Annex 41 report (Fazio et al., 2007) listed in the references.

Fig. 4.7 shows the configuration of the test room with the dimension of 3.62m long by 2.44m wide by 2.43m high. The wall system was built in the way of a typical residential construction, and its main components are listed in Table 4.2.

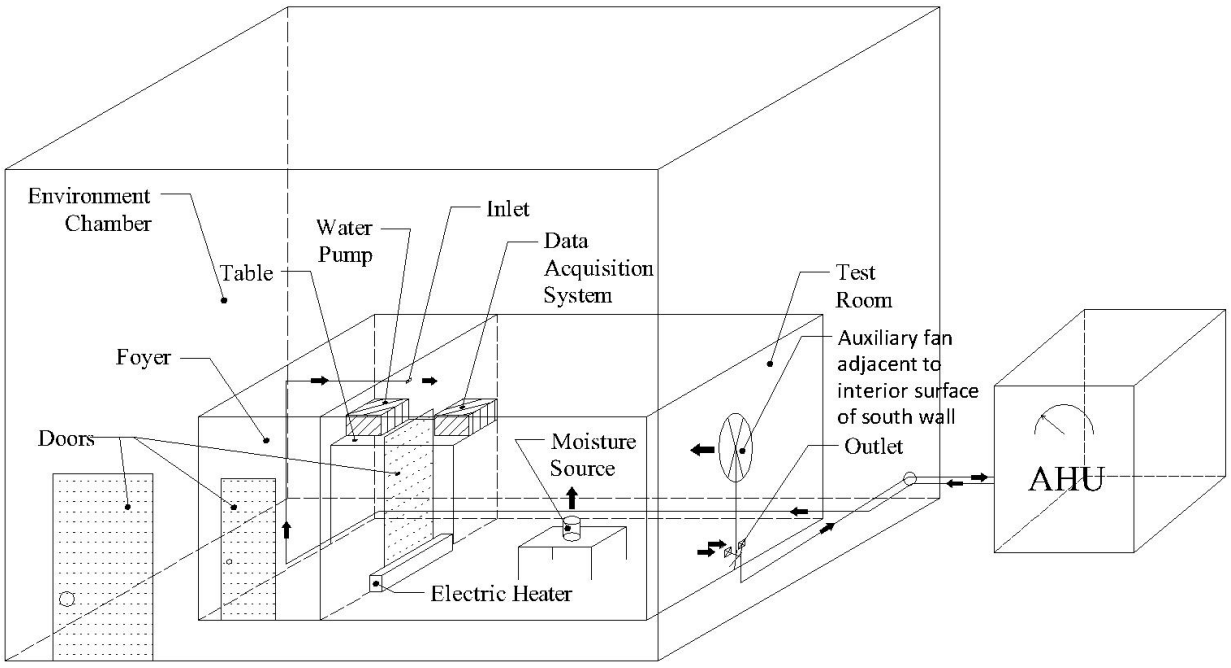

Fig. 4.7 Configuration of the test room connected with ventilation and moisture generation system

Table 4.2 Constituent layers of the wall assembly

Wall layers	Material
Outdoor surface	Vinyl siding
Air cavity	19 mm air
Air/weather barrier	Tyvek house wrap
Sheathing	Plywood (12.5 mm thick)
Stud cavity	Studs (2''×6'') 24'' cc and glass-fibre batt insulation
Vapor barrier	Polyethylene (0.15mm)
Indoor surface material	Gypsum board (12.5mm) and wood paneling (17.5 mm)

The inner layer of the west wall and east wall were covered with wood paneling; the rest of interior surfaces were covered by moisture impermeable material: 0.8 mm thick aluminum sheet (see Fig. 4.2). RH&T sensors, moisture pins, and thermocouples were embedded in the wall system (see Fig. 4.8) to monitor the wall's hygrothermal response. The details are described in the next section on monitoring.

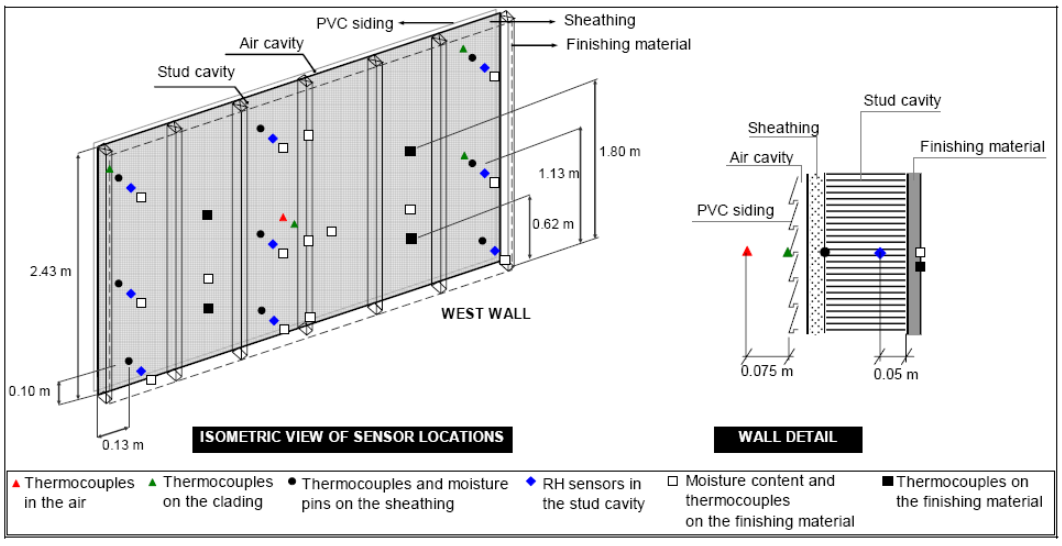

Fig. 4.8 Wall systems with sensors (from Fazio et al, 2007)

The entrances of the test room were located at north side. To avoid the disturbance of the entrance and to store the data acquisition system and moisture generation setups, a foyer room was built and; it was heated and subjected to outdoor winter weather condition during testing (see Fig. 4.5). At the bottom and back of the entrance door, an electrical baseboard heater (1 kW capacity) was attached. The heater was controlled by a thermostat to maintain the designed temperature inside the room.

4.3.3 Ventilation system

A closed-loop ventilation system, designed by Yang, Fazio, Ge & Rao (2011), circulated and conditioned the room air in this experiment. The system consisted of air handling unit (AHU), insulated piping, as well as inlet and outlet on the walls.

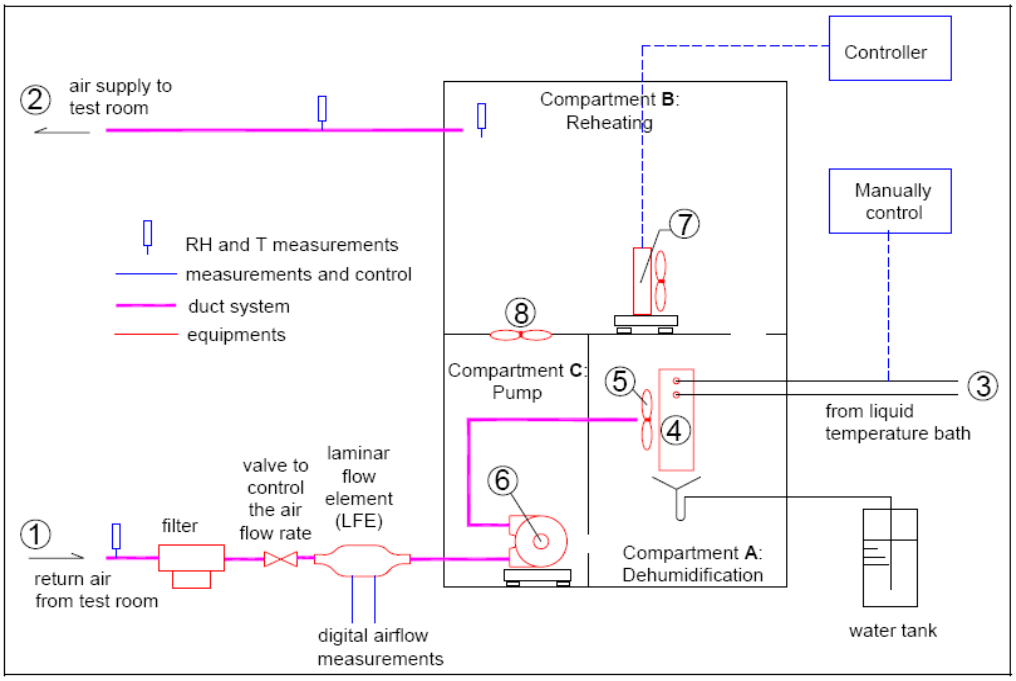

Fig. 4.9 Diagram of AHU (Air Handling Unit) (from Fazio et al., 2007)

The AHU (Fig. 4.9) maintained the conditions of supply air. The air (with water vapor) from the test room passed through a LFE (Laminar Flow Element) and went into the AHU chamber. A gate valve located between the LFE and the pump (6) could be turned manually to adjust the flow rate. Inside the AHU, the air passed through a liquid-to-air heat exchanger (4) which was cooled by the chilled water at constant temperature provided by a recirculating chiller (Fig. 4.10). Condensation on the dehumidifier was collected by the water tank and measured by a load cell located beneath the water tank. The cool and dehumidified air was heated up again by a heater (7) regulated by a PID (proportional integral and differential) controller to the desired temperature. The conditioned air was then supplied to test room through the insulated pipe (Fig. 4.10 b).

a) Recirculating chiller

b) Insulated pipe transports the supply and return air

Fig. 4.10 Equipment and pipe used in ventilation system

The position of the inlet and outlet inside test room can be seen Fig. 4.11. The inlet located at a higher position on the north wall with 170mm distance to the ceiling. Its dimension was 96.5mm long by 21.8mm wide. The outlet had two openings into ducts which joined behind the wall panel. It was located on the south wall at 172mm distance

from the floor. Its dimension was 135mm long by 85mm wide. The distance of the centers of the two openings is 301mm.

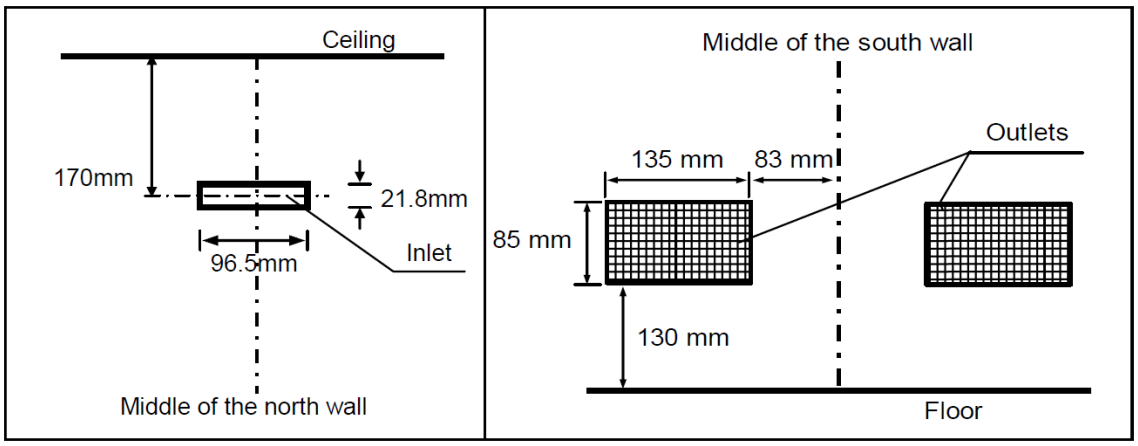

Fig. 4.11 Location and dimensions of inlet and outlets (from Fazio et al., 2007)

4.3.4 Moisture Generation System

The moisture generation system provided and monitored the water added into the test room. Three parts as shown in Fig. 4.12 completed the system. Distilled water in the water tank was pumped at a controlled flow rate into the stainless steel recipient. This recipient was heated by a hot plate and the content evaporated immediately. The water pump and hot plate were controlled on and off simultaneously by a multi-segment programmable timer. The water pump (peristaltic pump) was set at a set number of rotations per minute (RPM). The corresponding water amount pumped by the number of RPM is listed in Table 4.3.

Fig. 4.12 Moisture generation system

Table 4.3 Water transport amount corresponding to RPM (round per minute)

RPM	Corresponding water Pumped (gram/hour)
8.25	14
15	25
20	33
25	42
35	58.5
55	91

4.4 Monitoring and measuring

Over 200 sensors were used to monitor the hygrothermal responses. The sensors were sampled by a Data Acquisition System (DAS) and data were stored in a computer. The sensors set up and measurement were grouped and introduced according to their type and location in the test hut.

4.4.1 Inside Test Room

There were totally 33 RH&T sensors distributed inside the test room to measure the temperature and RH for the air, as shown in Fig. 4.13. The test room was divided by a grid of 6 along north-south direction and by 5 along west-east direction. The grid lines were denoted by letters (A, C, D, E, F, G) and numbers (1, 2, 3, 4, 5) respectively. 13 poles were positioned on some grid points as shown in Figure 4.13. The positions of these poles are shown as the small solid circles in the figure. For each pole, up-to three sensors were installed at heights of 62 mm, 124 mm and 185 mm from the floor, corresponding to the number of 1, 2, and 3 respectively. The sensors were labeled by the position of the pole and the height on the pole. For example, sensor A_11 was located on the pole on axes A and 1, and at the first height of 62 mm from the floor. After the preliminary test, some RH&T sensors were moved, but the name of labels did not change. Figure 4.13 shows the distribution of the RH&T sensors in the experiment. All the RH&T sensors except for the one marked by the big solid circle near the moisture source in Figure 4.13 are the RH&T HMP50 with an accuracy of 2% (Fig.14a). The big solid circle is the RH&T HMT333 with the accuracy of 1% (Fig. 14b), and is named as RH_room1 in the experiment. The temperature and RH values measured by these sensors were used to calculate the moisture content in the air in Eq. 3.49, and the measurement of sensor RH_room1 was utilized to represent the indoor environmental condition in the comparison of RH changes in different test cases.

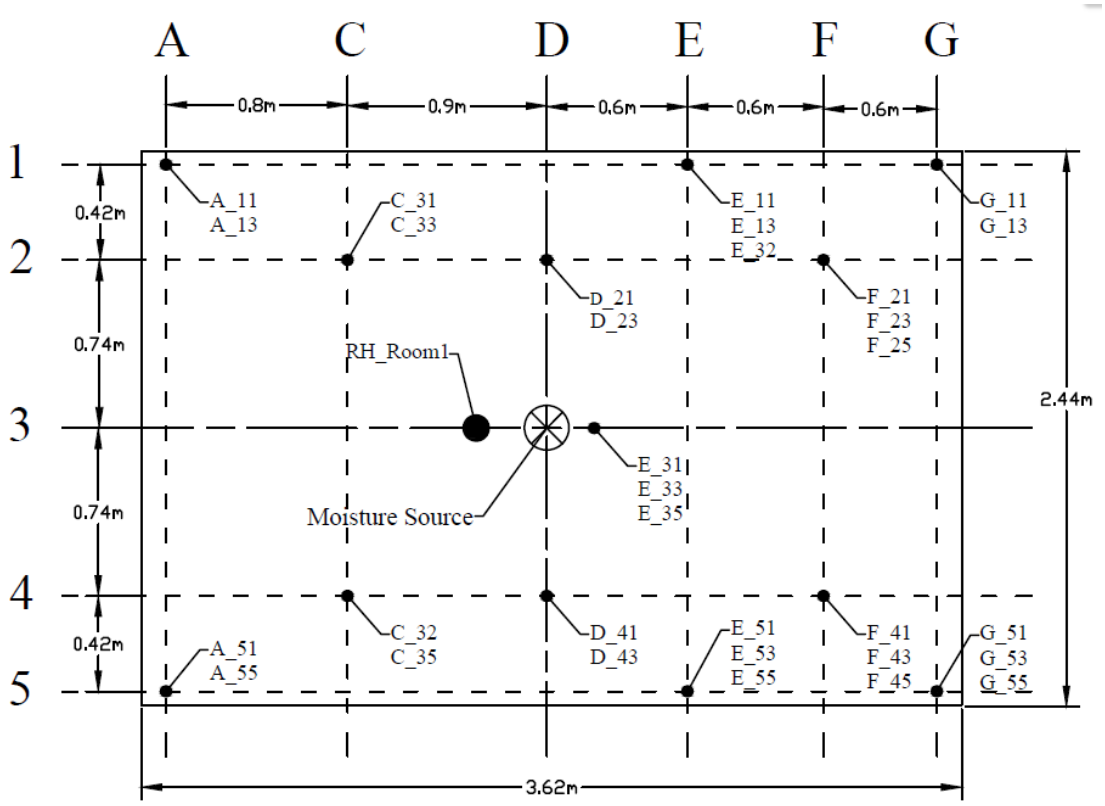

Note: The solid square represents the interior surface of the test room. For each solid circle, up-to three sensors were installed on a pole at heights of 62 mm, 124 mm and 185 mm from the floor, respectively.

Fig. 4.13 RH&T sensors distributed in the test room

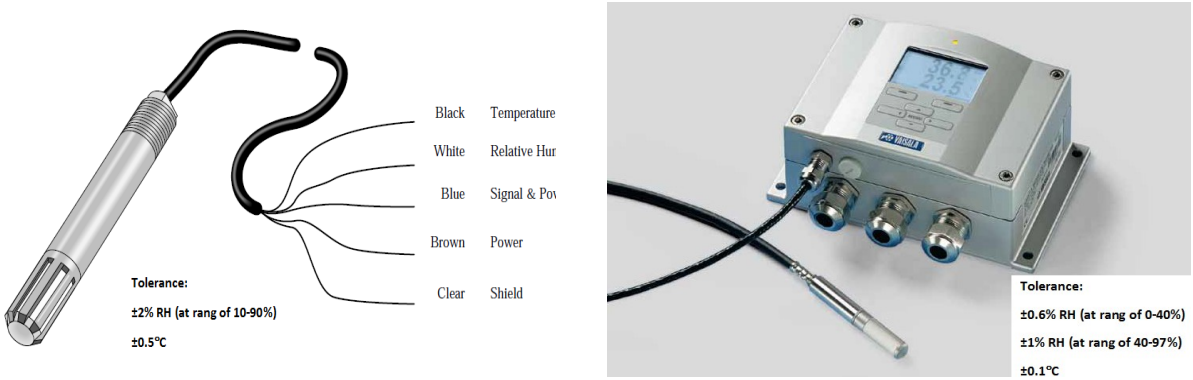

a)

b)

Fig. 4.14 RH & T sensors used in the experiment: a) HMP50 Temperature and RH Probe and b) HMT333 Humidity and Temperature Transmitter (both from Vaisala)

4.4.2 Sensors in wood paneling

Totally, 36 pairs of gold-plated copper pins were embedded in the wood paneling (Fig. 4.15). These moisture pins measured the wood's moisture contents. Since the moisture pins can only provide one-point information, and in this experiment the moisture distribution inside the wood paneling was not uniform, then there is a limitation using this measurement to calculate the moisture absorption amount by the wood paneling. These sensors measurements were utilized to monitor the moisture content changes but not for the calculation in this experimental study.

Fig. 4.15 Moisture pins utilized in the experiment (from Fazio et al., 2007)

4.4.3 Sensors inside stud cavities

In order to monitor the disturbance of temperature and relative humidity level inside the wall system, 14 RH&T sensors (Fig. 4.8) were installed at the centers of several wall cavities 2" from the drywalls. These sensors monitored the influence of the heat and moisture generated in the room on the temperature and RH distribution across the wall.

4.4.4 Inlet and outlet

Two RH&T sensors (HMT333) were installed inside the pipes to both the inlet and outlet to monitor the condition of supply air and return air. These data were used to calculate the moisture taken in/away by the ventilation system. The position of the RH&T sensors is shown in Fig. 4.16.

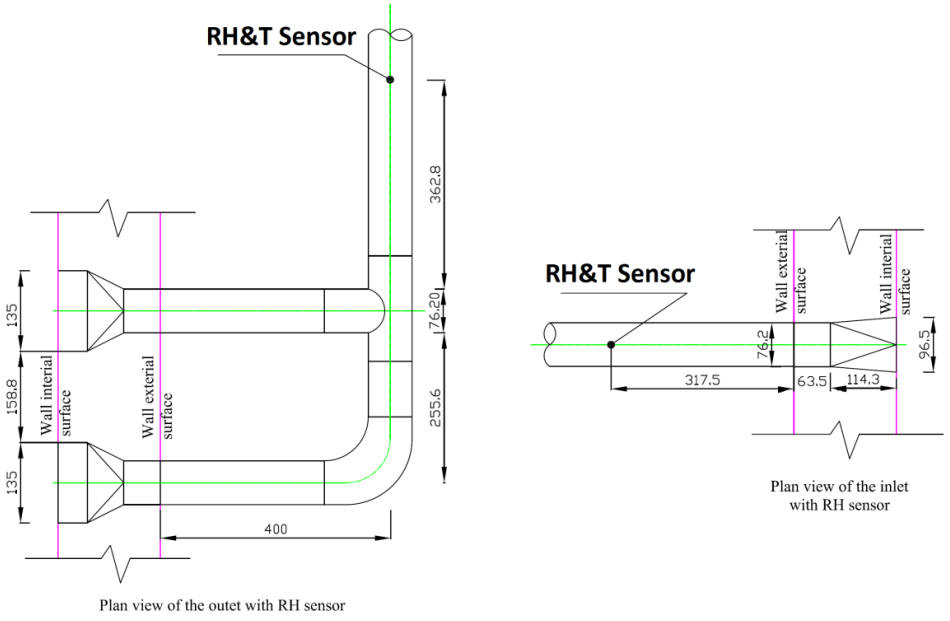

Fig. 4.16 Locations of RH&T sensor for outlet and inlet (from Fazio et al., 2007)

4.4.5 Other places

The thermocouples were attached on the electrical baseboard heater and on the cover of the hotplate to measure the temperature. This measured data was used in the numerical simulation.

There were some other RH&T sensors and thermocouples located inside AHU, buffer room zone, outside of test hut. These sensors were used to monitor the experiment

operation and to make sure the test functioned normally. Their measurements were not used in the experimental data analysis.

4.5 Preliminary Test Results

In this section, the preliminary experimental results are presented. As explained in previous sections, this experiment consists of two test steps, the non-hygroscopic test and hygroscopic test. In order to save the experimental testing time, all the non-hygroscopic tests were conducted first. Then the non-hygroscopic covers (plastic sheets) were removed, and the second steps of the tests were carried out.

The test results are shown from the observations of the indoor humidity changes first. The impact of the ventilation rate on indoor environment has been investigated by many other researches (Sandberg 1983; Roulet et al. 2002; Feriadi 2003). This experiment confirms this impact on indoor humidity level changes obtained by the ventilated condition cases. The moisture content changes inside wood paneling correspond to the room environment change and are illustrated by the measurements of the moisture pins embedded under the surface of the wood paneling. To precisely evaluate the wood paneling moisture buffering performance, the airtightness of the test room is investigated. The air leakage rates of the room under different indoor temperatures are evaluated. Finally, summary of the experimental protocol is presented.

4.5.1 Moisture changes and distributions inside test room

The changes of the relative humidity of air inside the room are not the same under different test conditions, and the moisture distribution inside the room is not uniform. For the hygroscopic test, the moisture is generated at the center of the room, diffuses to the whole room, and interacts with the envelope system. Figs. 4.17 and 4.18 show the relative humidity and temperature changes at the different locations from the beginning of the moisture generation in case 3 which is non-ventilation, 42 gram/hour MGR, and winter outdoor condition (-5 °C and 60 %RH). The differences among RH measured inside the room can reach to a maximum of about 10%. The temperature disturbances caused by the hot plate can be observed. The average room temperature rises half degree inside the room during the moisture generation.

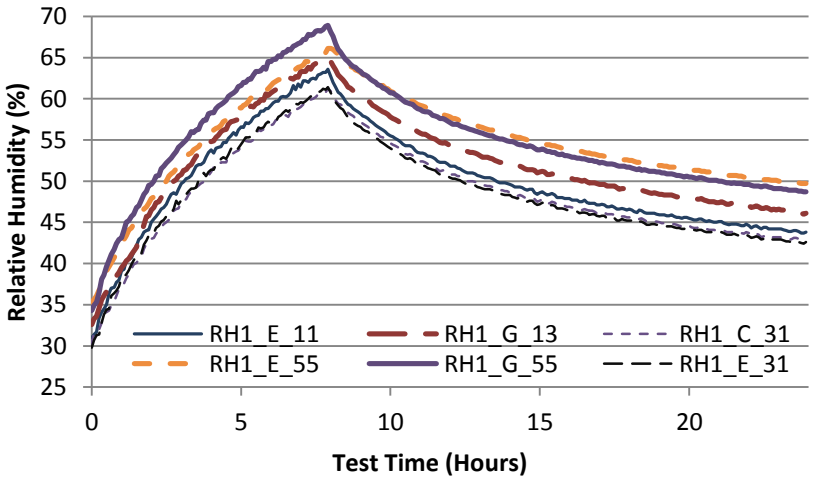

Fig. 4.17 RH distribution inside test room measured at different locations (see Fig. 4.13 for locations) in case 3 (00ACH, 42g/h)

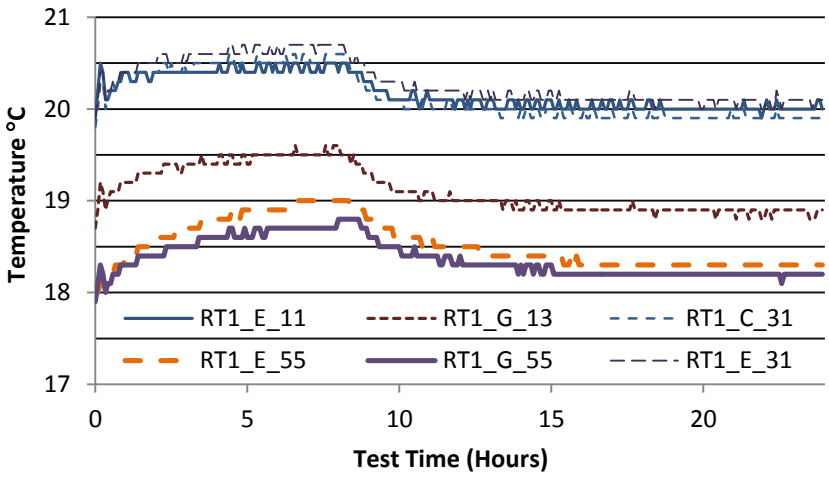

Fig. 4.18 Temperature distribution inside test room measured at different locations (see Fig. 4.13 for locations) in case 3 (00ACH, 42g/h)

The change of the ventilation rate influences the relative humidity level inside the test room. This change can be seen from Fig. 4.19, where, for the same generation rate of 42g/h, the indoor relative humidity level increases by 26.5% at 0.5 ACH and by 23% at 0.75ACH. The higher the ventilation rate is, the lower the indoor RH increases.

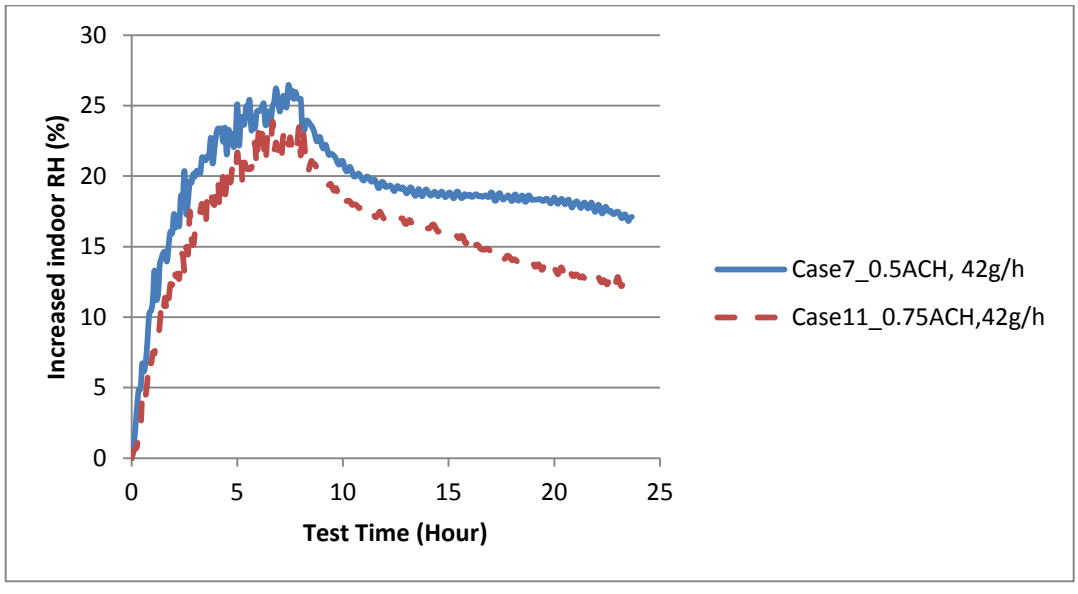

Fig. 4.19 RH changes in the test room at ventilation rates of 0.5ACH and 0.75ACH

4.5.2 Changes in the moisture content of the wood paneling

Variations in moisture contents of the wood paneling can be observed from the moisture pins measurements. For wood material, the electronic measurements based on pairs of metal probes/pins inserted into the materials are accurate for the moisture content range between 7% to the fiber saturation point (FSP) at about 28%. The utilization of metal probes to study the moisture changes inside the wall system has been widely adopted such as Teasdale (2006), Maref et al. (2003), and Simonson (2005). The advantage of using the electrical resistance measurement method is that it can directly obtain the moisture content in the dynamic transfer process. However, in this research, the whole panel moisture ab/desorption amount needs to be determined. The moisture distribution in the vertical, horizontal, and transverse direction will not be uniform during the transient moisture transfer process. The point measurement of the moisture pin is of limited value in the whole panel moisture change calculation. So the moisture pin calculation method was not used in the experimental analysis, but the pins were used to monitor the moisture changes inside the wood paneling. Fig. 4.20 shows the moisture content changes in the case of 00 ACH ventilation rate, 42 g/h MGR, and winter outdoor condition. The sensor notation adopted from the SRO project (Fazio et al. 2007) consists of three parts separated by underscores. The first part identifies the type of the sensor, and gMC1 in the figure means a resistive moisture content probe. The second part indicates the panel name where the sensor is located, for example, E1 means the first panel of the East wall. The third part shows the height index of the sensor. Ten heights were used with the index of 10 to 90. From Fig. 4.20, an average of

1% to 2% increases of moisture contents at the surface of the wood paneling is observed.

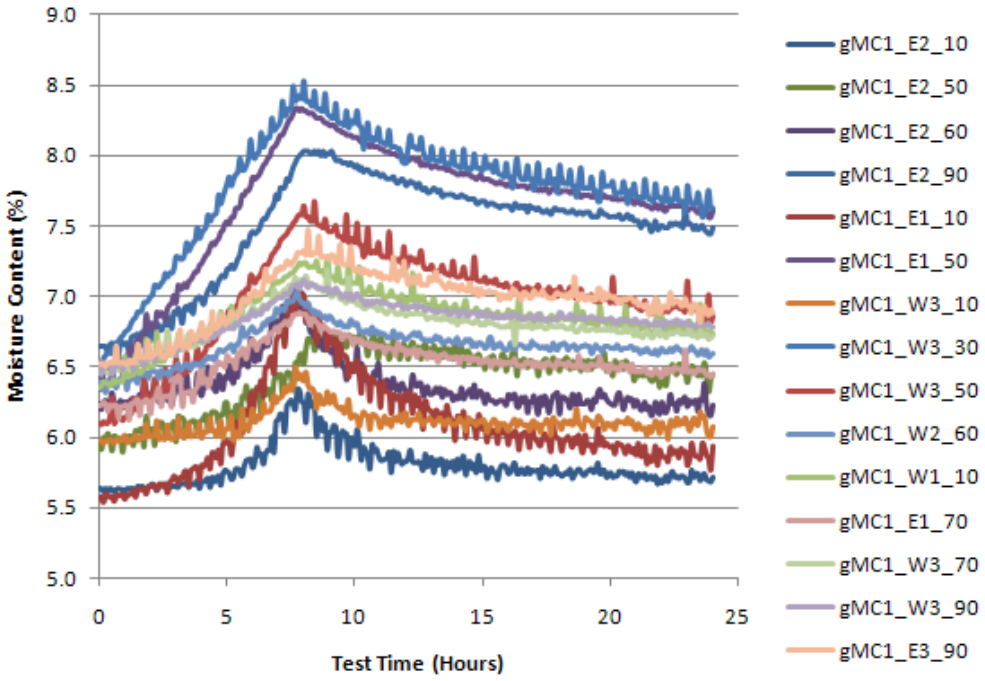

Fig. 4.20 Moisture contents measured by moisture pins in case 3 (00 ACH, 42g/h)

4.5.3 Temperature and humidity levels inside wall cavities

The measurements by the RH&T sensors located inside the wall cavities are shown in Fig. 4.21 and 4.22 for the case of 00 ACH, 42g/h MGR and winter outdoor conditions. For the RH&T sensors inside the cavities, a similar notation of the moisture pins was utilized. The notation of the RH&T sensor consists of three parts: the first part is the type of the sensor; the second part is the panel name where the sensor is located, for example, W2 means the second panel of the West wall; the third part is the height position of the sensor in the cavity. The height of the cavity is divided into 4, and index 1, 3, and 5 denote the height position of the 3 separation points from the ceiling to the floor. From

Figs. 4.21 and 4.22, a half degree temperature rise was observed, which corresponds to the indoor environment change caused by the hot plate. But the RH value in the cavities does not have significant change, which means that the vapor diffusing through the vapor barrier is a very little amount, and this is further studied by the numerical simulation presented in Chapter 7.

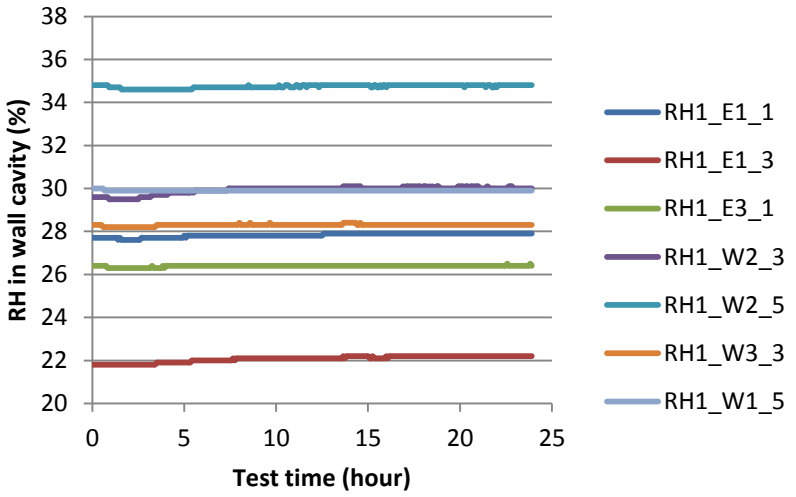

Fig. 4.21 RH variations measured by RH&T sensors inside wall cavities in case 3 (00ACH, 42g/h)

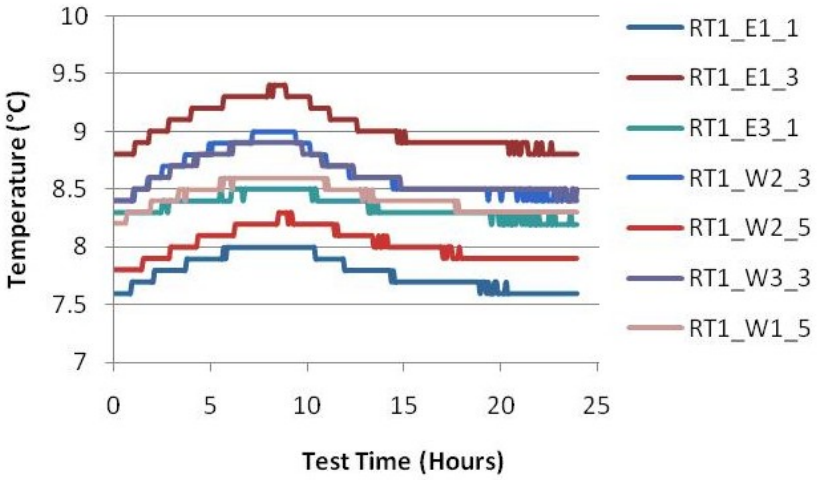

Fig. 4.22 Temperature variations measured by RH&T sensors inside wall cavities in case 3 (00ACH, 42g/h)

4.5.4 Repeatability of the test results

Differences in moisture responses of hygroscopic materials between the first and the two subsequent test cycles were found in some other studies (e.g. Osanyintola and Simonson, 2006). However, in this thesis research, the difference among the different cycles was found to be insignificant (Fig. 4.23). This insignificant difference was due to the consecutive tests in the hygroscopic tests. In the experiment, the formal test was preceded by a three-month preliminary test to examine the experimental setup and systems (ventilation, moisture generation, data acquisition, sensors function). During the preliminary test, the wall system was periodically subjected to room factor changes similar to those applied in the formal experiment at the same outdoor conditions (-5 °C, 68 %RH). The preliminary test ensured that the wood paneling was exposed to representative real life conditions and duration before the formal test began. Since the same wood paneling was used in the experiment, these repeated preliminary tests subjected the wood paneling to repeated load cycles similar to the consecutive cycles applied in other studies mentioned in previous sentences. Figure 4.23 shows no moisture response difference between the first and the two subsequent cycles in a preliminary test.

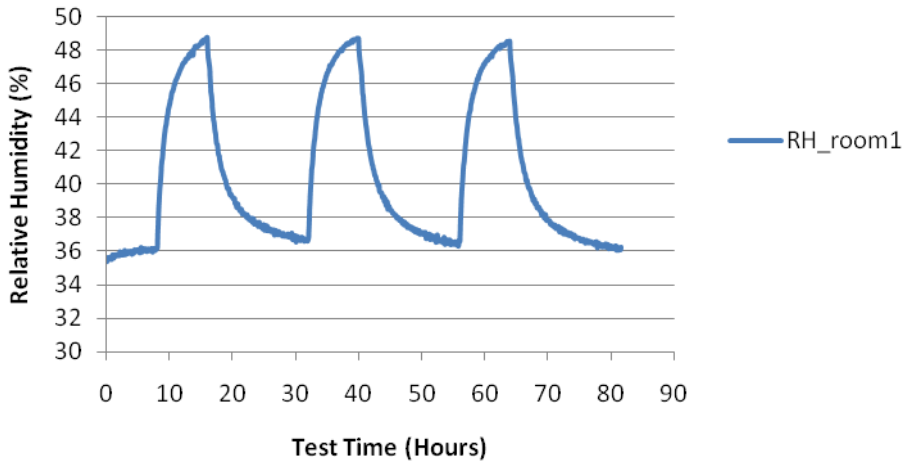

Fig. 4.23 Three cycles test measurement in the preliminary test showing no moisture response difference between the first and the two subsequent cycles

4.5.5 Equilibrium state in the case with 24 hours moisture generation

Fig. 4.24 and 4.25 show the measurements of indoor relative humidity and temperature in case 13. In this case, the moisture is generated at the rate of 42 g/h for 24 hours, and the ventilation rate is 0.5ACH. It is observed that under this test condition, the indoor temperature and humidity levels do not change at the end stage of the moisture generation. The heat and moisture have reached to equilibrium state. At this stage, the amount of the heat and moisture generated from the source is balanced with the amount losses through the ventilation, air leakage, and diffusion through the envelope. The whole system is under steady state. The measurements of the temperature and relative humidity levels were utilized to validate the simulation work which is introduced in Chapter 6.

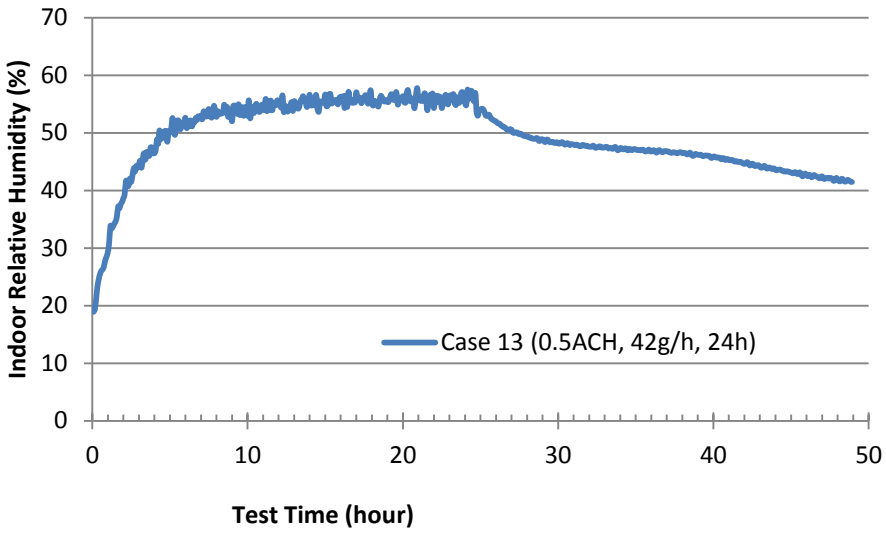

Fig. 4.24 Indoor RH changes in case13 with 24 hours moisture generation time

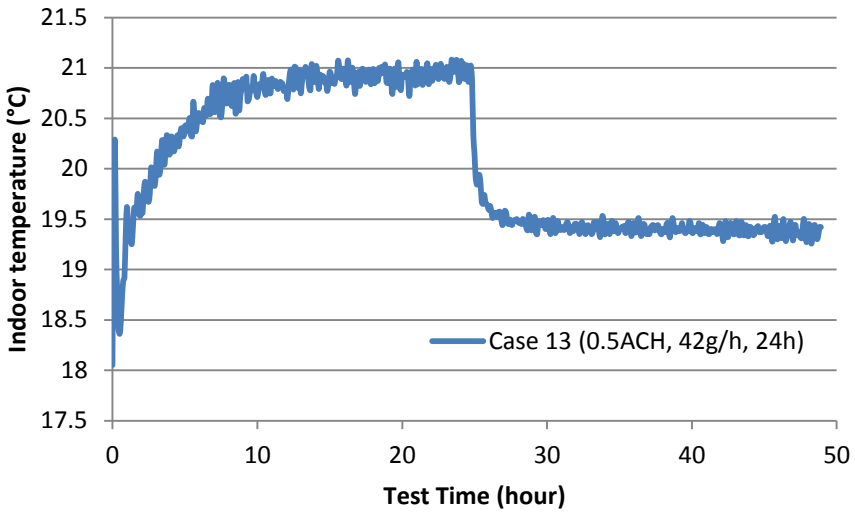

Fig. 4.25 Indoor temperature changes in case13 with 24 hours moisture generation time

4.5.6 Investigation on air leakage of the test room

Air leakage occurs in the test hut. The moisture losses due to the infiltration and exfiltration can be calculated through the product of the mass flow rate of the air and

the difference in humidity ratios between the infiltrating air and exfiltrating air. Under non-hygroscopic tests, after the moisture generation, the vapor pressure inside the room is higher than the outside. Fig. 4.26 shows the indoor RH level changes for the cases of non-ventilated condition at different test conditions. In the first 8 hours of the test, the indoor RH level increases as the moisture is generated from the moisture source. After the 8th hour cycle, the indoor humidity level begins dropping due to the air leakage. The air leakage rate is calculated through the decreases of the humidity ratio after the moisture generation stops in the non-hygroscopic tests with non-ventilation conditions. After the 8th hour, the decline of the moisture content in the test room is caused by the air leakage and is governed by:

$$Q \cdot w = -V(dw/dt) \tag{4.1}$$

where Q = air leakage rate (m^3/min)

w= humidity ratio (g/kg)

V= volume of the test room (m^3)

t = time (min)

Since the experimental data was recorded every 5 minutes, the unit in the leakage calculation is adopted as m^3/min rather than m^3/s.

Integration of Eq. 4.1 gives:

$$Q(t) = \frac{V}{t}(\ln \frac{w_0}{w}) \tag{4.2}$$

where w_0 is the humidity ratio at the time when moisture concentration begins recording.

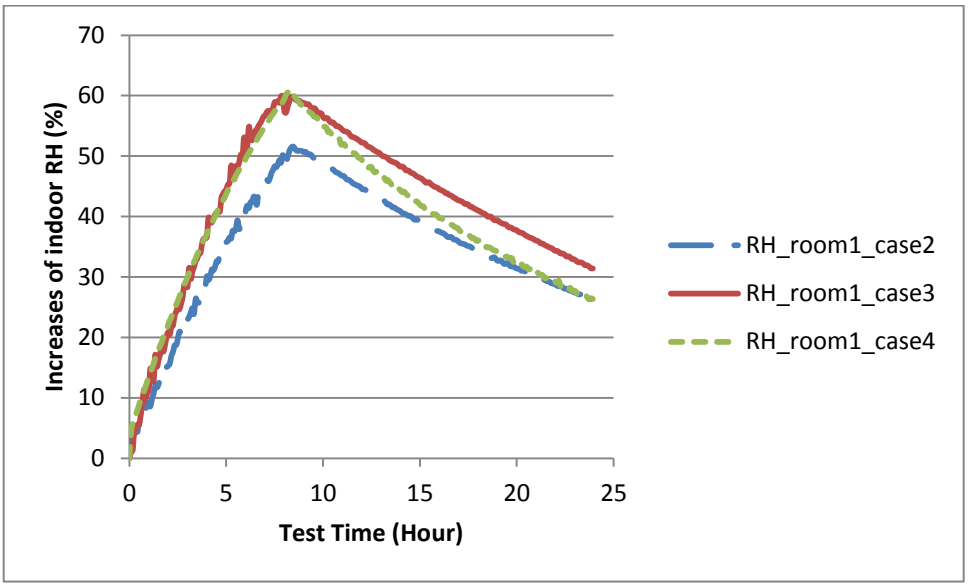

Fig. 4.26 Increases of indoor RH measured by sensor RH_room1at the center of the room in cases 2 (33g/h), 3 (42g/h), and 4 (42g/h, with auxiliary fan on)

The expression of the air leakage rate is a natural logarithm function over time. To avoid measurement errors at the moment when the moisture generation stopped, the data collected in the last 10 hours (14^{th} hour to 24^{th} hour) in a daily cycle is used in the calculation. Eq. 4.2 for cases 1 to 6 is calculated and plotted in MATLAB (Fig. 4.27).

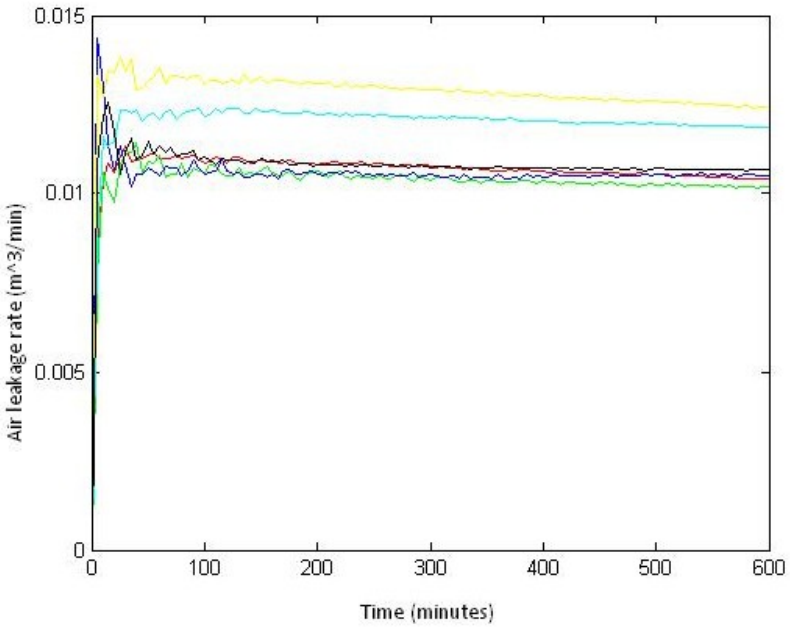

Fig. 4.27 Air leakage rates in cases 1-6 (red for case 1, green for case 2, blue for case 3, cyan for case 4, yellow for case 5, and black for case 6).

Fig. 4.27 shows that in each test case, the air leakage rate is about constant in the moisture decay period. The air leakage rates in cases 4 and 5 (Fig. 4.27) are higher than the rates in other cases. The higher leakage rates are due to the higher temperature in these two test cases. Fig. 4.28a shows the air leakage rate against the room temperature. A higher indoor temperature results in a relative higher air leakage rate, but the difference is only 0.002 m^3/min. The constant air leakage value in each test case and the consistent air leakage calculation result in the test cases with same indoor temperature indicate that the evaluation of the air leakage rate for the test hut is reliable without significant uncertainty. And as previously elaborated, this uncertainty in estimating the air leakage will not bring significant error in the calculation of moisture buffering effect for the two test series methods. Therefore, the linear relationship

between the air leakage rate and temperature is estimated by the least square method and is plotted as Fig. 4.28b. This linear function is applied to the ventilated test cases according to the average temperature in those cases.

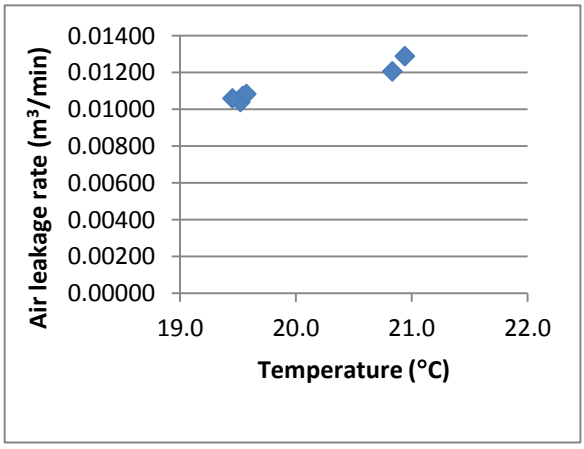

(a) Air leakage rate at different room temperatures

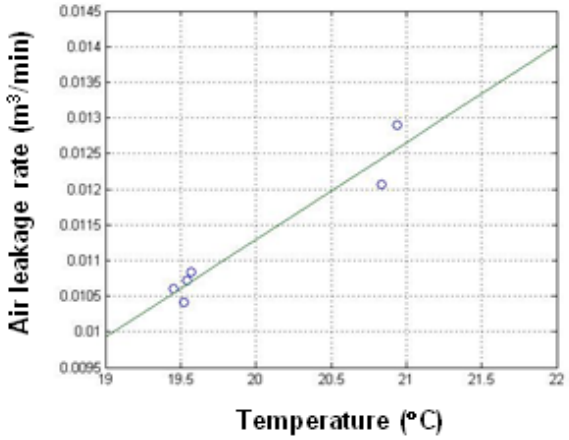

(b) Air leakage rate correlated with room temperature

Fig. 4.28 Air leakage rates at different temperatures (a) and their correlation (b)

4.6 Summary

In this chapter, the experimental setup, protocol, and preliminary results have been presented. The objectives of the experiment are to study the moisture buffering performance of wood paneling at room level, to investigate the influence of room factors on the buffering effect of wood paneling and on the indoor environment with the buffering effect of the wood paneling. The experiment consisted of 13 tests (Table 4.1): series 1, consisting of tests 1 to 6, had no ventilation in the test hut; series 2, consisting of tests 7 to 13, had ventilation. Each test was carried out in two steps. In step 1, the walls were covered with plastic sheets to avoid interaction between the hygroscopic material (wood paneling) and the moisture in the air. In step two, two of the walls with wood paneling were exposed to the air in the room. The moisture buffering performance of wood paneling under different test conditions can be calculated and presented in terms of the moisture ab/desorption kinetic curves, whose equation expression has been deduced. The test conditions are the different combinations of the room factors including ventilation condition, moisture generation loads, and the initial condition of the indoor relative humidity.

The preliminary results of the experimental tests have been presented in this chapter. The measurements of the indoor RH&T sensors show that the relative humidity and temperature inside the room are not uniformly distributed. The data from the moisture pins embedded inside the wood paneling indicate that the moisture content inside the wood paneling increases as the moisture is generated inside the room, and decreases

after the moisture generation stops. The moisture diffused through the vapor barrier to reach the wall cavity is only a small amount while the temperature inside the cavity increases and decreases corresponding to the indoor temperature changes. This information is obtained from the sensors inside the wall cavities. The air leakage of the test room is investigated through the decreases of the indoor moisture level after the moisture generation stops. The correlation of the air leakage rate with the indoor average temperature is obtained.

The following chapter presents the experimental results of moisture buffering performance of wood paneling at different room conditions. The experimental analysis of the indoor environment influenced by the room factors and the moisture buffering effect caused by the wood material is performed.

CHAPTER 5

EXPERIMENTAL RESULTS OF MOISTURE BUFFERING PERFORMANCE OF WOOD PANELING AND ITS EFFECTS ON INDOOR ENVIRONMENT

The preliminary test results in Chapter 4 show that the moisture distribution inside the test room is not homogenous. In order to take into account the non-homogeneous condition of indoor humidity, and therefore reduce sensor's measurement errors, the mathematical expression of the moisture buffering performance of wood paneling is developed in this chapter. A new index, EDRH (Effective Dampened Relative Humidity), is used to represent the moisture buffering effect of wood paneling on indoor environment. The experimental results including the buffering performance under different test conditions, the buffering effect influenced by room factors, and the magnitude of the room level buffering effect related to the characteristics of the structure are discussed. The discussion is based on the mathematical expression and calculation. The data analysis shows that the moisture response of the hygroscopic material at room level varies in different test scenarios. This variation is influenced by room factors, including ventilation conditions and the amount of moisture generation, and to a lesser degree by the indoor initial humidity conditions. Hence, the buffering effect cannot be predicted based on the material performance alone.

5.1 Mathematical expression of Moisture Buffering Performance (MBP) and Effective Dampened Relative Humidity (EDRH)

The moisture buffering performance of the wood paneling, which is defined as the dynamic moisture ab/desorption process during the test circle, can be expressed as Eq. 3.49, in Chapter 3. Since all parameters in the equation can be measured and determined by the sensors in the experiment, this equation represents a moisture ab/desorption curve as the function of time (t). Because the initial value of the moisture absorption is zero in the experiment, the maximum value of this equation can represent the moisture absorption performance. In this thesis, in some circumstances, the maximum value of Eq. 3.49, instead of the entire 24 hr temporal profile of ad/desorption, is used to represent the moisture buffering performance of the wood paneling.

The preliminary test results show that the moisture distribution inside the test room is not homogenous. The moisture distribution inside the room is a function of space and time, i.e.:

$$w_i(t) = w_i(x, y, z, t) \tag{5.1}$$

$$w_i^n(t) = w_i^n(x, y, z, t) \tag{5.2}$$

$$w_i(t_0) = w_i(x, y, z, t_0) \tag{5.3}$$

$$w_i^n(t_0) = w_i^n(x, y, z, t_0) \tag{5.4}$$

Then in Eq.3.49, the indoor humidity ratio is calculated as the average value of all the RH&T measurements.

Taking into account the non-homogeneous moisture distribution inside the test room, a new index, Effective Damped Relative Humidity (EDRH), is defined in this thesis to represent the moisture buffering effect caused by the hygroscopic material inside a room, which in this project is the wood paneling. Since this experiment investigates the dynamic moisture exchange between the wood material and its surrounding air, as well as its buffering effects, the highest RH value dampened by the hygroscopic material, i.e. the EDRH index is used to indicating the buffering effects. This index refers to the maximum difference of the average relative humidity in the test room between the two test conditions, and is expressed as:

$$EDRH = \frac{P_t * \Delta w_{\max}}{P_s * (0.622 + \Delta w_{\max})} \tag{5.5}$$

where P_t is the barometric pressure (Pa), and P_s is the vapor saturation pressure at 21°C, $\Delta w_{\max}$ is the difference of average humidity ratio increases in the air within the test hut between non-hygroscopic and hygroscopic tests and can be calculated from the measurement data by:

$$\Delta w_{\max} = \frac{1}{\rho V} MAX\left\{\left(\sum_{j=1}^{k} \rho v_j w_j^n(t) - \sum_{j=1}^{k} \rho v_j w_{ij}^n(0)\right) - \left(\sum_{j=1}^{k} \rho v_j w_j(t) - \sum_{j=1}^{k} \rho v_j w_{ij}(0)\right)\right\} \tag{5.6}$$

where ρ is the air density at 21°C, V is the room volume, j is the jth RH&T sensor, w_j is the humidity ratio measured by jth sensor, v_j is the volume around jth sensor and equals

to 1/33 of the room volume for all *j* values, and k is the total number of the RH&T sensors in the test room and equals to 33.

5.2 Moisture buffering performance of wood paneling under non-ventilated conditions

In the non-ventilated test stage, the air supply vents of the test room were blocked. The test room was subjected to moisture loads at different generation rates with different initial conditions and with or without an auxiliary fan to produce forced convection on the surface of the south wall. There were a total of 6 test cases in this stage as listed in Table 4.1. The purpose of these tests was to investigate wood paneling moisture responses under different room factors and to compare the performances to cases in the second stage in which ventilation was applied.

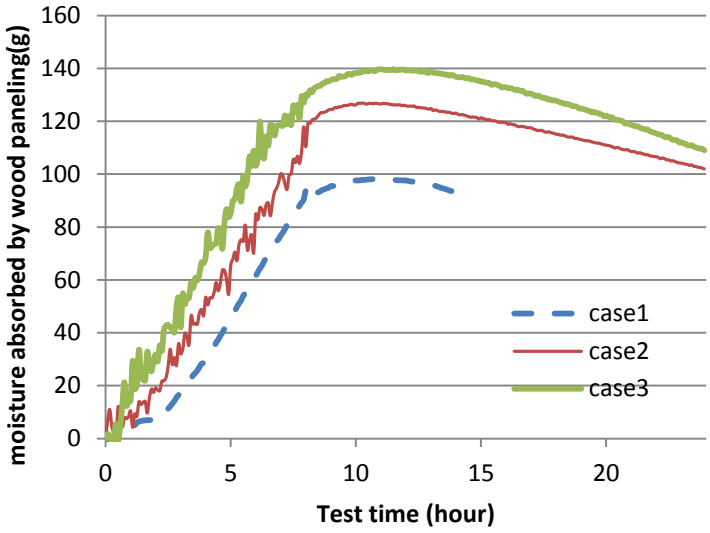

Fig. 5.1 Moisture absorbed by wood paneling in case 1 (25g/h MGR, 25%RH initial condition, as show in Table 2), case 2 (33g/h, 20%RH) and case 3 (42g/h, 30%).

Fig. 5.1 shows the temporal profiles of moisture absorption in the first three cases with the measured moisture generation rates (MGRs) at 25.8 g/h, 32.7 g/h, and 42.2 g/h, respectively. The maximum amounts of moisture absorbed are 98 gram, 127 gram and 140 gram, respectively. It is expected that the moisture absorbed by the wood paneling increases as the MGRs increase in the tests. The higher MGR results in a higher humidity level in the test room, which leads to higher moisture absorption. In case 1, a total of 206 gram of water is evaporated into the room, 47.5% of which is absorbed by the wood paneling. The corresponding percentages in cases 2 and 3 are 48.6% and 41.5% with respect to the evaporated water amount of 261 gram and 337 gram, respectively. In each test case, part of the moisture is absorbed by the wood paneling, part of the moisture exfiltrates through air leakage, while the rest of the moisture remains in the room air after the 24-hour test period. The high humidity level at the end of the test period stops the wood paneling from releasing the absorbed moisture and return to its initial moisture level as shown in Fig. 5.1

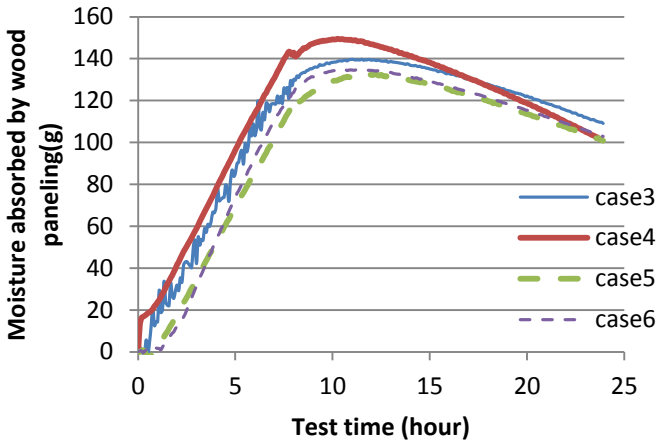

Fig. 5.2 Moisture absorbed by wood paneling in cases 3, 4, 5, and 6 (with the same 42g/h of water evaporation rate, with 30%, 28%, 33% and 25% initial RH, respectively, and with the auxiliary fan on in case 4).

Fig. 5.2 shows the moisture responses in the wood paneling in cases 3 to 6. These four test cases have the same MGR of 42 g/h, but with different initial room conditions or, as in case 4, with the auxiliary fan turned on. The maximum moisture absorbed in these four test cases is 139 gram, 150 gram, 133 gram and 135 gram, respectively. Case 4 has the highest maximum moisture absorption, and its release slope is steeper than the other three cases. In case 4, the air movement in the test room caused by the fan helps the wood paneling to absorb more moisture during the generation period and to release moisture faster during the decay period. The differences in the moisture absorption of the other three cases are small. This indicates that the initial room condition has only a small effect on the maximum moisture absorption amount in the wood paneling. The small difference in the moisture absorption may be attributed to the nonlinear isotherm absorption property of the pine used for wood paneling. For the same moisture load, with different starting points, the nonlinear absorption property of wood material results in different levels of moisture absorbed.

In all 6 cases, moisture absorption of the wood paneling continues after the moisture generation ends, since under non-ventilated conditions, the indoor humidity levels do not drop immediately after the moisture generation stops, thus allowing the wood paneling to continue to absorb moisture. Table 5.1 lists the maximum moisture

absorption amount and its corresponding time in each case. The moisture generation ends at the 8th hour, and the maximum moisture absorption in these non-ventilated cases occurs at hour 10.2 to 11.6. An average of 3 hours delay is observed.

Table 5.1 Maximum moisture absorbed by the wood paneling in a 24 h cycle and corresponding time in non-ventilated test cases

Case Number	Time required for maximum moisture absorption to occur		
	Moisture generation rate (g/h)	Maximum moisture absorption(gram)	Time (h)
1	25	98.1	10.8
2	33	126.8	10.2
3	42	139.6	11.5
4	42	149.5	10.5
5	42	132.5	11.6
6	42	134.0	11.2

5.3 Moisture buffering performance of wood paneling under ventilated conditions

Fig. 5.3 shows the ab/desorption responses of wood paneling based on the calculation of Eq.3.49 using experimental data. Comparing with non-ventilated condition tests, ventilation has a significant effect on the maximum moisture absorbed by the wood paneling. The MGRs in tests under ventilated conditions are equal to or larger than those in the non-ventilated conditions tests. Except for case 10, in which the generation rate reaches 91 g/h, the amounts of maximum moisture absorbed in this test series are

less than the amounts in the previous test series (cases1-6). This reduction in moisture absorption is due to ventilation which reduces the indoor humidity level.

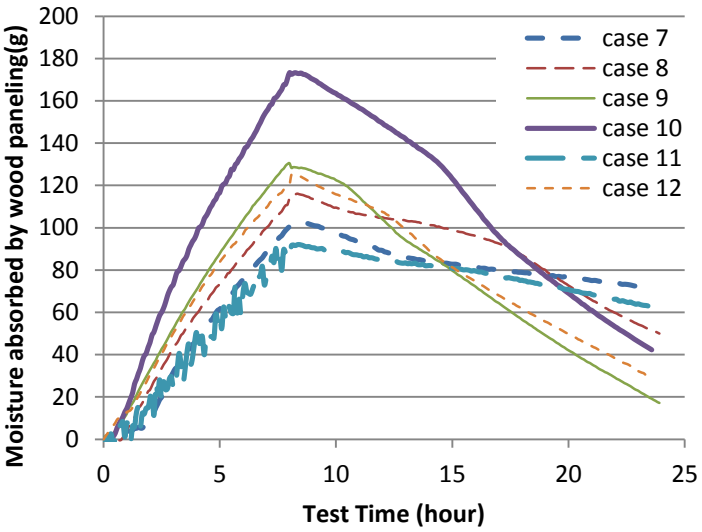

Fig. 5.3 Moisture absorbed by wood paneling in ventilated cases

The moisture buffering performance of wood paneling at room level is influenced also by the MGRs and indoor initial humidity levels. In case 7, with a ventilation rate of 0.5 ACH and a MGR at 42 g/h, the maximum moisture absorbed (102 grams) over 8 hours is 14 grams less than that of case 8 with the same ventilation rate, but a higher MGR of 58 g/h. With the same ventilation rate, a higher MGR results in a higher indoor humidity level. Consequently, the wood paneling absorbs more moisture. This process can also be observed in case 10, in which the generation rate is 91 g/h and the amount of maximum moisture absorption amount reaches 173 gram. Fig. 5.4 shows that in these three test cases the indoor RH increases since the moisture begins generating. Under the same ventilation rate of 0.5 ACH, the increases in the indoor relative humidity levels

are 26%, 32.5% and 43% and the moisture absorption amounts are 102 gram, 116 gram and 173 gram, respectively, corresponding to MGRs at 42 g/h, 58 g/h and 91 g/h. hence the moisture absorbed by the wood paneling increases as the MGR increases. However, the increases in absorption are nonlinear with respect to the increases of the MGRs.

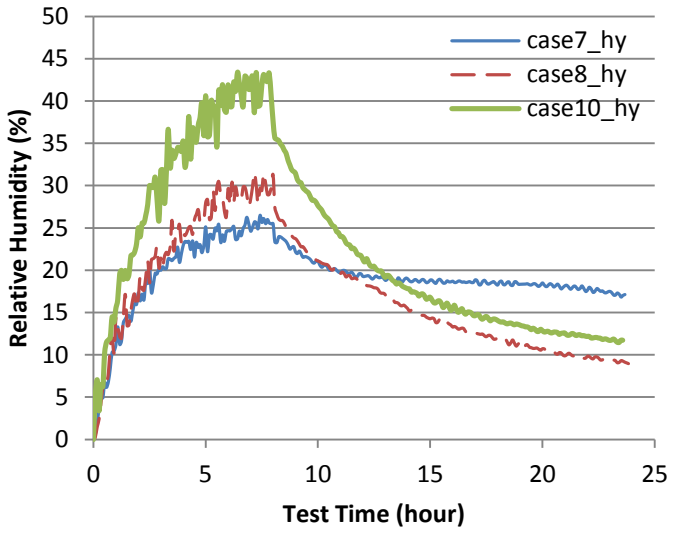

Fig. 5.4 Indoor RH increments in the hygroscopic test of cases 7 (0.5ACH, 42g/h), 8 (0.5ACH, 58.5g/h), and 10 (0.5ACH, 91g/h)

Under non-ventilation condition, the auxiliary fan at the south wall helps the wood paneling to absorb moisture faster during the uptake stage and to release moisture faster after the moisture generation ends. A similar influence is observed under the ventilation condition. About 25% more moisture is absorbed in the case with the fan on (case 9 compared to case 8). This higher absorption is not caused by the higher indoor humidity level. In fact, when the fan is turned on, the indoor RH increases are lower as shown in Fig. 5.5. Two reasons lead to the lower indoor RH level in case 9. One is the result of the more moisture absorbed by the wood paneling, and the other one is that

the fan makes the indoor moisture content more uniform, which increases the ventilation efficiency. Even with a lower indoor humidity level, the moisture absorbed is higher. This absorption increase would indicate that the forced convection caused by the fan can significantly increase the moisture exchange between the wood paneling and its surrounding air.

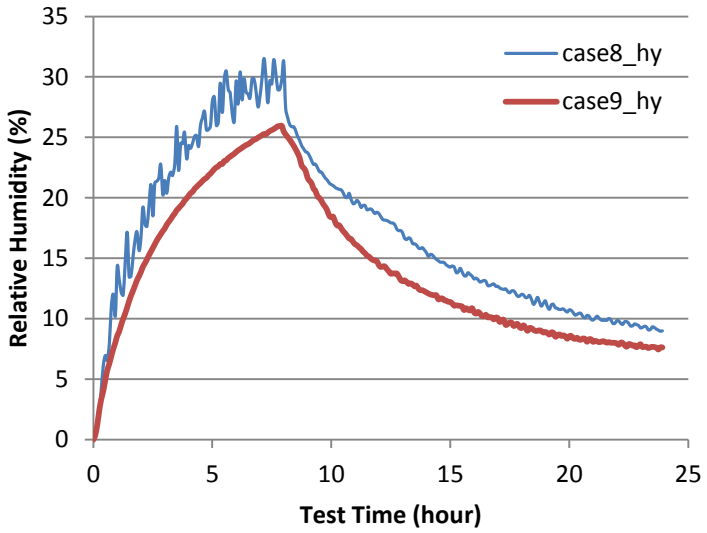

Fig. 5.5 Indoor RH increments in the hygroscopic test of cases 8 (fan off) and 9 (fan on) both with 0.5ACH, 58.5g/h

5.4 Investigation of moisture buffering effect on indoor environment

Under the same MGR, the ventilation rates of 0.5 ACH and 0.75 ACH have different impact on the moisture absorption of wood paneling and on the indoor environment. It is expected that the higher ventilation rate provides a faster air movement in the test room, and results in more moisture absorption. However, the moisture responses of the wood paneling depend not only on the condition of the wall surface, but also on the

indoor environment. Fig. 5.12 shows that under 42 g/h MGR, the indoor RH increases, measured at the same RH&T sensor (sensor room-1) at 0.5 ACH (case7) and 0.75 ACH (case 11), are 26% and 23%, respectively. The higher ventilation rate carries away more moisture and results in a lower indoor humidity levels. The lower humidity level makes the wood paneling absorb less moisture. The moisture amount absorbed by the wood paneling at 0.75 ACH is 10 gram less than that at 0.5 ACH (Fig. 5.3). On the other hand, the less absorption helps to increase indoor humidity levels. This opposing influence can also be observed in the lower ventilation rate of 0.5 ACH. For the same MGR, the indoor humidity levels at 0.5 ACH ventilation rate are higher than those at 0.75 ACH case due to the lower moisture amount carried away; then this higher RH level results in a higher moisture absorption amount in wood paneling. Again, the higher absorption dampens the indoor humidity level. This process is the buffering effect, and it keeps the indoor environment at a balance. In summary, the ventilation rate varies the indoor humidity level, and this variation is dampened by the hygroscopic material.

The influence of ventilation on the indoor environment can also be seen in the non-hygroscopic test for which there is no hygroscopic material interaction involved. In the non-hygroscopic test of cases 7 (0.5ACH, 42g/h) and 11 (0.75ACH, 42g/h) as shown in Fig. 5.12, the RH levels increases are by 35% and 32%, respectively. Without the influence of the hygroscopic materials, the MGR has a larger impact on the indoor humidity levels. Compared with the hygroscopic tests, about 8% RH increase in case 7 and 9% RH increase in case 11 are observed. The dampened RH by the hygroscopic

material is the moisture buffering effect. The RH increases measured at different locations are noted to vary in each test case. For example, in the hygroscopic test, the RH increase measured by sensor C31 is 28% in case 7 and 24% in case 11 (Fig. 11). Whereas sensor RH_room 1 is observed to measure 1.5% different from sensor C31 in case 7 and 1% difference in case 11. In order to take into account the non-homogeneous indoor moisture distribution and avoid sensor's measurement errors, the average dampened RH based on Eq. 5.5 is adopted to represent the moisture buffering effect caused by the wood paneling.

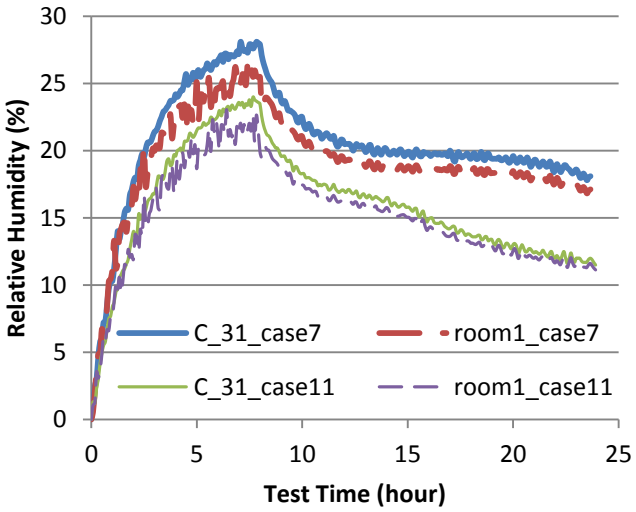

Fig. 5.6 Indoor RH increment measured at two locations in the hygroscopic cases 7 (0.5ACH, 42g/h) and 11 (0.75ACH, 42g/h)

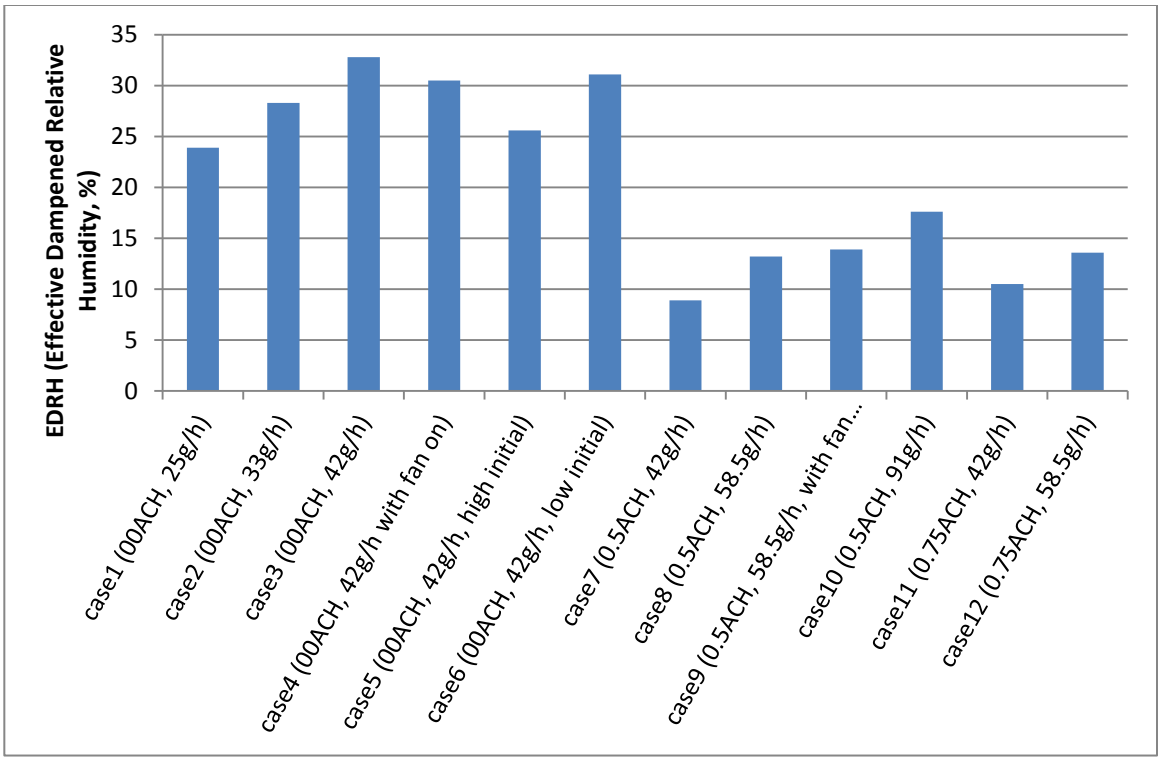

* EDRH is defined as the highest RH value dampened by the hygroscopic material in the experiment

Fig. 5.7 EDRH in all test cases 1-12 calculated from Eq. 5.5

In Figure 5.7, a significant difference of the moisture buffering effect between the non-ventilation condition (case 3) and ventilated condition (cases 7 to 12) can be observed. For the same MGR of 42g/h, the dampened relative humidity is 32.8% for the non-ventilated condition of case 3, 8.9% for the 0.5 ACH conditions of case 7, and 10.5% for 0.75 ACH condition of case 11. When comparing the wood paneling moisture responses in these three test cases, it can be noted that the dampened RH does not change in accordance with the wood paneling's moisture response. Over 8 hours, for the non-ventilated condition of case 3, the wood paneling absorbs 131 grams of moisture which is 29 grams more than the moisture absorbed in cases 7 and 45 grams more than the

moisture absorbed in case 11. The large value of the different moisture buffering effect between the non-ventilated condition (case 3) and the ventilated condition (cases 7 to 12) indicates that the indoor environment changes between the hygroscopic and non-hygroscopic steps in the non-ventilated test series are quite different from those in the ventilated test series. The dampened RH in non-ventilated cases is from 23% to 33%, while the EDRH in ventilated cases is only from 9% to 17%. This difference is partially caused by the presence of the hygroscopic material, which has different moisture buffering performance under different room conditions. It is also caused by the influence of the ventilation: for the non-hygroscopic test step, the indoor environment changes significantly under the non-ventilated condition, as shown in Fig. 5.8. Figure 5.8 shows that for the same moisture load, the non-hygroscopic test has much larger RH increase than the hygroscopic test. This is one reason why the EDRH in non-ventilated cases has higher values than in ventilated cases as shown in Figure 5.7.

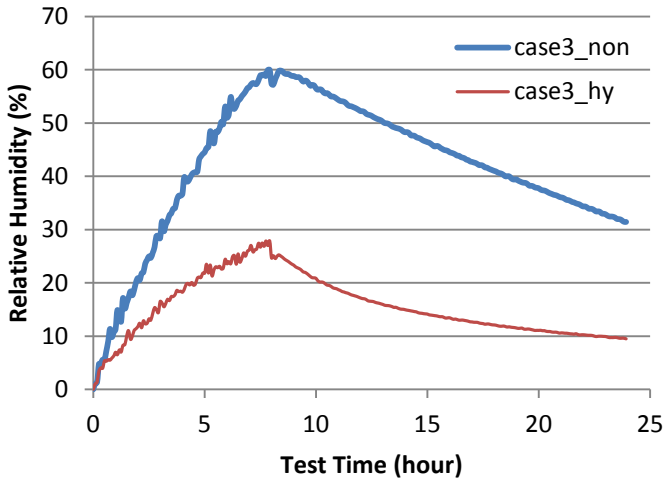

Fig. 5.8 Indoor RH increment in the non-hygroscopic and hygroscopic tests of case 3 (non-ventilated, 42g/h)

The influence of the ventilation on moisture buffering effect can be seen from another point of view. Under the same ventilation rate of 0.5ACH, cases 7 (0.5ACH, 42g/h), 8 (0.5ACH, 58.5g/h) and 10 (0.5ACH, 91g/h) have different moisture absorption amounts due to the different MGRs. When their absorption amounts are compared with the corresponding EDRH values, the influence of ventilation on moisture buffering effects can be observed. The moisture amounts absorbed by the wood paneling in these three test cases are 102 grams, 116 grams, and 173 grams, respectively. If there were neither ventilation nor air leakage, by calculation, these amounts of moisture removed from the room would represent a dampening effect of 25.7%, 29.2%, and 43.5% in the RH of the room, respectively, at 21°C. However, due to ventilation, the EDRH values from Figure 5.7 are only 8.9%, 13.2%, 17.6% for each case. Hence, the moisture buffering effects are reduced significantly by the ventilation conditions. This reduction can be seen in other ventilated test cases as well.

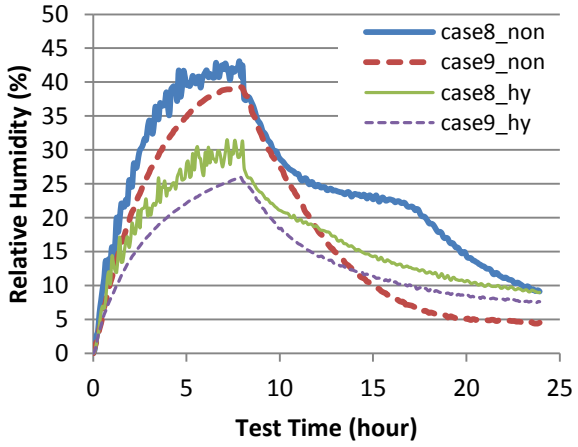

Fig. 5.9 Indoor RH increment in the non-hygroscopic and hygroscopic tests of cases 8 (0.5ACH, 58.5g/h) and 9 (0.5ACH, 58.5g/h, with fan on)

The larger buffering effect due to the more moisture absorption in the higher MGR cases can be observed by comparing case 10 (173g, 32.8%), which has the largest MGR of 91g/h, to all other ventilated cases (Fig. 5.7); case 8 (116g, 13.2%) to case 7 (102g, 8.9%) with an MGRs of 58.5g/h and 42g/h, respectively, and the same ventilation rate of 0.5ACH; and case 12 (125g, 13.7%) to case 11 (92g, 10.8%) with MGR of 58.5g/h and 42g/h, respectively, and the same ventilation rate of 0.75ACH. An exception to this relationship that the more moisture absorption can result in significant buffering effect is case 9 (13.8%) with an MGR of 58.5g/h and a ventilation rate of 0.5ACH, yet, in case 9, the wood paneling absorbs 130 grams of moisture, which is 14 grams more than the amount absorbed in case 8. This exception is attributed to the influence of the fan in case 9. Fig. 5.9 shows the RH measurements in the non-hygroscopic steps and hygroscopic steps in these two test cases. In the hygroscopic test of cases 9, the smaller increases in the indoor RH correspond to the larger moisture absorption. Whereas, the improved ventilation efficiency in case 9 due to the auxiliary fan results in a lower RH increment in both the non-hygroscopic and hygroscopic steps. Overall, the EDRH value in case 9 is about 5% higher than the EDRH in case 8. From these results, it is deduced that the fan can increases the moisture absorption by about 10% and the EDRH by around 5%.

5.5 Discussions

The moisture buffering performance of wood paneling at room level reflects the moisture sorption isotherm of the panel material and is influenced by the room

ventilation and the local conditions of the air near the material surface. Table 5.2 summarizes the moisture absorbed by the wood paneling, the increases of indoor RH levels caused by moisture generation, the ratio of moisture absorbed to RH changes, and the EDRH values in all the test cases. Under both non-ventilated and ventilated conditions, the moisture absorbed increases as the indoor RH rises, which corresponds to the sorption isotherm curve of the material. The ventilation lowers the indoor humidity, which reduces moisture absorption. For example, under non-hygroscopic tests, comparing cases 3 and 7, which have the same MGR of 42 g/h, case 3 with the non-ventilated condition has a relatively larger indoor RH increment (60 %) than the ventilated case 7 (35 %). This trend is consistent with the notion that, since more moisture remains in the test hut under the non-ventilated conditions, the more moisture is absorbed by the wood paneling. It is noted that values of moisture absorbed per unit increase in RH in the non-ventilated group are relatively larger than those in the ventilated group (Table 5.2). The increases in the ratio of moisture absorbed over RH increases may be explained by the fact that under non-ventilated conditions, the peaks of RH increases last longer, thus increasing moisture absorption (the nominator). This higher moisture absorption can be verified by observing the column of "ratio of moisture absorbed/ moisture generated" in Table 5.2, in which the percentages of moisture absorbed by wood paneling over the total moisture generated amount in the non-ventilated group are larger than those in the ventilated group.

One would anticipate that the higher air movement near the walls in ventilated cases should result in greater moisture absorption compared to that in the non-ventilated cases. However, this change in air movement for 0.5 ACH does not appear sufficient to cause a significant difference in the moisture absorption by the paneling. When moisture is generated, under non-ventilated conditions, the air movement near the wall surfaces is generated by natural convection due to the temperature difference between the wall surface and the indoor air, while under ventilated conditions it is a mixed convection with a low air flow coming from the inlet. Although it is difficult to quantify the differences in these two conditions, it may be assumed that their differences may not be significant.

These differences in air movement and in moisture absorption become significant, however, when an auxiliary fan is introduced to agitate directly the air over the panel surfaces as it was done in test case 9. This case has the largest proportion value, 5.0 g/% in Table 5.2. The premise that the fan improves absorption by the wood paneling can also be observed from the moisture sorption kinetic curves, Figures 5.2 and 5.3, in which cases 4 and 9 have the steepest rates of moisture absorption and release among the cases with the same moisture generation rate.

The presence of the hygroscopic material brings a significant change to the indoor environment, which can be seen from the comparisons of indoor humidity levels between non-hygroscopic and hygroscopic tests. The difference between these two

tests can be expressed by the EDRH index. The EDRH values in the test cases vary from 8.8 % to 17.5 % under ventilated conditions and are much larger under non-ventilated conditions, for instance, it is 32.8 % in case3. These high EDRH values indicate that the moisture buffering effect caused by hygroscopic material at the indoor surface layer of the enclosure is not negligible, and has to be taken into account in the prediction of the indoor environment.

Table 5.2 Moisture absorbed by wood paneling, their proportion to the moisture loads, and the indoor RH level increments in all test cases

Ventilation conditions	Case #	Ventilation rate (ACH) and fan$^{\zeta}$ condition (on or off)	Moisture generation, (gram)	Moisture absorption, (gram)	Ratio of moisture absorbed/ moisture generated (-)	Increase in indoor RH (%)*	Moisture absorbed per unit increase in RH (g/%)	EDRH values
Non-ventilated test cases	1	0 (off)	206.6	98.1	0.474	17.2	5.7	23.9%
	2	0 (off)	261.8	126.8	0.484	25.3	5.0	28.3%
	3	0 (off)	337.5	139.6	0.413	27.8	5.0	32.8%
	4	0 (on)	336.2	149.5	0.444	27.4	5.5	30.5%
	5	0 (off)	342.2	134.8	0.393	33.9	4.0	25.6%
	6	0 (off)	342.9	132.5	0.386	24.1	5.5	31.1%
Ventilated test cases	7	0.5 (off)	334.5	102.2	0.305	26.5	3.9	8.9%
	8	0.5 (off)	468.7	116.1	0.247	31.5	3.7	13.2%
	9	0.5 (on)	472.2	130.5	0.276	25.9	5.0	13.9%
	10	0.5 (off)	729.2	173.3	0.237	43.4	4.0	17.6%
	11	0.75 (off)	338.3	92.0	0.271	23.8	3.9	10.5%
	12	0.75 (off)	466.3	125.1	0.268	28.6	4.4	13.6%

* An RH increment is the measured difference between the indoor RH values at the start and end of the moisture generation cycle.

$^{\zeta}$Auxiliary fan at south wall

However, this buffering effect is not the dominant factor on the indoor humidity level for the ventilated tests. The room factors, i.e. the MGR and the ventilation rate, dominate the variation in the indoor environment. The buffering effect can only dampen this variation. This relative impact of various factors on the humidity level can

be seen from the comparison of the indoor environment change in any two pairs of ventilated test cases in Figures 5.10-5.13. At the ventilation rate of 0.5 ACH, the indoor RH level at the location of the RH&T sensor room-1 in the non-hygroscopic tests varies by 7 % due to the increased MGR from 42 g/h to 58.5 g/h (Fig. 5.10). The difference of this RH level in the hygroscopic tests is 5 %. Hence, about 2 %RH is dampened due to the presence of the hygroscopic material. At a ventilation rate of 0.75 ACH, the same increase of MGR from 42 g/h to 58.5 g/h produces differences in the RH value of 8 % and 5 % in the non-hygroscopic tests and hygroscopic tests, respectively (Fig. 5.11). For this case, the dampened RH value is 3 %. Figures 5.10 & 5.11 show that the indoor humidity responses of the test hut to the 130 g moisture load corresponding to an 8 h MGR is about 7 and 8 %RH variation at the relative low ventilation rate of 0.5 and 0.75 ACH, respectively; and the wood paneling has the buffering effect of dampening the RH by 2 and 3% out of the 7 and 8 %RH variation, respectively. Similarly, a change in ventilation from 0.5 to 0.75 ACH results in a RH variation of 4 % at a MGR of 42 g/h and of 3 % at a MGR of 58.5 g/h (Figures. 5.12 and 5.13). By inspection of these two figures, the buffering effect caused by wood paneling is about 1 % in Figure 5.12 and less than 1 % in Figure 5.13. From the above comparisons, it is observed that the room characteristics can cause up to 8 % variation in RH levels and that wood paneling can moderate these variations by up to 30 %.

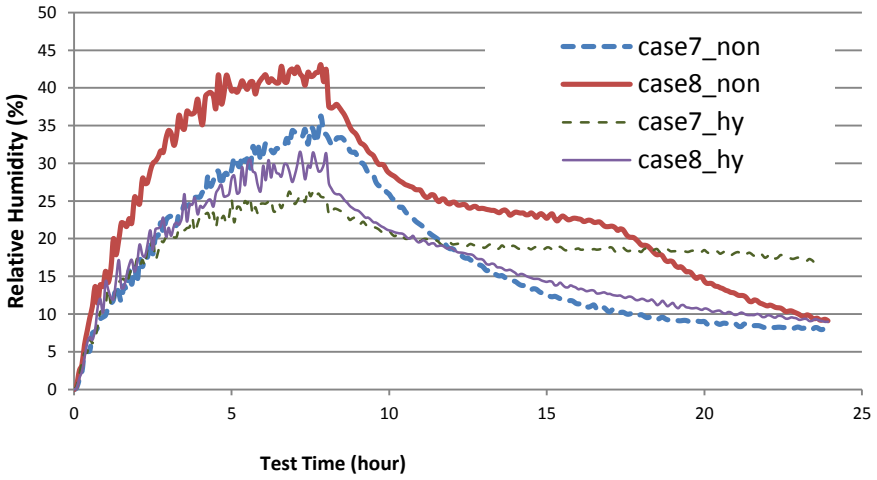

Fig.5.10 Impact of MGR on indoor RH levels at 0.5 ACH for cases 7 and 8

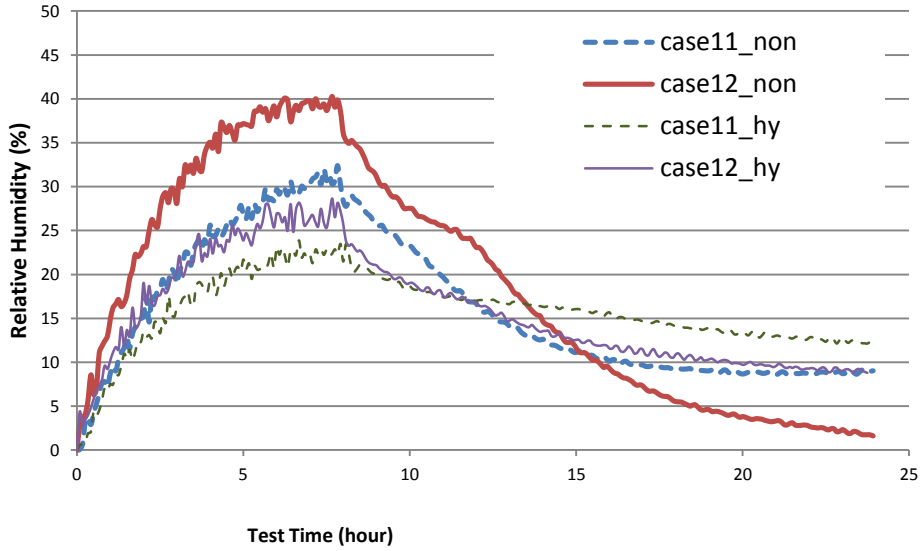

Fig.5.11 Impact of MGR on indoor RH levels at 0.75 ACH for cases 11 and 12

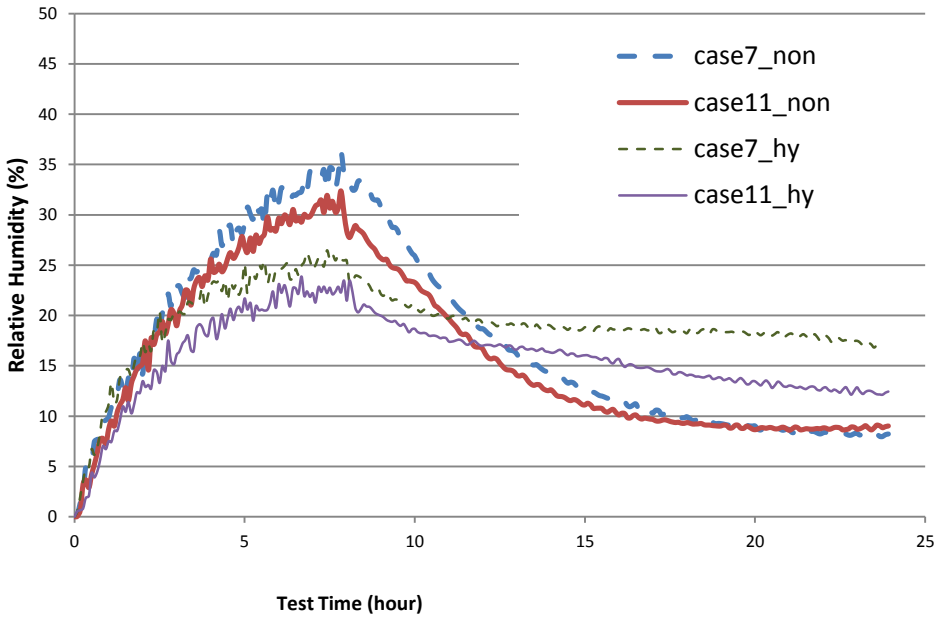

Fig.5.12 Impact of ventilation rate on indoor RH levels at 42g/h MGR for cases 7 and 11

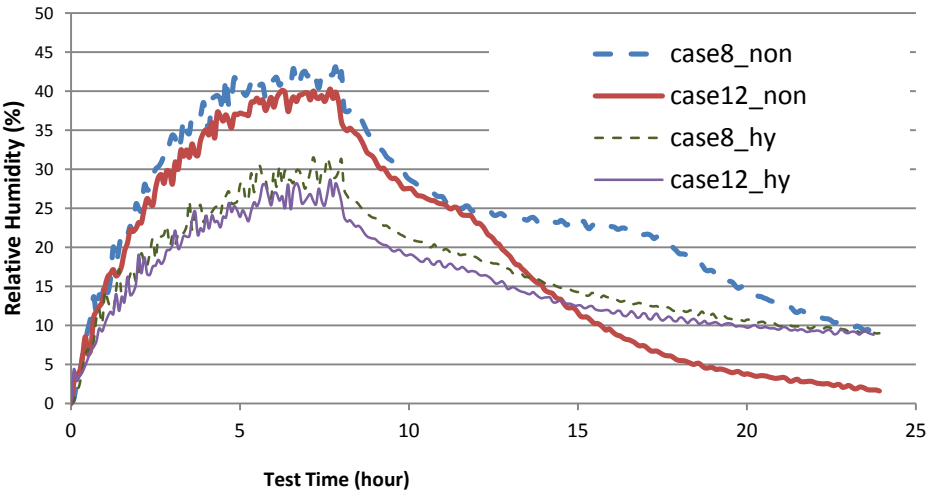

Fig.5.13 Impact of ventilation rate on indoor RH levels at 58.5g/h MGR for cases 8 and 12

5.6 Conclusions of the experimental investigation

The subject of moisture buffering has received considerable attention in the last decade. Some studies advocate the use of moisture buffering to moderate indoor humidity and to reduce energy consumption, while others indicate that the buffering effect may not be so significant in moderating indoor humidity levels. The main reason for the inconsistent findings is the lack of large-scale experimental investigation on the hygroscopic material buffering performance at the room level and its impact of this performance on the room environment. The whole building simulation may present the moisture transport process inside the room and into the enclosure, but many assumptions limit the analysis of the influence of room factors on the material buffering performance and the corresponding buffering effect.

This large scale experiment studies the room level moisture buffering performance of wood paneling and its buffering effect on the indoor environment. The study shows that the moisture response of hygroscopic material at room level varies under different room conditions. This variation is influenced by the room factors, including ventilation conditions, moisture loads, and to a more limited extent, by the indoor initial humidity conditions. For example, at 0.5 ACH ventilation rate, when moisture load increases from 42g/h to 58.5g/h, the moisture absorption amount of the wood paneling increases by 10%; with an auxiliary fan blowing against one of the walls, the absorption amount increases to 30%.

The moisture buffering effect of the wood paneling is related to its moisture responses at the room level. However the buffering effect cannot be predicted based on the material performance alone. When EDRH, defined as the highest RH value dampened by the hygroscopic material in the experiment, is used to represent the moisture buffering effect caused by the wood paneling, it shows that this value is related to the moisture absorption amount, the moisture generation conditions, the ventilation rate, and even the ventilation efficiency. By studying the relationship of the wood paneling buffering effect, its room level performance and the room factors, it is found that room factors are the dominating factors for the variation in the indoor environment.

By comparing the moisture buffering differences between the non-hygroscopic test and hygroscopic test, the study shows that this buffering effect is not negligible in the prediction of the indoor humidity level. At a ventilation rate of 0.5 ACH and MGR of 42 g/h, the indoor RH level is dampened by 8% by the wood paneling; while at a ventilation rate of 0.5 ACH and 91g/h, the dampened level reaches 17%. When the moisture load in the test room is increased from 42g/h to 58.5g/h, at a ventilation rate of 0.75 ACH, the indoor humidity increases by 8% and the moisture buffering of the wood paneling dampens the RH by 3%; while at the moisture load of 42g/h, the change in ventilation rate from 0.5 ACH to 0.75 ACH causes the indoor humidity to decrease by 4%, and the dampening of the RH, caused by wood paneling, by 1%.

From the above comparisons, it is observed that the room characteristics can cause up to 8% variation in RH levels and that wood paneling can moderate these variations by up to 30%.

CHAPTER 6

DEVELOPMENT OF COUPLED CFD MODEL FOR WHOLE BUILDING HEAT, AIR AND MOISTURE (HAM) TRANSPORT

In this chapter, the simulation model is introduced. The main purpose of the simulation is to calculate the indoor temperature and humidity levels taking into account the influence of wood paneling's moisture ad/desorption in a single numerical environment. In the experiment, the wood paneling was used as the interior finishing of the wall and was subjected to the air movement and humidity condition changes inside the room. The experimental results show that the moisture interaction between the wood paneling and indoor air is not negligible, and the dominant factors influencing the indoor environment are the room factors of moisture loads and ventilation conditions. The numerical model is first validated for the experimental test conditions, and then it is used to investigate the influence of more room factors on the indoor environment and on heat/moisture transport inside the wall system.

In this chapter, the simulation objective and review of the application of the COMSOL in building science studies are introduced first. The development process of the numerical model and its comparison with experimental results follow.

6.1 Numerical simulation in COMSOL

6.1.1 Objectives of the numerical simulation

The moisture transport in whole building can be simulated either by zonal-model or by coupled CFD model. For zonal-model, only the average indoor conditions and the average performance of the walls can be simulated. The CFD model has the advantage that overcomes the limitation of the zonal-model, but encounters another limitation. In currently available CFD software, there is no CFD model that the simulation of mass transfer can be extended from fluid region to solid region directly. In the whole-building moisture transport studies, the mass coupling between the indoor environment and the wall system is achieved by third party programming. Basically, the moisture flux on the surface of the wall calculated by CFD is used as the input for the wall model to determine the distribution of the moisture inside the wall material at each time step, and the mass fraction on the wall surface is calculated and sent back to the CFD model as the boundary condition for the next time step.

As reviewed in Chapter 2, in the Annex 41 research project (2004-2008) of the International Energy Agency (IEA), which was carried out to explore the complex physics governing the whole building heat, air and moisture (HAM) transfer, there were several models developed throughout this initiative to couple 3D CFD simulations with hygrothermal models of walls. For instance, Neale et al. (2007) solved the heat and moisture transport in air and porous materials by developing a simplified hygrothermal model in MATLAB that was coupled to FLUENT software. By using this model, the

moisture surface coefficient is calculated and compared with the Chilton and Colburn analogy results. But the finite difference model is difficult to extend or modify to fit new simulation conditions. Steeman et al. (2009a) used the effective penetration depth (EPD) approach to couple CFD and moisture transport inside the wall. By using this EPD model, the profile of indoor temperature and relative humidity can be obtained in the whole building simulation, and the local moisture behavior of the wall can be evaluated. While the EPD models do allow the simplified quantification, it has been argued that the reliance on the moisture penetration depth concept necessitates comprehensive material properties (Janssen and Roels, 2009). In the EPD model, the penetration depth, which is an estimation value based on the calculation of the sudden moisture level change on the surface of the material, has to be known in the model. This may limit the application and accuracy of the model.

Besides the Annex 41 project, other recent studies were carried out to couple CFD simulations with hygrothermal models of walls. Amissah (2005) coupled a 1D HAM model to a low-Reynolds number k–ε turbulence model, with independent execution and information exchanged at every time step. The HAM model supplied realistic boundary conditions for the CFD simulation, while CFD results supported direct modeling of convective mass transfer. Erriguible et al. (2006) coupled indirectly a 2D CFD model with a 2D hygrothermal material model. In these models, similar limitations can be found, and the main reason is that all these models are not simulated in one single simulation environment.

The objective of this thesis numerical simulation is to establish a coupled CFD model in a single simulation environment to study the HAM transport in the test hut influenced by the room factors. The experimental investigation presented in previous chapters shows that the moisture ab/desorption by the wood paneling has significant influence on the indoor environment, and the indoor temperature and humidity profiles vary under different test conditions. These test conditions consist of several parameters of the room factors including moisture generation rates and ventilation conditions. To predict indoor temperature and humidity levels, both the influences of the inner hygroscopic material of the wall (wood paneling in the experiment) and the room factors need to be taken into account. Even though the experimental work has extensively investigated the relationship of indoor environment changes with the room factors in the non-hygroscopic and hygroscopic tests, the parameters tested in the experiment and moisture transfer through the wall system are not fully investigated due to the limitation of the experimental facility, of the methodology and even of the time constraints in carrying out the tests. So a numerical method is utilized to further investigate the indoor environment and moisture transport process in the test room and inside the wall system influenced by the moisture loads and ventilation conditions.

In this chapter, a numerical model is presented, which couples CFD simulation of momentum, heat, moisture transport in the test room with the diffusion process of heat/moisture in the wall system. By utilizing this model, the distribution of the temperature and relative humidity inside the test room, the velocity profiles along the

wall surfaces and the ventilation condition including not only the ventilation rates but also the vent positions can be studied. Currently, numerical simulations model only steady-state processes. The numerical model was developed based on test case 13 with the 24 hour moisture generation period in which the indoor temperature and humidity level reached to equilibrium state. The implementation of this model and the parameters investigated by the model will be presented in detail in the next chapter.

To develop this model in a single simulation environment, the COMSOL software, a partial differential equation (PDE) based simulation environment, was used. In the following section, the introduction of this software and the application and validation of the COMSOL models for moisture buffering studies are reviewed.

6.1.2 Multi-physics models of COMSOL

Many science and engineering problems can be described by PDEs (Partial Differential Equations) and studied by simulation techniques. COMSOL (COMSOL 2008) is a powerful interactive environment for the modeling and solving these equations. In the COMSOL environment, the PDEs can be defined in the coefficient form, general form and weak form.

For a single dependent variable *u*, a linear or almost linear PDE is given in the coefficient form as follows (COMSOL 2008):

$$d_a \frac{\partial u}{\partial t} + \nabla \cdot (-c\nabla u - \alpha u + \gamma) + \beta \cdot \nabla u + au = f \qquad in\ \Omega \qquad (6\text{-}1a)$$

$$n \cdot (c\nabla u + \alpha u - \gamma) + qu = g - h^T \mu \qquad on\ \Omega \qquad (6\text{-}1b)$$

$$hu = r \qquad on\ \Omega \qquad (6\text{-}1c)$$

where

d_a is the mass coefficient

c is the diffusion coefficient

α is the conservative flux convection coefficient

β is the convection coefficient

a is the absorption coefficient

γ is the conservative flux source term

f is the source term

q is the boundary absorption coefficient

g is the boundary source term

μ is the Lagrange multiplier

In the coefficient form, the physical terms such as advection fields and sources are easy to identify. However, this form is not suitable for nonlinear problems due to the linearization algorithm. A general form is provided for the nonlinear problems in COMSOL as:

$$\nabla \cdot \Gamma = F \qquad in\ \Omega \qquad (6\text{-}2a)$$

$$-n \cdot \Gamma = G + (\frac{\partial R}{\partial u})^T \mu \qquad on\ \Omega \qquad (6\text{-}2b)$$

$$0 = R \qquad on\ \Omega \qquad \text{(6-2c)}$$

where Γ, F, G, R are coefficients which can be functions of the spatial coordinates, the solution u or the space and time derivatives of u .

There are many application modes available in the COMSOL environment that are built based on the PDEs. These modes, such as acoustics, diffusion, and heat transfer, provide predefined templates and interfaces that are easy for users to set up the simulation environment for that area of physics. For some particular fields of physics, the specialized modules are provided with the standardized terminology, material libraries, and the equations adapted to the specific area. For example, in the Chemical Module, the porous media flow can be described by the Darcy's law application mode or by the Brinkman equations application mode. The former is a common approach for the mass and momentum transport in a homogenous porous media, while the latter is for the case where the transport of momentum by shear stresses in the fluid is of importance.

COMSOL has especially provided the ways for building multi-physics models for the coupled field analysis. This coupling can happen in the sub-domains or on the boundaries. In the sub-domain the COMSOL multi-physics feature can combine two or several application modes or PDEs into a single model by adding them to the simulation environment. For the coupling on the boundaries where PDEs are needed to describe the boundary, the weak form can be used.

The name of the weak form is derived from mathematics. In the Finite Element Analysis, a PDE is multiplied by a test function and is then integrated. By using integration by parts and applying the Neumann boundary condition, the weak form of the PDE is obtained. The weak formulation poses a weaker condition on the solution than the strong formulation. The general form of the weak formulation in COMSOL is given as:

$$0 = \int_{\Omega} (\nabla v_l \cdot \Gamma_l + v_l F_l) dA + \int_{\partial\Omega} v_l (G_l + \frac{\partial R_m}{\partial u_l} \mu_m) ds \qquad \text{(6-3a)}$$

$$0 = R_m \qquad on\ \Omega \qquad \text{(6-3b)}$$

Note that the only automatically generated field variables are the shape function variables as default when the weak solution form is used. The test function variables, their space derivatives, time derivatives, and coupling variables can be defined in the software.

The three forms of the PDE description in COMSOL provide sufficient methods to present many scientific and engineering phenomena. In this thesis, the multi-physics feature of the COMSOL is utilized to model the momentum, heat and moisture transport process in the whole test hut. The simulation domain includes the room sub-domain and wall sub-domain. Before presenting the model development in detail, the application and validation of the COMSOL software in building science are reviewed in the next section.

6.1.3 Review of COMSOL application in building science

COMSOL has been used as a simulation tool in the building science research study recently. Van Schijndel (2008) established a simulation environment implemented in the software package MATLAB with the use of Simulink and COMSOL to model the dynamic heat, air and moisture processes in buildings and systems. The moisture transport through the wall system was modeled in COMSOL by taking advantage of its multidisciplinary application that COMSOL model can be exported directly to MATLAB and its family products and become an integral part of the dynamic system simulation. In that research, the reliability of the COMSOL simulation in building physics was evaluated through two different building problems, a 2D dynamic air flow problem and a 1D dynamic non-linear moisture transport in a porous material problem, and validated by the experiment measurements.

In the CRD project, Li, Rao, Fazio (2009) simulated moisture transport process across the 2D cross section of wood frame wall systems. The developed model coupled the moisture transport under non-isothermal condition and with the heat transfer for the wall assemblies. The governing equations for these two processes are defined as Eq.6.4 in which the air convection in the insulated cavity was calculated through the Darcy-Boussinesq equation or incompressible Navier-Stokes equation depending on the appropriate situation (Li, Rao, Fazio, 2009).

$$C\frac{\partial P_{suc}}{\partial t} = \nabla(-\delta_p \varphi \frac{dP_{sat}}{dT}\nabla T) + \nabla\left((K_l - \delta_p P_{sat}\frac{\partial \varphi}{\partial P_{suc}})\nabla P_{suc}\right) + \nabla(u \cdot \rho_v) \qquad \text{(6-4a)}$$

$$(\rho C_d + wC_w)\frac{\partial T}{\partial t} = \nabla\left((\lambda + L_v\delta_p\varphi\frac{dP_{sat}}{dT})\nabla T\right) + \nabla(L_v\delta_p P_{sat}\frac{\partial\varphi}{\partial P_{suc}}\nabla P_{suc}) - \nabla(v\rho_a C_{pa}T)$$

(6-4b)

The vapor and liquid transport with the air convection effects inside the wall assembly was included in the model. The wall assembly reflected the wall system situation in the CRD project. This COMSOL model was compared with the benchmark cases of HAMSTAD project and WUFI-PRO simulation results, as well as the experimental data obtained in the CRD project. The comparison showed good agreement between the COMSOL simulation and the others.

Lin (2007) used COMSOL to build a 3D model simulating the temperature distribution and air flow inside a dome covered zone and compared with his own 3D-TAF model. The dimensionless momentum and energy equations were derived by adding the buoyancy effect into the Navier-Stokes equation and by balancing the change in energy as equal to the heat source minus the diffusive heat flux. Combined with mass conservation, the governing equations described the absorption of solar radiation over the exterior wall surface, the conductive heat transfer through the wall, and the convective heat transfer due to the temperature changes inside the dome zone. By setting appropriate solver parameters, the converged solution was obtained and compared with the 3D-TAF model. Close agreement between the calculation of 3D-TAF model and the result of COMSOL simulation was found.

The application of COMSOL multi-physics and its coupling models validation can be further found in other studies, such as the study of the heat storing capacity of concrete walls with air cavities by Zhang and Wachenfeldt (2009); benchmarking the robustness and accuracy of COMSOL solver by Pepper and Wang (2009); the modeling of gas flow through porous sandstone and its experimental validation by Perera et al. (2011); and the numerical simulation of variably saturated flow with comprehensive geochemical reactions in two- and three-dimensional domains by Wissmeier and Barrya (2011). The studies reviewed above showed the reliability of the software as a simulation tool to perform multi-physics analysis in building science. In the following section, the development of the numerical model simulating the test room condition, the coupling process of the air movement inside the test room, and the heat/moisture transport inside both the test room and the wall system regions are presented.

6.2 Establishing a numerical model to simulate the test room

6.2.1 Mechanism of Heat, Air and Moisture (HAM) transport in the experiment

The objective of the simulation is to investigate the influences of room factors including moisture loads and ventilation conditions on the HAM transport inside the test room and the wall system. To numerically study these influences, the relationship of the room factors and the quantity of the temperature and humidity level in the test room and inside the wall need to be mathematically described and solved. To establish the relationship in the numerical model, especially in the CFD model which needs large

computational resources, the problem needs to be defined with some assumptions. The assumptions made about the system should not affect the accuracy of the mathematical model. The problem's spaces, i.e. the simulation domain and sub-domains are introduced in this section, the governing equations and the coupling process, as well as some assumptions are explained in the following sections.

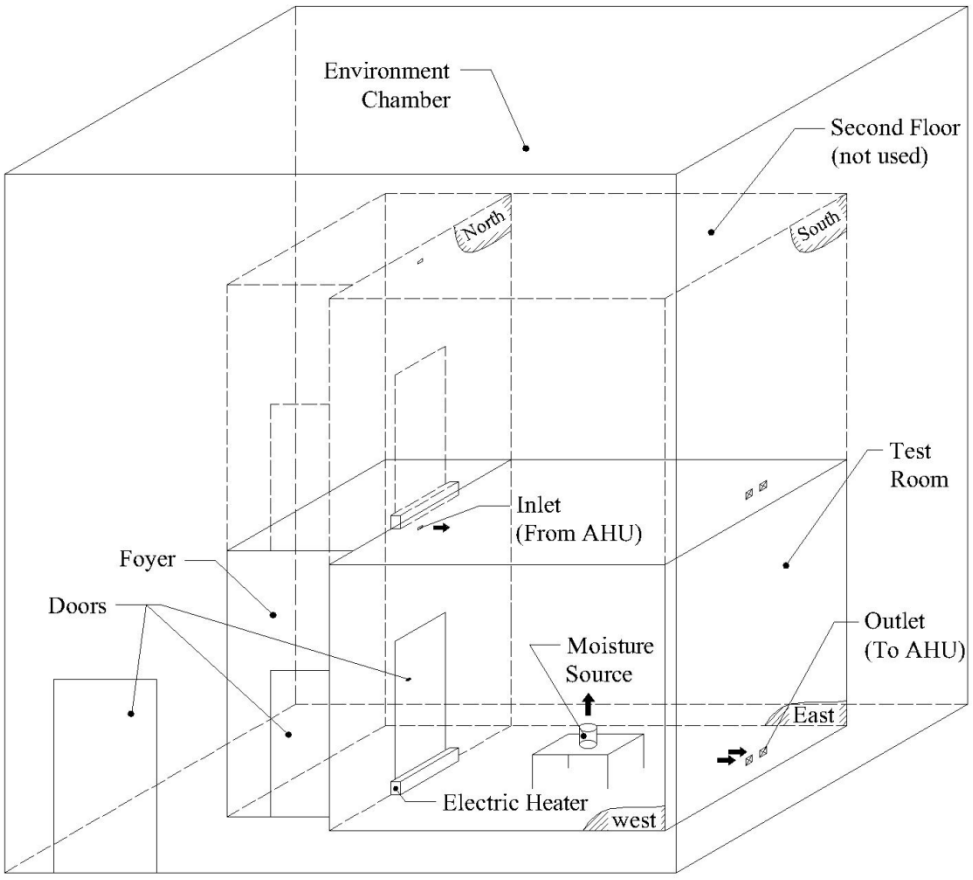

Fig. 6.1 Configuration of two-story test hut in the environmental chamber

Figure 6.1 shows the schematic drawing of the test hut in the environmental chamber. As described in the experimental protocol, all the surfaces of the room except for the east wall and west wall are covered by the aluminum metal sheets and, thus, have no

moisture interaction with the indoor air. The wood paneling is mounted on the east and west wall surfaces to study the buffering effect caused by the pine wood. The heat/moisture source, including a hot plate and a steel recipient located at the center of the room, provides moisture loads on the test room. The test room is heated by an electric board installed below the door sill on the interior. The test room is ventilated by the air handling unit. The inlet is located at the top of the center line of the north wall, 170mm from the ceiling, and the outlets are at the bottom of the south wall, 130mm from the floor. In the experiment, the investigated ventilation rates are 0.5 and 0.75ACH.

The air movement in the test room is driven by two forces. The ventilation system generates the air velocity in the inlet and exhausts the air from the outlet. Ventilation is the first cause of the indoor air movement. However, since the ventilation rate is relatively low in the experiment, the velocity at the inlet is small. For the 0.5ACH ventilation rate, the average air velocity at the inlet is 1.4m/s. The other force driving the air movement is the buoyant force caused by the hot plate at the center of the room as the heat/moisture source in the experiment. To identify the relationship of the two forces, the Reynolds and Grashof numbers are calculated. The ratio of Grashof number to the square of Reynolds number is about 0.75, which indicates that a mixed convection is occurring during the testing. The Gr number is about 1.5×1011, which implies that the air flow is turbulent.

For moisture transport, the moisture generated from the steel recipient is transported

by the convection mechanism inside the room, and interacts with the wood paneling. At the steady state, part of the moisture diffuses through the wall system, and the rest is exhausted through the outlet. The heat has a similar transport process.

The simulation domain should include the interior space of the test room and the wall system. In this thesis study, only the steady state is simulated. For the wall, the wood paneling is considered as a separated, independent sub-domain, while the rest of the wall layers are another sub-domain. To take advantage of the symmetry of the test room, half of the room is simulated in the geometrical model. Three simulation sub-domains are Sub-domain 1 corresponding to the test room, sub-domain 2 representing the wood paneling, and sub-domain 3 for the rest of the wall layers respectively, as illustrated in Figure 6.2.

In sub-domain 1, the convection of heat and mass (moisture) are coupled with the turbulent momentum. Between sub-domains 2 and 3, the heat/mass transfer inside the wall system is coupled with the indoor heat/mass transports through the continuity of the fluxes on the wall surfaces. The governing equations in the three sub-domains and their coupling process are presented in the following sections.

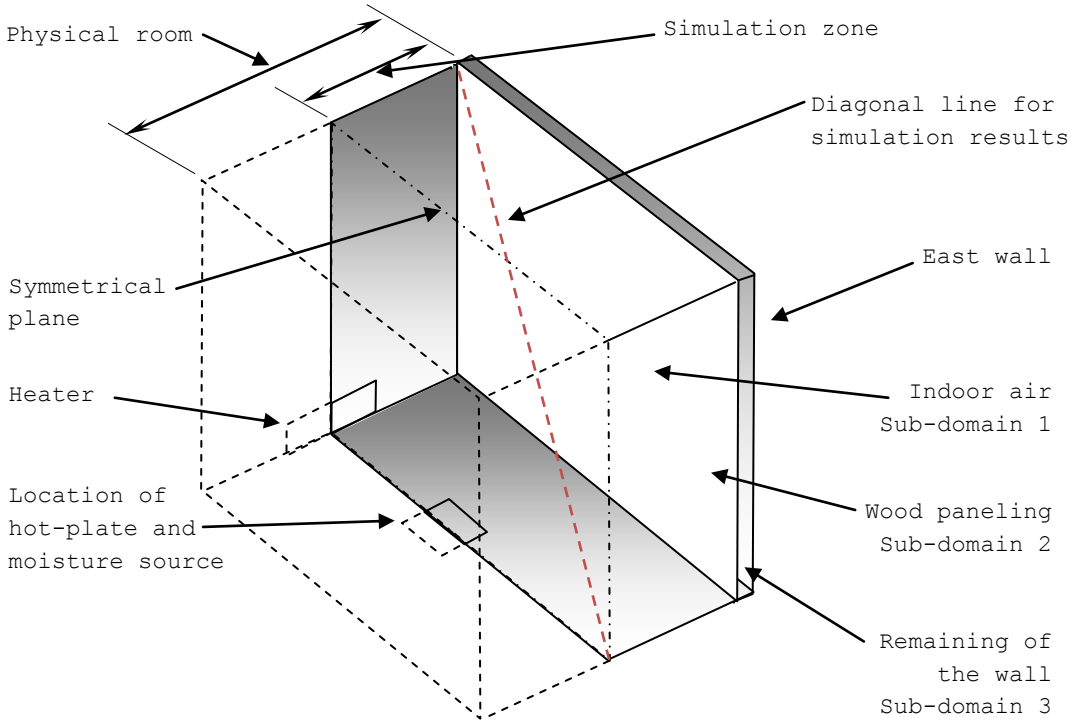

Fig.6.2 Schematic of the simulated room, showing the three sub-domains and the symmetrical plane

6.2.2 Governing equations and coupling process

The air movement inside the test room is turbulent with mixed convection condition as analyzed in the previous section. In COMSOL, two turbulence models are available: the k-ε model and the k-ω model. Theoretically, the k-ε model is based on the assumptions that the Re number is moderate or high and the turbulence in boundary layers is in equilibrium. The k-ω model provides a better prediction in the free shear flows close to wall, but is less accurate in the free-stream flow simulation. In addition the k- ω model is harder to reach convergence. Meanwhile, the accuracy of CFD simulation results is

related not only to the turbulent model selection, but also it depends on the wall surface conditions. The wood paneling wall surface in the experiment is a non-smooth surface, and thus both the turbulent models may bring in some simulation errors. Between k-ε and k-ω, k- ε has more advantages for this simulation model. In this 3D simulation of the momentum, heat and mass coupling in different regions, using k- ε model is a fair trade-off of saved computational resources compared to the more complicated turbulence model.

For the k-ε model, the governing equations for the momentum transport inside the test room can be presented as:

$$\rho(\vec{V}\cdot\nabla)\vec{V} = \nabla\cdot[PI + (\eta+\eta_T)(\nabla\vec{V} + (\nabla\vec{V})^T - (2/3)(\nabla\cdot\vec{V})I) - (2/3)\rho\kappa I] + \vec{F} \qquad (6.5)$$

$$\nabla\cdot(\rho\vec{V}) = 0, \qquad \rho = \rho(P_0, T) \qquad (6.6)$$

where $\vec{V}$ is the velocity (m/s), P is static pressure (Pa), P_0 is the reference pressure (Pa), $\vec{F}$ is the body force (N/m^3), I is the unit tensor (-), ρ is the density (kg/m^3) of the moist air, η_T is the turbulent viscosity (N·s/m^2) calculated by:

$$\eta_T = \rho C_\mu k^2 / \varepsilon \qquad (6.7)$$

where is a model constant (-), which is equal to 0.09 in the model, k is the turbulent kinetic energy (m^2/s^2), and is the dissipation rate of turbulent energy (m^2/s^3) which are determined by:

$$\rho\frac{\partial k}{\partial t} - \nabla\cdot[(\eta+\eta_T/\sigma_k)\nabla k] + \rho U\cdot\nabla k = \frac{1}{2}\eta_T(\nabla U + (\nabla U)^T)^2 - \rho\varepsilon \qquad (6.8)$$

$$\rho\frac{\partial\varepsilon}{\partial t}-\nabla\cdot[(\eta+\eta_T/\sigma_\varepsilon)\nabla\varepsilon]+\rho U\cdot\nabla\varepsilon=\frac{1}{2}C_{\varepsilon1}\frac{\varepsilon}{k}\eta_T(\nabla U+(\nabla U)^T)^2-C_{\varepsilon2}\rho\varepsilon^2/k \quad (6.9)$$

where $C_{\varepsilon1}$, $C_{\varepsilon2}$, σ_k, σ_ε are model constants (-) and are equal to 1.44, 1.92, 1.0 and 1.3 respectively.

These governing equations describe the turbulent mixed convection of indoor air movement in the sub-domain 1. Since the buoyancy force is one of driving forces, the air density as a function of indoor temperature distribution inside the test room is given together with the Navies-Stokes equation as Eq. 6.5-6.9, and the z direction of the body force in this equation is equal to that of gravity. To account for the turbulent characteristics of the flow, the viscosity of the fluid is defined by the software function eta, which is a function of indoor temperature. The sub-domain settings of the k- ε turbulent model are shown in Figure 6.3.

Figure 6.3 shows the interface of COMSOL in defining the room sub-domain regarding the k-ε turbulence model settings. The turbulent model is selected from the software, the parameters describing the test room conditions are defined according to the test room conditions. The air density is an internal function of COMSOL, and it is a function of pressure and temperature. In the experiment, the pressure is assigned to the standard atmospheric pressure, and the temperature is room temperature T_f which is calculated from the heat transfer model. The viscosity of the air is also an internal function and is a function of indoor temperature. The body force in Eq.6.5 is calculated by the product of the density and gravitational acceleration.

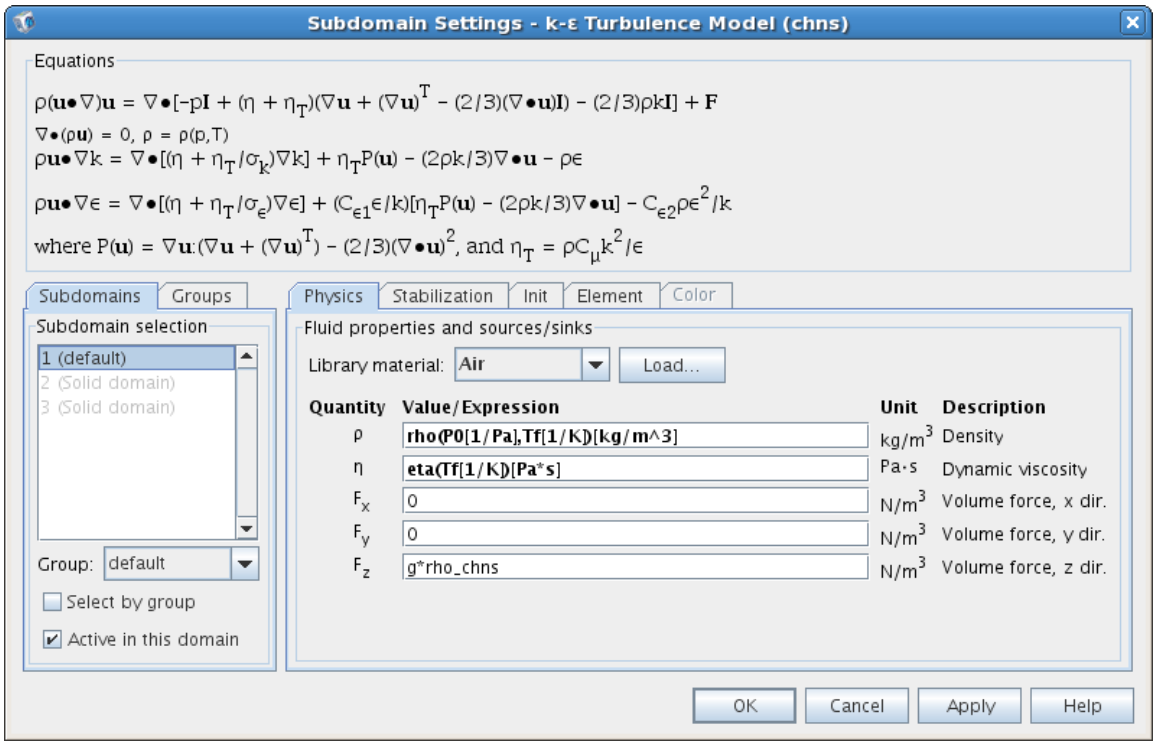

Fig. 6.3 Interface of sub-domain settings for momentum transport inside the test room

The heat and moisture transports in this sub-domain are governed by the equation of heat transfer and of the mass convection and diffusion as follows:

$$\nabla \cdot (-(K + K_T)\nabla T) = Q - \rho C_P \vec{V} \cdot \nabla T \qquad (6.10)$$

where T is temperature (K), Q is the heat source (W/m^3), K is the thermal conductivity (W/(m·K)), C_p is the specific heat capacity (J/kg·K) of the moist air, and is the turbulent conductivity (W/m·K), which depends on the turbulent Prandtl number (Pr_T) and turbulent viscosity,

$$K_T = C_p \eta_T / \mathrm{Pr}_T \qquad (6.11)$$

$$\nabla \cdot (-D\nabla c) = R - \vec{V} \cdot \nabla c \qquad (6.12)$$

where *D* is the diffusion coefficient (kg/m^3·s), *c* is the moisture concentration (kg/m^3), and *R* is the reaction rate for mass species (kg/m^3·s).

The coupling procedure among momentum, heat and mass transport is achieved by solving the equations above. The simultaneous computation of the parameters associated with air velocity, heat and moisture transport, enables in fact to build a coupled model. The air density in the momentum transport equation is calculated using the temperature given by the heat transfer equation; while the velocity in heat and mass transport equations and the turbulent kinetic viscosity in heat transfer equations (Eqs. 6.10 and 6.11) are based on the momentum equation.

The governing equation of the heat transfer in sub-domain 2 is the heat conduction equation:

$$\nabla \cdot (-K \nabla T) = 0 \tag{6.13}$$

The conductivity of wood paneling is measured in a previous project (Wu, Fazio, Kumaran, 2008) and given in Appendix A.

The governing equation of the moisture transfer in wood paneling can be deduced by the mass conservation. In this sub-domain, the moisture storage rate is equal to the divergence of the moisture flux. For the steady state simulation, the storage rate is equal to zero, and then the governing equation has the form:

$$\frac{\partial c}{\partial t} = \nabla \cdot (-\delta \nabla P_v) = 0 \tag{6.14}$$

where δ is the permeability of the wood (kg/Pa·s·m), and P_v is the vapor pressure (Pa).

In the governing equation, in order to have the same variable with the one used in indoor mass transport, moisture concentration c, instead of the variable P_v, the Eq.6.14 need to be further deduced as:

$$\begin{aligned} 0 &= \nabla \cdot (-\delta \nabla P_v) \\ &= \nabla \cdot (-\delta \nabla (\phi P_{sat})) \\ &= \nabla \cdot (-\delta (P_{sat} \nabla \phi + \phi \nabla P_{sat})) \\ &= \nabla \cdot (-\delta \frac{P_{sat}}{\xi \rho} \nabla c - \delta \phi \frac{dP_{sat}}{dT} \nabla T) \\ &= \nabla \cdot (-\delta \frac{P_{sat}}{\xi \rho} \nabla c) + \nabla \cdot (-\delta \phi \frac{dP_{sat}}{dT} \nabla T) \end{aligned} \qquad (6.15)$$

where ϕ is the relative humidity (-), ξ is the moisture capacity of wood (kg/kg), ρ is the density of the wood (kg/m3), and P_{sat} is the saturation vapor pressure (Pa). The relationship of the relative humidity and moisture capacity can be found in Chapter 3. The saturation vapor pressure is a function of temperature (ASHRAE 2005), and is given (when T - 273.15 > 0 °C) as:

$$\begin{aligned} P_{sat} = \exp(&-5.8002206 \times 10^3 / T + 1.3914993 - 4.8640239 \times 10^{-2} * T + 4.1764768 \times 10^{-5} * T^2 \\ &- 1.4452093 \times 10^{-8} * T^3 + 6.5459673 * \log(T)) \end{aligned} \qquad (6.16)$$

In COMSOL, the convection and diffusion equation of mass has the form:

$$\nabla \cdot (-D \nabla c) = R - \vec{V} \cdot \nabla c \qquad (6.17)$$

Since in the wood paneling, the air velocity is zero, comparing with Eq.6.15, the coefficient D and R are obtained as:

$$D = \delta \frac{P_{sat}}{\xi \rho} \tag{6.18}$$

$$R = \nabla \cdot (\delta \phi \frac{dP_{sat}}{dT} \nabla T) \tag{6.19}$$

Note that the coefficient D in fact is the moisture diffusivity, as presented in Section 3.1.4.

The continuity of the mass flux is the boundary condition of mass transfer for the interior boundary between sub-domains 1 and 2 as presented in Eq.20. This continuity assumption is the same as the ones in other models which are currently utilized in many HAM transport studies as reviewed in section 6.1.1, such as the EPD model, and MC model.

$$q_{hr} = q_{hw} \tag{6.20}$$

where q_{hr} is the moisture flux calculated on the wall surface based on indoor humidity gradient, and q_{hw} is based on the humidity gradient inside the wall.

For the heat coupling between the sub-domains 1 and 2, the thermal wall function, a heat flux defined as Eq.6.21, connects the heat transfer equations in the two sub-domains.

$$q = \frac{\rho C_P C_\mu^{1/4} k_w^{1/2} (T_w - T)}{T^+} \tag{6.21}$$

where q is the heat flux (W/m^2), C_μ and k_w are the model constants (-), T_w is the

temperature at wall (K), and dimensionless temperature T^+ is calculated by

$$T^+ = \frac{\mathrm{Pr}_T}{k_r}\ln(\delta_w^+) + \beta \tag{6.22}$$

where k_r is the von Karman constant (-), is a model constant (-), and is a dimensionless wall offset (-).

The coupling process of the heat transfer between indoor air and the wall is shown in Figures 6.4 and 6.5. The heat flux of the thermal wall function in the sub-domain 1 is calculated by Eq.6.21 as shown in Figure 6.4. This flux is input as the inward heat flux in the wall sub-domain as shown in Figure 6.5, but with a negative sign. In this way, the continuity of heat flux is achieved between the indoor air and the wood paneling. Note that in Figure 6.5, the second item of the right side of the boundary equation is zero, so h is set to zero, and the value of T_{inf} can be set as any value.

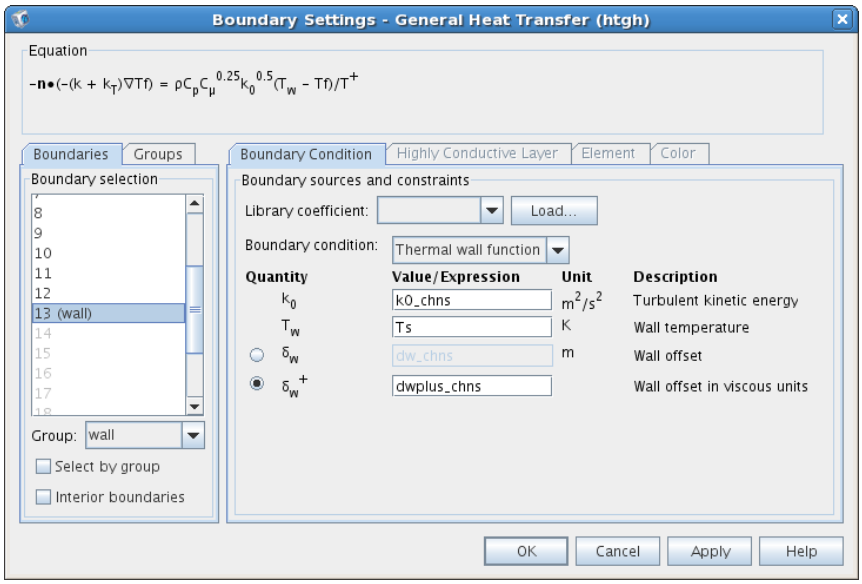

Fig. 6.4 Boundary settings on the room side of the interface of heat coupling between indoor air and wood paneling

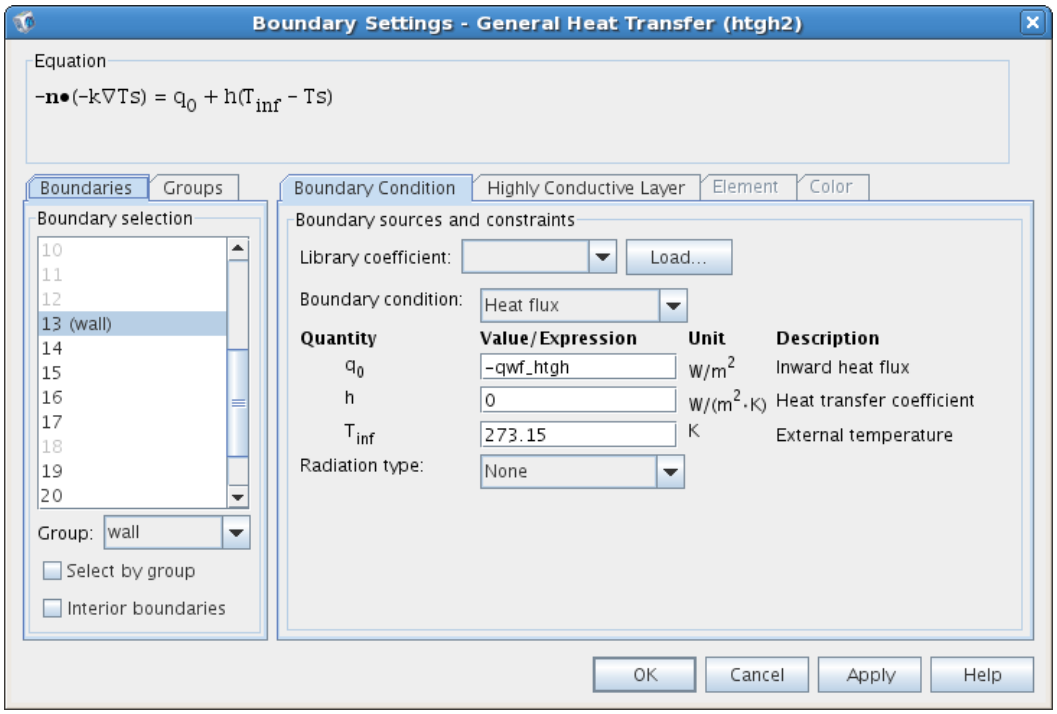

Fig. 6.5 Boundary settings on the wall side of the interface of heat coupling between indoor air and wood paneling

Sub-domain 3 includes the remaining layers of the wall. The material properties of all the layers are listed in Appendix A. The governing equations in sub-domain 3 are the same as those used in sub-domain 2. To reach the convergence solution and reduce the iterative time, an effective wall is used to simulate the heat and vapor transports in sub-domain 3. The effective properties are calculated based on the properties of each wall layer, for example, the effective thermal conductivity is calculated as:

$$k_{eff} = \frac{\sum_{i=1}^{n} d_i}{\sum_{i=1}^{n} \frac{d_i}{k_i}} \qquad (6.23)$$

where and are the thermal conductivity and thickness of the th component.

6.2.3 Boundary conditions, meshing, and solver parameters for the numerical model

The boundary conditions are assigned to the turbulent air movement, heat transfer and moisture transport. For the momentum transport in the test room, the inlet boundary conditions are the inlet air velocity which is calculated based on the ventilation rate and the two turbulent quantities related to the k-ε turbulent model. COMSOL provides two parameters specifying the characteristics of the k-ε turbulent in the inlet boundary: turbulent length scale LT and turbulent intensity IT. The chosen values of the two parameters were referred to the COMSOL user manual in the part of the Chemical Module related to the introduction of the turbulent boundary conditions. The inlet boundary for the momentum transport is set as Figure 6.6. The outlet boundary is the default option, i.e. pressure, no viscous stress. The pressure at the outlet is set to zero in the numerical model.

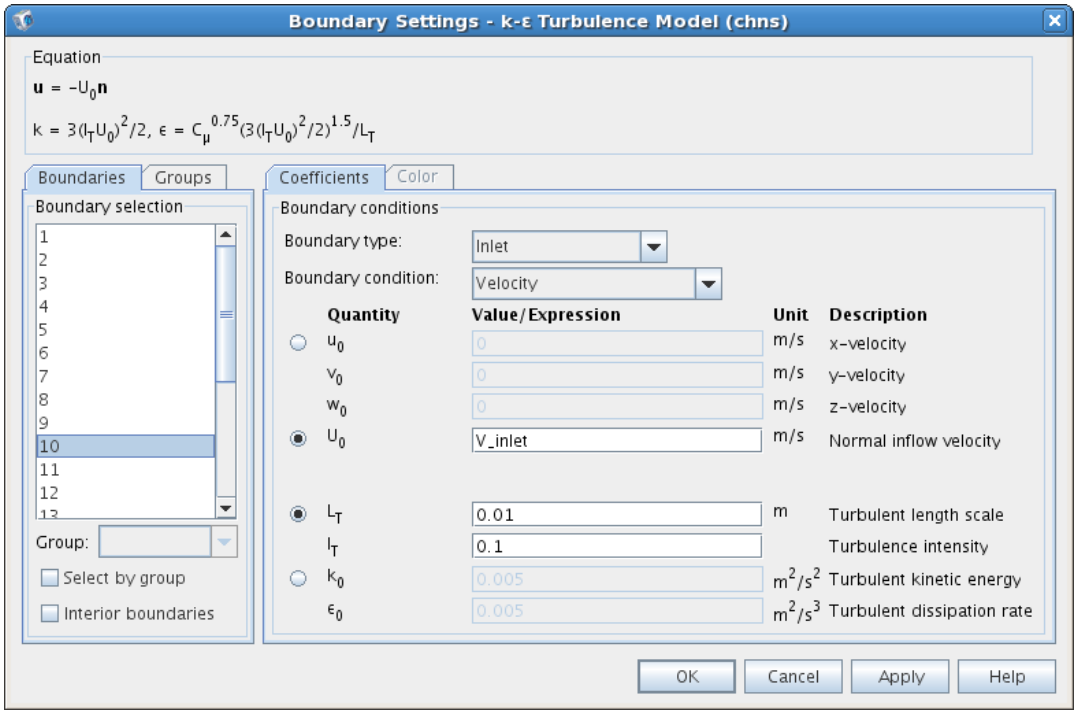

Fig. 6.6 Inlet boundary conditions of the k-ε turbulence model

For the heat transport inside the test room, the inlet boundary condition is the temperature of the supply air, and the outlet boundary condition is the convective heat flux. Since the RH&T sensor located at the outlet in the experiment is far from the ventilation vent, the temperature of the outlet in the sub-domain1 is unknown. The convective flux boundary condition assumes that the energy passes through this boundary in terms of the convective flux mechanism. It is useful boundary condition where the outlet temperature is unknown in the convection-dominated energy balances. The surface of the electric heater is 40 °C, and surface of the hotplate is 100 °C. These two values were measured in the experiment. The similar boundary conditions are set for the mass transport inside the test room. The inlet boundary condition is the moisture flux calculated by the ventilation rate and humidity ratio of the supply air. The

outlet boundary condition is convective flux for moisture. The boundary condition at the steel recipient is the moisture flux calculated by the moisture generation rate. On the walls, since there is no air movement, there is no need to set momentum boundary conditions. The boundary equation at the outside surface of the exterior wall is the outdoor air's temperature for the heat transfer equation, and the outdoor air's moisture content for the moisture diffusion equation.

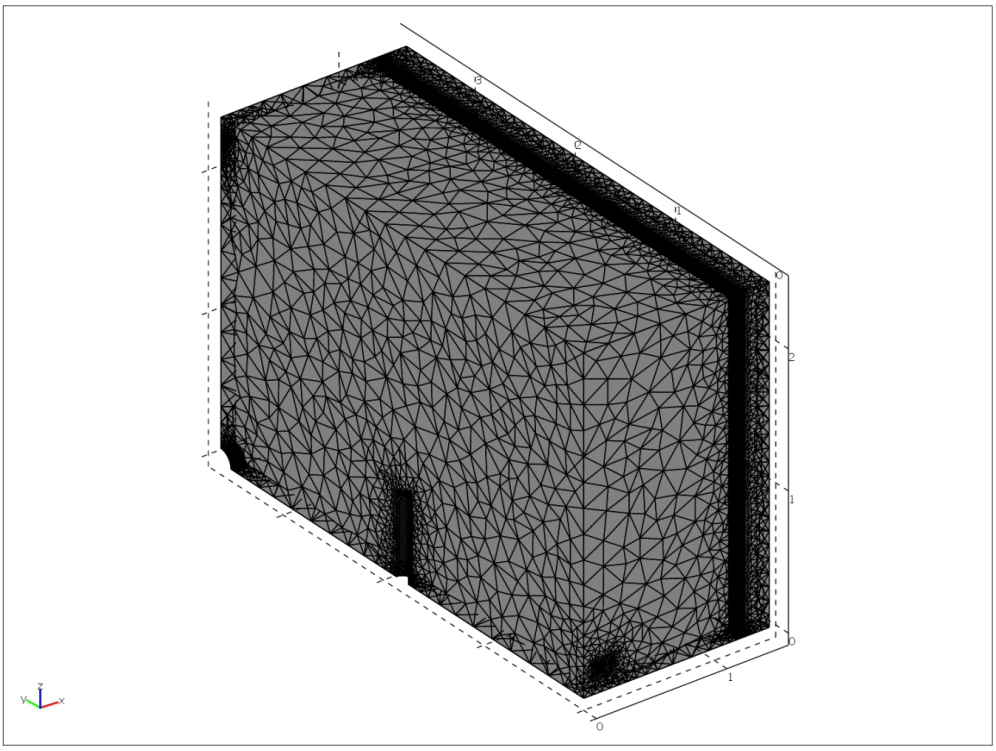

Fig. 6.7 Image of meshes assigned on the whole simulation domain

The unstructured mesh is assigned for the entire calculation domain. The mesh maximum sizes are set to 0.01m at the inlet surface, 0.02m at surfaces of the outlet, steel recipient and inner wall surface, and 0.04 m at heater surface. The rest of the

global size of the mesh is set at 0.29m. The mesh consists of 188,799 elements in sub-domain 1 and 46,975 elements in sub-domains 2 & 3. In total, the 834,546 degrees of freedom are solved in this simulation. The mesh image of the numerical model is shown in Figure 6.7.

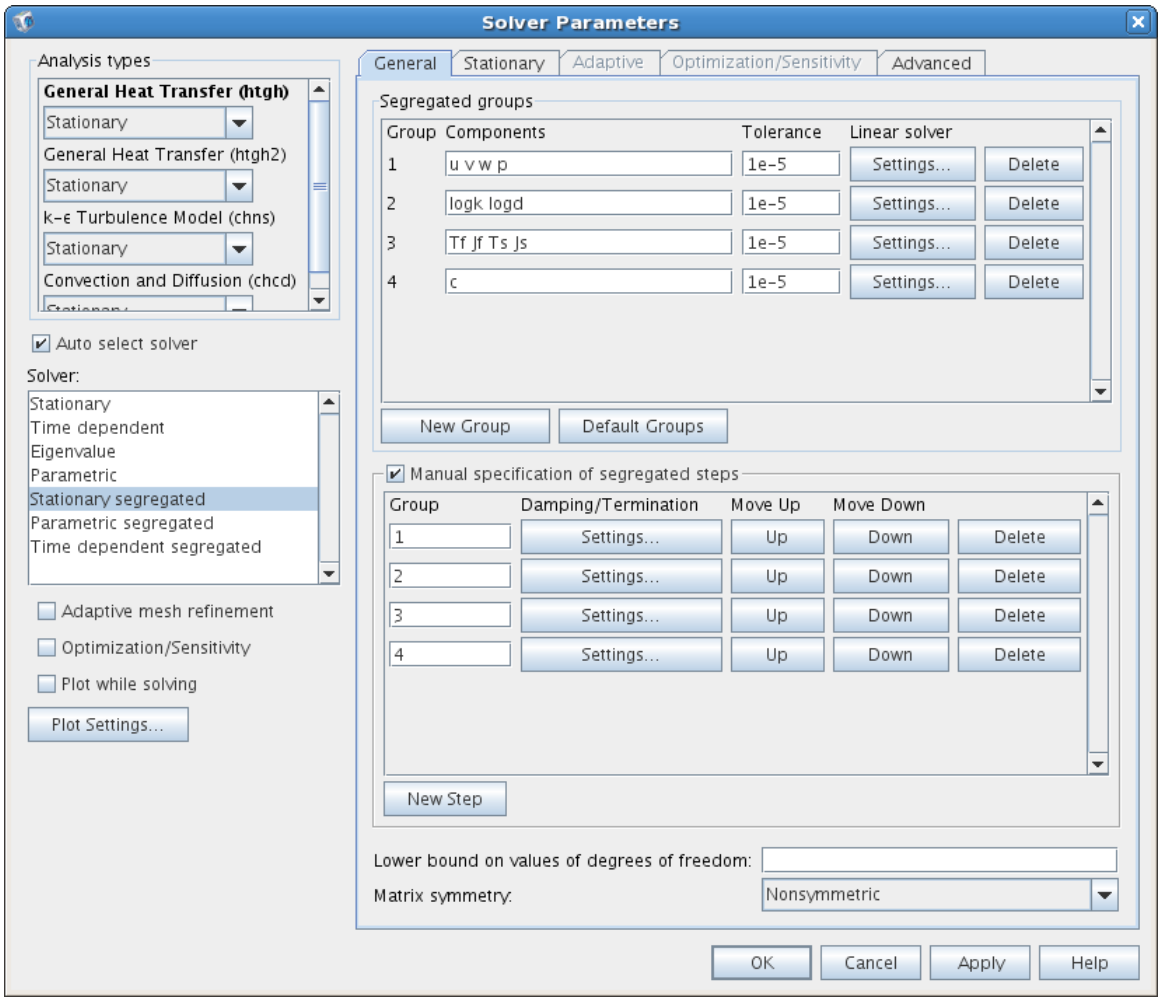

Fig. 6.8 Solver settings for solving the coupling equations of HAM

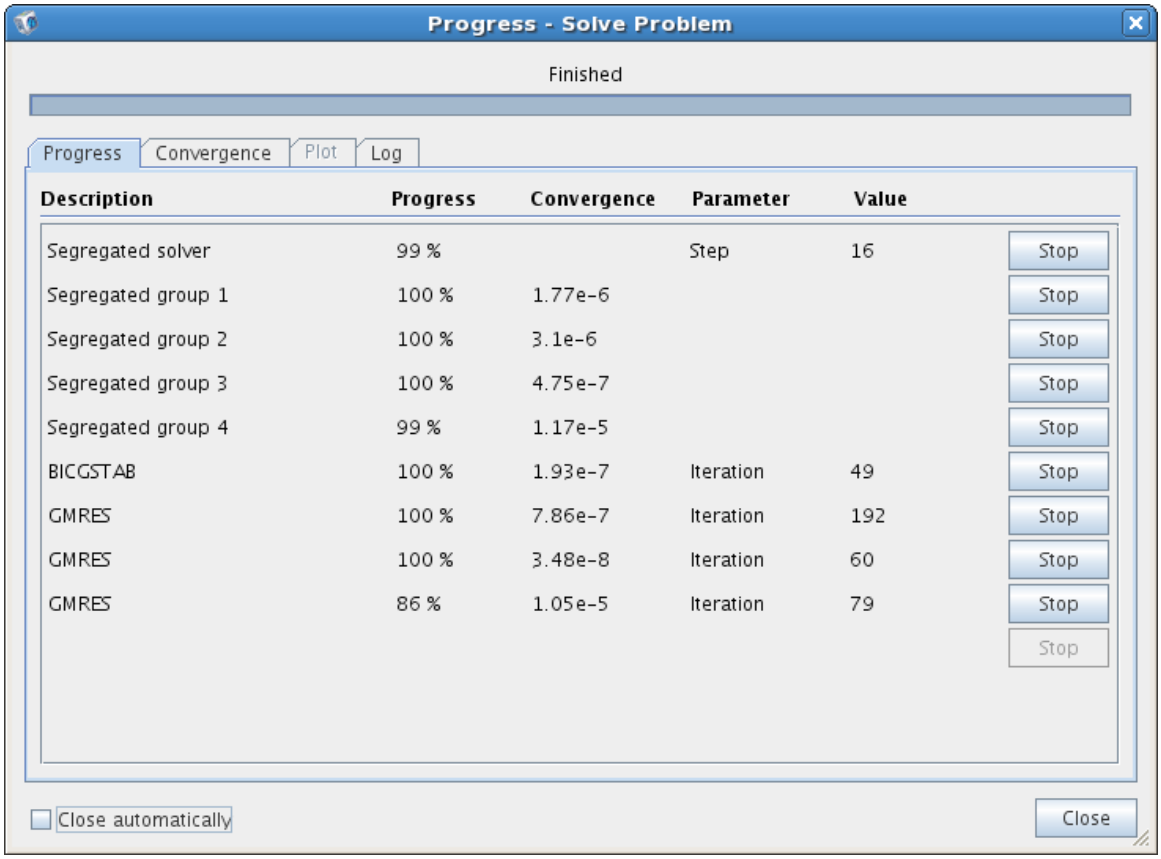

Fig. 6.9 Solver progress showing the model convergence tolerance

The default stationary segregated solver which is for stationary multi-physics PDE problems is selected with some adjustments as shown in Figure 6.8. By using this solver, the solution steps are split into sub-steps. In this coupled model, the coupled physics are grouped into four depending on the independent variables. For each segregated group, the tolerance and linear solver for this group's variables can be controlled through the setting options. The tolerance values for each segregated group are shown in Figure 6.8, and the solving convergence of the numerical model is shown in Figure 6.9. Under the linear solver level, the pre-conditioner solver and the maximum number of iterations for each level of the solvers can be defined. In this numerical model, the GMRES solver

which is an iterative solver for non-symmetric problems is selected as the linear solver for each segregated group. The geometric multi-grid solver is used as a pre-conditioner for each linear system solver. The solvers selection is based on the manual of COMSOL Multi-Physics. Since the order of the moisture content is expected to be much lower than the order of temperature and velocity, the variable scaling for mass is defined as 10^{-4} manually.

6.3 Comparisons to experimental results

Figures 6.10 & 6.11 show the temperatures in all sub-domains and RH in sub-domain 1, respectively. Except for the regions near the heater, hotplate, and inlet, the differences in the temperatures and RH levels inside the room are small (less than 1 °C and 3% RH). This is in close agreement with the experimental measurements (Figure 6.12). The accuracy of the sensors in the experiment is ±0.5°C for temperature measurements and ±2% for RH measurements. The maximum temperature difference in the experimental measurements is about 1°C (Figure 6.12 a), while the RH difference is 5% (Figure 6.12 b). The higher temperatures are recorded by sensor E_11, C_31 and E_31, while the higher RHs are recorded at G_13 and E_35. The same phenomenon is observed in the simulation results, reflecting higher values of temperature and RH at the corresponding locations of the mentioned sensors (Figure 6.12).

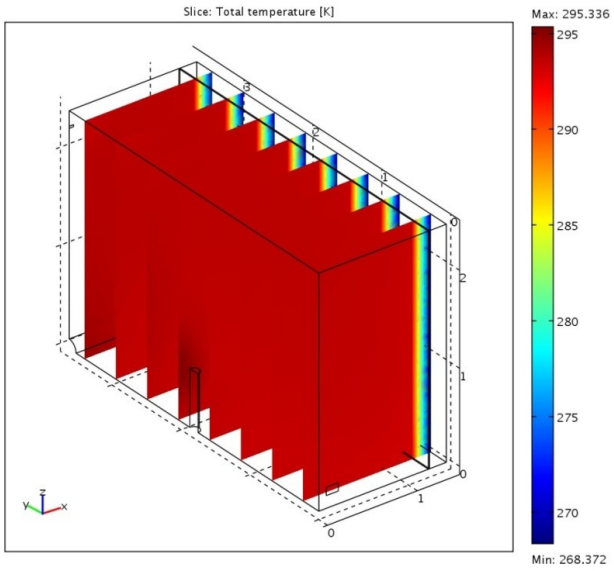

Fig. 6.10 Simulation result showing temperature distribution in test room and temperature gradient across the wall

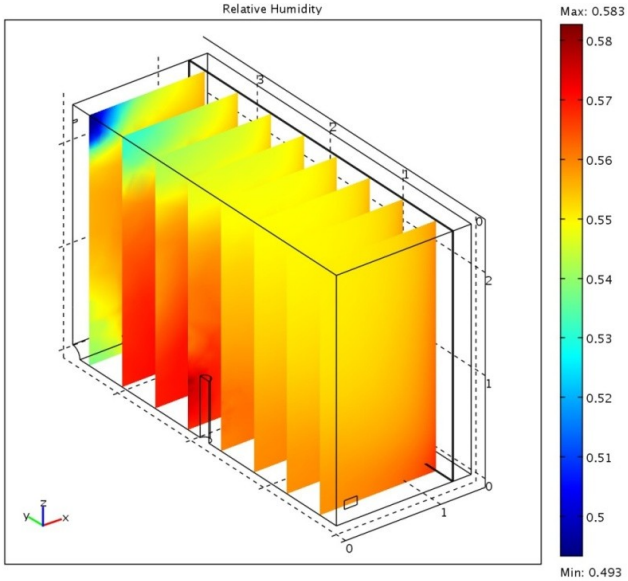

Fig. 6.11 Simulated RH distribution inside test room without showing the moisture gradient across the wall

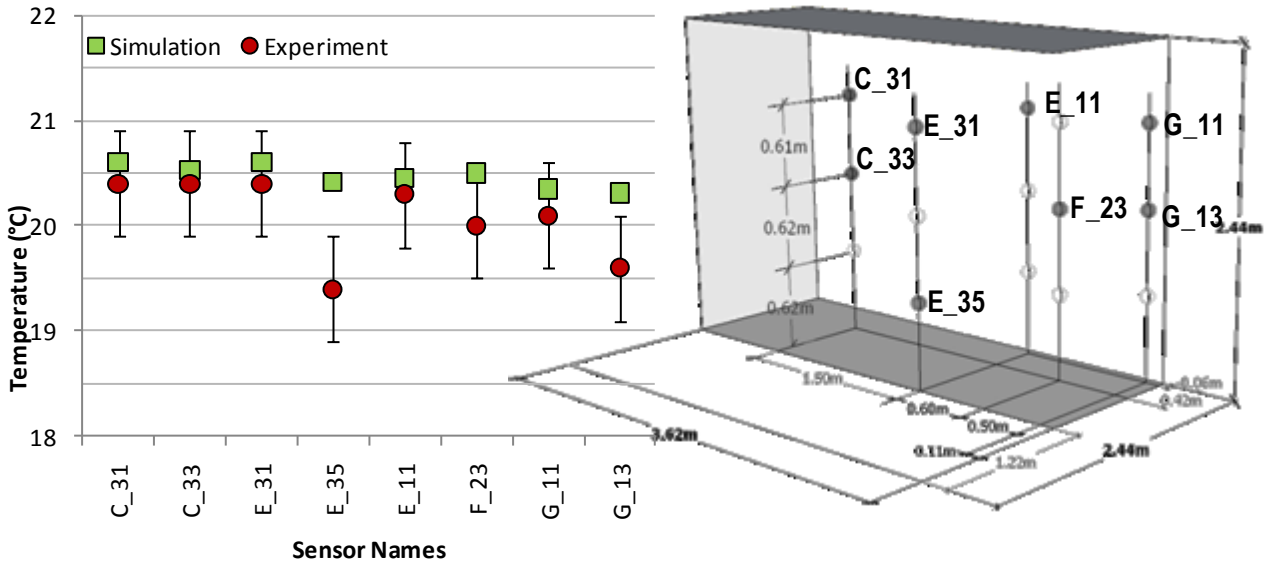

a) Comparison of indoor air temperatures between CFD simulation and measurements with ±0.5°C error band in case 1

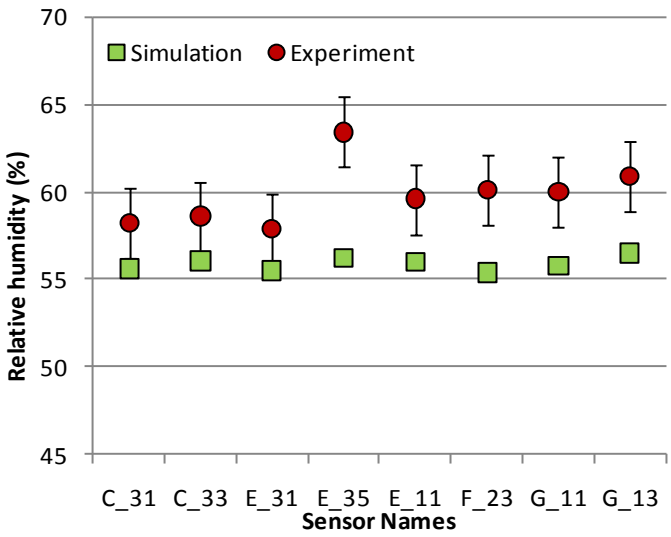

b) Comparison of indoor relative humidity levels between CFD simulation and measurements with ±2% error band in case 1

Fig. 6.12 Comparison between numerical simulation and experimental results

The overall temperature and moisture concentration profiles obtained from the simulation of the indoor air conform to the experimental data, as illustrated in Figure 6.12. The air temperatures measured by sensors are slightly lower than those obtained from the simulations. The fact that the test room is not completely airtight and the other interior surfaces, except for the east and west walls, are assumed as adiabatic in the simulation may be the causes of the temperature differences. The RH results provided by the experiment are higher than those obtained by the simulations. This higher result is because the computation of the RH in the model depends on the temperature results. The RH value is, in fact, inversely proportional to the temperature; therefore a higher temperature implies a lower RH value, if the moisture content in the air is kept constant.

On the other hand, the difference in the amplitude of the results among sensors in the experimental test can be attributed partly to the sensors' accuracies.

6.4 Summary

COMSOL is an engineering, design, and finite element analysis software environment for the modeling and simulation of any physics-based system. It is utilized in the numerical study of this thesis to establish the coupled CFD model of simulating the HAM transport in the experimental test conditions. The ways that the software couples multi-physics problems through the predefined application models and PDEs in the three forms, i.e. coefficient form, general form and weak form are introduced at the beginning of this

chapter. The review of the robustness and application of the software in building science studies follows. The related literature review shows that COMSOL Multi-physics is a reliable solver and simulation software for various physics, especially coupled phenomena, i.e. multi-physics. Based on this review, COMSOL is adopted to fulfill the objective of this thesis numerical research: to investigate the influence of room factors including moisture loads and ventilation conditions on the indoor environment taking into account the heat/mass interaction between indoor air and hygroscopic wall system.

The numerical model which couples the momentum, heat, and mass transport inside the test room and through the wall system in a single simulation environment, i.e. COMSOL, has been presented in this chapter. The coupling of the HAM inside the test room is achieved by establishing the relationships of the variables in the momentum, heat and mass conservation equations. These relationships including the density of air as a function of indoor temperature, the turbulent conductivity in heat equation related to the turbulent Pr number and turbulent viscosity in the momentum equation, the identities of the velocity in heat and mass equations with the velocity solved by momentum equation. The coupling of heat and moisture between different sub-domains, i.e. between indoor air and hygroscopic materials of walls is achieved by the continuity assumption of mass flux and thermal wall function. Since the air movement in the test room is characterized as turbulent under mixed convection condition, the assumption of the continuity of the moisture flux neglects the turbulent influence of the moisture interaction between the indoor humidity air and the hygroscopic wall. The

influence of this limitation on simulation results will be presented in the next chapter when the heat/mass transport through the wall system is investigated.

There are some advantages of this numerical model. First, it overcomes the main limitations existed in currently available CFD coupled models of the whole building HAM transport study. As reviewed in the beginning sections of this chapter, currently the coupling of CFD with the moisture transport in walls is achieved through the third party programming, i.e. not in a single simulation environment. Except for the assumption of continuity of the mass flux which is the same as the one used in this thesis' coupled model, there are some other limitations in those models. For example, when the finite difference method is used to couple the mass diffusion equation to CFD model, the complicated geometries cannot be simulated due to the limitation of this method; when penetration depth method is used in the coupled model, the value of the penetration depth has to be known, but in reality, this value can only be estimated (refer to Chapter 3: basic theory). Second, this thesis' coupled model has great application potential. Since this model is built in a single simulation environment, despite the complicated coupling process, the model can be extended in studying the HAM transport in the whole simulation domain.

This numerical model is validated by comparing its results with the experimental measurements. Close agreement is obtained in the indoor temperatures and relative humidity profiles. The simulation results show that the distribution of indoor temperature and moisture are not uniform, and the north side region has slightly higher

values. The higher value is observed by the sensors measurements, and will be explained in the next chapter.

The next chapter presents the application of the model in studying the impact of room factors on the indoor environment. The moisture loads and ventilation design are the room factors investigated numerically. Some of the parameters were tested in the experiment, but were not explained in terms of the mechanism of HAM transport. Other parameters, such as the position of the ventilation vents which were not studied in the experiment, are studied in the numerical simulation. The heat/moisture transport in walls under the room condition with the simulated room factors is also investigated.

CHAPTER 7

NUMERICAL INVESTIGATION OF HYGROTHERMAL RESPONSE IN A ROOM AND THROUGH ITS ENVELOPE

The numerical model coupling air, heat and moisture transport inside the test room and through the wall system has been presented in Chapter 6. In this chapter, the application of the numerical model on the investigation of the influence of room factors on HAM responses of the experimental room is developed. The scope of the numerical study and the investigation parameters are introduced first. Then, the impacts of the room factors on indoor environment are studied. The aspects which cannot be studied in the experiment work, such as the influence of the ventilation vents design, the heat/moisture fluxes influenced by room factors, and the potential damage caused by mold growth are investigated in this chapter by using the numerical model.

7.1 Implementation of the model

The moisture buffering effect of the wood paneling on the changes in the indoor environment has been studied and presented through the experimental work in Chapters 4 and 5. The buffering effect is the influence on the indoor environment due to moisture ad/desorption of the hygroscopic materials under the dynamic state of the moisture loads, i.e. the 8 hours moisture generation followed by 16 hours of no generation in a one-day cycle. In the experiment, there is a 3-day test case in which the

moisture is generated for 24 hours following by 48 hours of no moisture generation. The preliminary test results show that in this test case, at the end of the moisture generation, the indoor temperature and relative humidity level had reached a state of equilibrium under the ventilation rate of 0.5ACH. The other room factors, the moisture generation rate and ventilation rate under the equilibrium state, were not studied due to the unavailability of the environmental chamber. Meanwhile due to the limitation of the experimental facilities, it was not possible to further study experimentally the influence of ventilation design parameters such as the vents position and to study the heat/mass transfer through the wall system.

In this numerical investigation, the influence of more room parameters on the indoor environment under steady sate is firstly studied. The numerical model presented in Chapter 6 is built based on the mixed condition of the indoor air convections, which means it is for low ventilation rates. So, in the numerical investigation, the parameters of ventilation rates are the low ventilation rates of 0.5ACH, 0.75Ach and 1CAH. The first two rates have been tested in the experiment, but in a dynamic state. The moisture generation rates tested in the experiment are 42g/h, 58.5g/h and 91g/h, but not for every ventilation rate. In the numerical study these three moisture generation rates are studied under all three ventilation rates. Besides these parameters, the influence of the ventilation vent positions on the indoor environment is investigated. The position of the ventilation vents can be regarded as one room factor, but it is not designed in the experimental study. The study of the impacts of the vents position is a supplement to the experimental work in this research. In addition, the numerical model shows the

results as well as the visualization of the transport mechanisms which help to explain these results. The heat and mass transport through the wall system under each simulated case is investigated. The heat and moisture fluxes are calculated. Finally, the relative RH values in the simulation domain are evaluated for the potential mold growth. The risk regions in each simulation case are summarized.

In total, the model described in Chapter 6 is implemented in 12 cases to study the influence of the moisture loads, ventilation rates, and positions of the inlet and outlet on the indoor environment and on the heat and moisture transport through the envelope. Case 1 replicates the same conditions used in the experimental setting, which has a ventilation rate of 0.5ACH and a moisture generation rate of 42 g/h. To study the influence of the moisture generation rates, cases 2 and 3 simulate two moisture loads of 58.5 g/h and 91 g/h respectively while having the same ventilation rate as case 1. To investigate the influence of ventilation rates on the indoor environment, cases 4, 5, 6 and cases 7, 8, 9 are simulated at different ventilation rates of 0.75ACH and 1ACH, respectively, each subjected to three the different moisture loads of 42 g/h, 58.5 g/h, and 91 g/h. Cases 10 to 12 investigate the impact of the position of the ventilation vents, which have the same conditions as cases 1, 4 and 7 but change the position of the inlet and outlets. In these three cases (cases 10 to 12), the inlet is moved from the upper region of the north wall to the bottom region along the vertical center line of the wall, and the outlets are moved from the bottom region of the south wall to the upper region. The room factors including ventilation rates and moisture loads in all 12 cases are summarized in Table 7.1. The locations of the inlet and outlet in cases 10 to 12,

together with the comparison to the unchanged positions in cases 1 to 9 are listed in Table 7.2. For all cases, the supply air condition is 20 °C, 45% RH, corresponding to the values used in the experiment. The outdoor conditions are those specified in the experiment (-5 °C, 68%RH) as well.

Table 7.1 Ventilation rates and moisture rates in simulations

	42 g/h	58.5 g/h	91 g/h
0.5ACH	Case 1 & case 10	Case 2	Case 3
0.75ACH	Case 4 & case 11	Case 5	Case 6
1ACH	Case 7 & case 12	Case 8	Case 9

Table 7.2 Location of ventilation vents for all cases

	Cases 1 to 9	Cases 10 to 12
Height of inlet center (m)	2.26	0.25
Height of outlet center (m)	0.172	2.2

7.2 Impact of ventilation rates on indoor humidity level

Figures 7.1-7.3 show the profiles of the indoor relative humidity along the diagonal line from the bottom center of the south wall to the upper corner of the north and east wall (indicated by the red dash line in Figure 6.2) for cases 1 to 9. As shown in Figure 7.1, under the same moisture generation rate of 42 g/h, the indoor RH values are 55 % (case 1), 49 % (case 4) and 45 % (case 7), respectively, corresponding to the ventilation rate of 0.5ACH, 0.75ACH and 1ACH. The indoor humidity levels decrease as the ventilation rate increases because the higher ventilation can carry away more moisture and lower the moisture concentration in the test room. The RH decreases with the ventilation rate

increases from 0.5ACH to 0.75ACH, and to 1ACH can also be observed in Figures 7.2 and 7.3 in which the moisture generation rates are 58.5 g/h and 91 g/h respectively.

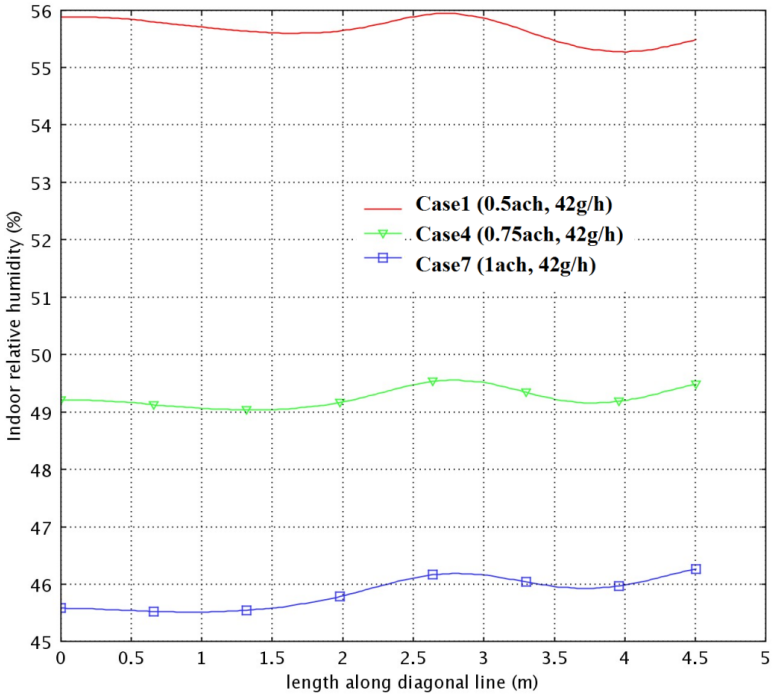

Fig. 7.1 RH values along the diagonal line (from bottom center of the south wall to the upper corner of the north and east wall, see Figure 6.2) for cases 1, 4 and 7 with same moisture generation rate of 42g/h

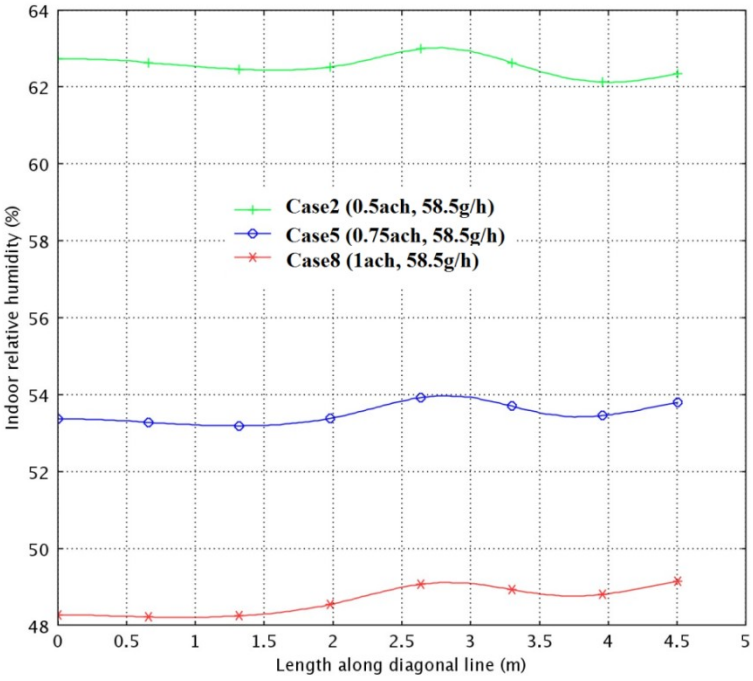

Fig. 7.2 RH values along the diagonal line for cases 2, 5 and 8 with same moisture generation rate of 58.5g/h

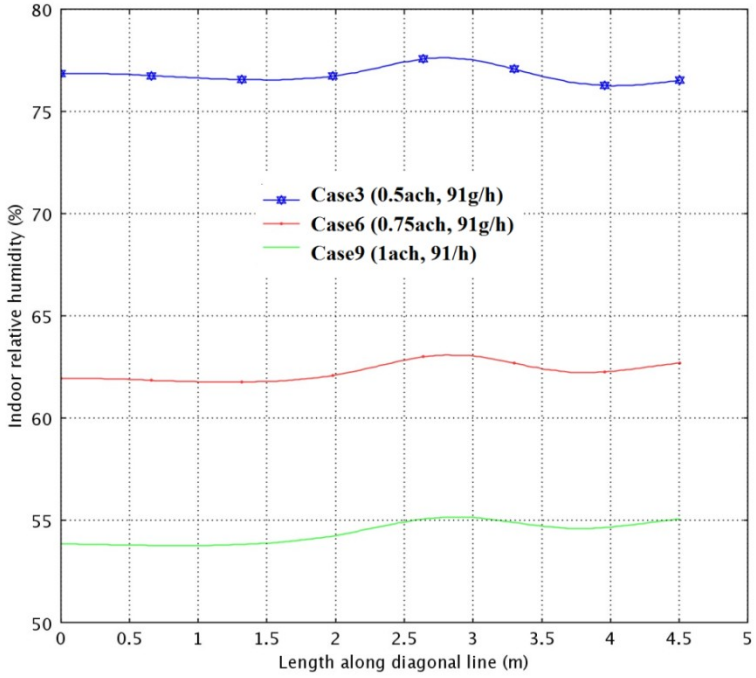

Fig. 7.3 RH values along the diagonal line for cases 3, 6 and 9 with same moisture generation rate of 91g/h

The condition of the supply air in cases 1 to 9 is 45 %RH and 20°C with a humidity ratio of 6.559×10-3 kg/kg. The increased humidity level over the condition of the supply air in each simulated case can be regarded as the humidity responses of the test room to the moisture loads and ventilation conditions. The profiles of the humidity ratio in each case can be obtained from simulation results. Taking the value of the humidity ratio at midpoint of the diagonal line to represent the indoor humidity condition, the increased relative humidity (IRH) is calculated as the RH value increases between the indoor RH value (the value at the midpoint) and the supply air RH value, which is constant for all simulated cases. Figure 7.4 shows the IRH for cases 1 to 9. The increments in humidity levels decrease as the ventilation rate increases. The largest IRH is in case 3 in which the moisture load is 91 g/h, and the ventilation rate is 0.5ACH. When the moisture loads do not change, as the ventilation rate increases from 0.5ACH to 1ACH, the IRH decreases significantly. As shown in Figure 7.4, at the moisture rate of 91 g/h, the IRH decreases from 32% (case 3) at 0.5ACH to 9% (case 9) at 1ACH; and at the moisture rate of 58.5 g/h, the corresponding IRH decrease is from 17% to 4% between cases 2 and 8. At 1ACH, the 42g/h moisture generation causes only 1% increase in the RH of the test room.

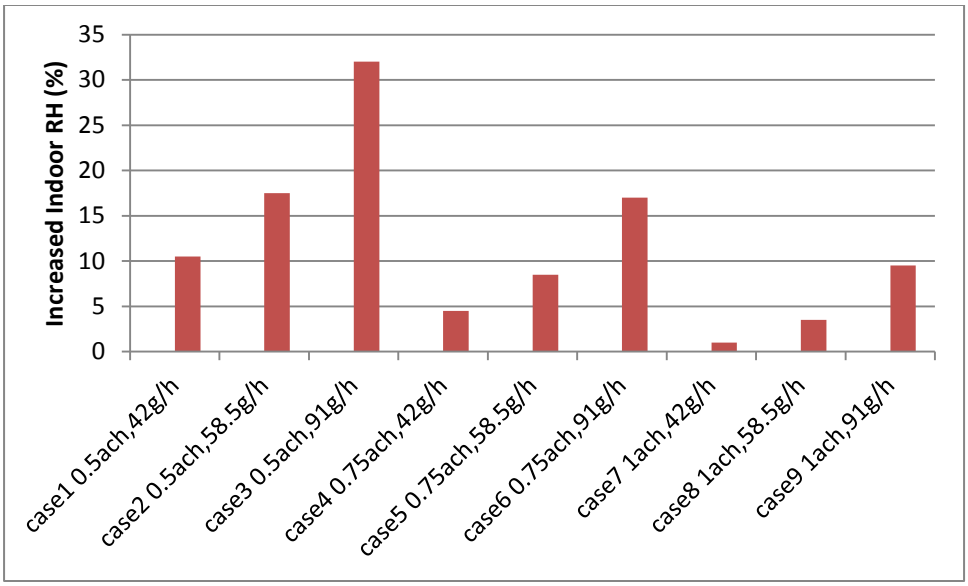

Fig. 7.4 Increased relative humidity (IRH) in cases 1 to 9 at the center of the half room simulated

7.3 Impact of moisture generation rates on indoor humidity level

The impact of moisture generation rates on the indoor humidity level can be observed when the indoor moisture concentration profiles along the diagonal line are grouped into different ventilation rates as shown in Figures 7.5 to 7.7. Figure 7.5 shows the indoor moisture concentration profiles of the three cases (cases 1, 2 and 3) with different moisture generation rates under the same ventilation rate of 0.5ACH. When the moisture generation rate increases from 42 g/h (case 1) to 58.5 g/h (case 2), the indoor moisture concentration at the midpoint of the diagonal line increases from 0.0098 kg/m^3 to 0.0112 kg/m^3. An increase of about 0.0015 kg/m^3 is observed in the moisture concentration. The increase of moisture concentration is 0.0024 kg/m^3 when the moisture generation rate changes from 58.5g/h to 91g/h. The indoor moisture

concentration increases as the moisture generation rate becomes higher. Figures 7.6 and 7.7 show the moisture concentration profiles along the diagonal line under the ventilation rate of 0.75ACH and 1ACH respectively. Under the ventilation rate of 0.75ACH, the increased values of the moisture concentration corresponding to the moisture generation rate changes from 42 g/h to 58.5 g/h and from 58.5 g/h to 91 g/h are 0.0008 kg/m^3 and 0.0016 kg/m^3 respectively; and under 1ACH, these two increments are 0.0005 kg/m^3 and 0.001 kg/m^3, respectively. It is noted that for the same changes of moisture loads, the variation of moisture concentration at higher ventilation rates is smaller than that at lower ventilation rates.

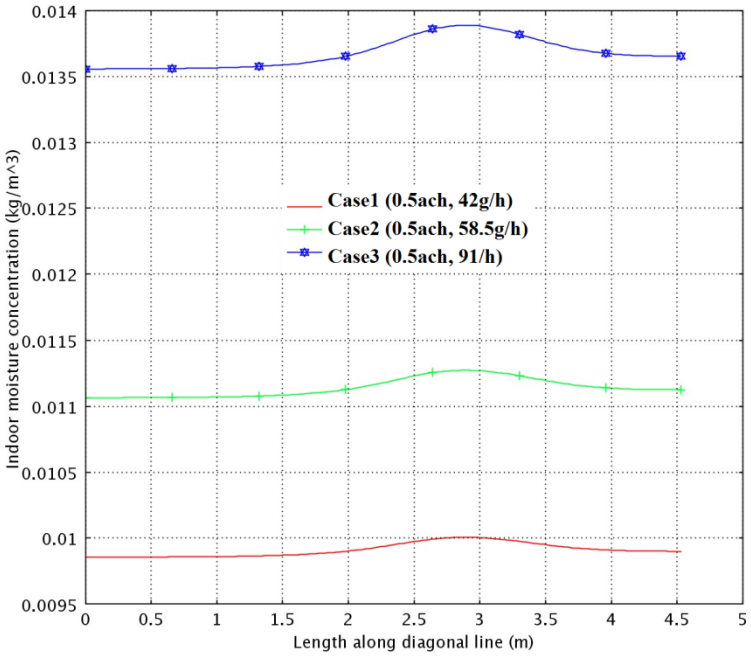

Fig. 7.5 Moisture concentration profiles along the diagonal line for cases 1, 2 and 3 with same ventilation rate of 0.5ACH

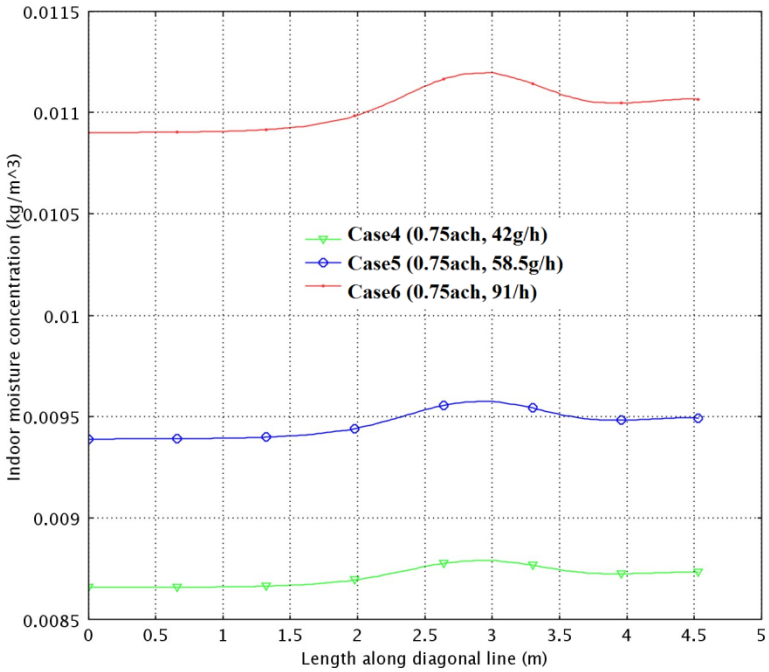

Fig. 7.6 Moisture concentration profiles along the diagonal line for cases 4, 5 and 6 with same ventilation rate of 0.75ACH

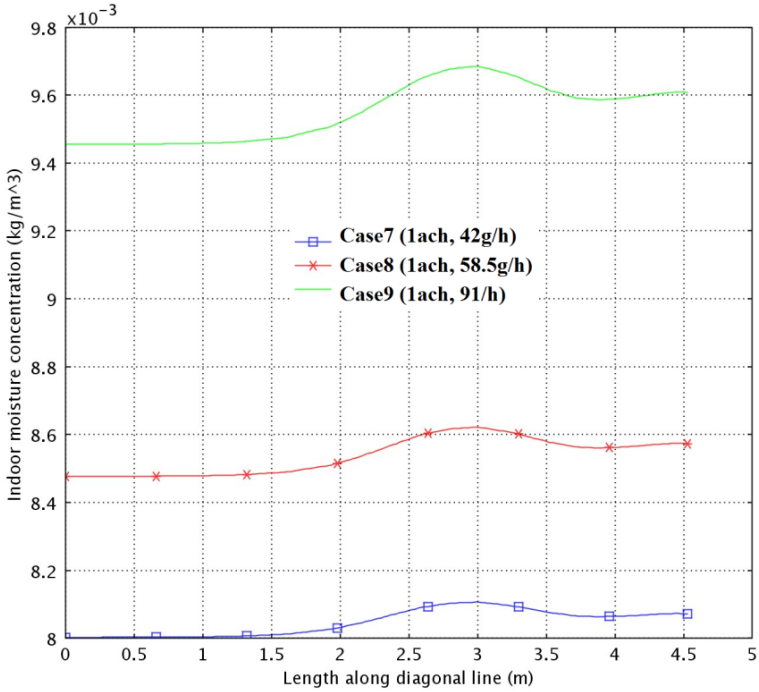

Fig. 7.7 Moisture concentration profiles along the diagonal line for cases 7, 8 and 9 with same ventilation rate of 1ACH

7.4 Impact of ventilation vents design on indoor environment

The influences of the position of the ventilation vents on indoor environment are investigated by simulation cases 10 to 12 in which the position of the inlet is moved down to the bottom of the north wall while the outlets are moved to the upside of the south wall as shown in Table 7.2. To compare the simulated results of the cases with changed positions of the vents to those of cases with unchanged ventilation positions,

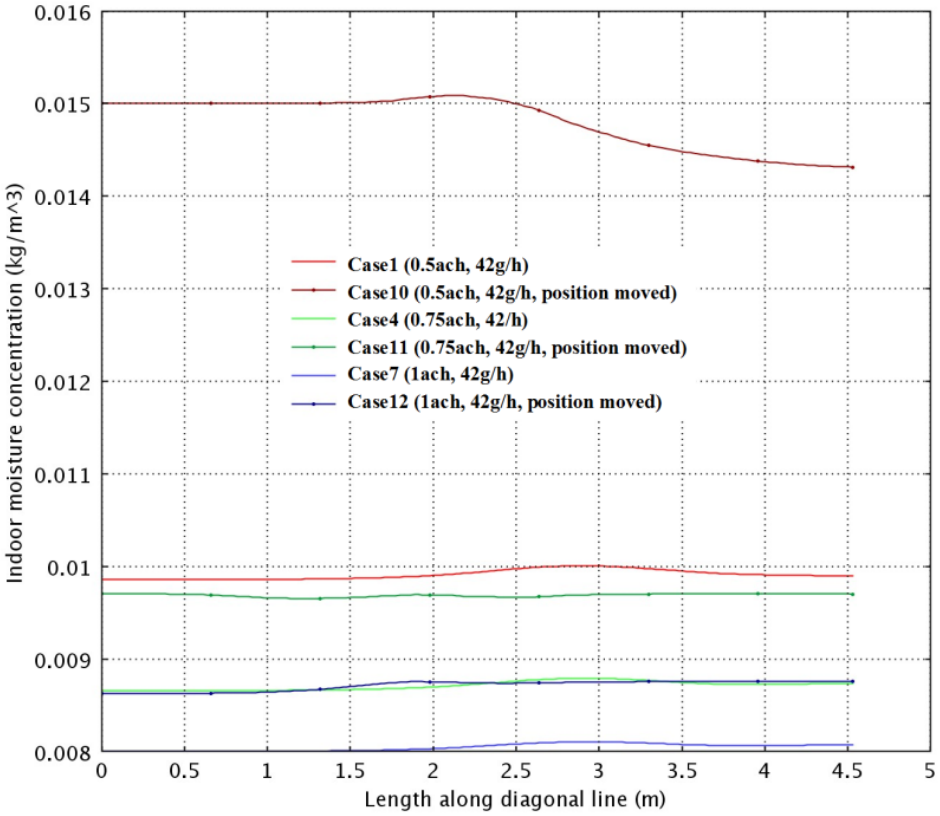

Fig. 7.8 Moisture concentration profiles along the diagonal line for cases 1&10, cases 4&11, and cases 7&12

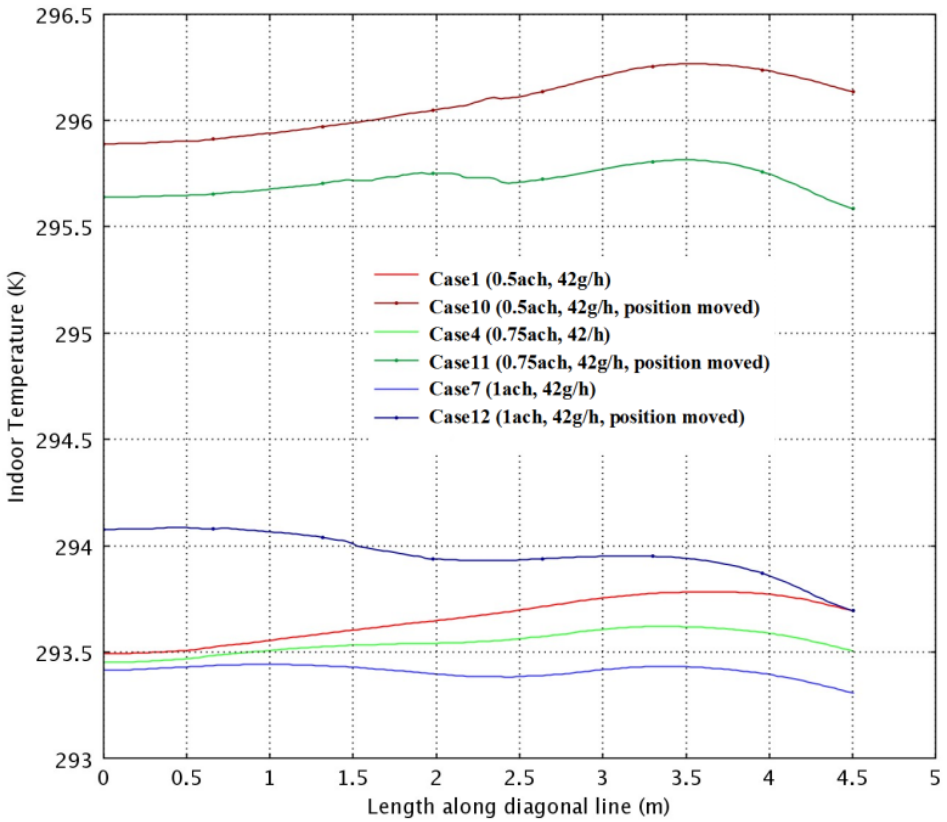

Fig. 7.9 Temperature profiles along the diagonal line for cases 1&10, cases 4&11, and cases 7&12

the profiles of indoor moisture concentration and temperature along the diagonal line for each compared pair are shown in Figures 7.8 and 7.9. These pairs include: cases 1 & 10 (0.5ACH, 42 g/h, red lines), cases 4 & 11 (0.75ACH, 42 g/h, green lines), cases 7 & 12 (1ACH, 42 g/h, blue lines). The figures show that the positions of the inlet and outlet have a large impact on the indoor environment, especially when the ventilation rate is low. In case 10, the average temperature inside the test room is about 2.5 °C higher than that in case 1, which has the same ventilation rate of 0.5 ACH and the same moisture generation rate of 42g/h but different location of the ventilation vents (see

Table 7.2), and the moisture concentration increase of 0.005 kg/m^3 higher, which corresponds to 18 % higher in RH increase than that of case 1. The large difference is due to the existing heat/mass source at the center of the room. This ventilation vent position is not an efficient ventilation design in this scenario. The lower ventilation efficiency keeps more heat and moisture generated by the source inside the room and leads to the significant changes in the indoor conditions. Figures 7.10 and 7.13 show the air flow streamlines in cases 1 and 10 respectively. When the positions of the vents do not change in case 1, the air inside the test room circulates clockwise and mixes well with the heat and moisture coming from the generation source. While in case 10, the buoyant force due to the hotplate separates the air circulation into two parts. One part of the air on the north side, i.e. the side near the electric heater, circulates counter-clockwise due to the jet coming in from the supply vent; while the other part of the air on the same side circulates clockwise due to heating by the electric baseboard. These opposite circulations reduce air movement and heats up the air on that side. On the south side, the air circulates clockwise due to the center hotplate. The separated circulations trap heat and moisture, and make the air inside the room not well mixed. This results in a high value of temperature and RH.

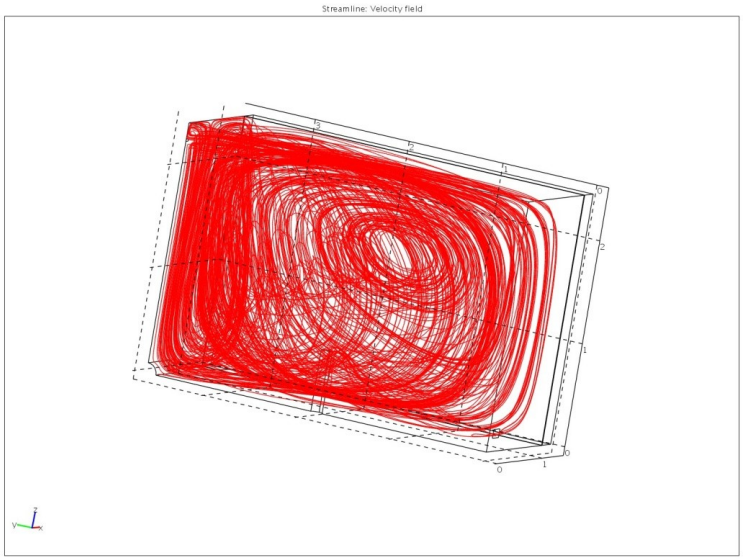

Fig. 7.10 Streamlines illustrating the clockwise air movement in case 1 (0.5ACH, 42g/h)

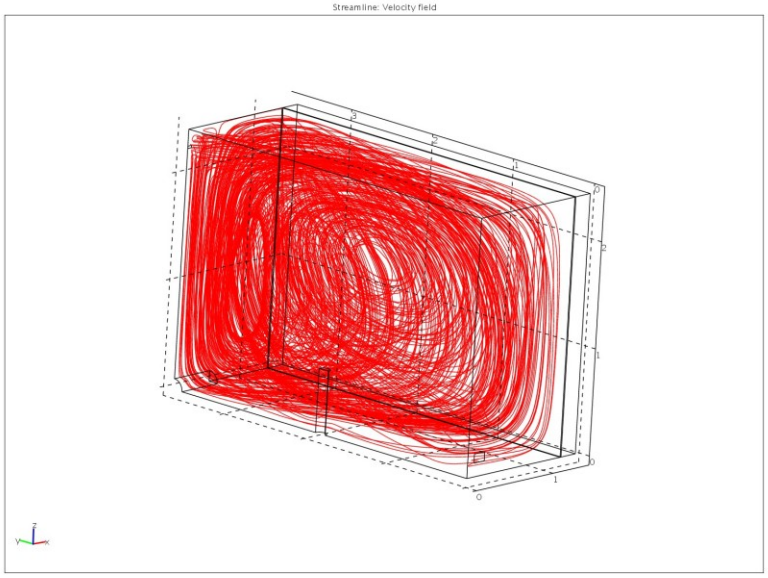

Fig. 7.11 Streamlines illustrating the clockwise air movement in case 4 (0.75ACH, 42g/h)

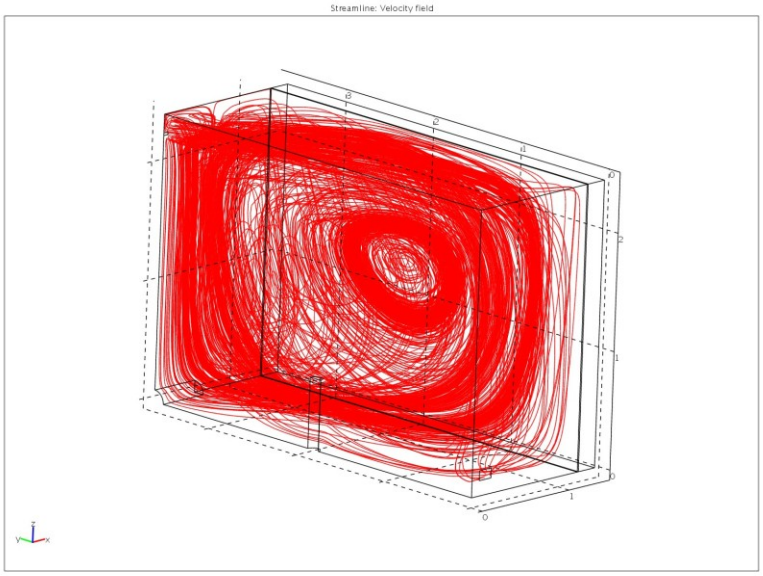

Fig. 7.12 Streamlines illustrating the clockwise air movement in case 7 (1ACH, 42g/h)

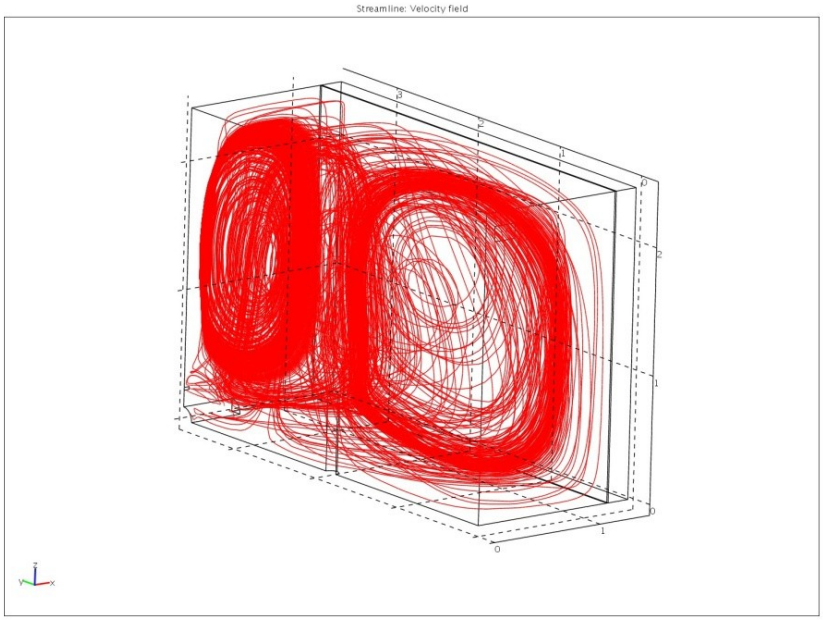

Fig. 7.13 Streamlines illustrating the separated air flow in case 10 (0.5ACH, 42g/h, vents position moved, see Table 7.2)

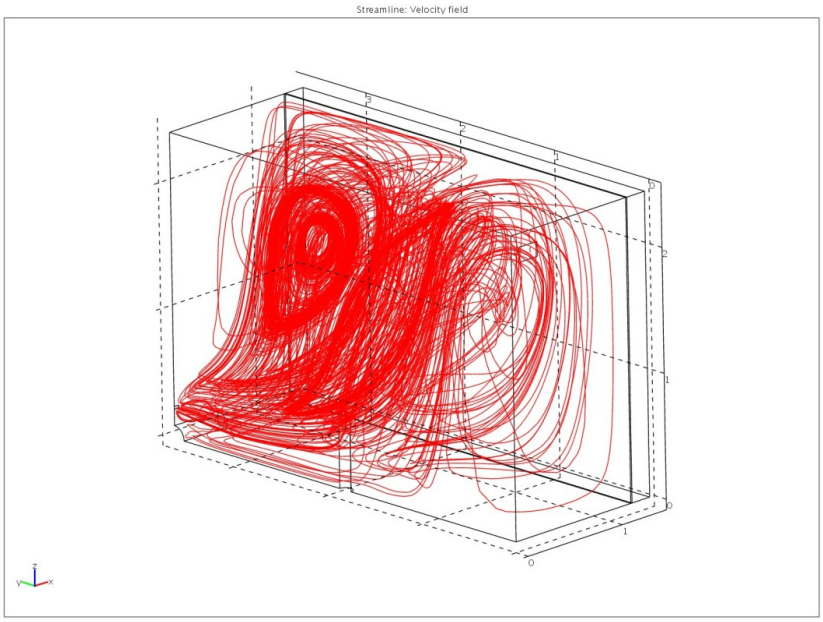

Fig. 7.14 Streamlines illustrating the separated air flow in case 11 (0.75ACH, 42g/h, vents position moved, see Table 7.2)

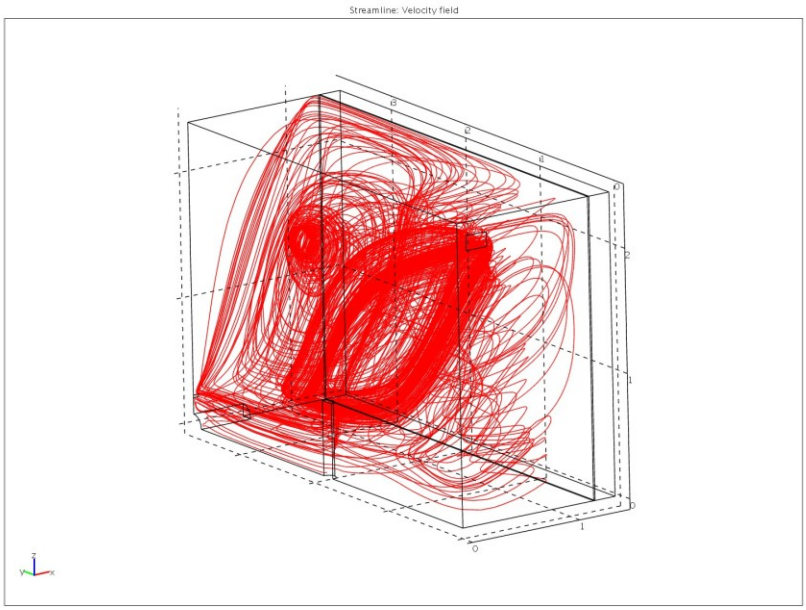

Fig. 7.15 Streamlines illustrating the separated air flow in case 12 (1ACH, 42g/h, vents position moved, see Table 7.2)

The ventilation efficiency is improved when the ventilation rate increases as shown in Figure 7.14 for case 11. In this simulation case, the vent position is same as in case 10, but with a higher ventilation rate of 0.75ACH. The streamline pattern shows that the circulation on the north side close to inlet wall becomes smaller, and indicates more humid air circulating on the south side. The increased air circulation on the south side which is close to the outlet can carry away more heat and moisture. In case 11, the moisture concentration is 0.001 kg/m^3 more than that in case 4 which has the same moisture generation rate of 42g/h and the same ventilation rate of 0.75ACH, and the temperature in case 11 is 2.1 °C higher. The differences of the moisture concentration and the temperature between cases 4 and 11 which have the ventilation rate of 0.75ACH are smaller than those between cases 1 and 10 which have the ventilation rate of 0.5ACH. When the ventilation rate reaches 1ACH, the differences of the moisture concentration and temperature between case 7 and case 12 become much smaller. In case 12 (with changed position), the indoor temperature is 0.5°C higher than case 7 (with unchanged position), and the moisture concentration is 0.0008 kg/m^3 higher, which corresponds to 4.5 % RH at room temperature. Figure 7.15 shows the air flow pattern of case 12. From this figure, one can observe that the circulation on the north side becomes much smaller than that in case 11, which indicates that higher ventilation efficiency is obtained. By comparing the flow patterns between the cases with unchanged vent positions and the cases with changed positions shown in Figures 7.10 to 7.15, the influence of the position of the ventilation vents on indoor air movements can be observed. When the ventilation vents are not changed as in cases 1, 4, and 7, the air

flows clockwise inside the test room (Figures 7.10 to 7.12). The increased ventilation rate accelerates the air velocities but does not change the air clockwise moving direction. When the vents positions are changed, the air movement inside the room is changed both in direction and magnitude. The CFD simulation provides an extension to the experimental results and a visualization of the air flows which help to explain changes in the indoor environment when room factors are varied.

The air flow pattern in case 1 shown in Figure 7.10 also explains why the north side of the test room has relative higher temperature and RH values as shown in the simulated patterns of Figures 6.9 and 6.10. The clockwise air flow moves the moisture and heat generated from the hotplate to the north side and results in a higher value of temperature and humidity level in this region.

7.5 Investigation of the impact of ventilation conditions on heat and moisture fluxes across the wall

Different ventilation conditions have different impact on heat and moisture transfer through the envelope. Since the same outdoor conditions are employed in the simulation of all cases, the heat and moisture fluxes in the walls are related to the indoor temperatures, the RH profiles, and the velocities along the wall surface.

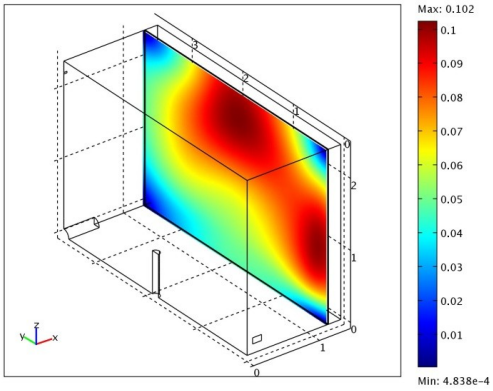

a) case 1 (0.5 ach, inlet/outlet at 2.26 /0.172 m)

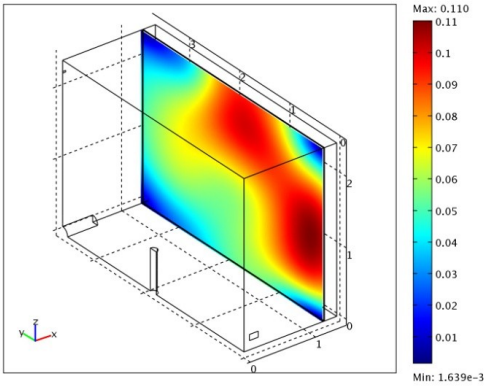

b) case 4 (0.75 ach, inlet/outlet at 2.26 /0.172 m)

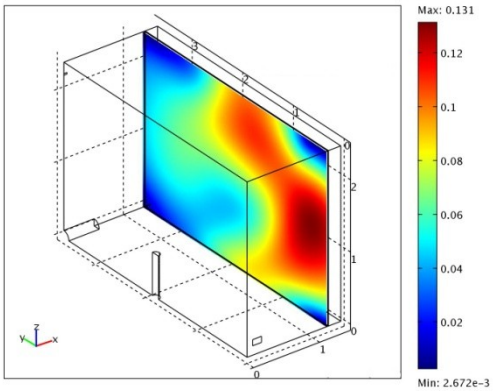

c) case 7 (1 ach, inlet/outlet at 2.26 /0.172 m)

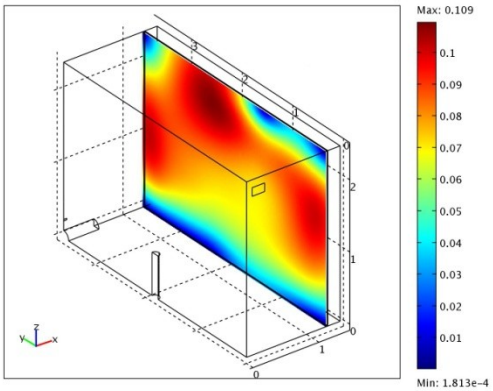

d) case 10 (0.5 ach, inlet/outlet at 0.25 /2.2 m)

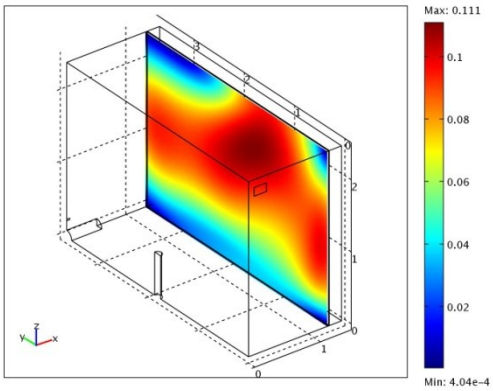

e) case 11 (0.75 ach, inlet/outlet at 0.25 /2.2 m)

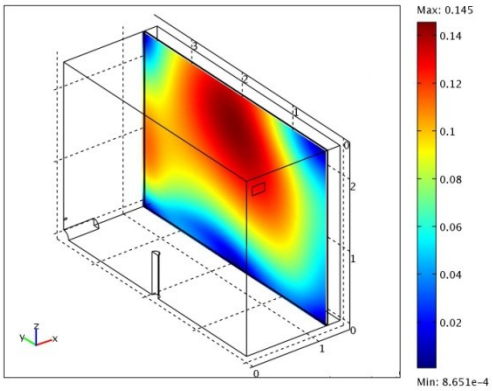

f) case 12 (1 ach, inlet/outlet at 0.25 /2.2 m)

Figure 7.16 Velocity maps on plane at 0.02 m from the east wall, at different ach, with inlet/outlets at different heights, and with the same moisture generation rate of 42 g/h

Figure 7.16 shows the air velocity profiles along the wall surface in cases 1, 4, 7 (42 g/h for each case, and with ventilation rate of 0.5, 0.75 and 1ACH respectively) and cases 10, 11, 12 (same conditions with the previous three cases, but with the changed vents positions) respectively. For different ventilation rates and different positions of the ventilation vents, the air flow patterns near the wall surface are different. The maximum velocities near the wall surface in each case are 0.102 m/s, 0.110 m/s, 0.131 m/s (for cases 1, 4 and 7), and 0.109 m/s, 0.111 m/s, 0.145 m/s (for cases 10, 11 and 12), respectively. Cases 7 and 12 have the largest maximum velocities due to their highest ventilation rate of 1ACH. The maximum velocities near the wall surface in case 7 are 28% higher than case 1, and in case 12, the maximum velocities are 42% higher than case1.

Table 7.3 Total heat and moisture fluxes passing through the intestitial boundary between sub-domains 2 and 3

Case number	*Indoor Temperature [K]*	*Heat Flux [W]*	*Indoor Moisture Concentration [kg/m^3]*	*Moisture Flux [kg/s]*
Case 1 (0.5ACH,42g/h)	293.7	45.99	0.0100	5.32×10^{-8}
Case 4 (0.75ACH,42g/h)	293.6	46.01	0.0088	4.49×10^{-8}
Case 7 (1ACH,42g/h)	293.4	46.03	0.0081	4.03×10^{-8}
Case 10 (0.5ACH,42g/h)	296.1	50.62	0.0150	8.65×10^{-8}
Case 11 (0.75ACH,42g/h)	295.7	50.11	0.0096	5.18×10^{-8}
Case 12 (1ACH,42g/h)	293.8	47.09	0.0088	4.50×10^{-8}

Note: cases 10 to 12 are the cases with the position of ventilation vents moved (see Table 7.2)

It is expected that the higher velocity close to the wall surface will lead to higher surface coefficients and increase the heat and mass fluxes through the wall systems. However, the influences of the increased air velocity values in these simulation cases are not significant. Table 7.3 lists the indoor temperature, moisture concentration and the

integration of heat/moisture fluxes across the interstitial boundary between sub-domains 2 and 3 in the above cases, which corresponds to the interface between the wood paneling and the dry wall. For the unchanged ventilation positions (cases 1, 4 and 7), even though the maximum air velocity in case 7 is about 28% higher than case 1, and about 20% higher than case 4, the heat fluxes in these three cases are almost the same (45.99, 46.0 and 46.03 W respectively). The moisture fluxes do not increase as the velocity becomes larger (5.32×10^{-8}, 4.49×10^{-8}, and 4.03×10^{-8} kg/s respectively), but vary according to the indoor humidity levels. For cases 10 to 12 which are with the changed ventilation positions, the heat and moisture fluxes decrease as the indoor temperature and humidity level decrease from 22.95 °C and 0.015 kg/m^3 MC in case 10 to 20.65 °C and 0.0088 kg/m^3 MC in case 12. Case 10 has the largest heat and moisture fluxes (50.6 W, 0.015 kg/m3) due to its highest indoor temperature and moisture concentration values, and case 12 has the smallest flux values (47.09 W, 0.0088 kg/m3) due to its lowest indoor temperatures and humidity levels, despite case 12 having the largest velocity in these three cases. The reason that the velocities close to wall surfaces do not significantly influence the heat and moisture transfer inside the wall is that the absolute differences of the velocities among these cases are small. The insignificant influences of the velocities near the wall surface show that under mixed convection conditions, the indoor temperature and humidity levels dominate the heat and moisture fluxes through the wall system. In this simulation, the interaction of the heat and moisture between indoor air and wall surface is achieved by the continuity equations of the fluxes (Eqs. 6.20 to 6.22). The simulation shows that at the ventilation rate of 1.0 ACH or less, the

velocity near the wall surfaces has insignificant influence on heat and moisture transport across the wall system. This insignificant influence indicates that for mixed convection simulation, the assumption of the constant heat and mass surface coefficients can be applied to the inside wall boundaries without significantly affecting the simulation results.

7.6 investigation of potential damages caused by mold growth

Mold growth is an important topic in the indoor environment studies because molds not only cause costly damages to household structures, but can also put occupants' health and wellbeing at risk. The transport of microbial volatile organic compounds in wall cavities has been investigated in some previous studies (Hachem, Fazio, Rao and Bartlett, 2009; Rao, Fazio, Bartlett, Yang, 2009; Hachem, Chaubey, Fazio, Rao and Bartlett, 2010). This numerical model can be utilized to predict the potential damages caused by molds based on the criteria of the mold growth in the mold studies. The studies found that for mold growth there are four requirements: water, suitable temperature, food, and air. Since molds absorb nutrients through microscopic threads, it is relatively easy to have the last two requirements, food and air, in an indoor environment. Then the water and temperature are the critical conditions to be controlled in order to avoid mold growth. Viitanen and Salonvaara (2001) concluded that the temperature over 0°C creates a favourable condition for mold growth if accompanied with high relative humidity for long enough time. Kowalski (2000) listed all of the major pathogenic and allergenic fungi, by genus, that have been found growing indoors, and Clarke et al (1998) summarized

the relative humidity and temperature conditions for the growth of six generic mold categories as shown in Figure 7.17. The study indicates that at room temperature, 75% RH is the critical value for mold growth.

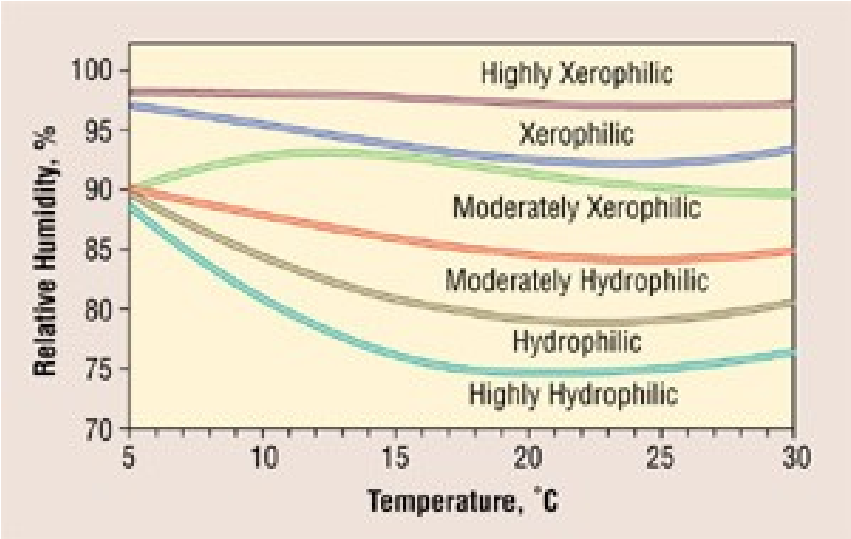

Fig. 7.17 Effect of Temperature and Relative Humidity on Mold Growth Rates, based on data from Clarke et al (1998)

In this thesis, the RH color maps on the wood wall surface and inside the wall system are obtained from simulations to study the potential regions for the mold growth under different room factors. Figure 7.18 shows a color map of RH on the surface of wood paneling in case 1 (0.5ACH, 42g/h). The bottom corner of the east and north walls has

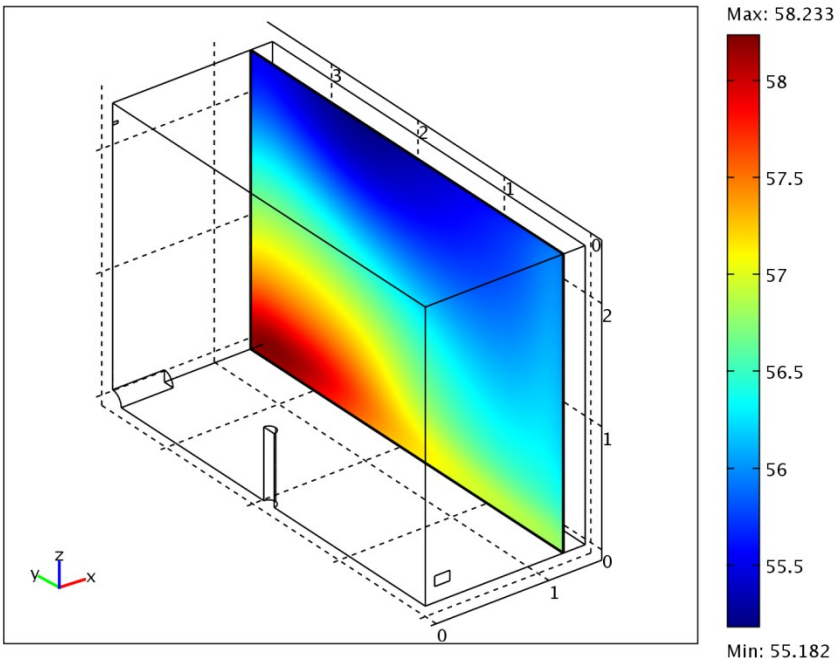

Fig. 7.18 RH profiles on the east wall surface in case 1 (0.5ACH, 42g/h)

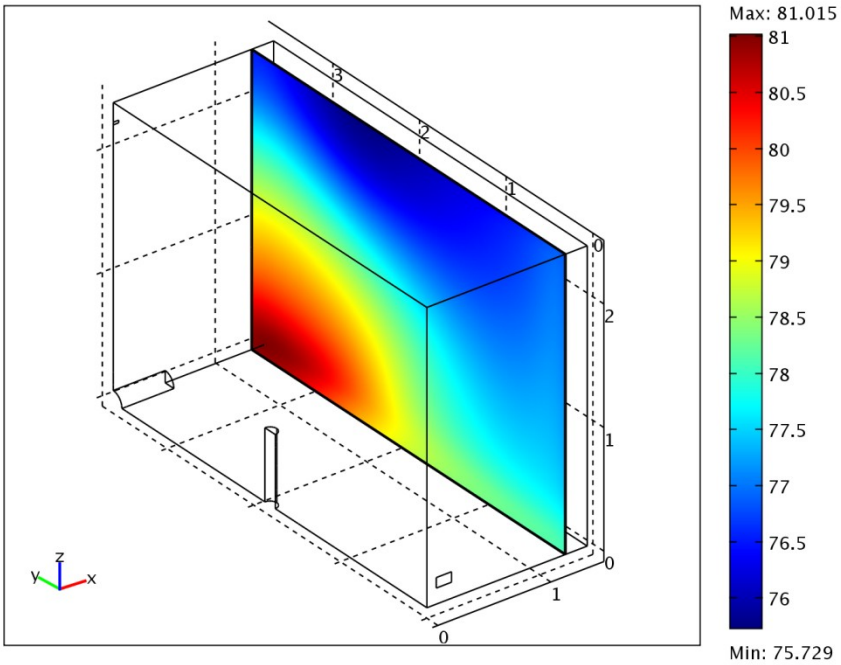

Fig. 7.19 RH profiles on the east wall surface in case 3 (0.5ACH, 91g/h)

the highest RH value in this simulation scenario. The highest value is less than 60% in this case, which can be regarded as unfavourable condition for mold growth. The RH value in this region increases as the moisture generation rate becomes larger. Figure 7.19 shows the RH profiles in case 3 (0.5ACH, 91g/h). The highest RH value is 81% which indicates potential mold growth.

The region of the highest RH value is located at the bottom corner of east and north wall in these two presented cases. Similar places of high RH value are observed in other cases with the unchanged position of the ventilation vents, i.e. in all cases 1-9. The bottom region of the wall has the lower temperature because the heated air moves up and the RH value is inversely proportional to the temperature. Meanwhile, the ventilation moves the moisture to the north side when the air clockwise circulates in the test room. When the position of the ventilation vents change, the movement pattern of the indoor air also changes as illustrated in the previous sections. Then the region of the highest RH value is different. Figures 7.20 to 7.22 show the RH profile along the wood wall surface in cases 10-12. Since the ventilation rate has great impact on the moving direction of the indoor air, the region with the highest RH values changes in these three cases. The figures indicate that the highest RH value is located at the bottom corner of the east wall and south wall in case 10, at the bottom of the east wall in case11, and at the bottom of the east wall but close to the corner of east and north wall in case 12.

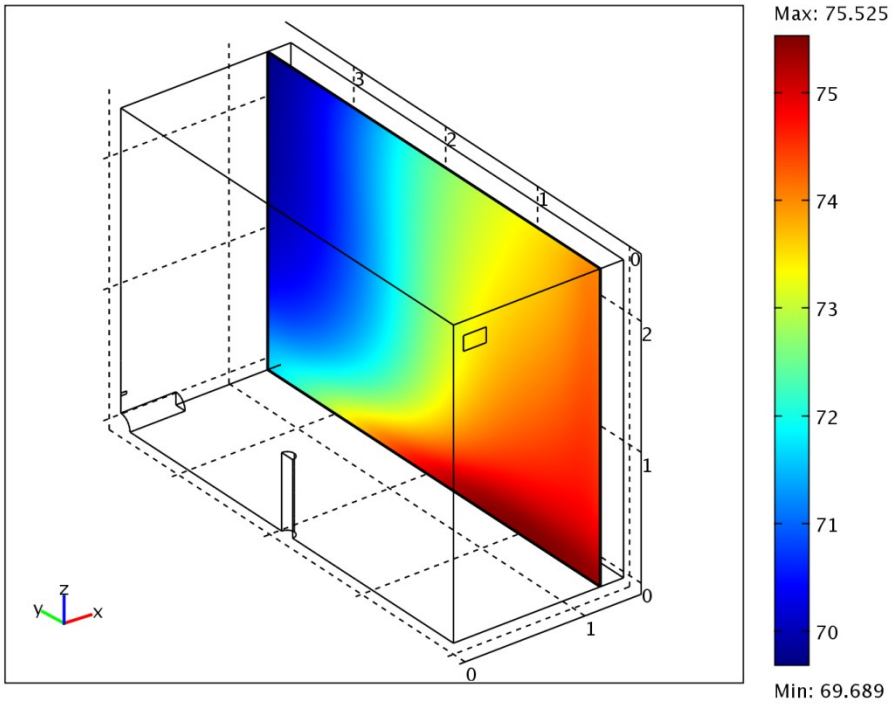

Fig. 7.20 RH profiles on the east wall surface in case 10 (0.5ACH, 42g/h, changed vent position

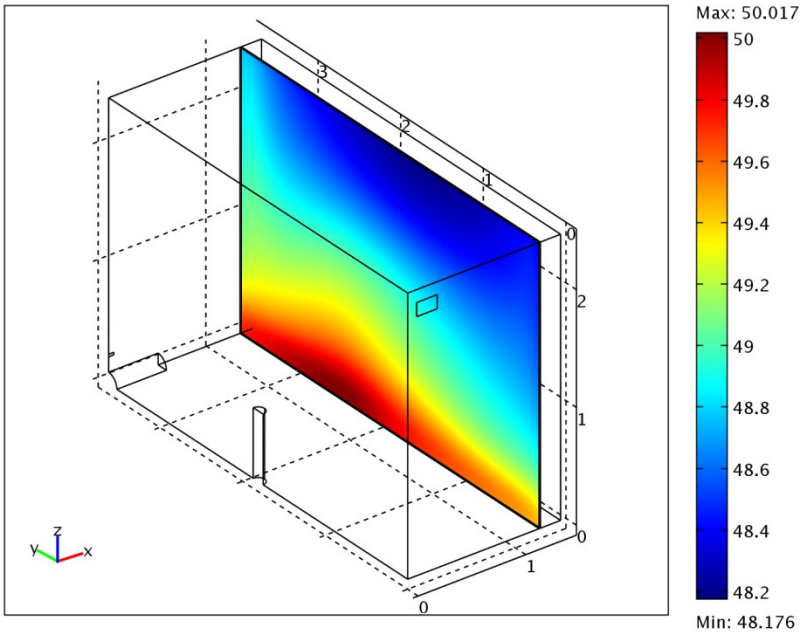

Fig. 7.21 RH profiles on the east wall surface in case 11 (0.75ACH, 42g/h, changed vent position)

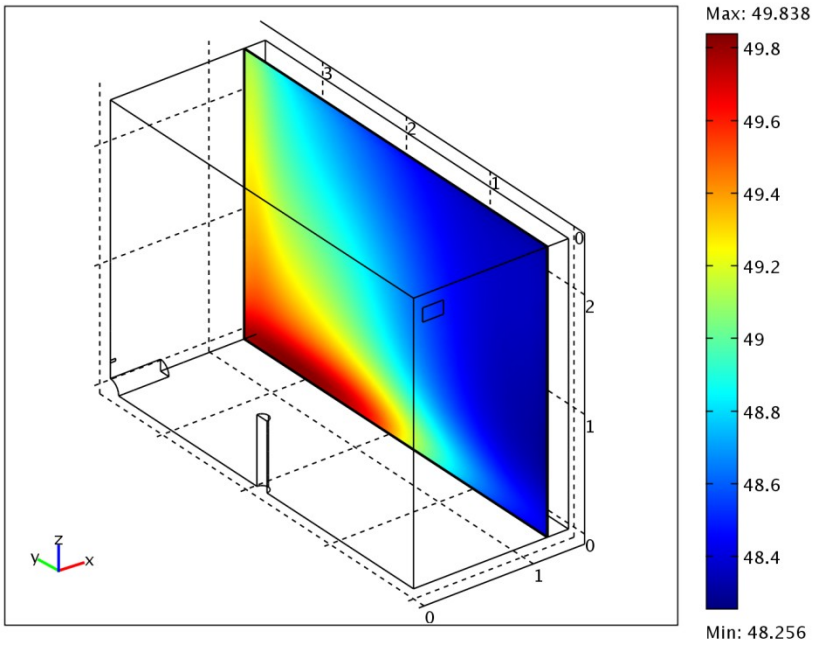

Fig. 7.22 RH profiles on the east wall surface in case 12 (1ACH, 42g/h, changed vent position)

The RH values on the wall surface are not uniform and are different in different cases. Table 7.4 summaries the highest and lowest values of RH along the wood surface in all simulated case. The value of the highest RH increases as the moisture generation rate increases; and this value decreases as the ventilation rate increases. For the unchanged vent position, the condition of the favourable mold growth happens in case3 which has the 91g/h moisture generation rate. This simulation result indicates that for 0.5ACH ventilation rate, the critical moisture generation rate for the mold growth is between 58.5 g/h and 91g/h. When the ventilation rate becomes higher than 0.75ACH, the moisture generation rate can be as large as 91g/h without causing any favourable mold growth condition. For the changed vent position, at 0.5ACH ventilation rate, the

moisture generation rate of 42g/h has reached the critical condition of mold growth. This analysis indicates that the ventilation design also has great impact on indoor mold growth.

Table 7.4 Range of RH values along the east wall surface in all simulated cases

Case number	Ventilation rate (ACH)	Moisture generation rate (gram/hour)	Highest RH value (%)	Lowest RH value (%)
1	0.5	42	58.2	55.2
2	0.5	58.5	65.7	61.9
3	0.5	91	81	75.7
4	0.75	42	51.5	48.9
5	0.75	58.5	56.2	53
6	0.75	91	65.7	61.5
7	1	42	48	45.7
8	1	58.5	51.1	48.4
9	1	91	57.4	53.9
10	0.5*	42	75.5	69.7
11	0.75*	42	50	48.2
12	1*	42	49.8	48.2

*with ventilation vent positions changed

The color maps for RH and temperatures along the vertical cross sections at 5 locations of the east wall can be observed in Figures 7.23 & 7.24. Figure 7.23 shows that the RH values inside the wall system are higher than the values on the wood wall surfaces. The higher value of the RH is due to the lower temperature distributions inside the wall system. In the experiments, the outside temperature is -5 °C. There is a temperature gradient from the high indoor temperature region to the low outdoor temperature region, as observed in Figure 7.24. It is noted that in the center region of the wall, the temperature change with respect to the distance change in the direction crossing the wall from indoor to outdoor is not the same. This non-uniform temperature gradient

may be caused by the presence of the heat source at the center of the room. The governing equation of the heat transport takes into account not only the convection mechanism of the heat transfer but also the diffusion process of the heat transfer. The non-homogenous temperature distribution on the wood wall surface results in the different heat fluxes in the different regions of the wall. The non-uniform temperature gradient in the wall system leads to the non-homogenous distribution of RH as shown in Figure 7.23. The non-homogeneous distributions of temperature and relative humidity are consistent with the measurements of the thermocouples and moisture pins as presented in Chapter 4.

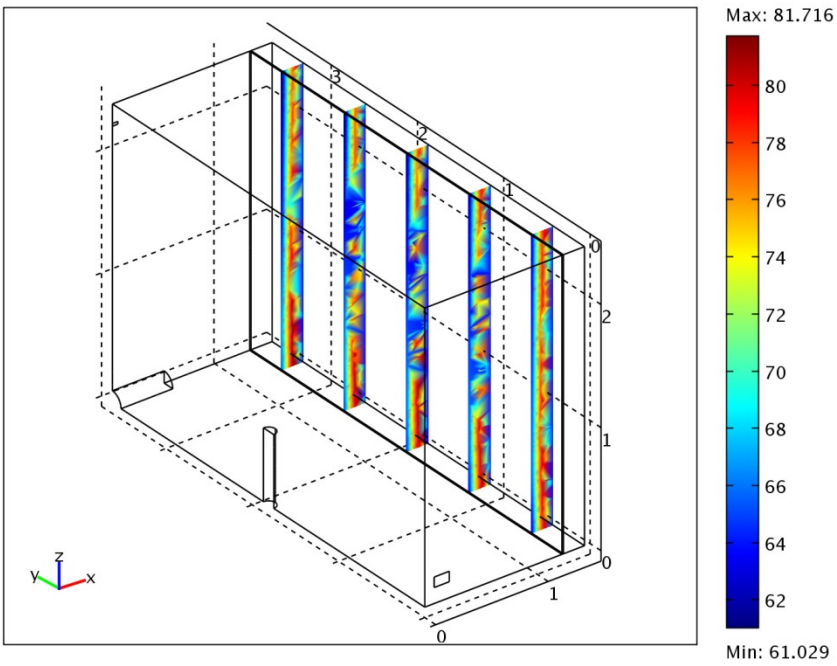

Fig. 7.23 RH color maps in the cross section of the wall for case 1

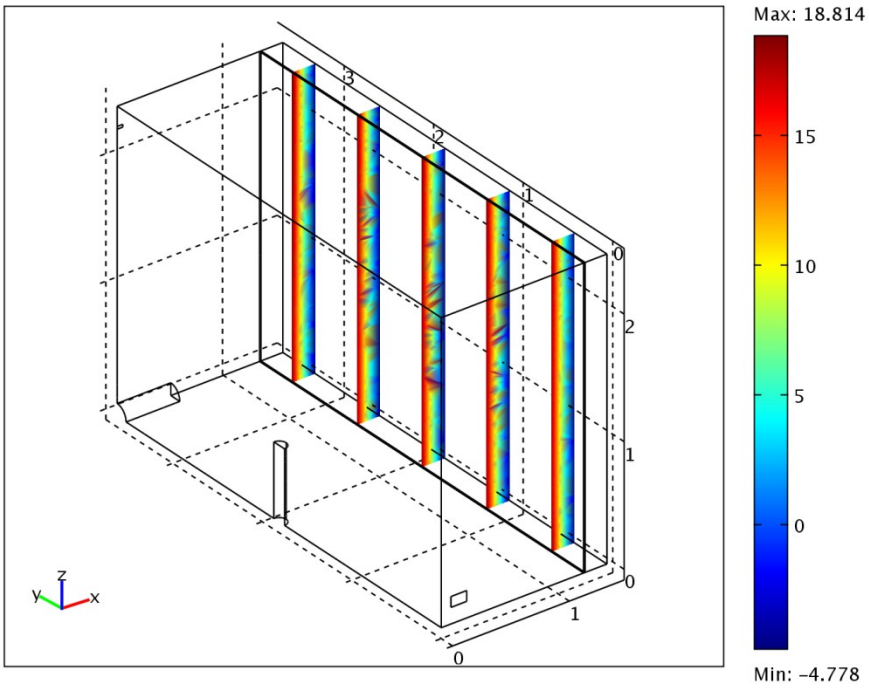

Fig. 7.24 Temperature color maps in the cross section of the wall for case 1

The highest value of the RH has reached 81% in this case (case1 with 0.5ACH and 42g/h). However, it does not mean that the mold will be necessarily generated. The temperature of the region where the highest RH value is located is in the range of 5-8°C. According to the mold growth criteria as presented in Figure 7.17, in this range of the temperature, the favourable RH condition for mold growth is over 85%. The simulation results also show that the highest RH value to be located at the middle layer of the wall. Since the effective wall is simulated in the wall sub-domain in this numerical model, the position of the potential mold growth inside the wall may not be accurate. To precisely predict the mold growth inside the wall requires a model that sufficiently defines the characters of the different layers of the wall and the contact properties of the region between any two layers in the wall. This model characteristic is beyond the scope of this

thesis. From the Figures 7.23 and 7.24, the simulation results indicate that the potential damage region of the wall system is in the bottom region of the middle layers.

7.7 Summary

A CFD model, coupling momentum, heat and moisture transport inside a test room and through multilayered wall systems, has been developed. The coupling among the governing equations and between the indoor air domain and the wall system domain is implemented in a single simulation environment -- COMSOL. This direct coupling model has great application potential. Using this model, the indoor condition, HAM transport in the wall, and other coupled processes can be directly simulated.

Based on this model, the influence on the heat & moisture transports in the indoor air and through its envelope by moisture loads, ventilation rates, and position of inlet and outlets are investigated. The simulation results show that the humidity response of the test room varies significantly under the range of the moisture loads from 42 to 91 g/h, and the ventilation rates changes from 0.5 to 1ACH. The largest variation is 35% RH increase in simulation case 3, in which the ventilation rate is 0.5 ACH and moisture generation rate is 91 g/h; while the lowest RH increase is 1% in simulation case 7, in which the ventilation rate is 1 ACH and moisture generation rate is 42 g/h.

The position of the ventilation vents has the most significant effect on the indoor environment especially under the low ventilation. The moved positions of the vents change the air flow pattern inside the test room significantly and decrease the

ventilation efficiency. Due to the existence of the heat and moisture source inside the test room, the low ventilation efficiency increases the indoor temperature and humidity level. At the ventilation rate of 0.5ACH, and under the moisture load of 42 g/h, the increased temperature and RH value are 2.5 °C and 18% respectively. The influence of the ventilation change becomes smaller when the ventilation rate increases. At the condition of 1ACH and 42 g/h, the increased temperature and RH values are 0.5 °C and 4.5 %.

Simulations show that under mixed convection condition, the indoor temperatures and moisture levels, which change with the ventilation condition, dominate the heat and moisture transport through the wall system. The velocity profile along wall surface has less effect on the heat and mass transfer inside the walls.

The mold growth occurs when the relative humidity has reached to certain level at regions where temperature is mild. The simulation results show that for the cases with unchanged vent positions, the bottom corners between east/west and north walls are the places that have the highest RH values, and for the cases with the changed vent positions, the bottom region of east/west wall is where mold most likely would grow. The RH levels in some region of the wall system are higher than the indoor RH values where the temperature would be higher than the temperature in the wall. Depending on the temperature distribution, the region with high RH values also may be at risk for mold growth. For all simulated cases, the high risk region is located at the middle layer of the wall assembly.

The limitation of this model is that the mass coupling on the wall surface is based on the direct continuity of mass flux calculation. Even though this continuity is adopted in most other simulation studies, the model with this limitation may not truly represent the turbulent effects on the mass transfer in this region. However, the simulation results show that the velocity profiles on the wall surface is not a dominant factor influencing moisture transfer inside the wall system, and the agreement of the RH and temperature distribution inside the test room with the experimental measurement indicates that under mixed convection conditions, this model can correctly predict the indoor environment with the HAM responses of the wall system taken into account. In this thesis, this model deals with the steady state simulation, the models that investigate the dynamic HAM responses of the test room and its wall system are recommended for future studies.

CHAPTER 8

CONCLUSIONS, CONTRIBUTIONS AND FUTURE WORK

8.1 Summary of the thesis study

Indoor humidity levels are important for building performance and the inhabitants. The durability of building components is directly related to the humidity condition of their surroundings and within themselves. The materials in concealed spaces inside buildings can get damaged if they are persistently under high levels of moisture concentration. The indoor humidity level is related to the room factors including moisture loads and ventilation conditions and to the moisture ab/desorption capacity of hygroscopic materials for interior finishing or furnishing of the building. The phenomenon of the indoor humidity level being dampened by the dynamic moisture interactive process between hygroscopic materials and indoor air is recognized as moisture buffering effect. The buffering effect and the moisture ab/desorption performance of hygroscopic materials under different room factors were experimentally studied in this thesis. The steady state indoor environments influenced by room factors taking into account the moisture interactive process between indoor air and enclosure were investigated numerically in this thesis. The CFD technique was employed in the numerical investigation.

A literature review on the experimental and numerical investigations on moisture buffering and whole building indoor environment was carried out in this thesis. This review found that the moisture buffering effect of hygroscopic materials had been extensively studied at the material level, i.e. the characterization of the buffering property of materials. However, the buffering property of the material may not be representative of the buffering performance of the material at the room level because the indoor hygrothermal condition, room factors, and moisture buffering of hygroscopic materials influence each other. The buffering effect of hygroscopic materials on the indoor environment has been observed in some large-scale experimental studies, but the measurement of the buffering effect values under different room conditions and the explanation of the buffering effect related to the buffering property of hygroscopic materials and room factors have not been found in existing studies. The literature review also found that a CFD model in a single simulation environment to study the HAM transport including the moisture interaction between the indoor air and the envelope is needed, but yet to be developed. Using this kind of CFD model, detailed information of the moisture transport in a building and inside its envelope could be obtained, and the indoor humidity level influenced by the room factors could be predicted by the simulation of HAM transport processes involved.

To study the moisture buffering effect at the room level experimentally and to simulate the HAM transport in the whole domain of the room air and its enclosure numerically, the fundamental theories of the hygroscopic material properties, the governing equations describing HAM transport in the convection and diffusion processes, the

analogy between mass transfer and heat transfer, and the formulation of this thesis experiment have been presented.

The thesis presents the experimental facilities, setup, procedures, methodologies, parameters, preliminary results, measurements of indoor humidity level changes, calculations based on the formulation, and analysis. To study the moisture buffering effect of the hygroscopic material at room level, the panels made of pine wood were installed on the inner layer of the walls in the test room. The tests were performed with the room under different test loads in 12 pairs of cases, i.e. 24 test scenarios, to study the indoor humidity level influenced by moisture buffering effects under different room factors. Through these tests, the findings of the moisture buffering performance of wood paneling at room level, the impact of room factors on wood paneling moisture ab/desorption and on indoor humidity level change, the buffering effect values at room level corresponding to the test parameters change were obtained.

The fully coupled CFD model to simulate HAM transports in the simulation domains of test room and wall was established. This model was built in COMSOL Multi-physics, a PDE basis simulation environment. The governing equations of the momentum, heat, and mass transport were coupled by correctly defining the relationship of the independent variables according to the characteristics of the fluid flow inside the test room. The coupling process of heat/moisture between the indoor air and wood paneling were established by defining the fluxes equations in the interface of the two regions. These equations were solved in the whole building domain, i.e. the test room and wall

system. In COMSOL, the algorithm of solving PDEs is based on finite element method. Then the PDE discretion, i.e. the meshing was developed. The general applications of CFD techniques were not elaborated in the thesis, but the special points, such as the solver selection, were demonstrated. The numerical model was implemented in 12 cases. These cases studied the influence of moisture loads, ventilation rates, and ventilation vents design on the indoor environmental changes and on the heat/moisture transport through wall. The potential damage of the test hut caused by mold growth was also simulated by investigating the RH distribution in different regions of the simulation domain.

8.2 Findings and Conclusions

Findings and conclusions obtained from experimental work:

- The two-step experimental methodology had advantages of evaluating the moisture buffering performances of hygroscopic material at room level. This method made possible the testing of the buffering performance of wood paneling being as part of the wall system in a real room setting, and minimized the errors of the sensors' measurements and of the air leakage investigation in the experimental data calculation and analysis.
- The moisture buffering performance of wood paneling under different test conditions can be represented by the kinetic curves of the moisture ab/desorption process during the 8/16 hours moisture add/release cycle. The

curves reflected the material property of Moisture Sorption Isotherm but varied from one test condition to another. The variation was caused by the room factors which lead to different indoor humidity levels and different surface conditions of the wood paneling. For example, at moisture load of 58.5 gram/hour, the maximum moisture absorption amount of the wood paneling increased by 7.8% when the ventilation rate changed from 0.5ACH to 0.75ACH; this amount increased by 12.4% when an auxiliary fan was turned on to increase the air flow in the test room.

- The moisture buffering effect of wood paneling on the indoor humidity level can be evaluated by the index EDRH. EDRH was defined as the highest RH value dampened by the hygroscopic material in the experiment. The study found that this value was not consistent with the buffering performance of the wood paneling. The buffering effect of hygroscopic material cannot be predicted based on the buffering property or performance only. The room factors have to be taken into account in the buffering effect prediction.
- To further study the buffering effect under different room factors, the buffering effect was evaluated by the indoor humidity level change with respect to a room factor change. The study found that without the presence of the hygroscopic material (non-hygroscopic test) the indoor relative humidity value increased by 8% at the ventilation rate of 0.75ACH when the room factor of moisture generation rate increased from 42g/h to 58.5g/h; this increase of 8% in the RH value decreased to 5% with the presence of the hygroscopic material

(hygroscopic test). The difference of the RH values, i.e. 3%, was the buffering effect caused by the wood paneling corresponding to the moisture generation rate change under the specific tested ventilation condition (0.75ACH in this case). From the experimental data analysis, it was concluded that the room characteristics caused the variation of indoor RH level ranging from 4% to 8% for the room factors tested, and the wood paneling could moderate these variations by the range of 25% to 37.5%.

Findings and conclusions obtained from numerical investigation:

- COMSOL Multi-physics provides simulation environment that the coupling of HAM equations and of the heat/moisture transfer between indoor air and enclosure can be directly achieved without third party programming. In this thesis, the fully coupled model was established in this single simulation environment. This model has several advantages: (i) it overcomes the main limitations of the currently available CFD coupling models in simulating the whole building HAM transport, and (ii) it has great application potential such as for the aspects investigated in this thesis including influences of room factors on indoor environment, ventilation design, heat/moisture transport through wall system, and prediction of mold growth.
- The numerical simulation found that under steady state conditions, for the small range of ventilation rate changes, i.e. from 0.5ACH to 1ACH, the difference of the variation of indoor humidity level for the moisture loads changing from 42g/h to

91g/h was large. For example, at a ventilation rate of 1ACH and moisture generation rate of 91g/h, the maximum indoor RH level during the experimental test increased up to 32% from the beginning of the moisture generation, while at ventilation rate of 0.5ACH and moisture generation rate of 42g/h, the indoor RH level increased 1% only.

- The position of ventilation vents has great impact on indoor environment, especially under low ventilation rates and can change the direction of air flows. The changed air flow circulation influenced the ventilation efficiency. This influence was significant at the ventilation rate of 0.5ACH. Compared with the unchanged vents position, at this ventilation rate, the indoor RH value increased by 18%.
- The heat/moisture transport through the wall system is related to the indoor environment and interior wall surface condition. Under mixed convection condition, the transport is influenced mainly by indoor temperature and humidity levels. The surface condition has less impact on the transport. The simulation results indicate that for mixed convection simulation, the assumption of the constant heat and mass surface coefficients can be applied on inside wall boundaries without significantly affecting the simulation results.
- The simulated potential damage caused by mold growth in the test room was at the two bottom corners of the east/west and north walls for the cases with the unchanged vent positions, and at the bottom region of the east/west wall for the cases with the changed vent positions. At the bottom region of the room, the

lower temperature resulted in higher relative humidity levels, which were the favorable condition for mold growth. For the wall system, the simulation found that the highest RH value was located at the middle layers of the wall system. The accurate location for the wall system need to be further investigated.

8.3 Contributions

- A two-step experimental methodology and the formulation for the experimental test were developed. The methodology made the room level tests of moisture buffering performance for hygroscopic materials available, and it can be utilized to further study the topics related to the HAM transport at room level.
- Air leakage of the test room was investigated in the experiment. The formulation and data processing for the calculation of air leakage were presented in the thesis. This investigation method can be applied in other tests to evaluating the air tightness of a room.
- The moisture buffering performance of wood material at room level was experimentally evaluated and presented by kinetic curves. Such curves have not been found in the literature review.
- The nature of buffering effect caused by hygroscopic material under different room conditions has been explained and its values at room level have been obtained.
- The relationship of indoor environment, buffering effect, room factors has been elaborated through the experimental data analysis.

- A index, EDRH -- the highest RH value dampened by the hygroscopic material, has been proposed to quantify the influence of hygroscopic material on indoor moisture levels
- A new CFD coupling model has been developed in a single simulation environment to overcome the limitations in existing coupling models. This new model has great application potential such as prediction of indoor environment, evaluation of ventilation design, and assessment of mold growth risk.
- Dominant factors of influencing heat/moisture transport through wall systems under indoor mixed convection conditions were identified.

8.4 Recommended future work

The indoor environment influenced by moisture buffering effect and room factors has been experimentally investigated in this thesis study. The buffering effect caused by hygroscopic material -- wood paneling, and the room factors including moisture generation rates and ventilation rates were studied. The relationship of indoor environment, buffering effect, and room factors has been elaborated through the experimental data analysis. Some additional parameters such as higher ventilation rates, other hygroscopic materials can be further investigated using this experimental method. The recommended study regarding the influence of room factors and moisture buffering on the indoor environment is about the solar effect and ventilation strategy. Studies of solar energy and ventilation strategy have been found in the literatures. However, their

combined influences on indoor environment and how moisture buffering effect works in these conditions have not been studied, but are expected to be significant in indoor environment control. The experimental study on these topics can also establish the data foundation for the related numerical simulation.

The fully coupled steady state model of the momentum, heat, and moisture transport inside the test room and through the wall system has been established in a single simulation environment in this thesis study. The indoor environment influenced by room factors and heat/moisture transfer through the wall system have been numerically studied. This model can be further developed and implemented to study transient processes. The simulation of the turbulent effects of mass transfer in the interface of wood paneling and indoor air is recommended for further development in the numerical model. This development will be helpful in investigating the moisture surface coefficient at the interior wall surfaces.

8.5 Related publications by author et al.

Li Y, Fazio P, Rao J. “An investigation of moisture buffering performance of wood paneling at room level and its buffering effect on a test room”, Building and Environment, 2012; 47(1):205-216.

Li, Y. Fazio, P. Rao, J. "Numerical investigation: the influence of room factors on HAM transport of a full-scale experimental room", accepted for publication by the Building and Environment Journal

Li, Y. Fazio, P. Rao, J. (2010) "Numerical Modeling of Hygrothermal Response in a Full-Scale Experimental Room and through the Envelope", proceedings of the Thermal Performance of the Exterior Envelopes of Whole Buildings XI International Conference, Florida, USA, Dec 6-9.

REFERENCES

Abadie, M., Mendes, N. 2006. Comparative analysis of response-factor and finite-volume based methods for predicting heat and moisture transfer through porous building materials. *Journal of Building Physics,* v 30, n 1, p 7-37

Abadie, M. O., Mendonça, K. C. 2009. Moisture performance of building materials: From material characterization to building simulation using the moisture buffer value concept. *Building and Environment*, v 44, n 2, p 388-401

Adan, O., Brocken, H., Carmeliet, J., Hens, H., Roels, S., Hagentoft, C.-E., 2004 Determination of liquid water transfer properties of porous building materials and development of numerical assessment methods: Introduction to the EC HAMSTAD Project, *Journal of Thermal Envelope and Building Science*, v 27, n 4, April, p 253-260

Alturkistani, A., Fazio, P., Rao, J., Mao, Q., 2008. A new test method to determine the relative drying capacity of building envelope panels of various configurations. *Building and Environment,* v 43, n 12, December, p 2203-2215

Amissah, P., (2005), "Indoor air quality – combining air humidity with construction moisture", Doctoral Thesis, University of Strathclyde, Glasgow, U.K.

Atthajariyakul, S. and Leephakpreeda, T. 2004. Real-time determination of optimal indoor-air condition for thermal comfort, air quality and efficient energy usage. *Energy and Buildings*, v 36, n 7, p 720-33

ASHRAE, 2005. ASHERAE Handbook 2005 – Fundamentals. Atlanta: American Society of Heating, Refrigerating and Air conditioning Engineers.

Barbosa R., Mendes, N. 2008. Combined simulation of central HVAC systems with a whole-building hygrothermal model. *Energy and Buildings*, v 40, n 3, p 276-288

Bennett, C.O., Myers, J.E. 1982. *Momentum, heat, and mass transfer*. McGraw-Hill, NY.

Carmeliet, J., Roels, S. 2001. Determination of the isothermal moisture transport properties of porous building materials. *Journal of Thermal Envelope and Building Science*, v 24, n 3, p 183-210

Cerny, R., Jirickova, M. 2006. Effect of hydrophilic admixtures on moisture and heat transport and storage parameters of mineral wool. *Construction & Building Materials*, v 20, n 6, p 425-434

Cerolini, S., D'Orazio, M., Di Perna, C., Stazi, A. 2009. Moisture buffering capacity of highly absorbing materials. *Energy and Buildings*, v 41, n 2, p 164-168

Chen, Z.Q., Shi, M.H. 2005. Study of heat and moisture migration properties in porous building materials. *Applied Thermal Engineering*, v 25, n 1, p 61-71

Clarke, J.A., Johnstone, C.M., Kelly, N.J., McLean, R.C., Anderson, Rowan, N.J., and Smith, J.E. 1998. A technique for the prediction of the conditions leading to mould growth in buildings. *Building and Environment*, v.34, n 4, p 515-521

COMSOL 3.5 Multiphysics User's Guide, COMSOL AB, 2008

Cornick, S.M., Kumaran, M.K. 2008. A comparison of empirical indoor relative humidity models with measured data. *Journal of Building Physics*, v 31, n 3, p 243-68

Cunningham, M.J. 1992. Effective penetration depth and effective resistance in moisture transfer. *Building and Environment*, v 27, n 3, p 379-386

Cunningham, M.J. 2003. The building volume with hygroscopic materials - An analytical study of a classical building physics problem. *Building and Environment*, v 38, n 2, p 329-337

Davies, M., Tirovic, M., Ye, Z., Baker, P.H. 2004. A low cost accurate instrument to measure the moisture content of building envelopes in situ: a modelling study. *Building Services Engineering Research & Technology*, v 25, n 4, p 295-304

Delgado, J.M.P.Q., Ramos, N.M.M., De Frietas, V.P. 2006. Can moisture buffer performance be estimated from sorption kinetics? *Journal of Building Physics*, v 29, n 4, p 281-99

Derluyn, H. , Janssen, H., Diepens, J., Derome, D., Carmeliet, J. 2007. Hygroscopic behavior of paper and books. *Journal of Building Physics*, v 31, n 1, p 9-34

El Diasty, R., Fazio, P., Budaiwi, I. 1993. Dynamic modelling of air humidity behaviour in a multi-zone space. *Building and Environment*, v 28, n 1, p 33-51

Erriguible, A., Bernada, P., Couture, F., Roques, M., 2006. Simulation of convective drying of a porous medium with boundary conditions provided by CFD. *Chemical Engineering Research & Design*, v 84, n A2, p 113-23

Fang, L., Clausen, G., Fanger, P.O. 1998. Impact of temperature and humidity on the perception of indoor air quality. *Indoor Air*, 8, 80-90

Fazio, P., Alturkistani, A., Rao, J. and Mao, Q., (2009), A new testing method to evaluate the relative drying performance of different building envelope systems using water trays. *Journal of ASTM International,* Vol. 6, No. 9.

Fazio, P., Athienitis, A., Marsh, C., Rao, J. 1997. Environmental chamber for investigation of building envelope performance. *Journal of Architectural Engineering*, v 3, n 2, p 97-102

Fazio, P., Rao, J., Alturkistani, A., Ge, H., 2006. Large scale experimental investigation of the relative drying capacity of building envelope panels of various configurations.

Proceedings of the 3rd International Building Physics Conference - Research in Building Physics and Building Engineering, p 361-368

Fazio, P., Vera, S., Rao, J., Yang, X., Ge, H. 2007. Datasets of whole-building HAM indoor conditions for one-room and vertical two-room experimental setups. A sub-project report for Annex 41, International Energy Agency.

Feriadi H. 2003. Thermal comfort for natural ventilated residential buildings in the tropical climate. PhD. dissertation, National University of Singapore, Singapore.

Gudum, C. 2003. Moisture Transport and Convection in Building Envelopes Ventilation in Light Weight Outer Walls. PhD thesis, Lund University, Sweden.

Hachem, C., Chaubey, Y., Fazio, Rao, J. and Bartlett, K., 2010. Statistical Analysis of Microbial Volatile Organic Compounds in an Experimental Project: Identification and Transport Analysis. Indoor and Built Environment, v19, n2, p275-285

Hachem, C., Fazio, P., Rao, J. and Bartlett, K., 2009. Identification and transport investigation of microbial volatile organic compounds in full-scale stud cavities. Building and Environment, v44, n8, P1691-1698

Hagentoft, C., Kalagasidis, A., Adl-Zarrabi, B., Roels, S., Carmeliet, J., Hens, H., Grunewald, J., Funk, M., Becker, R., Shamir, D., Adan, O., Brocken, H., Kumaran, K., Djebbar, R. 2004. Assessment method of numerical prediction models for combined heat, air and moisture transfer in building components: benchmarks for one-dimensional cases. *Journal of Thermal Envelope and Building Science*, v 27, n 4, p 327-352

Hameury, S. 2005. Moisture buffering capacity of heavy timber structures directly exposed to an indoor climate: A numerical study. *Building and Environment*, v 40, n 10, p 1400-1412

Hamlin, T. and Gusdorf, J., 1997. Airtightness and energy efficiency of new conventional and R-2000 housing in Canada, CANMET Energy Technology Centre (CETC), Ottawa, Ontario.

Hutcheon, N.B. and Handegord, G. 1983. Building science for a cold climate. NRC, Canada.

Jaguste, D.N. and Bhatia, S.K. 1995. Combined Surface and Viscous-Flow of Condensable Vapor in Porous-Media. Chemical Engineering Science. v 50, n 2, p 167-182.

Janssen, H., Blocken, B., Carmeliet, J. 2007. Conservative modelling of the moisture and heat transfer in building components under atmospheric excitation. *International Journal of Heat and Mass Transfer*, v 50, n 5-6, p 1128-40

Janssen, H. and Roels, S., 2009, Qualitative and quantitative assessment of interior moisture buffering by enclosures, Energy and Buildings, 41(4): 382-394.

Jirickova, M., Cerny, R. 2006. Chloride binding in building materials. Journal of Building Physics, v 29, n 3, p 189-200.

JIS A 1470-1 (2002). Test Method of Adsorption/Desorption Efficiency for Building Materials to Regulate an Indoor Humidity-Part 1: Response Method of Humidity, Japanese Industrial Standards, Japan.

Kalamees, T., Vinha, J., Kurnitski, J. 2006. Indoor humidity loads and moisture production in lightweight timber-frame detached houses. *Journal of Building Physics*, v 29, n 3, p 219-46

Karagiozis, A., Salonvaara, M.. 2001. Hygrothermal system-performance of a whole building. *Building and Environment*, v 36, n 6, p 779-787

Karoglou, M., Moropoulou, A., Krokida, M.K., Maroulis, Z.B. 2007. A powerful simulator for moisture transfer in buildings. *Building and Environment*, v 42, n 2, p 902-912

Kong, F., Zheng, M. 2008. Effects of combined heat and mass transfer on heating load in building drying period. *Energy & Buildings*, v 40, n 8, p 1614-22

Kumaran, M.K., Mukhopadhyaya, P., Cornick, S.M., Lacasse, M.A., Rousseau, M., Maref, W., Nofal, M., Quirt, J.D., Dalgliesh, W.A., 2003. An Integrated methodology to develop moisture management strategies for exterior wall systems. Proceedings of the 9th Canadian Conference on Building Science and Technology, Vancouver, B.C., pp. 45-62

Kumaran, M.K., Lackey, J., Normandin, N., van Reenen, D., and Tariku, F., 2002. Summary report from task 3 of MEWS project. Institute for Research in Construction, National Research Council, Ottawa, Canada, (NRCC-45369), pp. 1-68.

Kunzel, H.M., Kiessl, K. 1997. Calculation of heat and moisture transfer in exposed building component .*International Journal of Heat and Mass Transfer*, v 40, n 1, p 159-67

Kunzel, H.M., Holm, A., Zirkelbach, D., Karagiozis, A.N. 2005. Simulation of indoor temperature and humidity conditions including hygrothermal interactions with the building envelope. *Solar Energy*, v 78, n 4, p 554-61

Li, Qinru, Rao, Jiwu, Fazio, Paul. 2009. Development of HAM tool for building envelope analysis. *Building and Environment*, v 44, n 5, p 1065-1073

Lin, Y. 2007, Three-dimensional thermal and airflow (3D-TAF) model of a dome-covered house in Canada. Ph.D. Thesis, Concordia University (Canada), AAT NR30127

Lstiburek, J. 2002. Moisture, building enclosures, and mold. *HPAC Heating, Piping, Air Conditioning Engineering,* v 74, n 1, p 77+80-81

Lstiburek, J., Pressnail, K., Timusk, J. 2002. Air pressure and building envelopes. *Journal of Thermal Envelope and Building Science*, v 26, n 1, p 53-91

Malek, K. and Coppens, M.O. 2003. Knudsen self- and Fickian diffusion in rough nanoporous media. Journal of Chemical Physics. 119(5): p 2801-2811.

Maref, W., Lacasse, M., Booth, D. 2003. Assessing the hygrothermal response of wood sheathing and combined membrane-sheathing assemblies to steady-state environmental conditions. National Research Council of Canada, ISBN 90 5809 565 7

McCullough, E.A., Myoungsook Kwon, Shim, H. 2003. A comparison of standard methods for measuring water vapour permeability of fabrics. *Measurement Science & Technology*, v 14, n 8, p 1402-8

Mortensen, L.H., Woloszyn, M., Rode, C., Peuhkuri, R. 2007. Investigation of microclimate by CFD modeling of moisture interactions between air and constructions. *Journal of Building Physics*, v 30, n 4, p 279-315

Mudarri, D.H., 2010. Building Codes and Indoor Air Quality. U.S. Environmental Protection Agency, Office of Radiation and Indoor Air, Indoor Environments Division. http://www.epa.gov/iaq/pdfs/building_codes_and_iaq.pdf

Murakami, S., Kato, S., Kim, T. 2001. Indoor climate design based on CFD coupled simulation of convection, radiation, and HVAC control for attaining a given PMV value. *Building and Environment*, v 36, n 6, p 701-709

Murakami, S., Kato, S., Zeng, J. 2000. Combined simulation of airflow, radiation and moisture transport for heat release from a human body. *Building and Environment*, v 35, n 6, p 489-500

Neale, A., 2007. A study in computational fluid dynamics for the determination of convective heat and vapour transfer coefficients. Thesis of M.A.Sc., Concordia University 117, AAT MR28889

Noble, J. and Arnold, A. E. 1991. Experimental and mathematical modeling of moisture transport in landfills. Chemical Engineering Communications, 1563-5201, Volume 100, Issue 1, P 95 – 111

Ojanen, T., Salonvaara, M., 2004. Comparison of measured and simulated moisture buffering results. Paper to IEA ECBCS Annex 41, Working meeting, Glasgow.

Osanyintola, O. F. and Simonson, C. J. 2006. Moisture buffering capacity of hygroscopic building materials: Experimental facilities and energy impact. *Energy and Buildings*, v 38, n 10, p 1270-1282

Osanyintola, O. F., Talukdar, P., Simonson, C. J. 2006. Effect of initial conditions, boundary conditions and thickness on the moisture buffering capacity of spruce plywood. *Energy and Buildings*, v 38, n 10, p 1283-1292

Pavlik, Z., Jirickova, M., Cerny, R., Sobczuk, H., Suchorab, Z. 2006. Determination of moisture diffusivity using the time domain reflectometry (TDR) method. *Journal of Building Physics*, v 30, n 1, p 59-70

Perera, M.S.A., Ranjith, P.G., Choi, S.K., Airey, D. 2011. Numerical simulation of gas flow through porous sandstone and its experimental validation. *Fuel*, v 90, n 2, p 547-554

Peuhkuri, R., Rode, C., Hansen, K. K. 2008. Non-isothermal moisture transport through insulation materials. *Building and Environment*, v 43, n 5, p 811-822

Phillipson, M.C., Baker, P., Davies, M., Ye, Z., MclMaughtan, A., Galbraith, G., McLean, R. 2007. Moisture measurement in building materials: an overview of current

methods and new approaches. *Building Services Engineering Research & Technology*, v 28, n 4, p 303-16

Plagge, R., Scheffler, G., Grunewald, J., Funk, M. 2006. On the hysteresis in moisture storage and conductivity measured by the instantaneous profile method. *Journal of Building Physics*, v 29, n 3, p 247-59

Qin, M., Belarbi, R., Ait-Mokhtar, A., Nilsson, L. 2008. Non-isothermal moisture transport in hygroscopic building materials: Modeling for the determination of moisture transport coefficients. *Transport in Porous Media*, v 72, n 2, p 255-271

Qin, M, Belarbi, R., Aït-Mokhtar, A., Seigneurin, A. 2006. An analytical method to calculate the coupled heat and moisture transfer in building materials. *International Communications in Heat and Mass Transfer*, v 33, n 1, p 39-48

Qin,M., Belarbi, R., Ait-Mokhtar, A., Nilsson, L.-O. 2008. Simultaneous heat and moisture transport in porous building materials: evaluation of nonisothermal moisture transport properties. *Journal of Materials Science*, v 43, n 10, p 3655-3663

Quintard, M., Bletzacker, L., Chenu, D., Whitaker, S. 2006. Nonlinear, multicomponent, mass transport in porous media. *Chemical Engineering Science*, v 61, n 8, p 2643-2669

Rao, J., Fazio, P., Bartlett, K., Yang, D.-Q., 2009. Experimental evaluation of potential transport of mold spores from moldy studs in full-size wall assemblies. Building and Environment. v44, n8, p1568-1577

Reddy, J.N. 2001. The finite element method in heat transfer and fluid dynamics. CRC Press, ISBN: 9780849323553

Rode C., Peuhkuri R., Mortensen L.H., Hansen K., Time B., Gustavsen A., Ojanen T., Ahonen J., Svennberg K., Harderup L.E., Arfvidsson J. 2005. Moisture buffering of

building materials. Report BYG·DTU R-126. ISSN 1601 – 2917, ISBN 87-7877-195-1

Rode, C., Grau, K. 2008. Moisture buffering and its consequence in whole building hygrothermal modeling. *Journal of Building Physics*, v 31, n 4, p 333-60

Rode, C., Holm, A., Padfield, T. 2004. A review of humidity buffering in the interior spaces. *Journal of Thermal Envelope and Building Science*, v 27, n 3, p 221-226

Rode, C., Peuhkuri, R., Time, B., Svennberg, K., Ojanen, T.. 2007. Moisture buffer value of building materials. ASTM Special Technical Publication, v 1495 STP, p 33-44

Roels, S., Carmeliet, J., Hens, H., Adan, O., Brocken, H., Cerny, R., Pavlik, Z., Ellis, A. T., Hall, C., Kumaran, K., Pel, L., Plagge, R., 2004. A Comparison of different techniques to quantify moisture content profiles in porous building materials. *Journal of Thermal Envelope and Building Science,* v 27, n 4, p 261-276

Roels, S., Janssen, H. 2006. A comparison of the Nordtest and Japanese test methods for the moisture buffering performance of building materials. *Journal of Building Physics*, v 30, n 2, p 137-161

Roels, S., 2008. Experimental analysis of moisture buffering. Report of Annex 41 Moist-Eng Subtask 2. NUR 955, ISBN 978-90-334-7058-5

Roulet, C.A., Sekhar, S.C., Tham, K.W., Cheong, K.W. 2002. Ventilation, indoor environment quality and climate - Comparison of European and Singapore office buildings. *International Journal of Ambient Energy*, v 23, n 2, p 108-112

Salonvaara, M., Holm, A., Kunzel, H. and Karagiozis, A. 2004. Moisture buffering effects on Indoor Air Quality – experimental and simulation results. Conference Proceedings Performance of Exterior Envelope of Whole Buildings IX, CD-ROM, Clearwater, Florida, December 5-10.

Sandberg M. 1983. Ventilation eAciency as a guide to design. ASHRAE Transaction. 89:455–79.

Sasic Kalagasidis, A., Karlsson, H., Hagentoft, C. 2008. A Simulation tool for temperature and moisture dependent transport of VOC's in buildings. Proceedings of the 7th Symposium on Building Physics in the Nordic Countries, Reykjavík, Iceland

Saito, H., 2005 a. Simple parameters for moisture buffering effect to predict indoor humidity variation. IEA-Annex 41, Moist-Eng, Working meeting, Montreal

Satio, H., 2005 b. Review of researches regarding moisture sources in Japan. IEA-Annex 41, Moist-Eng, Working meeting, Montreal

Simonson, C. J., Salonvaara, M., Ojanen, T. 2004. Heat and mass transfer between indoor air and a permeable and hygroscopic building envelope: Part I - Field measurements. *Journal of Thermal Envelope and Building Science*, v 28, n 1, p 63-101

Simonson, C.J., Salaonvaara, M., Ojanen, T. 2004. Heat and mass transfer between indoor air and a permeable and hygroscopic building envelope: Part II - Verification and numerical studies. *Journal of Thermal Envelope and Building Science*, v 28, n 2, p 161-185

Simonson, C.J., Ojanen, T., Salonvaara, M. 2005. Moisture performance of an airtight, vapor-permeable building envelope in a cold climate. *Journal of Envelope & Building Science*, v 28, n 3, p 205-26

Simonson, C.J., Osanyintola, O.F. 2006. Moisture buffering capacity of hygroscopic building materials: Experimental facilities and energy impact. *Energy and Buildings*, v 38, n 10, p 1270-82

Song, F., Zhao, B., Yang, X., Jiang, Y., Gopal, V., Dobbs, G., Sahm, M.. 2008. A new approach on zonal modeling of indoor environment with mechanical ventilation. *Building and Environment*, v 43, n 3, p 278-286

Steeman, H.J., Janssens, A., Carmeliet, J., De Paepe, M. 2009a. Modelling indoor air and hygrothermal wall interaction in building simulation: Comparison between CFD and a well-mixed zonal model. *Building and Environment*, v 44, n 3, p 572-583

Steeman, H.-J., Janssens, A., De Paepe, M. 2009b. On the applicability of the heat and mass transfer analogy in indoor air flows. *International Journal of Heat and Mass Transfer*, v 52, n 5-6, p 1431-1442

Steiger, M., Kiekbusch, J., Nicolai, A. 2008. An improved model incorporating Pitzer's equations for calculation of thermodynamic properties of pore solutions implemented into an efficient program code. *Construction and Building Materials*, v 22, n 8, p 1841-50

Straube, J., Burnett, E. 2001. Overview of hygrothermal (HAM) analysis methods. Moisture Analysis and Condensation Control in Building Envelopes, ISBN: 0-8031-2089-3. ASTM Manual 40, Ch. 5.

Svennberg, K., Hedegaard, L., Rode, C., 2004. Moisture buffering performance of a fully furnished room. Proceedings of Performance of Exterior Envelopes of Whole Building IX, Clearwater beach, Florida, CD-Rom, 5-10 December.

Svennberg, K., Lengsfeld, K., Harderup, L.-E., Holm, A. 2007. Previous experimental studies and field measurements on moisture buffering by indoor surface materials. *Journal of Building Physics,* v 30, n 3, p 261-74

Tan, G., Glicksman, L.R. 2005. Application of integrating multi-zone model with CFD simulation to natural ventilation prediction. *Energy and Buildings*, v 37, n 10, p 1049-57

Teasdale St-Hilaire, Anik. 2006. Hygrothermal performance of different wood-frame wall assemblies wetted by simulated rain infiltration. Doctoral Theses, Concordia University.

Teodosiu, C., Rusaouen, G., Hohota, R. 2003. Influence of boundary conditions uncertainties on the simulation of ventilated enclosures. *Numerical Heat Transfer*, Part A (Applications), v 44, n 5, p 483-504

Van Schijndel, A.W.M. 2008. Estimating values for the moisture source load and buffering capacities from indoor climate measurements. *Journal of Building Physics*, v 31, n 4, p 319-31

van Schijndel, A.W.M., Schellen, H.L., Wijffelaars, J.L., van Zundert, K. 2008. Application of an integrated indoor climate, HVAC and showcase model for the indoor climate performance of a museum. *Energy & Buildings*, v 40, n 4, p 647-653

Viitanen,H., Salonvaara, M. 2001. Failure criteria: Moisture analysis and condensation control in building envelopes. ASTM Manual series 50: Chapter 4.

Wang, Q.G., Ahmet, K., Yue, Y., L, L.Y. 2005. Determination of the unsaturated hydraulic diffusivity of porous construction materials from transient moisture profiles utilizing pin-type resistance sensor array. *Journal of Materials Science*, v 40, n 4, p 1013-1015

Weber, M., Kimmich, R. 2002. Rayleigh-Benard percolation transition of thermal convection in porous media: computational fluid dynamics, NMR velocity mapping, NMR temperature mapping. *Physical Review E (Statistical, Nonlinear, and Soft Matter Physics*), v 66, n 5, p 56301-1-13

Whitaker, S. 1986. Flow in porous media I: A theoretical derivation of Darcy's law. Transport in Porous Media, v 1, n 1, p 3-25.

White, F. 1988. Heat and Mass Transfer. Prentice Hall, ISBN: 9780201170993

Wissmeier, L., and Barry, D.A. 2011. Simulation tool for variably saturated flow with comprehensive geochemical reactions in two- and three-dimensional domains. *Environmental Modeling and Software,* v 26, n 2, p 210-218

Woloszyn, M., Rode, C., 2008a. Modeling principles and common exercise. Report of Annex 41 Moist-Eng Subtask 1. NUR 955, ISBN 978-90-334-7057-8

Woloszyn, M., and C. Rode. 2008b. Tools for performance simulation of heat, air and moisture conditions of whole buildings. *Building Simulation* 1(1): 5-24.

Woloszyn, M., Kalamees, T., Olivier A., M., Steeman, M., Sasic Kalagasidis, A. 2009. The effect of combining a relative-humidity-sensitive ventilation system with the moisture-buffering capacity of materials on indoor climate and energy efficiency of buildings. *Building and Environment*, v 44, n 3, p 515-524

Wu, Y., Fazio, P., Kumaran, K. 2008. Moisture buffering capacities of five North American building materials. *Journal of Testing and Evaluation*, Vol. 36, No. 1, 34-40.

Yang, X., Fazio, P., Rao, J., Ge, H. 2009. Experimental evaluation of transient moisture buffering of interior surface materials in a full-scale one-room test setup. Proceedings of the Fourth International Conference in Building Physics (IBPC4), Istanbul, June 15-18.

Yang X, Fazio P, Ge H and Rao J. 2011. Evaluation of moisture buffering capacity of interior surface materials and furniture in a full-scale experimental investigation, Building and Environment, In Press.

Yang, X., Vera, S., Rao, J., Ge, H. and Fazio, P., 2007. Full-scale experimental investigation of moisture buffering effect and indoor moisture distribution. Thermal

Performance of External Building Envelopes of Whole Buildings X international Conference, Florida, USA, Dec. 2-7.

Yang, X. 2010. Investigation on moisture buffering of hygroscopic materials by full-scale experiments and HAM simulations. Thesis of PhD. Concordia University 237, AAT NR67328

Zhang, J. S. 2005. Combined heat, air, moisture, and pollutants transport in building environmental systems. *JSME International Journal, Series B: Fluids and Thermal Engineering,* v48, n 2, p 182-190

Zhang, Z.L., and Wachenfeldt, B.J. 2009. Numerical study on the heat storing capacity of concrete walls with air cavities. *Energy and Buildings,* v 41, n 7, p 769-73

APPENDIX A: MATERIAL PROPERTIES

Properties of the materials used in wall system in the experiment setup are listed in Tables A.1. and A.2. The values are also used as inputs in the CFD simulations. These data were adopted from the database created in CRD, SRO projects, WUFI software, as well as some publications (Rode and Grau, 2008; Wu et al. 2008; Janssen and Roels, 2009).

Table A.1 Material properties

Materials of the wall	Thickness (m)	Density (kg/m3)	Heat Capacity (J/kg·K)	Thermal Conductance (w/m·K)	Sorption Isotherm *	Permeability (kg/m·s·Pa)	Vapor Resistance Factor[-]
Vinyl siding	0.0012	1500	1260	0.16	-	-	-
Air cavity	0.019	1.292	1005	0.0243	-	-	-
Air barrier	0.00064	1033	1880	0.1	-	2.82E-14	993.17
Plywood	0.0125	456	1880	0.089	-	1.86E-12	142.5
Wood stud	0.152	465	2390	0.096	-	3.23E-12	117.6
Insulation	0.152	11.51	1260	0.04	-	1.30E-10	1.3
Polyethylene	0.00015	1739	1260	0.159	-	4.75E-15	3280
Gypsum board	0.0125	592	870	0.15	w_{s1},m_1,n_1	Table A.2	-
Wood paneling	0.0175	520	1880	0.12	w_{s2},m_2,n_2	Table A.2	-

*In equation A.1, w_{s1}=805, m_1=-8416.602, n_1=1.652; w_{s2}=588, m_2=-625.404, n_2=1.4639

Table A.2 Vapor permeability of gypsum board and wood paneling

RH %	Permeability (kg/m·s·Pa)		RH (%)	Permeability (kg/m·s·Pa)	
	Gypsum	Wood		Gypsum	Wood
10	3.00 E-11	1.01 E-13	60	3.94 E-11	1.86 E-12
20	3.17 E-11	1.08 E-13	70	4.17 E-11	3.37 E-12
30	3.34 E-11	3.22 E-13	80	4.42 E-11	6.18 E-12
40	3.53 E-11	5.77 E-13	90	4.68 E-11	1.16 E-11
50	3.73 E-11	1.03 E-12	100	4.96 E-11	2.26 E-11

For the moisture sorption isotherm, an empirical relation is used:

$$w = w_s \times [1 + m \cdot \ln(RH)^n]^{\frac{1-n}{n}} \quad \text{(A.1)}$$

where w_s is the saturated moisture content of material (kg/m^3).

APPENDIX B: COMPARISON STRATEGY IN EXPERIMENTAL CALCULATION AND ANALYSIS

In the experiment, a two-step experimental method was developed to calculate the moisture buffering performance of wood paneling and to analyze the variation of indoor environment with respect to the room factors change. This method utilizes a comparison strategy to reduce the errors caused by both the uncertainties of the sensors and in the air leakage estimation. This appendix illustrates how the comparison strategy can reduce the experimental errors.

When temperature T and relative humidity value RH are given, the humidity ratio can be calculated as:

$$w = \frac{0.622 \times P_{sat} \times RH}{P_t - P_{sat} \times RH} \qquad \text{(B.1)}$$

where P_t is the barometric pressure (Pa), P_{sat} is the vapor saturation pressure and is calculated as (ASHRAE, 2005):

$$P_{sat} = \exp(-5.8002206 \times 10^3 / T + 1.3914993 - 4.8640239 \times 10^{-2} * T + 4.1764768 \times 10^{-5} * T^2 - 1.4452093 \times 10^{-8} * T^3 + 6.5459673 * \log(T)) \qquad (B.2)$$

Using Eqs. B.1 and B.2, the humidity ratio at the position of each RH&T sensor can be obtained. Figures B.1 to B.4 show the indoor humidity ratio of cases 7 and 8 in the non-hygroscopic test and hygroscopic test respectively. In each of these figures, there are two curves. One of them represents the humidity ratio measured by a RH&T sensor located in the test room named E_32, and the other curve is the humidity ratio obtained by the average value of measurements by all the RH&T sensors in the test room. The value measured by sensor E_32 has some differences to the average value in each scenario. These differences are caused either by the non-homogeneous indoor humidity condition or by the sensor's uncertainty (±1.0 °C and ±2 %RH). The difference, for

example, in hygroscopic test of case 7 is 0.8 g/kg or 10% (calculated by dividing the difference with respect to the average value) away from the average value. These differences indicate that using the measurement of a single sensor to represent the whole region condition can bring in some errors.

However, when the two-step method is applied, these errors can be significantly reduced. Figures B.5 shows the humidity ratio difference between the two calculation results: one is calculated by using the average value of the indoor humidity ratio in non-hygroscopic test of case 7 to minus the average humidity ratio value in hygroscopic test of this case; the other calculation is conducting the same minus by using the values measured by the sensor E_32. The difference of the two calculations presented in Figure B.5 is insignificant: the difference is between -0.15 to 0.05 g/kg. A similar result can be seen in Figure B.6 where the difference of the two calculations conducted in case 8 is presented. In this case, the difference is between -0.1 to 0.05g/kg. Figures B.1 to B.6 show that by using the two-step method, the errors caused by a single sensor measurement can be significantly reduced. In the experiment, only one RH&T sensor was installed in the inlet and outlet respectively. Some errors may exist when using one measurement to represent the inlet and outlet condition. By using this method, these errors can be significantly minimized. The comparison strategy used in the two-step method also works in the analysis of moisture buffering effect when the room factors change. Figure B.7 shows the humidity ratio differences between the calculations in the hygroscopic tests of cases 7 and 8 in which the room factor of moisture generation rate changes from 42g/h to 58.5g/h. One calculation is using the average value of the indoor humidity ratio in hygroscopic test case 8 minus the average value in hygroscopic test case 7, and the other calculation is using the measurement of sensor E_32 instead of the

average value. The difference in Figure B.7 is between -0.1 to 0.05g/kg. This insignificant difference indicates that the measurement of one single sensor can be utilized when two cases conditions are compared without losing significant accuracy.

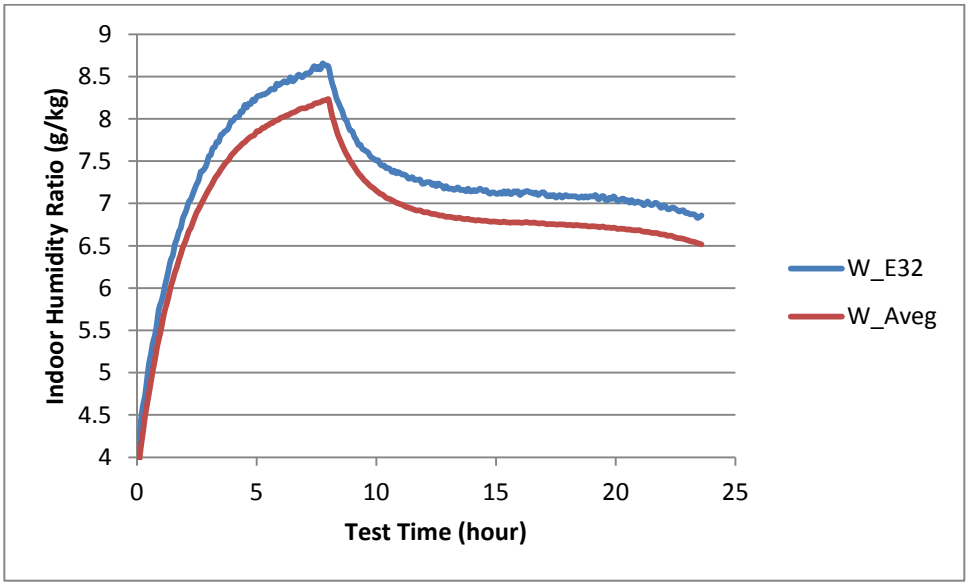

Fig. B.1 Average humidity ratio VS measurement by RH&T sensor E_32 in hygroscopic test of case 7

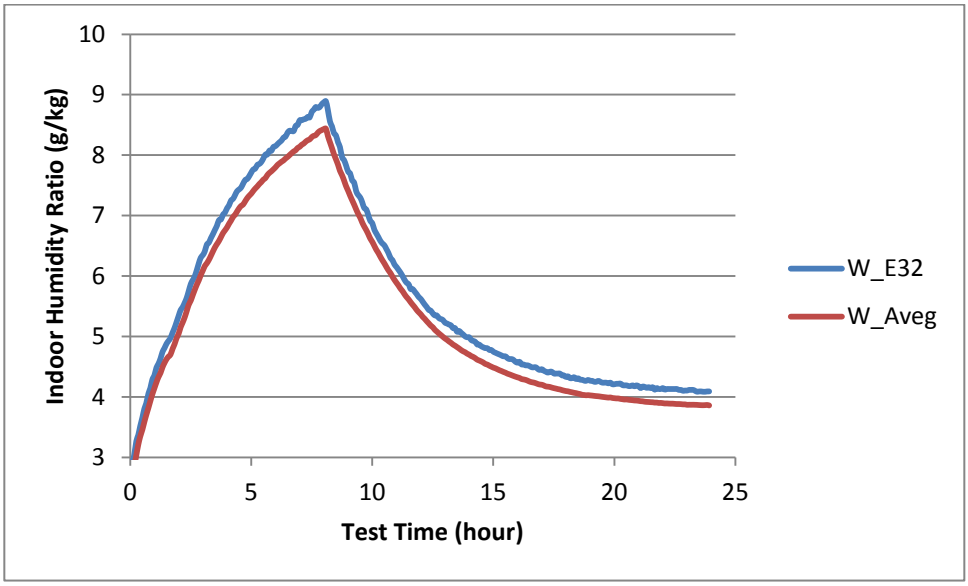

Fig. B.2 Average humidity ratio VS measurement by RH&T sensor E_32 in Non-hygroscopic test of case 7

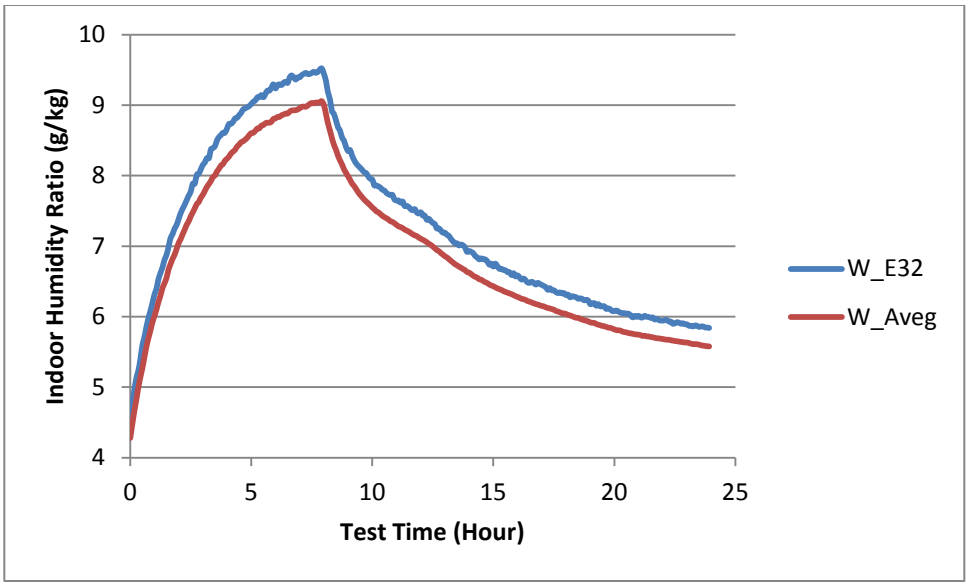

Fig. B.3 Average humidity ratio VS measurement by RH&T sensor E_32 in hygroscopic test of case 8

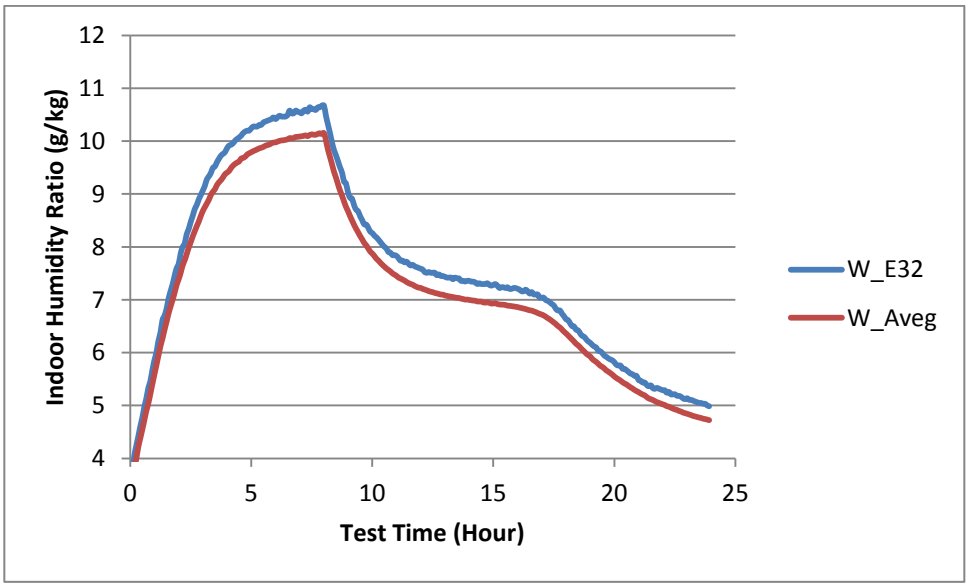

Fig. B.4 Average humidity ratio VS measurement by RH&T sensor E_32 in Non-hygroscopic test of case 8

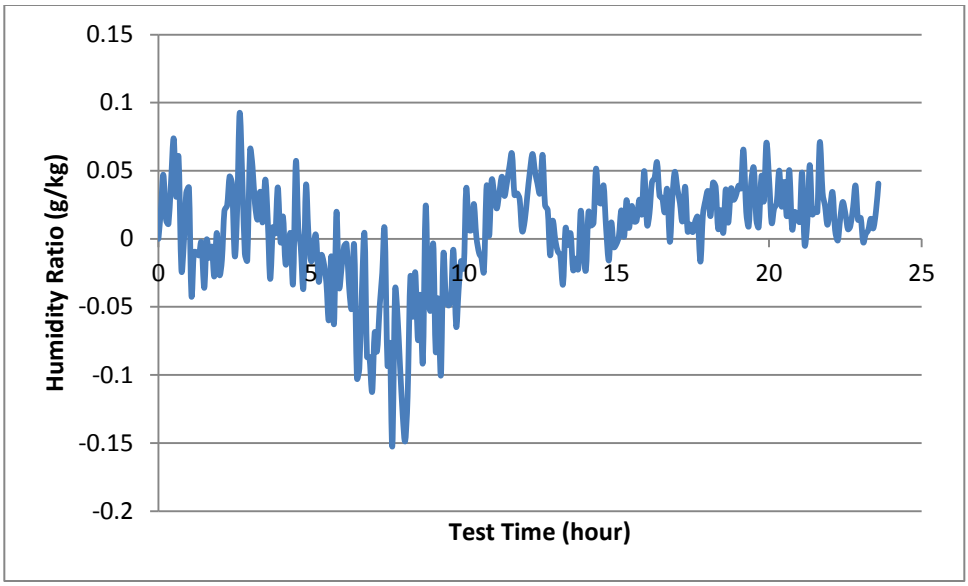

Fig. B.5 Calculation differences between two minus operations in case 7: one is the minus operation between non-hygroscopic test and hygroscopic test by using the average value of the humidity ratio, the other one is by using the humidity ratio measurement of sensor E_32

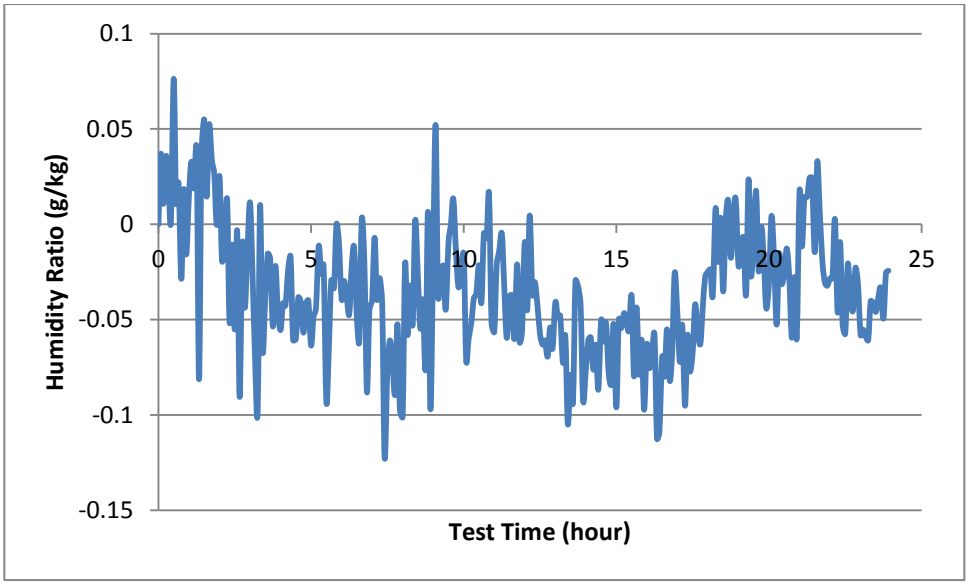

Fig. B.6 Calculation differences between two minus operations in case 8: one is the minus operation between non-hygroscopic test and hygroscopic test by using the average value of the humidity ratio, the other one is by using the humidity ratio measurement of sensor E_32

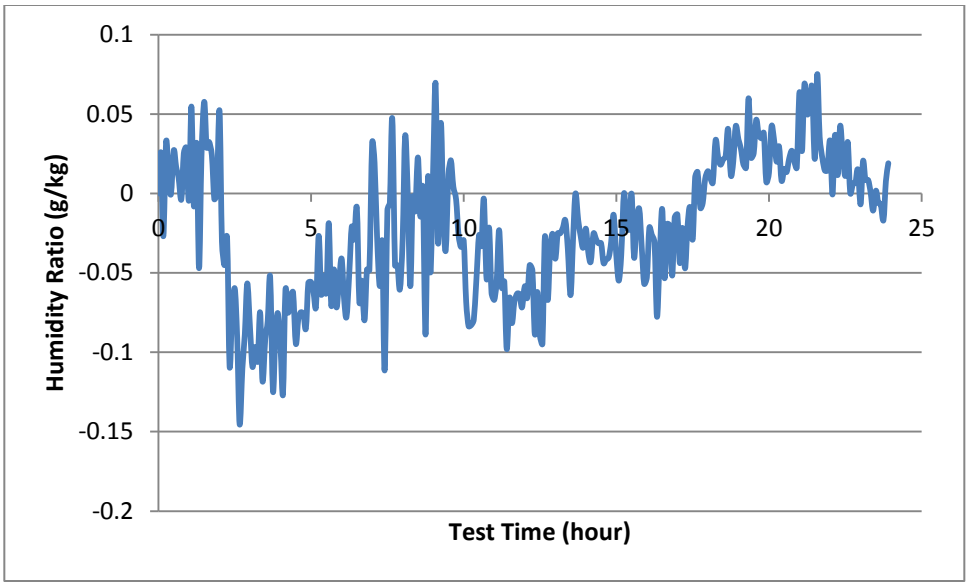

Fig. B.7 Calculation differences between two minus operations in hygroscopic tests of cases 7 and 8: one is the minus operation between cases 7&8 by using the average value of the humidity ratio, the other one is by using the humidity ratio measurement of sensor E_32

APPENDIX C: COMSOL MODEL REPORT

The fully coupled numerical model was established in the COMSOL simulation environment, in which the mechanisms of HAM transport in the test room and through wall system were described by partial differential equations. These equations can be presented in terms of coefficient form, general form, or weak form (if it is needed) as briefly introduced in Chapter 6. This appendix shows the numerical model setup from the geometry to solver selection. This setup information is presented by copying the interface figures or data from the model of simulation case1. The COMSOL version used is 3.5a 3.5.0.603

1. Constants and expression

Constants:

Constant	Value	Description
Q_inlet	10.73[m^3/h]	inlet air flow rate
A_inlet	0.04825*0.0218[m^2]	inlet area
A_outlet	0.135*0.085[m^2]	outlet area
V_inlet	Q_inlet/A_inlet	inlet air velocity
T_heater	40[degC]	heater temperature
T_steel	100[degC]	steel recipient temperature
P0	101325[Pa]	reference pressure
g	-9.81[m/s^2]	gravity constant
T_room	20[degC]	room temperature
T_outside	-5[degC]	outside temp
nv_s	0.85[m^3/kg]	specific volume
Q_m_inlet	Q_inlet/nv_s*Hr	inlet moisture flow rate

Expressions:

Function name: PSAT -- saturated water vapor pressure

Argument: a -- absolute temperature in (°K)

Expression:

exp (-5.8002206e3/a+1.3914993-4.8640239e-2*a+4.1764768e-5*a^2-1.4452093e-8*a^3+6.5459673*log (a))

2. Geometry: sub-domains of the model

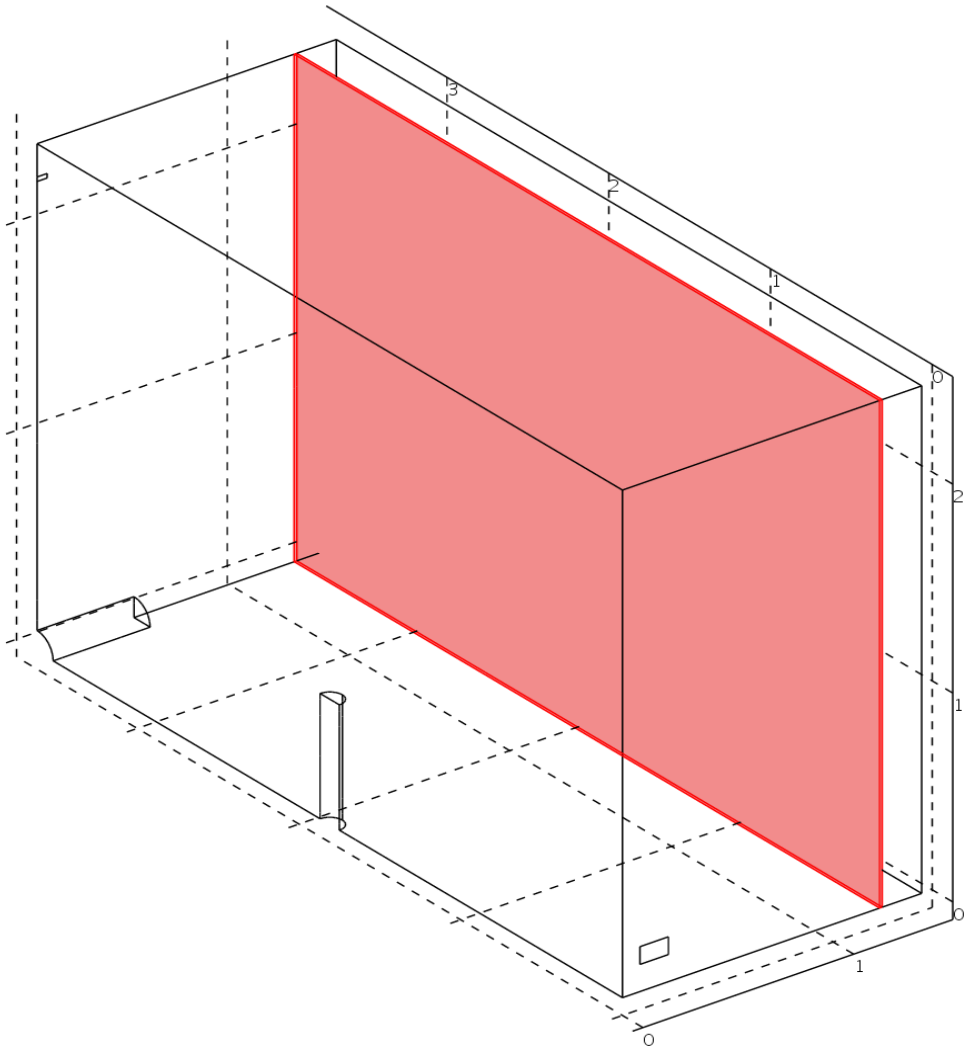

Fig. C.1 Three sub-domains of the numerical model: the color region is the sub-domain2, wood paneling; left side is the sub-domain 1, test room; right side is the sub-domain 3, rest wall assembly layers.

3. Meshing

Mesh parameter	Value
Number of DOFs (degree of freedoms)	834,546
Number of mesh elements	309,519
Number of vertex elements	34
Number of edge elements	1,103
Number of boundary elements	60,504
Minimum element quality	0.184

4. Multi-physics model

4.1 k-ε turbulent model in sub-domain 1

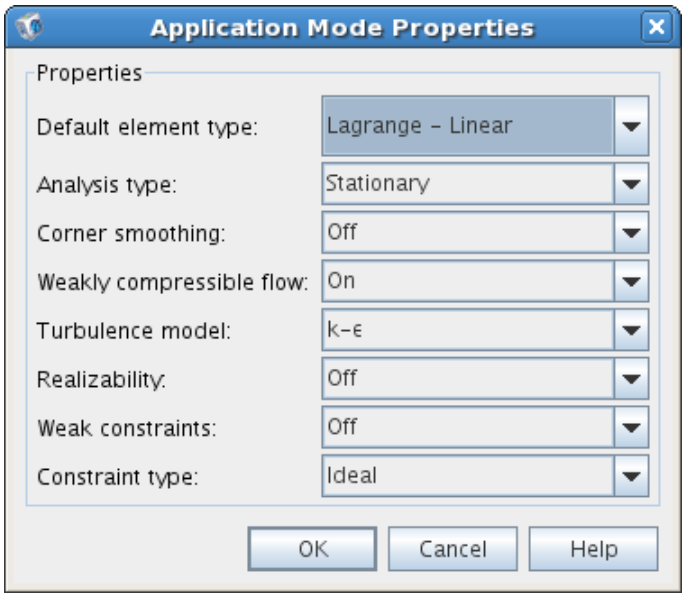

Fig.C.2 Summary of application mode properties for indoor air movement

4.2 Heat transfer model 1 in sub-domain 1

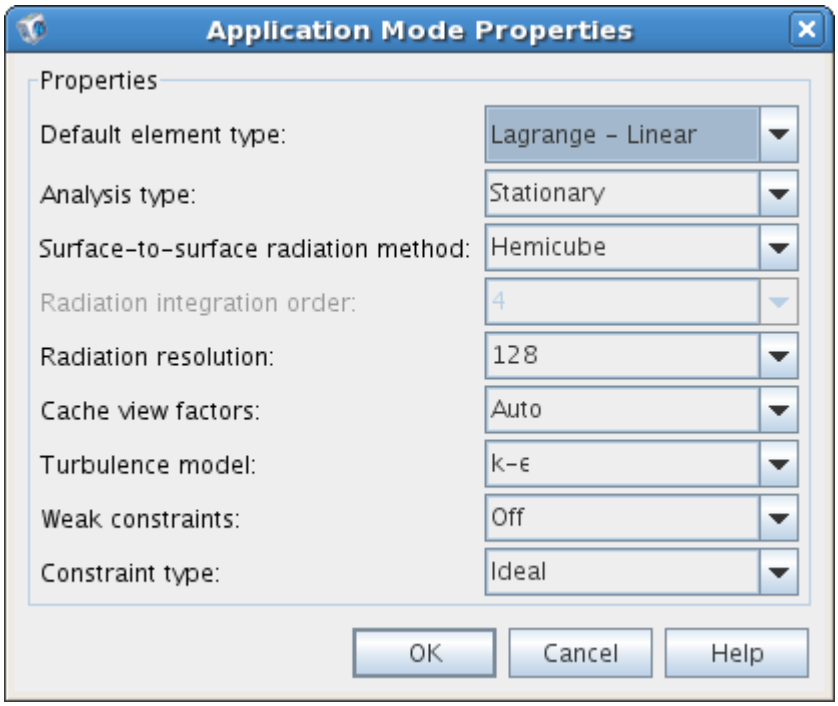

Fig.C.3 Summary of application mode properties for indoor heat transport

4.3 Heat transfer model 2 in sub-domain 2 and 3

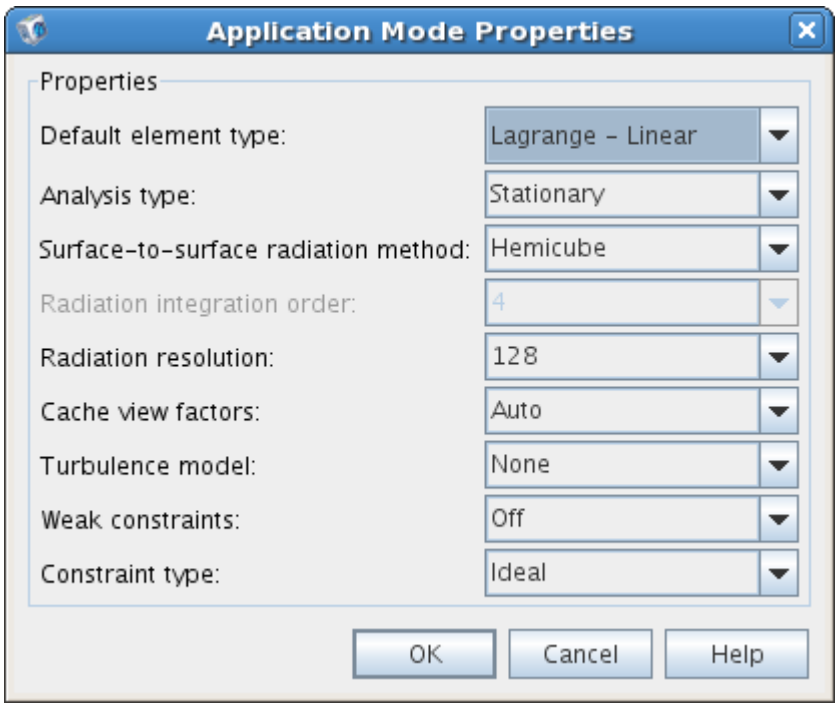

Fig.C.4 Summary of application mode properties for heat transfer inside wall system

4.4 Moisture transport model in sub-domains 1, 2 and 3

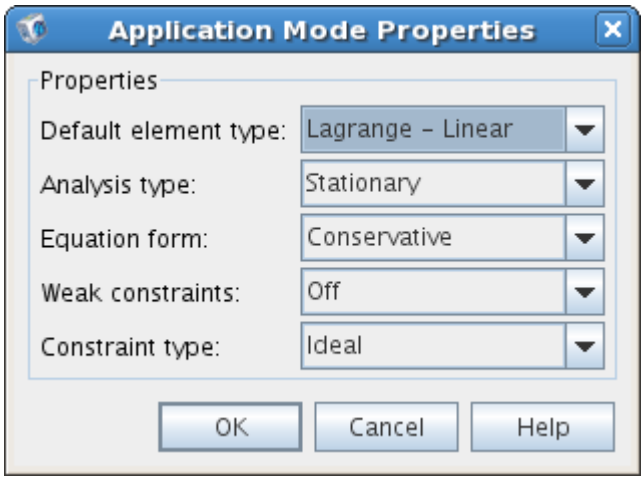

Fig.C.5 Summary of application mode properties for moisture transfer in whole simulation domain

4.5 General form equations

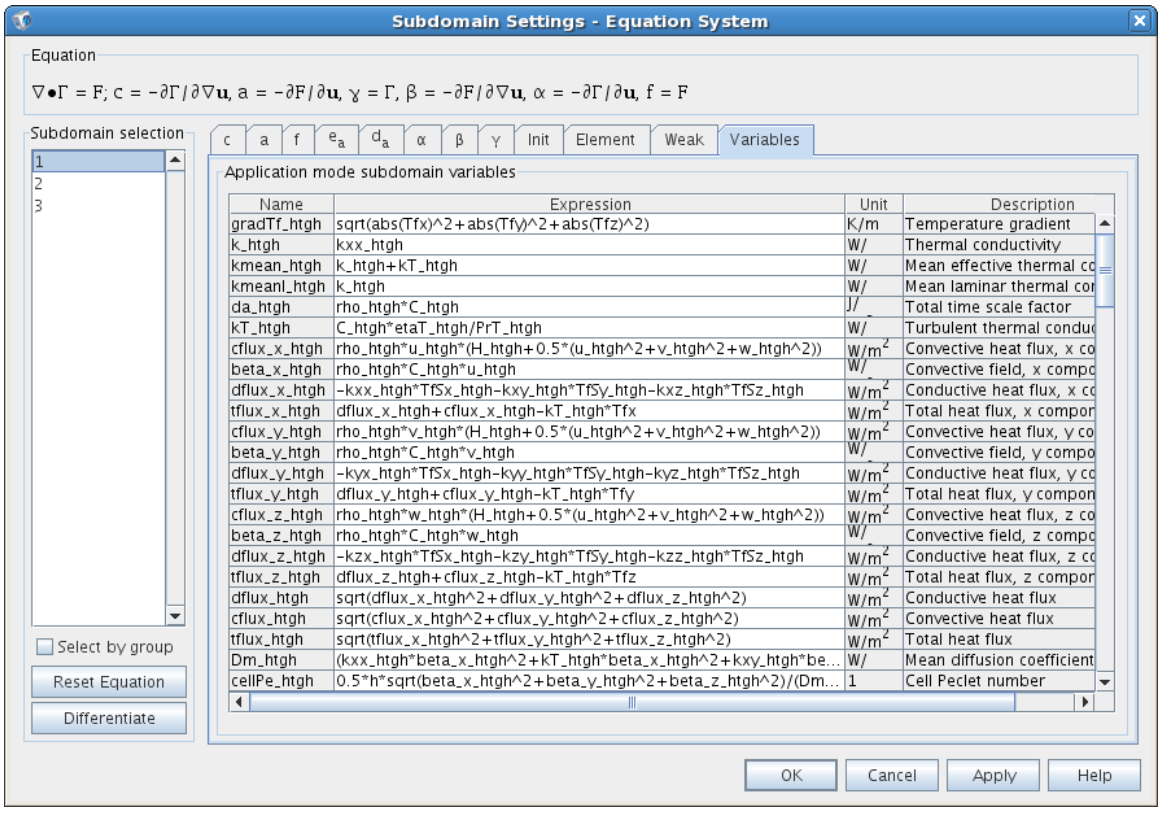

Fig.C.6 General Form of the governing equations defined in the coupling model with the variables list generated by COMSOL simulation environment

5. Solver parameters

Table c.1 Solver parameters manually defined for the coupling numerical model

Solver: Stationary segregated			**Group 1** **u, v, w, p**	**Group 2** **logk, logd**	**Group 3** **Tf, Jf, Ts, Js**	**Group 4** **c**
Linear system solver	Name		BiCGStab	GMRES	GMRES	GMRES
	Relative tolerance		1.0E-3	1.0E-3	1.0E-3	1.0E-6
	Preconditioner	Name	Geometric multigrid	Geometric multigrid	Geometric multigrid	Geometric multigrid
		Multigrid cycle	V-cycle	V-cycle	V-cycle	V-cycle
	Presmoother	Name	SSOR	SSOR	SSOR	Vanka
		Relaxation factor (omega)	0.8	0.8	0.8	0.8
	Postsmoother	Name	SSOR	SSOR	SSOR	Vanka
		Number of iterations	3	3	3	3
	Coarse solver	Name	PARDISO	PARDISO	PARDISO	PARDISO
		Pivoting perturbation	1.0E-8	1.0E-8	1.0E-8	1.0E-8
		Check tolerance	On	On	On	On
Damping	Damping technique		Constant	Constant	Constant	Constant
	Damping constant		0.3	0.3	0.3	0.3
	Jacobian update		On every iteration	On every iteration	On every iteration	On every iteration
Matrix symmetry			Non-symmetry	Non-symmetry	Non-symmetry	Non-symmetry
Termination technique			Tolerance	Tolerance	Tolerance	Tolerance
Maximum number of iterations			100	100	Constant	Constant
Manual scaling			1	1	1	1.0E-4